Thin film composite membranes via layer-by-layer assembly for pervaporation separation

by

Elnaz Halakoo

A thesis
presented to the University of Waterloo
in fulfillment of the
thesis requirement for the degree of
Doctor of Philosophy
in
Chemical Engineering

Waterloo, Ontario, Canada, 2019

AUTHOR's DECLARATION

I hereby declare that I am the sole author of this thesis.

This is a true copy of the thesis, including any required final revisions, as accepted by my examiners.

I understand that my thesis may be made electronically available to the public.

Abstract

The aim of this study was to develop LbL membranes based on polyethyleneimine and graphene oxide (PEI/GO) and to investigate them for three different applications, namely the pervaporative desalination of high-salinity water, dehydration of ethylene glycol (EG) and dehydration of ethanol (EtOH) and isopropanol (IPA). Salts are non-volatile, EG has a high boiling point, and EtOH and IPA can form an azeotrope with water. To prepare LbL membranes in this work, a chlorine-treated thin film composite (TFC) polyamide membrane was used as a substrate, and PEI and GO were used as polycation and polyanion, respectively. To the best of our knowledge, it is for the first time the aforementioned LbL membranes were prepared and investigated in pervaporation applications.

Chlorine-treatment of TFC polyamide was initially studied to determine the suitable chlorination conditions. It was found that pure water flux was more than doubled after chlorination with sodium hypochlorite at 6000 ppm for 2h at room temperature. The as-chlorinated membrane showed that the water permeation flux was almost tripled (i.e., 1.3 kg/m^2h) while the salt rejection decreased by 2% (i.e., 95.8%) for pervaporative desalination of 20 wt% feed salt concentration. The chlorine-treated TFC polyamide membranes with improved flux were used as substrates throughout this study.

First, attempts were made to improve the pervaporative desalination performance. PEI/GO LbL membrane formed on the surface of chlorine-treated TFC polyamide membrane for pervaporation desalination of high-salinity water was investigated for the first time, and for this reason, concentrations of PEI and GO were 0.02 monomol/L and 100 ppm, respectively. It was shown that the incorporating PEI and GO to the chlorine-treated TFC polyamide membranes improved the salt rejection. The PEI/GO LbL membrane was tested for the desalination of aqueous

solutions containing NaCl, Na_2SO_4, $MgSO_4$, and $MgCl_2$ salts, and a water flux as high as 8 kg/m^2h with a high salt rejection (>99.9%) was obtained for all the tested salts at various temperatures and feed concentrations. In order to assess the temperature dependence of the permeation flux through the membrane, the apparent activation energy for permeation of water was determined. The water permeation flux increased with an increase in temperature due to the augmented driving force and diffusivity in the membrane. The properties of the membranes surface were studied using Fourier transform infrared spectroscopy (FTIR), x-ray diffraction (XRD), atomic force microscopy (AFM) and contact angle measurements. Based on the experimental data and stability of the PEI/GO LbL membrane, the formation of the membranes through the LbL self-assembly with PEI and GO showed potential for applications in the treatment of high-salinity water such as industrial wastewater and concentrated reverse osmosis (RO) brine.

EG is one of the important substances in gas and chemical industries. Therefore, after the efficiency of PEI/GO LbL membrane with one bilayer was found and analysed for pervaporative desalination of salts, the PEI/GO membrane was further modified by increasing the number of bilayers for uses in the dehydration of ethylene glycol (EG) with and without the presence of salts in the feed. The effects of operating temperature and feed concentration on the membrane performance were studied. The nano self-assembly of GO and PEI with three bilayers showed a satisfactory performance; a permeation flux of 114 g/(m^2 h) and a separation factor of 213 were achieved at 35 °C for a feed water concentration of 2 wt%. The impact of inorganic salt in the feed on the pervaporation properties were tested by using NaCl as a model salt. The permeation flux decreased with feed salt concentrations while permeate water content increased. The effects of the number of PEI/GO bilayers on membrane performance were also investigated. Increasing number of bilayers from 1 to 15 caused separation factor to increase by 148% while the total permeation

flux decreased by 38%. It was for the first time in the literature that the resistance per bilayer and substrate resistance in LbL membranes were evaluated based on the resistance-in-series approach. FTIR and AFM were used to study the chemistry and morphology of the surface of the PEI/GO LbL membranes with different bilayers, respectively. Water contact angle measurements showed that the surface of the PEI/GO LbL membranes was hydrophilic (lower than 54°), which is advantageous for dehydration of EG.

Following dehydration of EG, the PEI/GO LbL membranes were crosslinked with glutaraldehyde (GA) to further improve the performance of membranes for pervaporation dehydration of EtOH and IPA. A two-level factorial design was used to determine the effects of three main factors in the membrane preparation (i.e., GA concentration, crosslinking time and temperature) on the permeation flux and separation factor. It was found that the GA concentration and crosslinking time were the most significant factors on the performance of the membranes for alcohol dehydration. The effects of operating temperature and feed concentration on the separation performance of the crosslinked LbL membrane were studied. For the crosslinked LbL membrane, total flux increased sharply with operating temperature, while separation factor showed little dependence on temperature. At 60 ºC, the crosslinked (PEI/GO) LbL membrane with seven bilayers had fluxes of 1.8 kg/m^{2}h and 1.5 kg/m^{2}h at 2 wt% water in feed, and the corresponding separation factors were 77 and 197 (respectively for EtOH/water and IPA/water mixtures). It was also showed that the membrane performance can be efficiently adjusted by altering the number of bilayers. The permeance ratio increased to 250 and 620 for water/EtOH and water/IPA systems, respectively, demonstrating that the membrane became much more permselective after deposition of the bilayers on the substrate. FTIR, AFM and contact angle measurements were used to study the surface chemistry, morphology and hydrophilicity of the (PEI/GO) LbL membranes with

different bilayers, respectively. The separation performance of the XL(PEI/GO)$_7$ membrane was monitored over an operation time of 210 h at 50 ºC to verify the membrane stability. The long-term data showed there were no significant variations in pervaporation performance, implying the feasibility of the crosslinked membrane for pervaporation processes.

For all target applications, the activation energies for permeation of each penetrant based on permeation flux (E_J) and membrane permeance (E_P) were calculated and discussed in detail. The activation energies of the different penetrants were compared as they were affected by the types of PEI/GO LbL membranes and the composition of the feed solutions to be separated.

Finally, suggestions for future work include optimization or modification of the PEI/GO LbL membrane preparation to further improve membrane performances for pervaporation applications. Field emission scanning electron microscopy (FESEM) and transmission electron microscopy (TEM) can be used to look at the PEI/GO LbL membranes with and without crosslinking in more detail in future studies.

Acknowledgement

First and foremost, I wish to thank my supervisor Professor Xianshe Feng for his support, insight, and patience. I appreciate all his contributions, both time and ideas, to making my Ph.D. experience productive and inspiring. Thank you, Prof, for allowing me to grow as a research scientist.

My sincere thanks go to my committee members, Professors Michael Pope, Sigrid Peldszus, and Christine Moresoli for their time, interest, and helpful comments. I would also like to thank Professor Raja Ghosh for kindly serving as my external committee member.

Of course, my Ph.D. work has been built on the work of my Master's degree under the supervision of Professors Takeshi Matsuura, Ahmad Fauzi Ismail, and Woei J. Lau. Thank you for all your inspiration, kindness, support, and for giving me a love for this exciting field.

I would like to acknowledge the financial support that I received from the Government of Ontario for the Ontario Trillium Scholarship (OTS). Research support from the Natural Science and Engineering Research Council (NSERC) of Canada is also acknowledged.

My time at the University of Waterloo was made enjoyable in large part owing to lovely friends and labmates: Sahar Hemmati, Muhammad Waqas Iqbal, Kiyoumars Zarshenas, Amir Mowla, Sara Xu, Michael Celarek, Han Wang, Xiaotong Cao, and Silu Chen.

Lastly, I must thank my family for their endless love and encouragement: my parents who support me in all my pursuits; my lovely siblings, Elham and Ali, who always cheer me up; and most of all my beloved, encouraging, and patient husband, Hossein, whose faithful support during the final stages of this thesis is highly cherished. Thank you all!

Elnaz Halakoo
University of Waterloo
September 2019

Table of Contents

List of Figures

List of Tables

List of Abbreviations

AFM	atomic force microscope
ANOVA	analysis of variance
ATR-FTIR	attenuated total reflectance-Fourier transform infrared spectroscopy
BAPP	polyimide membrane based on 3,3-bis[4-(4-aminophenoxy) phenyl] phthalide
BSA	bovine serum albumin
CA	cellulose acetate
Cl-TFC	chlorine-treated thin film composite
CMCNa	carboxymethyl cellulose
CS	chitosan
EDA	ethylenediamine
EG	ethylene glycol
EtOH	ethanol
f-CS	functionalized chitosan
FFV	fractional free volume
FO	forward osmosis
FTIR	Fourier transform infrared spectroscopy
GA	glutaraldehyde
GE	gelatin
GO	graphene oxide
H-PAN	hydrolyzed polyacrylonitrile
IP	interfacial polymerization
IPA	isopropanol
LbL	layer-by-layer
MD	membrane distillation
MF	microfiltration
MLR	multi linear regression
MPD	m-phenylenediamine
Na-Alg	sodium alginate
NF	nanofiltration

NTAC	5-nitrobenzene-1,3-dioyl dichloride
P84	polyimide
PA	polyamide
PAA	polyacrylic acid
PAM	polyallylamine
PAAM	polyacrylamide
PAH	poly(allylamine hydrochloride)
PAN	polyacrylonitrile
PECM	polyelectrolyte complex membrane
PEI	polyethyleneimine
PES	polyethersulfone
PET	polyethylene terephthalate
PD	polydopamine
PDDA	poly(diallyl dimethylammonium chloride)
PRO	pressure retarded osmosis
PSF	polysulfone
PSS	poly(styrene sulfonate sodium salt)
PVA	poly(vinyl alcohol)
PVDF	polyvinylidene fluoride
Ra	mean surface roughness of membrane
RO	reverse osmosis
TBAC	5-tertbutylbenzene-1,3-dioyl dichloride
TETA	triethylenetetramine
TFC	thin film composite
TMC	trimesoyl chloride
UF	ultrafiltration
UFS	urea formaldehyde and sulphuric acid mixture
VLE	vapor-liquid equilibrium
XL	crosslinked
XRD	X-ray diffraction

List of Symbols

A	Effective membrane area, m^2
c	Concentration, mg/L, kg/m^3
D	Diffusion coefficient, m^2/s
E_D	Activation energy for diffusion, kJ/mol
E_J	Activation energy based on permeation flux, kJ/mol
E_P	Activation energy based on membrane permeability, kJ/mol
ΔH_S	Heat of sorption, kJ/mol
ΔH_v	Heat of vaporization, kJ/mol
J	Permeation flux, $g/(m^2.h)$
L	Proportional coefficient related to chemical potential driving force
l	Membrane thickness, m
P	Permeability coefficient, m^2/s
ΔP	Pressure difference across the membrane, MPa
P	Partial vapor pressure, Pa
p^p	Permeate pressure, Pa
p^{sat}	Saturated vapor pressure, Pa
Q	Permeate quantity, g
R	Gas constant, 8.314 J/(K.mol)
R	Salt rejection, %
S	Solubility coefficient
T	Temperature, K, °C
Δt	Time interval, h
x	mole fraction
W	weight of membrane, g

Greek letters

α	Separation factor
γ	Activity coefficient
μ	Chemical potential

Chapter 1

Introduction

1.1 Motivation

Lack of access to potable water and sanitation are important challenges of our time. Globally more than one-third of people live in water-stressed countries, and this number is expected to increase to two-thirds by 2025 [1]. This worldwide challenge has motivated the search for advanced water treatment approaches. Membrane-based separation technologies are efficient, energy-saving, environmentally friendly, and versatile compared with conventional separation methods. According to the "Global Membrane Market for Industrial Water and Wastewater Treatment Forecasts and Analysis," the membrane market is growing at a Compound Annual Growth Rate (CAGR) of 11.1% and is expected to reach $18.22 billion by 2025 [2].

Pervaporation, an emerging membrane process for separating liquid mixtures, is mainly applied for treating organic-organic mixtures, azeotropic mixtures, anhydrous organic mixtures, dehydrating of organic solvents, thermally sensitive compounds, and eliminating trace organic compounds from contaminated water [3,4]. Dehydration is the most developed area of pervaporation applications, and desalination via pervaporation has gained interest in recent years [5,6]. The advantages of pervaporation over conventional technologies are that it is simple to

operate, needs no third component, consumes less energy, and does not introduce secondary contamination [4]. Moreover, this process has superior separation ability and energy efficiency, resulting in a 40-60% reduction in energy consumption [7]. Pervaporation can be used as a standalone unit or integrated with other unit operations, such as distillation, to form a hybrid process. For example, using a hybrid pervaporation-distillation process in ethanol-production can reduce operating costs (66% lower than a standalone distillation process) [8]. Table 1.1 compares separation options for a small-scale ethanol/water GFT plant [9]. Pervaporation has the lowest cost and consumes less energy than distillation and adsorption [9].

Table 1. 1 Separation options for small scale ethanol/water (Basic: 1000L/day, 99.5 wt% ethanol).

	Pervaporation	Distillation	Adsorption
System cost	$ 75,000	$ 140,000	$ 90,000
Pumps	3 kW	2 kW	2 kW
Steam	45 kg/h @ 1.8 bar	70 kg/h @ 7.3 bar	90 kg/h @ 7.3 bar
Entrainer		3 L/day	

An efficient pervaporation membrane requires a high permeation flux and reasonable selectivity. However, the permeation flux is usually low for pervaporation processes and still under-developed commercially [10]. For selective removal of water, hydrophilic membranes are frequently applied. Layer-by-layer (LbL) self-assembly of oppositely charged polyelectrolyte is one of the simple, yet low cost and efficient method to prepare hydrophilic membranes with thin surface layer [11,12]. LbL membranes have attracted significant interest in pervaporation applications due to their ultra-thin thickness, high hydrophilicity, and ionic crosslinked structures [11,13]. However, the low membrane stability, high preparation time and rate of membrane

swelling limit its use in pervaporation applications. These limitations can be improved by applying appropriate (1) substrate and (2) oppositely charged polyelectrolytes. Chlorine-treated thin film composite (TFC) polyamide membranes have an ultra-thin selective layer which reduces the number of polyelectrolyte deposition and save preparation time [14]. TFC polyamide negative surface charges make it ready for polycation deposition [15]. Controlled chlorination of polyamide membranes increases their permeation flux, surface negative charges and hydrophilicity [13].

In this study, branched polyethyleneimine (PEI) was used as a polycation as it has both secondary and primary amine groups in its structure. Graphene oxide (GO) nanosheets have great potential as building blocks for the fabrication of inexpensive and high-performance water purification membranes. GO nanosheets are negatively-charged due to the ionization of carboxylate groups when well-dispersed in water. Consequently, the nanosheets can be used as an anionic component to electrostatically bond to polycations such as PEI [16–18].

The main goal of this study was to prepare LbL membrane with improved pervaporation performance. No prior study in the literature has been investigated the preparation of PEI/GO deposition on the surface of chlorinated TFC polyamide membranes. It was hypothesized that depositing PEI and GO on the surface of chlorine-treated TFC polyamide membranes can build selective LbL membranes with enhanced properties for pervaporative desalination and dehydration. It was for the first time that the as-mentioned membranes were employed for pervaporation applications. Crosslinking of bilayers was also considered as a promising approach to decrease the degree of swelling and increase the stability of the PEI/GO LbL membranes. Glutaraldehyde (GA) was chosen as a crosslinker agent in this study. Its potential for crosslinking of PEI and GO was investigated as well.

1.2 Knowledge gap

As mentioned earlier, pervaporation is an energy-efficient process compared with conventional separation processes. However, the current industrial applications of pervaporation are relatively limited due to the lack of stable and cost-effective membranes under industrial operating circumstances (i.e., relatively high temperature and continuous exposure of the membrane to a feed solution). Low membrane permeation flux and selectivity are also common problems of pervaporation membranes. Therefore, in this study the focus was on improving pervaporation membrane performance via LbL self-assembly approach. To prepare appropriate membranes for pervaporative water desalination and solvent dehydration, the chemical properties and material selection of the membrane must be considered. In addition, to reach a higher permeation flux without sacrificing the separation factor is still the main challenge. Herein, it was tried to increase the permeation flux with chlorination of the TFC polyamide substrate and increase the selectivity by depositing hydrophilic PEI/GO bilayers. More efforts are required to prepare thin membranes with fewer defects, lower mass transfer resistance, more hydrophilicity, and stability. Composite membranes such as LbL membranes have promising structures.

LbL membranes with different pervaporation performances due to their different fabrication methods and configurations have been reported since 1998, and information on the preparation of LbL membranes and their pervaporative applications is highly desired. Moreover, there is a paucity of literature on using GO in LbL assembly for pervaporation applications. Although the self-assembly of PEI/GO on top of chlorinated TFC polyamide membranes for pervaporation applications are expected to offer a preferential passageway for the transport of water molecules, the membrane permeability and selectivity for different feed systems (i.e., salt/water, EG/water, EG/water/salt, EtOH/water and IPA/water) are still limited. To our knowledge, little work has been

carried out on the application of GO-based LbL membranes in pervaporative desalination of water and dehydration of solvents. Only a few studies reported in the literature demonstrated organic solvent dehydration in the presence of inorganic salt. As the thickness of an active layer of a membrane increases with the number of bilayers, more valuable information should be provided about the relation among membrane thickness, permeation flux, and selectivity, and there are key questions yet to be discussed about total resistance of a membrane.

To fill these knowledge gaps, the present research work intended to investigate the properties of PEI/GO LbL membranes and address the issues mentioned above and provide a better understanding of the GO-based LbL membranes in different pervaporation systems and conditions. The results can provide new references for LbL membrane fabrication.

1.3 Research objectives

The objective of this research was to investigate LbL membranes based on PEI and GO with improved separation performance and stability for desalination and dehydration applications via pervaporation. Membrane preparation, separation performance and mass transfer resistance were systematically studied and thoroughly discussed. The detailed research objectives are as follows:

1) To study the chlorine treatment of the TFC polyamide membranes for use as a substrate and improve the separation performance of chlorinated TFC polyamide membrane by deposition of PEI and GO for pervaporative desalination of high-salinity water.
2) To investigate the TFC membranes fabricated via self-assembly based on PEI/GO for pervaporative dehydration of ethylene glycol, with/without the presence of salt.

3) To improve the performance of the PEI/GO LbL membranes for pervaporative dehydration of ethanol and isopropanol by surface crosslinking of each bilayer using glutaraldehyde (GA).

1.4 Thesis layout

This thesis is organized into six chapters, as follows:

Chapter 1 briefly introduces pervaporation and background of the research, then outlines the objectives study.

Chapter 2 reviews the literature on pervaporation systems for water desalination and solvent dehydration. Information on the fundamentals and mass transport mechanism of pervaporation is provided. In addition, the development and features of layer-by-layer (LbL) assembly membranes are presented, and current studies that have been carried out to develop pervaporative LbL membranes are discussed.

Chapter 3 presents the chlorine treatment of TFC polyamide membranes in a controlled manner, followed by the deposition of PEI and GO for the pervaporative desalination of high-salinity water. The effects of operating temperature and feed concentration on membrane performance were investigated. Four types of salts (i.e., NaCl, Na_2SO_4, $MgCl_2$, and $MgSO_4$) were used as model salts in this study.

Chapter 4 investigates the separation performance of the PEI/GO LbL membranes for the dehydration of ethylene glycol, an important application in natural gas and chemical processing industries. The effects of the number of bilayers on pervaporation performance were studied. The effects of feed concentration, operation temperature on the pervaporative performance were also

investigated, using binary mixtures of ethylene glycol/water and ternary mixtures of ethylene glycol/water/salt. The stability of the membrane was also tested.

Chapter 5 deals with the design and fabrication of crosslinked PEI/GO LbL membranes for the dehydration of ethanol and isopropanol via pervaporation. A two-level factorial design was used to study the effects of three main factors (i.e., crosslinker concentration, crosslinking time and temperature) in the membrane crosslinking on the permeation flux and separation factor. The effects of feed concentration, operating temperature, and the number of bilayers on the pervaporative performance were further discussed. The stability of the crosslinked membrane was also tested at a relatively high temperature (i.e., 50 ºC).

Chapter 6 draws general conclusions and highlights the original contributions of the thesis work. Some recommendations for future research are also provided. Fig. 1.1 shows an overview of this thesis structure.

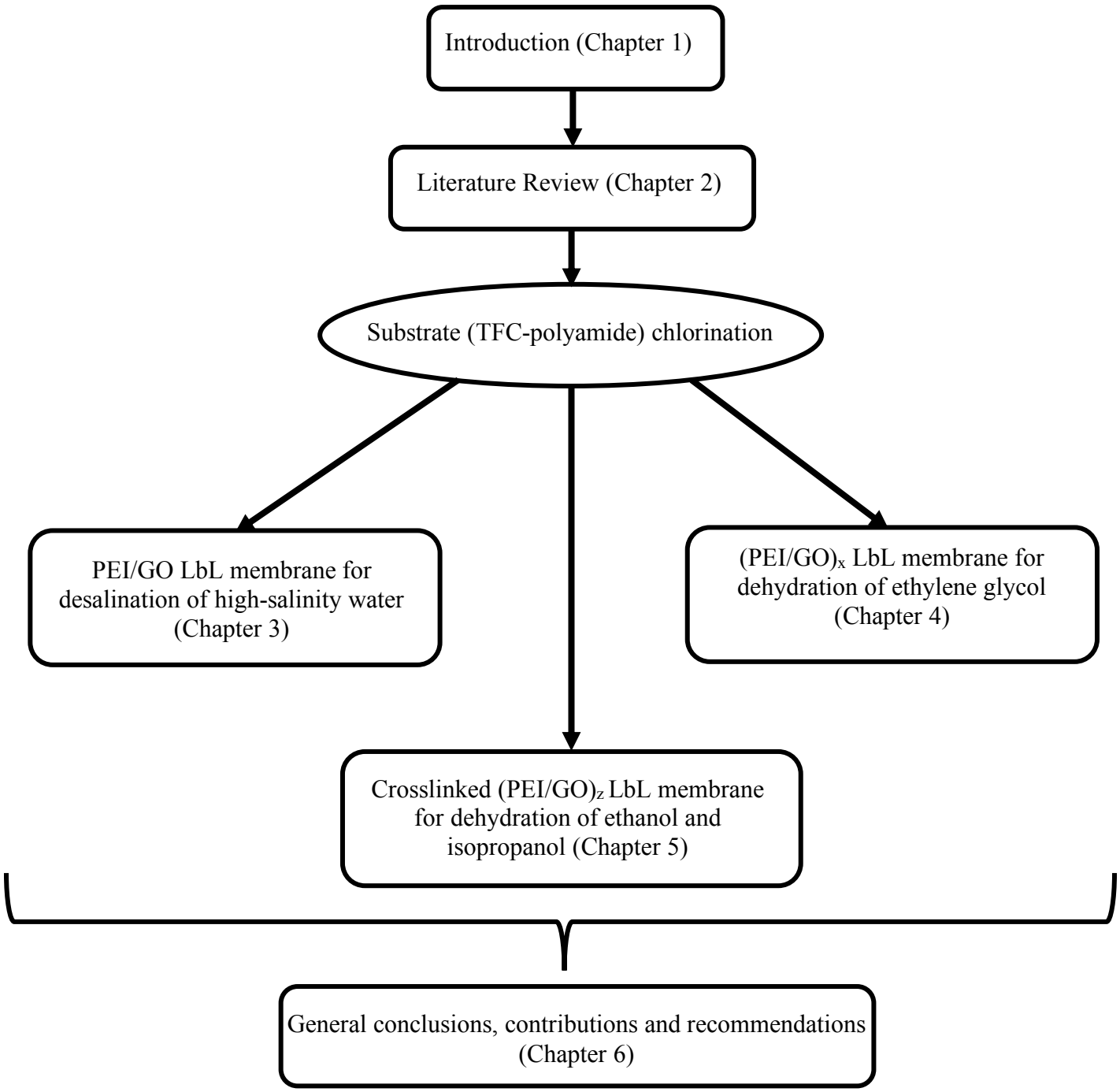

Figure 1. 1 An overview of the thesis structure.

Chapter 2

Literature Review

2.1 Pervaporation

The term pervaporation, which combines the words "permeation" and "evaporation," was first coined by Kober, who described selective permeation of water from aqueous solutions of albumin and toluene through cellulose nitrate film [19]. Since then, many studies have been carried out to develop this technology [10,19]. Pervaporation is a membrane-based technology for the separation of liquid mixtures. The difference in the partial vapor pressure of components between the feed side and the permeate side drives the process, which is usually maintained by a vacuum pump on the permeate side of the system [14,20]. In the pervaporation process, a heated feed-liquid mixture comes in contact with the upstream side of a non- porous or molecular-sieving porous membrane; permeate vapor is then preferentially removed from the downstream side by either a vacuum pump or an inert purge (generally air or steam). When cooled down (e.g., using a liquid nitrogen cold trap), the permeate vapor undergoes a phase change and forms a condensed permeate [10].

Permeating component with a higher affinity to the surface of the membrane and/or quicker diffusivity in the membrane can be preferentially removed from the feed mixture. Pervaporation involves a phase change from liquid (feed) to vapor (permeate). Technologies such as distillation

involving phase change are usually energy-intensive. However, pervaporation deals with the minor components of the liquid mixture, and selective membranes are employed [21].

2.2 Mass transport mechanism

The permeation of a component across a pervaporation membrane can be explained from both kinetic and thermodynamic perspectives. Thermodynamically, it involves the solubility of the permeating component into the membrane, whereas kinetically, it involves penetrant diffusion through the membrane. The coupled transport among different penetrants should also be considered since it influences the permeation of individual permeant. Additionally, these penetrants can swell the membrane and alter its microscopic structure, enhancing diffusion rates [4]. In principle, two approaches are widely used to address mass transport in pervaporation: 1) the solution diffusion model and 2) the pore flow model [5,10].

The solution diffusion model

Thomas Graham proposed the solution-diffusion model, the most popular transport mechanism in pervaporation, and the one most accepted in the membrane community [22]. The heated feed liquid mixture is in contact with the upstream side of the semipermeable membrane, and mass transfer takes place under the concentration gradient through the membrane. The vaporous permeate in downstream can be removed. Accordingly, the concentration gradient, which is related to partial vapor pressures of upstream and downstream sides of the membrane is considered to be the driving force for the process [5]. Differences in the amount of penetrant that dissolves in the membrane and the rate at which the penetrant diffuses through the membrane are the basis of separation in this model [23]. The transport of a permeating component across a membrane occurs in three consecutive steps (Fig. 2.1**)** [10]:

1) Sorption of the penetrant from the feed liquid side into the membrane side;

2) Diffusion of the penetrant in the active layer of the membrane;

3) Desorption of the penetrant to the vapor phase on the downstream side of the membrane.

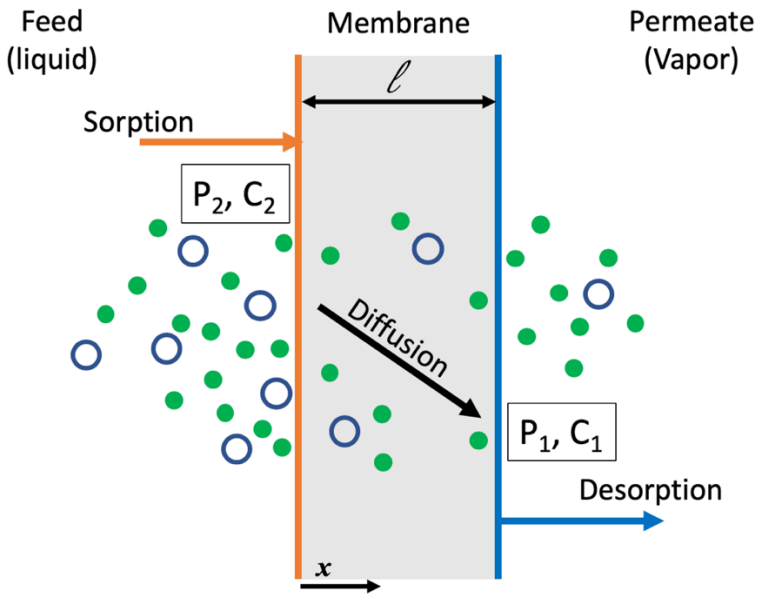

Figure 2. 1 Schematic diagram of the solution-diffusion model [23].

The separation performance of pervaporation membranes can be increased by improving solubility selectivity and/or diffusivity selectivity of the penetrant(s) [4]. The sorption and desorption steps are assumed to be fast enough to reach equilibrium. The second step, i.e. diffusion, is considered to be a rate-controlling step and can be described by Fick's first law [5]. The model can be applied to derive equations for the mass transport in dense membranes such as gas separation, reverse osmosis, dialysis, and pervaporation.

Furthermore, the solubility of a penetrant in a membrane is related to the condensability of the penetrants and membrane-penetrant interactions. The diffusivity is affected by the molecular size

and shape of the penetrants, the mobility of the polymer chains, the interstitial space between polymer chains or the fractional free volume of the membrane, as well as the interactions between the permeating components and the membrane [24].

Pore flow model

Okada and Matsuura proposed an alternative transport model based on pore flow considerations [25]. In this model, straight cylindrical pores with a length of δ are assumed to be on the surface of the membrane. Fig. 2.2 schematically shows the pore-flow model. The pores are perpendicular to the membrane surface and all of them are under isotherm condition. It is also postulated that the pores are filled with liquid to a depth of δ_1, and the remaining portion (δ_2) of the pores are filled with vapor. Accordingly, there is a liquid/vapor phase boundary somewhere inside the membrane pores. The mass transport of this model consists of three steps:

1) Liquid transport from the pore inlet to a liquid-vapor phase boundary;

2) Evaporation at the phase boundary;

3) Vapor transport from the boundary to the pore outlet.

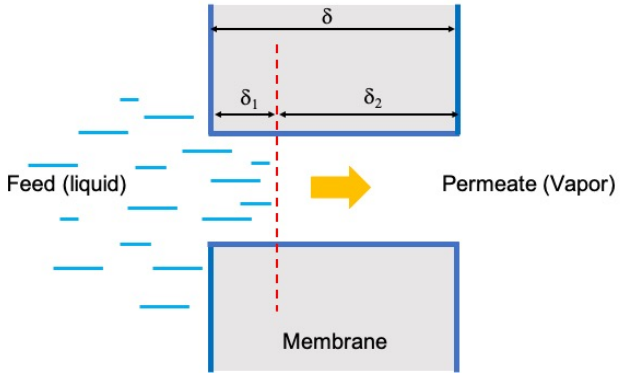

Figure 2. 2 Schematic diagram of pore-flow model [25].

This model simplifies the membrane structure and implies the combination of liquid-transport and vapor-transport sequentially [14]. The pore-flow model may disregard membrane-permeant interactions, and might not be suitable for cases where the feed solution causes the membrane to swell significantly.

2.3 Evaluation of pervaporation membrane performance

The membrane performance is expressed as the capability of a membrane to separate out the components of a mixture. Three specific factors must be taken into consideration. i) Membrane productivity, which is commonly described by permeation flux (*J)*. Note that the thickness of a membrane has a significant impact on permeation flux, and thinner membranes are desired. ii) Membrane separation efficiency, which can be defined in terms of selectivity (β) or separation factor (α). For α of unity, no separation takes place in the system. Note that concentration polarization can potentially affect selectivity. Concentration polarization occurs when there is an accumulation or reduction of permeable components at the boundary layer due to the selective transport through the membrane [26]. Commonly, the permeation flux and the selectivity are determined by experiments. iii) Membrane stability which maintains permeation flux and selectivity under system conditions for an extended period. Chemical, mechanical and thermal properties of the membrane have an essential effect on the membrane stability [10,20].

The flux (*J*) of the membrane can be directly determined experimentally by evaluating the total weight of the permeate (*Q*) during a specific period (*t*) over the effective surface area (*A*) of the membrane.

$$J = Q/(A \times t) \tag{2.1}$$

The separation factor α can be defined by the following equation:

$$\alpha = \frac{y_{wi}/y_{wj}}{x_{wi}/x_{wj}} \quad (2.2)$$

where y_w and x_w are the mass fractions of components *i* and *j* in the permeate and feed, respectively. Higher values of α mean that the membrane has achieved a greater degree of separation. If $\alpha \rightarrow \infty$, the membrane tends to be entirely selective [14].

Moreover, based on the solution-diffusion model, the flux *(J)* is described as follows [14]:

$$J_i = -L_i \, d\mu_i/dx \quad (2.3)$$

where $d\mu_i/dx$ is the chemical potential gradient of component *i*, and L_i is the coefficient of proportionality (not necessarily a constant). The effect of all the typical driving forces such as gradient in concentration, pressure, temperature, and electromotive force on flux can be described by the chemical potential gradient. The chemical potential can be expressed as follows:

$$d\mu_i = RTd\ln(\gamma_i c_i) + v_i dp \quad (2.4)$$

where c_i is the concentration and v_i is the partial molar volume of component *i*, and *p* is the hydrostatic pressure. If the activity coefficient and the molar volume are assumed to be constant values, and by considering ideal gas condition for the vapor phase, the permeation flux can be expressed as:

$$J_i = -\left(\frac{RTL_i}{c_i}.\frac{dc_i}{dx} + L_i v_i \frac{dp}{dx}\right) \quad (2.5)$$

In the solution-diffusion model, it is assumed that the hydrostatic pressure through the membrane remains constant, and the chemical potential gradient of a permeant across the membrane is described simply as a concentration gradient [14]. As a result, equation 2.5 can be rewritten as [5]:

$$J_i = -\frac{RTL_i}{c_i}\frac{dc_i}{dx} \quad (2.6)$$

Substituting the term RTL_i/c_i with D_i, equation (2.6) can be simplified as Fick's equation for steady-state permeation [27].

$$J_i = -D_i \frac{dc_i}{dx} = -\frac{D_i \Delta c_i}{x} \tag{2.7}$$

where D_i is the diffusion coefficient of component i in the membrane (m^2/s), x is the membrane thickness (m), and Δc_i is the concentration difference between component i at the membrane surface on the feed and permeate sides (kg/m^3). Based on equation (2.7), the flux is inversely proportional to the membrane thickness.

Flux and separation factor depend on both the intrinsic properties of a membrane and the operating parameters such as temperature, feed concentration, and pressure. Based on the solution-diffusion model, flux and separation factor can be used to determine the permeability *(P)* and selectivity *(β)*, intrinsic properties of the membrane. The permeability (P_i) is calculated as follows:

$$P_i = \frac{J_i l}{P_i^f - P_i^p} = \frac{J_i l}{\Delta P_i} \tag{2.8}$$

where l is the membrane thickness, P_i^f is the partial vapor pressure of component i in a vapor phase that is in equilibrium with the feed liquid, and P_i^p is the partial vapor pressure of component i in the permeate. According to equation 2.8, P is the thickness- and pressure-normalized permeation flux. In pervaporation, the feed is in a liquid phase; P_i^f can be calculated using Raoult's Law:

$$P_i^f = x_i \gamma_i P_i^{sat} \tag{2.9}$$

where x_i, γ_i and P_i^{sat} are the mole fraction of component i in the feed, the activity coefficient, and the saturated vapor pressure of component i, respectively. The partial vapor pressure (P_i^p) in the permeate is calculated assuming ideal gas behavior, by:

$$P_i^p = y_i P^p \tag{2.10}$$

where y_i and P^p are the mole fraction of component *i* in the permeate and the total pressure at the permeate side. When the permeate side is under a high vacuum, P^p approaches zero. As a result, the permeability can be evaluated from:

$$P_i = \frac{J_i\, l}{x_i \gamma_i P_i^{sat}} \tag{2.11}$$

To look into how the permeability coefficient is related to diffusivity and solubility, consider the pervaporation of a pure component through a flat membrane with a thickness of l, as indicated in Fig 2.1. P_2 and P_1 are the equilibrium vapor pressure of a component in the feed and the vapor pressure of the permeate. At steady-state permeation, the flux can be determined from the Fick's first law (equation 2.7) by integration across the membrane (from x=0 to x=1):

$$J = \frac{1}{l}\int_{C_1}^{C_2} D\, dc \tag{2.12}$$

For constant diffusivity coefficient D, the following equation can be written

$$J = \frac{C_2 - C_1}{l}\, D \tag{2.13}$$

where C_1 and C_2 are the concentrations of the penetrant in the polymer at the feed and permeate sides of the membrane, respectively. Therefore, the permeability of vapor through the membrane can be stated as:

$$P = \frac{J\, l}{P_2 - P_1} = \left(\frac{C_2 - C_1}{P_2 - P_1}\right) D \tag{2.14}$$

Equation 2.14 is valid for the permeation of pure component. To expand this definition to mixtures, P_1 and P_2 should be substituted with the relevant partial pressures (equations 2.9 and 2.10).

In pervaporation, the pressure (P_2) and concentration (C_2) of the feed-side are noticeably greater than those of the permeate side. Therefore, equation 2.14 can be simplified as:

$$P = \frac{C_2}{P_2}\, D \tag{2.15}$$

The equilibrium solubility coefficient, *S*, of vapor in a membrane measures the concentration of the vapor sorbed in the membrane at an equilibrium vapor pressure in the vapor phase [27–29]. From the theoretical point of view, the most appropriate definition of *S* is

$$S = \frac{C}{P} \tag{2.16}$$

After replacement of equation 2.15 by equation 2.16, the permeability in the pervaporation process can be expressed through the following expression:

$$P = DS \tag{2.17}$$

where *S* is calculated at the feed-side of the membrane (i.e., $S = \frac{C_2}{P_2}$). Strictly speaking, this equation is only valid when both *D*, *S* and thus *P* are constant [29].

From equation 2.17, permeability, *P,* which is an intrinsic property of a membrane depends on: 1) *S*, a thermodynamic term, describing the quantity of volatile penetrant molecules dissolved in the membrane matrix and 2) *D*, a kinetic term, describing the motion of penetrant molecules as they diffuse into the membrane (rate of migration through the membrane) [27,28]. Generally, the diffusivity and solubility coefficients depend upon penetrant size and shape and temperature. The diffusion coefficient is strongly sensitive to free volume (chain packing) in polymer chains and chain mobility, so the permeability coefficient is often directly correlated to free volume [28,30]. For instance, after crosslinking of a membrane, the diffusion rate of a penetrant across the membrane starts to decrease as the free volume in the polymer decreases. The solubility coefficient is sensitive to interactions between penetrants and the polymer [27]. Depending on the operating conditions, membrane preparation and feed solution, both D and S have significant effects on the permeability and selectivity (membrane performance).

In pervaporation, the effect of operating temperature on permeation flux often follows an Arrhenius type of equation [31]:

$$J_i = J_0 \exp\left(-\frac{E_J}{RT}\right) \quad (2.18)$$

where E_J is the activation energy for permeation, J_0 is a pre-exponential factor, R is the gas constant, and T is the absolute temperature. It should be noted that equation (2.18) has been widely used in pervaporation to calculate the activation energy of permeation from the logarithmic diagram of flux vs. the inverse of temperature. The activity coefficient and the saturated vapor pressure are also affected by temperature in different ways; therefore, E_J is only a rough characterization of the apparent activation energy of permeation that measures the overall temperature dependence of permeation flux.

The temperature dependence of D_i and S_i is usually expressed as [31]:

$$D_i = D_0 \exp\left(-\frac{E_D}{RT}\right) \quad (2.19)$$

$$S_i = S_0 \exp\left(-\frac{\Delta H}{RT}\right) \quad (2.20)$$

Therefore, the permeability coefficient can be described as:

$$P_i = P_0 \exp\left(-\frac{E_P}{RT}\right) \quad (2.21)$$

where $E_p = (E_D + \Delta H)$ is the real activation energy of permeation based on permeability, it consists of the activation energy of diffusion (E_D) and the enthalpy change of dissolution (ΔH) of the permeant in the membrane. A pre-exponential factor, P_0, is equal to D_0 multiplied by S_0.

The activation energy (E_p) can be calculated from the slope of the line for $\ln(J/\Delta P)$ vs. $1/T$. As mentioned earlier, the permeate pressure may be assumed to be zero. Therefore, by assuming a Clausius-Clapeyron equation for the saturated vapor pressure of the feed and insignificant temperature dependence of the permeant activity coefficient, the activation energy E_p can be estimated through the following correlation:

$$E_P = E_J - \Delta H_V \quad (2.22)$$

where ΔH_V is the heat of vaporization of the permeant. Evaluating E_J from lnJ vs. 1/T is more straightforward compared to calculating E_p from ln(J/ΔP) vs. 1/T data, especially when the permeate pressure is sufficiently low. Accordingly, equation (2.22) can be used to estimate E_p from the corresponding data of E_J. This equation explicitly shows how enthalpy change due to the phase change in pervaporation influences permeation. Note that E_p is the activation energy based on permeance that measures the temperature dependence of the permeability of the membrane, excluding the effect of temperature on the driving force for permeation (ΔP).

The selectivity (β) is the ratio of the permeability of components *i* and *j*:

$$\beta = \frac{P_i}{P_j} \quad (2.23)$$

In addition, the selectivity (β) of asymmetric membranes can also be evaluated as the ratio of the permeance of components *i* and *j*, when the actual selective layer thickness is unknown [4,20]:

$$\beta_{ij} = \frac{P_i/_l}{P_j/_l} \quad (2.24)$$

The salt rejection *(R)* can be experimentally determined:

$$R = \frac{C_f - C_p}{C_f} \times 100 \quad (2.25)$$

where C_f and C_p are the salt concentrations in feed and permeate, respectively [5].

The mass transport mechanism in non-porous uncharged polymeric membranes can be described by the solution-diffusion model. According to Kuznetsov et al. [32], pervaporation desalination can be considered as separation of a pseudo-liquid mixture including free water molecules and hydrated salt ions in water, similar to the separation of organic solutions by pervaporation. Water molecules are first adsorbed and then diffused into the fractional free volume (FFV) of the dense hydrophilic membrane, while salt is rejected. The water flux through the

membrane depends on the thickness of the membrane, the diffusion coefficient of water in the membrane and the hydrophilicity of the membrane, while the rejection of salts relies on the salt solubility and diffusivity (and plus permeability) through the membrane [33]. Xie et al. [34] reported that both NaCl and water diffusivity and permeability are directly proportional to membrane water uptake and FFV. They showed strong correlations between water flux and FFV, and between mass transfer coefficient and the FFV of membranes.

2.4 Membrane materials for pervaporation

To date, pervaporation has been used in different applications (as noted in Chapter 1). Among them, the dehydration of such organic solvents as alcohols, acids, ethers, and ketones is the most well-developed application [35–37]. Recently, desalination by pervaporation has drawn considerable attention from researchers. The available pervaporation membranes in the market are manufactured from a variety of materials such as polymeric, zeolite, and hybrid materials (composite) with different morphologies. Fig. 2.3 shows several types of membranes that are suitable to be used in pervaporation [5]. Polymeric membranes such as poly(acrylic acid), poly(vinyl alcohol), chitosan, and polyacrylonitrile are practical and feasible alternatives according to their ease of preparation and low fabrication costs; however, they may be subjected to a trade-off between permeability and selectivity [5,7]. Inorganic membranes have high thermal stability and good performance; however, they are expensive and brittle. Therefore, composite membranes are widely used, as they have features of both organic and inorganic materials.

For both dehydration and desalination, dense hydrophilic membranes are the primary choice. Water molecules diffuse through a membrane and then evaporate into the vapor phase on the other side of the membrane to generate clean water. Therefore, membrane-material selection for two

applications – the pervaporative desalination of high-salinity water and the dehydration of organics – are discussed in detail in the following.

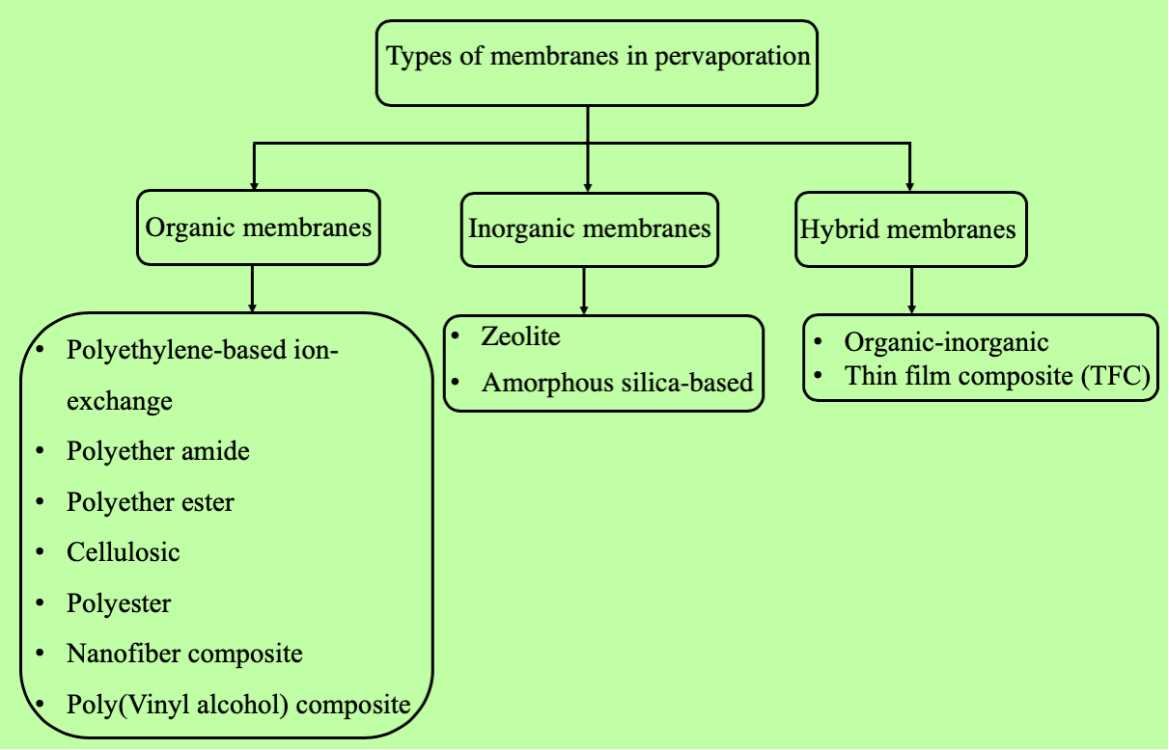

Figure 2. 3 Types of membranes used in pervaporation [4].

Membranes for pervaporative desalination

Table 2.1 summarizes some of the materials and performance of pervaporative membranes typically used for desalination. As mentioned earlier, hybrid organic-inorganic membranes, combining two different materials, have new properties such as improved permeation performance, modified membrane structure, and better stability. The chemical interactions between the organic and inorganic components are strong ionic/covalent bonding and weak

hydrogen bonding. The former is considered to help prevent the agglomeration of inorganic particles and the formation of non-selective voids at the organic-inorganic interface [38,39].

Table 2. 1 Summary of membranes and their performances in pervaporative desalination.

Membrane	NaCl (g/L)	T (°C)	Operation conditions on permeate side	Membrane thickness (μm)	J (kg/m^2.h)	R (%)	Ref.
Silicate-1 (S-1)	3	75°C	vacuum	6	11.5	99	[40]
ZSM-5	3	75°C	vacuum	3.3	12.5	99	[40]
Cellulose triacetate	100	50°C	Air sweep ($4.68*10^{-3}$ m/s)	10	2.3	99	[33]
Sulfonated polyethylene, cation exchanger	0-176	25-65°C	Air sweep (6 m/s)	100	0.8-3.3	_	[41]
Polyethylene, anion exchanger	35	45-65°C	Air sweep (>1.5 m/s)	50-180	1.5-3.0	_	[42]
Poly(vinyl alcohol)/maleic acid/silica	2	65°C	Vacuum	10	11.7	99.9	[34]
NaA zeolite	Sea water	69°C	Vacuum	_	1.9	99.9	[43]
NaA zeolite	29	77°C	Vacuum	_	4.4	99.9	[43]
Poly(vinyl alcohol)	30	70°C	Vacuum	0.1	7.4	99.9	[44]
ZSM-5	38	90°C	Vacuum	_	0.85	99	[45]
Polyetheramide	32	Solar energy (70°C)	Cooler tunnel	40	0.56	99.99	[46]
Carbonised template silica	3	20°C	Vacuum	_	3	97	[47]
Poly(vinyl alcohol)/polyacrylonitrile	5	20°C	Vacuum	0.62	9.04	99.5	[48]
Clinoptilolite-phosphate	1.4	95°C	Vacuum	_	15	95	[49]

Membrane	NaCl (g/L)	T (°C)	Operation conditions on permeate side	Membrane thickness (μm)	J (kg/m^2.h)	R (%)	Ref.
Graphene oxide/polyacrylonitrile	35	90°C	Vacuum	0.1	65.1	99.8	[50]

Membranes for pervaporative dehydration

Hydrophilic polymeric membranes are durable in water and can act as molecular sieves. These membranes may interact with water molecules by hydrogen bonding, ion-dipole interactions (in case of polyelectrolytes), and/or dipole-dipole interactions [51]. The water permselectivity of a membrane can be improved by enhancing the diffusion ratio of water to organics or by enhancing the sorption ratio of water to organics. Polymeric membranes such as poly(vinyl alcohol) (PVA), chitosan (CS), alginate, polysulfone (PSF), polyimide, polyamide, polyelectrolyte, and polyaniline have been used mainly for the dehydration of organic solvents. However, these hydrophilic membranes may swell excessively in water and exhibit poor stability.

When polymer chains are stretched, membranes swell. Therefore, the membrane flux increases while its selectivity decreases. The degree of swelling can be decreased by reducing the hydrophilicity of a membrane, leading to enhanced selectivity and decreased water flux. Through modification such as chemical crosslinking and/or blending, the membrane resistance to swelling may improve [52]. Chemical crosslinking introduces irreversible covalent bonds among polymer chains [4]. The degree of crosslinking influences a membrane performance. Network structures become more compact when the degree of crosslinking is greater between polymer chains. The result is a stiff membrane with relatively greater stability. Today, many attempts have been performed to increase the separation performance of membranes. For instance, one can modify the surface of a membrane by increasing the degree of crosslinking or by changing the hydrophilicity

[51]. Table 2.2 summarizes some of the materials and performance of membranes typically used for pervaporative dehydration of ethanol (EtOH) and isopropanol (IPA).

Table 2. 2 Summary of membranes and their performances in pervaporative dehydration.

Binary mixture (mass ratio)	Support	Active layer	Crosslinker/ modification	α	J (kg/m^2h)	T (°C)	Ref.
EtOH/water (50:50)	PVA	PVA	Amic acid	100	0.25	45	[37]
EtOH/water (90:10)	PVA	PVA	Dimethylolurea	115	0.12	60	[53]
EtOH/water (95:5)	PVA/PAAM	PVA/PAAM	-	45-4100	0.1- 0.06	75	[54]
IPA/water (90:10)	PVA	PVA	UFS solution	77	0.095	30	[55]
EtOH/water (90:10)	CS	CS	Glutaraldehyde	127	0.201	50	[56]
IPA/water (90:10)	CS	CS	Glutaraldehyde	196	0.197	60	[56]
IPA/water (95:5)	PSF	CS	Binded with PVA	400	0.4 - 0.8	50	[57]
EtOH/water (90:10)	Alginate	Alginate	Ionically crosslinked, Ca^{2+}	300	0.230	50	[58]
IPA/water (90:10)	Na-Alg	Na-Alg	Glutaraldehyde followed by HCl	356	0.012	30	[59]
IPA/water (90:10)	PSF	PVA/Na-Alg (80:20)	Maleic anhydride	1727	0.414	45	[60]
EtOH/water (90:10)	PSF hollow fiber	PSF	-	23.9	0.173	25	[61]
IPA/water (85/15)	P84	P84	-	5	2.578	60	[52]
EtOH/water (90:10)	BAPP	BAPP	-	22	0.27	25	[62]
EtOH/water (95:5)	PAN hydrolyzed with NaOH	PEI/PAA	Dynamic LbL	604	0.314	70	[63]
EtOH/water (95:5)	PES	PEI/PAA	Dynamic LbL	1207	0.140	40	[64]
EtOH/water (90:10)	Nylon-4	Nylon-4	-	4.5	0.35	25	[65]

PAAM: polyacrylamide; UFS: urea formaldehyde and sulphuric acid mixture; Na-Alg: sodium alginate; P84: polyimide; BAPP: polyimide membrane based on 3,3-bis[4-(4-aminophenoxy) phenyl] phthalide; PAN: polyacrylonitrile; PAA: polyacrylic acid; PES: polyethersulfone;

2.5 Methods for fabrication of pervaporation membranes

Pervaporation membranes can be either symmetric and dense, or asymmetric with a thin dense selective skin layer. Asymmetric membranes can be made from either one material or different ones (composite membranes). For the former type, a homogeneous polymer solution is precipitated in a non-solvent bath (usually water), forming a bottom porous layer and a dense top layer. The latter type allows more freedom during fabricating. They can be fabricated by solution casting, direct coating, interfacial polymerization, and layer-by-layer assembly [4,66].

Interfacial polymerization (IP) is a favored method for the fabrication of thin film composite (TFC) membranes. These membranes are widely used for RO and NF [14,24]. This method has been much less used for pervaporation, except for dehydration [4]. The IP mechanism involves a fast reaction between an amine-based monomer (typically between 0.1- 1%w/v) and an acyl chloride-based monomer (usually between 0.05-0.2% w/v) at the interface of the two immiscible monomers to form a polyamide layer. This condensation polymerization reaction can form a selective layer on a porous substrate (such as polysulfone and polyethersulfone). The polyamide TFC membranes are negatively charged due to the presence of carboxyl groups on their structures. Fig. 2.4 shows the IP reaction and the chemical structure of a typical polyamide membrane. Table 2.3 summarizes the performance of TFC membranes in the dehydration of organics.

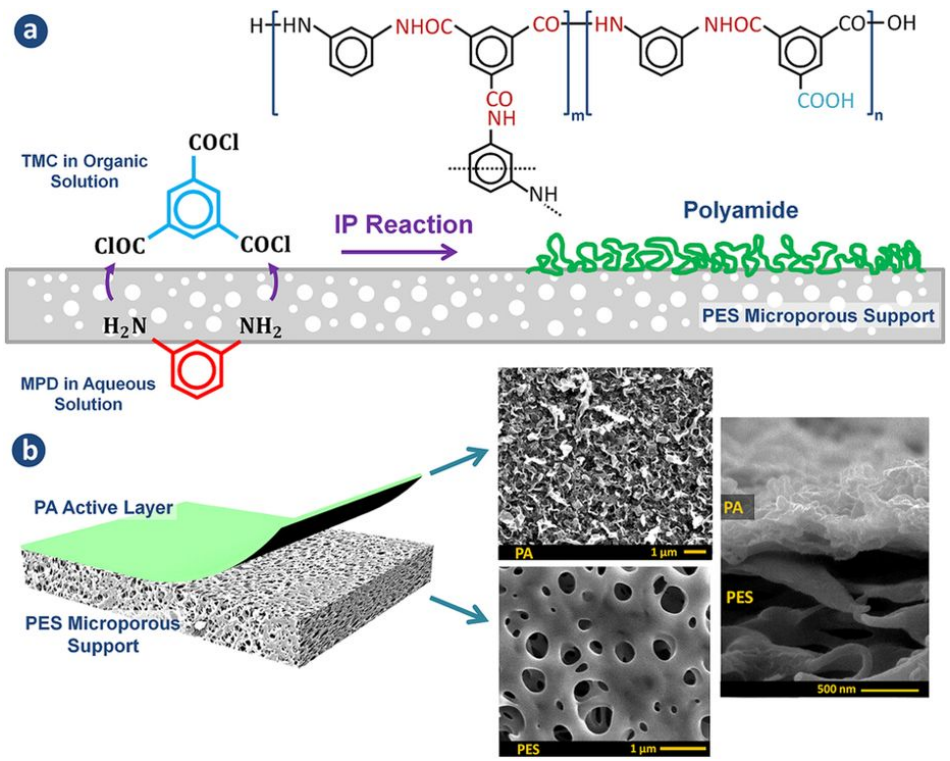

Figure 2. 4 Schematic representation of the IP reaction and the chemical structure of a typical polyamide membrane. The m and n in the polymer structure show the crosslinked and linear parts, respectively [67].

Table 2. 3 TFC membranes for the dehydration of organic solvents.

Binary mixture (mass ratio)	Support	Active layer	T (°C)	J (g/m^2h)	α	Ref.
IPA/water (90:10)	Modified PAN	MPD-TMC	25	181	22	[68]
EtOH/water (90:10)	Modified PAN	TETA-NTAC	25	537	491	[69]
EtOH/water (90:10)	Modified PAN	TETA-TBAC	25	452	301	[69]
EtOH/water (85:15)	Polyvinylidene fluoride [a]	MPD-TMC	50	1288	40	[70]
EtOH/water (85:15)	PES [a]	MPD-TMC-silicone coating	50	7501	60	[71]
IPA/water (90:10)	Modified PAN	EDA-TMC	25	213	105	[72]
IPA/water (90:10)	Modified PAN	TETA-TMC	25	370	171	[73]

MPD: m-phenylenediamine; TMC: trimesoyl chloride; TETA: triethylenetetramine; NTAC: 5-nitrobenzene-1,3-dioyl dichloride; TBAC: 5-tertbutylbenzene-1,3-dioyl dichloride; EDA:ethylenediamine; [a] Hollow-fiber membrane

Layer-by-layer assembly

Layer-by-layer (LbL) self-assembly is a technique developed to build up multilayer films with controlled thickness in nano-scale. LbL self-assembled membranes are formed under electrostatic (ionic) interactions between oppositely charged polyelectrolytes. The LbL membranes have been applied in the pervaporative dehydration of organic solvents since they are hydrophilic. However, water-induced swelling is an unavoidable concern during the pervaporation process. Chemically crosslinking the LbL membranes helps improve their performance and long-term stability [4]. Liu et al. found that crosslinking the LbL membrane formed from carboxymethyl cellulose/poly(diallyl dimethylammonium chloride) (CMCNa)/(PDDA) with glutaraldehyde (GA) resulted in better membrane resistance to swelling and good selectivity for IPA/water mixtures [74]. Zhang et al. reported that after crosslinking the outmost PEI layer on the PEI/PAA LbL membranes, the composite membranes showed a stable and relatively high performance for the dehydration of EtOH [75].

Polyelectrolytes

Polyelectrolytes are macromolecules with rich functionalities that can be dissociated into highly charged macromolecules in polar solvents such as water. Weak polyelectrolytes are partially dissociated in solvents, and strong polyelectrolytes may undergo complete dissociation in solvents. The polyelectrolytes can be classified into polycations and polyanions based on their charges. There are many polyelectrolytes with different charges, structures, and properties. Fig. 2.5 shows the chemical structures of the monomers of common polyelectrolytes used for preparing LbL membranes.

Polyanions

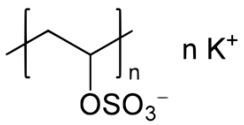

Poly(vinylsulfate)

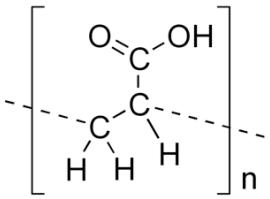

Polyacrylic acid

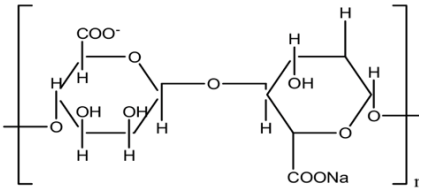

Sodium alginate

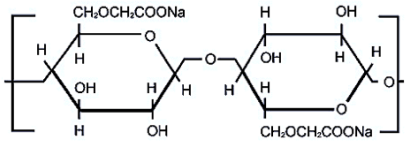

Sodium carboxymethyl cellulose

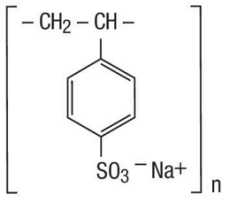

Poly(styrenesulfonate)

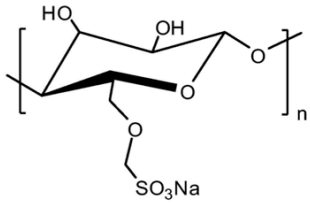

Sodium cellulose sulfonate

Polycations

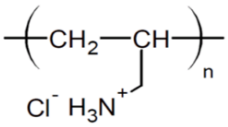

poly(allylamine hydrochloride)

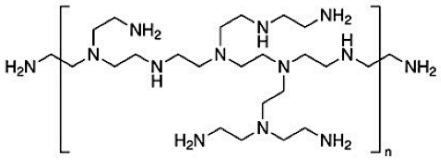

polyethyleneimine

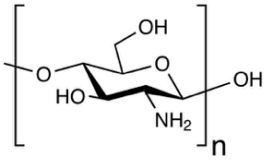

Chitosan

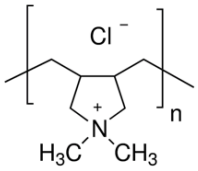

poly(diallyldimethylammonium chloride)

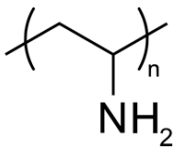

Polyvinylamine

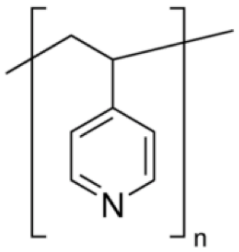

poly(4-vinylpyridine)

Figure 2. 5 Chemical structures of common polyanions and polycations.

Practically, polyelectrolyte complexes can be fabricated by (a) mixing or (b) interfacial complexation methods (Fig 2.6). Multilayered polyelectrolyte complex membranes are hydrophilic with ionic crosslinked structures.

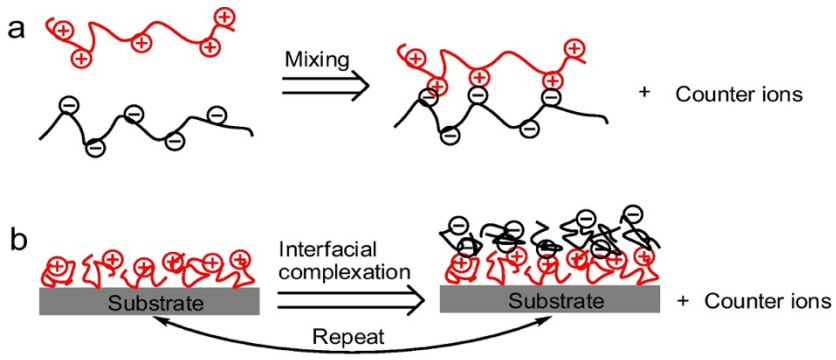

Figure 2. 6 Schematic diagram of polyelectrolyte complex formation via (a) mixing, and (b) interfacial complexation methods [11].

The mechanism of LbL assembly

The electrostatic attraction between a charged surface and a polyelectrolyte is the principal driving force for LbL self-assembly. As shown in Fig. 2.7, LbL self-assembled membranes are prepared in four steps. For illustration, a positively charged surface is considered. Polyelectrolyte solutions with low concentrations (usually below 0.2wt%) are used in LbL [75]. First, the polyanion is adsorbed onto the positively charged surface of a substrate due to electrostatic attraction; therefore, the surface becomes negatively charged. The adsorption of a polyelectrolyte layer by a charged surface is irreversible. The substrate surface is then thoroughly rinsed with DI water to remove excess polyanion molecules that have not been strongly adsorbed on the surface. Finally, a polycation is adsorbed by the negatively charged membrane surface, and the surface becomes positively charged again. The above steps can be repeated to form additional

polyelectrolyte layers. In each step of the assembly, a polyelectrolyte layer is adsorbed on the charged substrate and reverses the surface charge for the next layer. The number of layers can be controlled, and multilayers may have a thickness in the nanometer range [76].

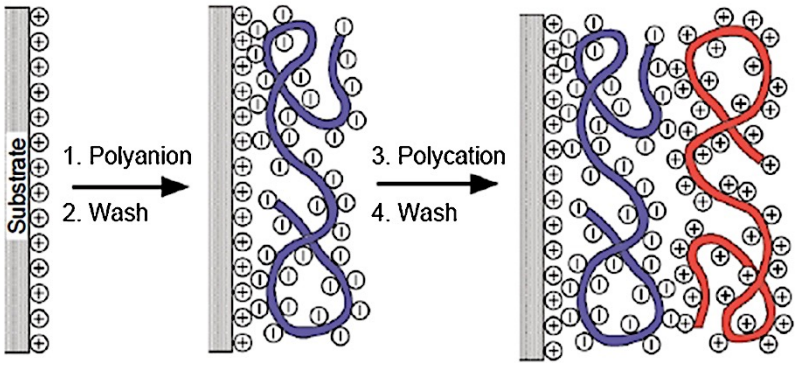

Figure 2. 7 Schematic of LbL adsorption of polyelectrolytes on the positively charged surface [77].

Charge overcompensation is a key feature in the formation of polyelectrolyte multilayers. When a negatively-charged substrate is in contact with polycations, the substrate surface will become positive due to excess positive charges in the cationic polyelectrolyte. This phenomenon is called charge overcompensation. Due to charge overcompensation, subsequent layers with opposite charges can be formed. Otherwise, the fabrication process would stop. Rinsing the membrane with water removes the weakly bound charged polyelectrolyte molecules and prevent their bulk reaction with oppositely charged polyelectrolyte molecules during the adsorption process [78,79]. The monolayer adsorption in the LbL self-assembly process is similar to the normal adsorption process. At a low ionic strength of polyelectrolyte chains, slight charge overcompensation can be provided by loops and tails in the polyelectrolyte. In contrast, strong charge overcompensation occurs at a high ionic strength [80]. The structure of the multilayer depends on the type, charge density, and molecular weights of the polyelectrolytes, and the process

conditions such as the ionic strength and pH of the solutions. In addition, the type of substrate also influences the structure of the deposited layer; however, its effect is generally limited only to the first three to six layers [81].

This LbL assembly is time-consuming since one layer may take almost half an hour to complete. Therefore, a procedure that decreases the preparation time of the polyelectrolyte multilayer is needed. Efforts have been made to accelerate the multilayer coating process. Applying a relatively dilute concentration of polyelectrolytes in the first few cycles of depositions, followed by depositions with more-concentrated polyelectrolyte solutions, has been proposed by Zhu et al. [12]. In addition to dip coating, a single-sided coating process has also been proposed to improve membrane permeability. It was demonstrated that good permselectivity could be achieved with less than ten cycles of deposition when this technique is used. The membrane performance performed well in separating water from isopropanol; a permeate concentration of over 99 wt.% water was achieved with a permeation flux of about 0.6 kg/(m^2 h) at a feed concentration of 90% IPA.

The growth of polyelectrolyte multilayers begins from the adsorption of the first layer on the charged substrate. The thickness of layers may change with each deposition step during the multilayer build-up. Linear growth of multilayer thickness is usually expected with an increase in a number of layers [82–86]. It has also been reported that the polyelectrolyte layer grows exponentially in thickness for the first few layers, followed by a linear growth [87]. Deposition conditions influence the growth of polyelectrolyte multilayers in the LbL self-assembly, including polyelectrolyte molecular weight [88], the pH of solution [89], charge density [79], polyelectrolyte concentration [90] and temperature. Moreover, the electric field also has an impact on self-

assembly [91–93]. The overall thickness of a polyelectrolyte film can be controlled by the number of depositions.

2.6 Stability of LbL membranes

The development of membranes with good performance and stability is a key research area in membrane science. Membrane stability is the ability of a membrane to keep both permeability and selectivity under desired operating conditions for a relatively long period of time. The chemical, mechanical, and thermal stability of a membrane can be assessed. As mentioned, swelling is a common phenomenon occurring in hydrophilic membranes during pervaporation [10]. Similar to water, ethylene glycol, ethanol and isopropanol are also hydrophilic, and thus these organic compounds may swell polyelectrolyte multilayers as well. Note that the hydrophilicity of a membrane is not the only reason that causes membrane swelling in solvents. Swelling increases the membrane permeability and decreases its selectivity, and if the membrane swelling is severe, the membrane may become non-selective.

When polyelectrolyte membranes are in contact with aqueous solutions, membrane swelling will occur because the polymer-polymer intermolecular forces are overcome by strong polymer-solvent interactions that lead to membrane instability. However, if the polymer-polymer intermolecular forces are high enough due to crosslinking, crystallinity, or strong hydrogen bonding, then membrane swelling will not be significant. There are studies on the stability of LbL membranes in different solvents. Carrière et al. [94] found that the swelling of poly(styrene sulfonate)/ poly(allylamine hydrochloride) films was related to the top layer. The films swell 25% less if the top layer deposited is poly(allylamine hydrochloride). Miller and Bruening [95] showed that the thickness of a membrane with 10 double layers of poly(styrene sulfonate)/ poly(allylamine hydrochloride) increased by 40% when immersed in a pH 6.3 buffer water solution, and the

membrane thickness further increased when the membrane was soaked in a pH 10 buffer water solution, due to membrane swelling. Degrees of membrane swelling as high as 800% have been reported in the literature [96]. Crosslinking can be applied to improve the membrane stability. The polymer chains are restricted when crosslinked, and the crosslinking often increases the selectivity and decreases the permeation flux. The membrane becomes more compact with an increase in the crosslinking density, and the polymer chains become more rigid. Therefore, the membrane is more discretional to the permeation of penetrant molecules, which favors the selectivity of the membrane, though the membrane permeability may be compromised [75]. Depending on the polymers, various types of crosslinking agents can be applied, such as trimesoyle chloride, sulfuric acid, glutaraldehyde, sulfosuccinic acid [97–100].

2.7 LbL deposition on polyamide substrate membrane

Many efforts have been made to prepare LbL membranes with a small number of deposition bilayers and reasonable performance by use of a nonporous substrate. However, the membrane permeability is decreased due to the high mass transport resistance in a nonporous substrate. Since pervaporation process is based on a solution-diffusion mechanism, using a composite membrane with an ultrathin active layer supported on a microporous substrate is preferred, to reduce the number of polyelectrolyte bilayers and reach a high permeation flux [13]. Zhou et al. [15] showed that the deposition of only a single layer of polyethyleneimine on the membrane surface enhanced salt rejection without significantly lowering the membrane permeability when an interfacially polymerized polyamide membrane was used as a substrate. In particular, the fouling resistance of the membrane to cationic foulants was increased due to charge reversal on the membrane surface. Xu et al. [13] used a TFC membrane based on the LbL self-assembly of polyethyleneimine and poly(acrylic acid) on an interfacially polymerized polyamide membrane for the dehydration of

ethylene glycol by pervaporation. The resulting membranes showed a good permselectivity and separation factor.

Chlorination of polyamide membranes

The surface properties of most polymer-based membranes generally change when they are exposed to hypochloric acid or sodium hypochlorite [101]. One of the main disadvantages of polyamide membranes is their sensitivity to chlorine solutions even at low concentrations. Impaired performance may result due to loss of structural integrity of constituent polymers. The chlorine substituents on the amide nitrogen or aromatic rings may cause physical deformation or cleavage at the amide linkage in the linear polymer chain [102]. The chlorine sensitivity of polyamide membranes varies, depending on the type of the polymer structure and the pH of feed water. A chlorine attack on amide nitrogen and aromatic rings leads to an increased passage of both water and salt. When exposed to chlorine, the polyamide membrane is generally more hydrophilic and has more negative zeta potential.

The N-chlorination of amide nitrogen includes the replacement of hydrogen by chlorine on amide nitrogen and leads to N-chloroamide (step A in Fig. 2.8). The N-bonded chlorine atom can be removed to provide molecular chlorine when exposed to further intramolecular Orton rearrangement, which will then attack the aromatic ring through electrophilic substitution, resulting in indirect ring chlorination (step B in Fig. 2.8). On the other hand, direct ring chlorination appears when active (electrophilic) chlorine attacks the aromatic ring bonded to the N-H groups of the amide linkages. In addition, the end amine groups are vulnerable to oxidation as well, due to their high reactivity [14,77,78].

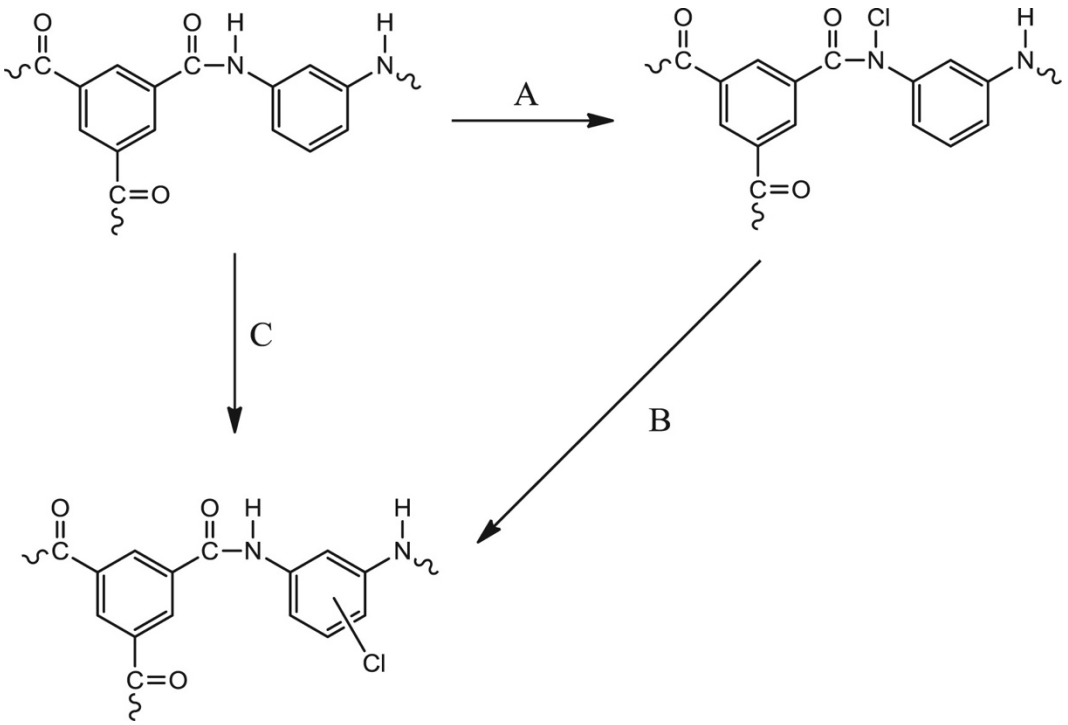

Figure 2. 8 Chlorination mechanisms of the fully aromatic polyamide membranes: (A) N-chlorination; (A) and (B) ring chlorination by Orton rearrangement; (C) direct ring chlorination [13,103,104].

Excessive chlorination can damage membranes severely. Xu et al. [13] fabricated a polyamide/chitosan (PA/CS) TFC membrane for desalination by RO; They then applied chlorine treatment using a dilute sodium hypochlorite solution to modify the surface of the commercial polyamide membrane followed by chitosan deposition. Chlorination makes the membrane surface more hydrophilic, with higher negative zeta potentials. Hegab et al. [18] modified the surface of commercial TFC RO membranes using graphene oxide (GO) functionalized chitosan (GO/f-CS) to improve their antifouling properties. The membranes were treated with 200 ppm of sodium hypochlorite to increase the free negatively charged carboxylic groups on the membrane surface before being coated with a GO/f-CS solution. Their results showed the GO/f-CS/polyamide

membranes have superior performance compared to the unmodified polyamide membrane in terms of hydrophilicity, water flux, NaCl rejection, and antifouling properties.

2.8 Graphene oxide

Graphene oxide (GO) nanosheets, prepared by chemical oxidation and ultrasonic exfoliation of graphite flakes, have great potential as building blocks for the fabrication of inexpensive yet high-performance water purification membranes [105]. Fig. 2.9 shows the chemical structure of GO, assumed to be one-atom thick and arranged in a honeycomb lattice bearing abundant oxygenated functional groups (i.e., carboxyl, hydroxyl, epoxy groups) [106]. The mechanical and electrical properties make GO an ideal material for making high performance membranes for water separation [17,18,107–109].

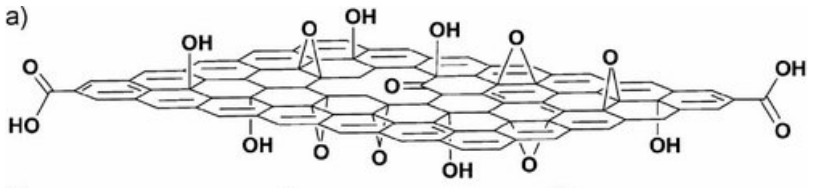

Figure 2. 9 Schematic structure of GO.

GO has long been known hydrophilic because it can simply disperse in water; however, some research based on molecular dynamics simulations showed that GO nanosheets may be amphiphilic [110–113]. It is described that the ionizable edges of GO are hydrophilic and its basal plane contains unoxidized graphitic regions. The amphiphilicity of GO depends on pH, nanosheet size and degree of reduction. Therefore, smaller nanosheets are usually more hydrophilic due to a

higher ratio of edge to basal plane. The size of hydrophobic basal plane can be adjusted by reduction of GO (rGO) at different degrees or removal of oxygen-containing functional groups. The hydrophilicity of GO nanosheets increases with higher pH, smaller size and a lower degree of reduction [110] GO nanosheets have been frequently applied for preparing hydrophilic membranes, whereas rGO has been used in hydrophobic (or less hydrophilic) membranes. Kim et al. [114] reported that one way to study the nature of GO is to observe how it reacts with oil/water and air/water interfaces. To prepare less/more hydrophilic GO, oxygenated functional groups on the edges (or maybe plane) can be manipulated [115]. More research is needed to have a better understanding of the properties of GO.

Assembling GO nanosheets on TFC membrane surfaces

There are two possible approaches to assembling GO nanosheets on the polyamide TFC membrane surface: 1) covalent-bonding using amide coupling to connect the carboxylic groups of GO nanosheets with the carboxylic groups of the polyamide TFC membrane, and 2) LbL self-assembly. Since GO nanosheets are extremely hydrophilic, LbL membranes prepared with GO are highly susceptible to dispersion in an aqueous environment. Unbonded GO layers can be easily spoiled with a gentle touch or detached from the membrane support by water rinsing; therefore, such a membrane is unable to survive cross-flow testing conditions [108]. To resolve this problem, GO layers must be bonded firmly to each other, and the outermost layer must be strongly connected to the support substrate. One approach is to form covalent bonding between GO layers by using proper cross-linkers such as trimesoyl chloride (TMC). Another promising approach is to bond stacked GO nanosheets through electrostatic interaction, which facilitates reactions and uses a lower amount of organic solvent, and reduces the quantity of by-products [17]. GO nanosheets are

negatively charged due to ionization of carboxylate groups in water, and the hydrophilicity and electrostatic repulsion cause the dispersion of GO at the individual sheet level in water [18,107,109]. These features make GO suitable for use in LbL self-assembly membranes for the dehydration of organic solvents via pervaporation due to the high selectivity of water [116]. The nanosheets can be considered as polyanions and electrostatically bound to positively charged polyelectrolytes.

Hu and Mi [17] reported that a GO membrane could be successfully prepared by the LbL assembly of negatively charged GO nanosheets and positively charged poly(allylamine hydrochloride) (PAH) on both sides of a charged porous poly(acrylonitrile)(PAN) support via electrostatic interaction; Fig. 2.10 is a schematic of the LbL assembly of GO membranes. The authors showed that each GO–PAH bilayer in the membrane is around 16.5 nm thick and dominated by GO (the mass of GO is 2–5 times higher than that of PAH), indicating multiple layers of GO nanosheets exist in each bilayer. They were able to design a high-performance forward osmosis (FO)/ pressure retarded osmosis (PRO) membrane with a water permeability one order of magnitude higher than a commercial FO membrane.

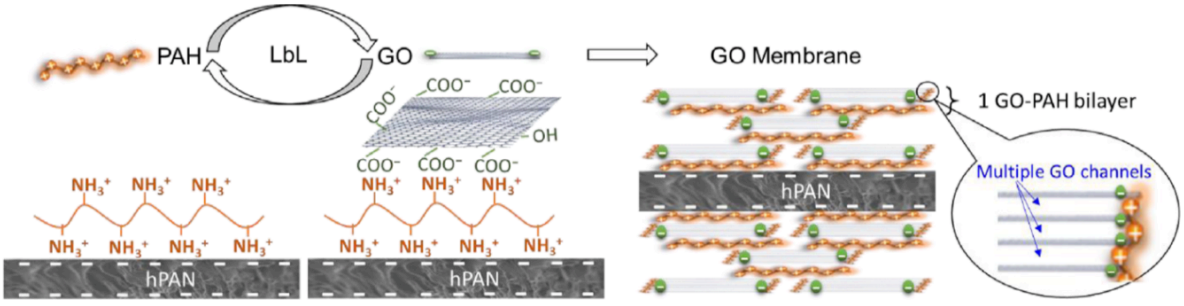

Figure 2. 10 Schematic diagram of LbL assembly of a GO membrane by alternately soaking an hPAN support substrate in 1 g/L PAH (pH 4) solution and in 1 g/L GO solution (pH 4) to deposit a prescribed number of GO–PAH bilayers on both sides of hPAN [17].

Zhao et al. [117] reported that the LbL self-assembly of GO and PEI on the surface of polyethylene terephthalate (PET) film showed excellent barrier performance to hydrogen gas. They investigated the effects of the pH of PEI solutions on the performance of the PEI/GO LbL film. The GO nanosheets adsorbed on the substrate were found to have the most uniform and dense structure when the pH of PEI and GO solutions was 3.5, with a thickness of 3.45 nm per bilayer. Yang et al. [118] also studied the LbL deposition of branched PEI and GO on a PET surface to investigate the oxygen barrier of these thin film assemblies, as shown in Fig. 2.11. On average, 0.01 and 0.05 wt.% concentrations of GO have a thickness of 4.3 and 5.0 nm per PEI/GO bilayer, respectively. They also mentioned that charge overcompensation could be achieved by using a high GO suspension concentration.

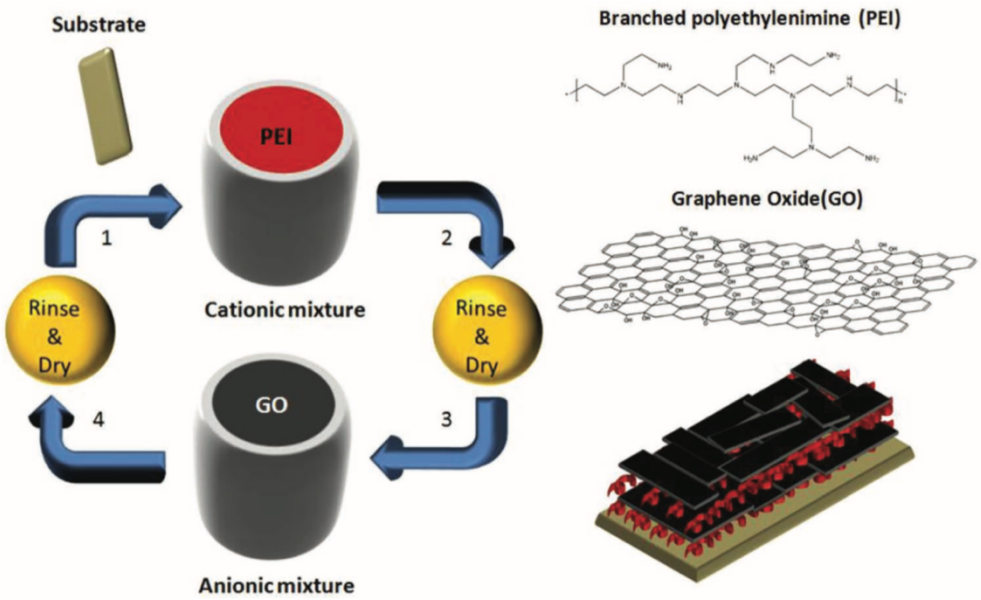

Figure 2. 11 Schematic diagram of preparing PEI-GO bilayers via the LbL self-assembly [118].

Chen et al. [107] investigated LbL film assemblies of positively charged branched PEI and negatively charged GO on a UV/ozone treated PET surface as the support to fabricate gas barrier films. Their results indicated that each bilayer contains the same amount of GO, so the multilayer film growth is regular and uniform. They showed that at a pH of 3.5, the electrostatic force between the branched PEI and the GO is strong due to the high amount of deposition. The LbL self-assembly exhibited the best barrier properties. Zhao et al. [109] fabricated ultrathin multilayer $(PVA/GO)_n$ films driven by hydrogen bonding interaction through the LbL assembly of poly(vinyl alcohol) (PVA) and exfoliated GO on quartz glass slides. The mechanical properties of the membranes were improved by assemblies of GO nanosheets in the polymer matrices, and a thickness of 3 nm per bilayer of PVA/GO was observed. Choi et al. [119] studied the coating of GO multilayers on the surface of TFC polyamide RO membrane via LbL deposition of oppositely charged GO nanosheets to improve membrane antifouling and chlorine resistance. Interestingly, the membrane performance after GO surface coating (regardless of the number of GO bilayers) remained unchanged within the measurement errors. Multilayered GO coating strongly affected the membrane antifouling performance. It was noted that a polyamide membrane with ten bilayers of GO/aminated-GO showed a lower degree of final flux reduction (~15%) after filtration for 12 h with an aqueous solution of bovine serum albumin (BSA) (100 mg/L) than that of a pristine PA membrane (~34%). Wang et al. [16] modified GO by PEI under sonication conditions. The positively charged PEI-modified GO and negatively charged polyacrylic acid was sequentially assembled on the hydrolyzed PAN substrate through electrostatic interaction. The LbL membrane was immersed in a polyvinyl alcohol solution and cross-linked with glutaraldehyde to obtain a defect-free layer for the pervaporation dehydration of different solvent-water mixtures. Hu and Mi [16] deposited GO nanosheets via LbL assembly on polydopamine-coated polysulfone support and

then cross-linked them by TMC. They reported that the flux of the GO membrane was about 4–10 times higher than that of most commercial NF membranes.

Chapter 3

Layer-by-layer assembly of polyethyleneimine/graphene oxide membranes for desalination of high-salinity water via pervaporation

3.1 Introduction

In recent years, worldwide demand for safe and fresh water has significantly increased due to population growth, industrial application, urban development, climate change, and contamination of available fresh water resources [1,67]. As a result, new sources of water are required. Desalination and water reuse have been applied to improve the fresh water supply beyond what is accessible from the hydrologic cycle [120,121]. Reverse osmosis (RO), a currently commercialized membrane-based technology, has been commonly exploited in the desalination of seawater. However, RO has been facing challenges stemming from its high fouling propensity (scaling), low water flux per unit of pressure applied, and low water recovery from sea-water desalination (35-55%). As a result, RO produces large volumes of concentrated brine as a by-product. Moreover, a high hydraulic pressure must be applied for water permeation through the RO membrane [120,122,123]. Membrane distillation (MD) is an alternative separation process which can be applied for desalination of high-salinity water [5,124] and has the potential for complete salt rejection. However, there are two major challenges of MD: membrane wetting and

membrane fouling due to the poor long term hydrophobicity of the membranes [125,126]. The deposition of such foulant as salt crystals on the membrane surface decreases the hydrophobicity of a membrane and results in increased membrane wetting [127–130]. Moreover, the current cost of fresh water production via MD is considered to be higher than that of RO [131].

To achieve high water recovery, pervaporation has been studied as an alternative in treating high-salinity water [34,50]. Pervaporation is effective for treating azeotropic mixtures, dehydration of organic solvents, and removal of organic compounds from contaminated water [4]. However, not much work has been done on the application of pervaporation for desalination of high salinity water. In pervaporation, the liquid feed mixture is in contact with the upstream side of the membrane, while the permeate side is kept at a low pressure by applying a vacuum or a flow of air to generate the driving force for mass transfer from the feed side of the membrane to the permeate side. The solution-diffusion model, the major transport mechanism of pervaporation, involves three consecutive steps: sorption of the penetrant from the feed liquid into the membrane, diffusion of the penetrant across the membrane, and desorption of the penetrant from the membrane to the vapor phase at the permeate side [4,132]. Desalination by pervaporation has advantages over RO and MD: Pervaporation is not operated under high pressure, no heavy piping and pumping are required. It is more fouling resistant than RO, with almost 100% rejection of ions and other non-volatile compounds [123,125,131]. In addition, pervaporation can be operated using various renewable energy sources - waste, solar, or geothermal [5,46]. In addition to solvent dehydration, pervaporation is deemed to have the potential for desalination of high salinity water such as industrial wastewater and concentrated RO brine [40,46,48].

To deploy appropriate membranes for desalination by pervaporation, the chemical properties and material selection of the membrane must be considered. Polymeric membranes with well-

defined nanostructures show high selectivity and permeability, as well as such other properties as antifouling and resistances to photodegradation and bacterial. Consequently, using nanomaterials has been regarded as one of the best potential approaches to developing high-performance membranes and relieving stresses on water supply [133]. Carbon-based two-dimensional nanomaterials have been of particular interest for the development of efficient membranes for water purification. Among the various nanomaterials, graphene oxide (GO) is mainly used in developing membranes for treating saltwater, including seawater, brackish water, and reverse osmosis concentrate [106,134]. GO is a nanosheet of carbon atoms tightly packed in a honeycomb lattice bearing a large number of oxygen-rich functional groups (i.e., carboxyl, hydroxyl, epoxide, and carbonyl groups).

Liang *et al.* investigated GO/PAN composite membranes for desalination of water via pervaporation and these membranes showed improved performance in treating high-salinity water [50]. The existence of GO in the membranes induced remarkable properties due to its intrinsic hydrophilicity, compatibility with the polymeric matrices, large negative zeta potential, and mechanical and thermal stabilities [135–139]. Water molecules can permeate the 2-D planar interconnected nanochannels formed between the stacked GO nanosheets, molecular-simulations predict a fast flow of water through GO membranes with near-zero friction results from the capillary-driven force formed by planar graphene nanosheets [140,141]. However, GO nanosheets are very hydrophilic, and unbonded GO layers can be peeled off and detached from the membrane support, especially in crossflow testing conditions [108]. Thus, to make GO-based membranes practical for water application requires sufficient bonding of the GO nanosheets to retain membrane integrity. One promising approach is to bond firmly stacked GO nanosheets via electrostatic interactions using layer-by-layer (LbL) self-assembly [17]. As the surfaces of GO

nanosheets are negatively charged once dispersed in water due to the carboxyl and hydroxyl groups [138], they can electrostatically bind to polycations such as polyethyleneimine (PEI) and poly(allylamine hydrochloride) (PAH) [17,142]. Recently, the LbL method has been applied for assembling oppositely charged polyelectrolytes to modify membranes used in nanofiltration (NF) [142], RO [143], forward osmosis (FO) [17] and solvent dehydration by pervaporation [144,145]. These membranes are environmentally friendly as all the assembly is achieved in aqueous solutions, whereas traditional membrane synthesis often involves the use of organic solvents [17]. Additionally, the thickness of a bilayer can be controlled by varying the assembly conditions [146]. The GO incorporated LbL membranes represent a new generation of ultrathin, high-flux, energy-efficient membranes for water-purification applications [147].

Interfacially polymerized thin-film composite (TFC) polyamide membrane has recently been used as a substrate in LbL self-assembly since it holds negative surface charges owing to the presence of carboxyl groups [143,145,148]. Membranes of this type have generally been studied for water desalination by NF and RO, and they have also shown great potential for pervaporation applications [145,149]. The main advantage of using TFC polyamide membranes as a substrate is that the number of polyelectrolyte layers needed to form permselective membranes can be reduced due to its ultrathin but relatively dense skin layer. However, the permeability of the resulting membrane is compromised due to its large mass transport resistance [143,145]. This issue can be addressed by modification of the membrane surface. Zhou et al. modified the surface of a polyamide TFC membrane by electrostatic deposition of only one layer of PEI, and improved antifouling properties, surface hydrophilicity, and salt rejection were achieved [148].

In the present study, we aimed to design and fabricate an LbL self-assembled membrane by using oppositely charged PEI and GO on top of a chlorine-treated polyamide TFC membrane for

pervaporative desalination of high-salinity water. The substrate was initially surface modified by chlorine treatment to improve the permeation flux of the resulting membrane. The amide bonds are sensitive to chlorine attack, and the extreme exposure to chlorine degrades the thin active polyamide layer of the TFC membrane due to cleavage of the amide-bonds and Orton transition [150]. Controlled chlorination with a dilute hypochlorite solution makes the membrane surface more hydrophilic and negatively charged without damaging the membrane structure, which favors subsequent electrostatic adsorption of polycations [151]. Xu et al. modified a polyamide TFC membrane surface by chlorine treatment, followed by deposition of supramolecular chitosan, and the resulting membrane showed a permeation flux of 57.7 L/(m^2 h) and a salt rejection of 95.4 % by RO for a feed NaCl concentration of 1500 mg/L at 0.8 MPa [143]. To our knowledge, only a few publications have explored the use of the LbL assemblies for pervaporation membranes, and the present study uses PEI and GO for self-assembly on top of chlorine-treated polyamide TFC membrane for pervaporative desalination of high-salinity water. For this purpose, NaCl, Na_2SO_4, $MgCl_2$, and $MgSO_4$ were used as model solutes. The effects of feed salt concentration and temperature on the pervaporation performance were evaluated.

3.2 Experimental

3.2.1 Materials

Graphite flakes were obtained from Alfa Aesar Chemical Manufacturing Company and used to synthesize GO. To oxidize graphite into GO, potassium permanganate ($KMnO_4$, >99%, Merck), phosphoric acid (H_3PO_4, 85% solution in water, Acros), hydrogen peroxide 30% (H_2O_2, 30%) and sulfuric acid (H_2SO_4, 95-98%), (both from Sigma-Aldrich) were used. Hydrochloric acid (HCl, 37%, Merck), ethanol (Sigma-Aldrich) and De-ionized (DI) water were used for rinsing the

synthesized GO. A commercially available thin-film composite polyamide membrane with non-woven fabric support produced by interfacial polymerization (supplied by GE water) was used as a substrate. Branched polyethylenimine, (PEI, average $M_w \sim$ 25,000, Sigma-Aldrich) was used as a polycation. Inorganic salts, including magnesium chloride ($MgCl_2$, J.T Baker Chemical Company), magnesium sulfate ($MgSO_4$, BDH Chemicals Ltd), sodium sulfate (Na_2SO_4, McArthur Chemical Co.) and sodium chloride (NaCl, EMD Chemical, Inc) were used in preparing feed solutions to simulate high-salinity water with which to determine the performance of pervaporation. A commercially available sodium hypochlorite solution (NaClO, 14.5% available chlorine, BDH Chemicals) was used for chlorine treatment of the TFC polyamide membrane. Deionized water (DI) water with a conductivity of less than 2 μs/cm (at 25 °C) was used throughout the study.

3.2.2 Chlorine treatment of polyamide membrane

It is well known that aromatic polyamide membranes are sensitive to chlorine attack. Thus, the polyamide TFC membrane was chlorine-treated in a controlled manner so that its dense skin layer became thinner and less compact without compromising the membrane integrity and its underlying porous layer [152]. Therefore, to avoid polyamide TFC membrane deterioration and improve its performance, chlorination was performed at moderate conditions. In this study, after rinsing with DI water, a TFC polyamide membrane was exposed to 6000 ppm chlorine solution for 2 h at room temperature. After chlorination treatment, the membrane was again thoroughly washed with DI water until the hypochlorite residue was completely removed from the membrane surface before subsequent deposition of polycation.

3.2.3 GO preparation and characterization

GO nanosheets were synthesized from graphite powder following an improved method. That provides a higher amount of hydrophilic oxidized graphene materials with fewer defects in the basal plane as compared to GO prepared by the original Hummers' method [153,154]. In short, 3 g of graphite flakes and 18 g of $KMnO_4$ were gradually added to an acid mixture composed of 360 mL of H_2SO_4 and 40 mL of H_3PO_4 under stirring condition. The reaction was then conducted at 50°C for 16 h. After the mixture was cooled to room temperature and poured in 400 mL of ice-water, 3 mL of H_2O_2 was added, causing a color change from dark purple to golden. The mixture was first centrifuged at 3500 RPM to decant away large aggregates and supernatant. Then, the remaining solid materials were washed with 10% HCl (2×) and ethanol (4×) solutions, respectively. For each washing step, the materials were centrifuged to remove the supernatant [153]. The resulting uniform and brown GO solution was used as an anionic solution in the self-assembly for membrane formation.

The X-Ray Diffraction (XRD) pattern of the GO nanosheets and the membranes were attained with an X-ray diffractometer (Bruker D8 Focus), scanned over a 2θ range of 5°-70° for GO and 5°-35° for the membranes, with a step increment of 0.1° and a count time of 3 sec/step. To confirm the existence of oxygen-containing groups on the prepared GO nanosheets, Fourier Transform Infrared spectrum of GO was obtained using a Nicolet 6700 FTIR spectroscopy from Thermo Electron Corporation in the wavelength range of 500 to 4000 cm^{-1}. The chemical structures of the membranes were also investigated using an attenuated total reflectance (ATR) technique with a spectrometer (Bruker, Tensor 27) in the range of 4000–500 cm^{-1}. The surface hydrophilicity of membranes was measured by conducting static contact angle measurement with a contact angle goniometer (VCA 2500 XE, AST Products) at room temperature. The average contact angle value

of five arbitrary locations was reported for each membrane sample (for an average water droplet size of 2 μL). The surface morphology and roughness of the membranes were characterized using a tapping mode atomic force microscopy (AFM) (Bruker Innova, USA).

3.2.4 Fabrication of GO-PEI LbL membranes

Fig 3.1 illustrates the step-by-step procedure to deposit PEI and GO on the negatively charged chlorine-treated polyamide TFC membrane via the LbL approach. The concentration of the polyelectrolyte solution and deposition time of the polyelectrolyte are two important factors in preparing LbL membranes as they affect the amount of the polyelectrolyte adsorbed on the membrane surface [155,156]. Different deposition times and polyelectrolyte concentrations have been used in the literature to prepare LbL membranes. Sun et al. [157] showed that at a given polyelectrolyte concentration, increasing the polyelectrolyte deposition time increased salt rejection while decreased water permeation flux. However, beyond 1 h of polyelectrolyte deposition had little influence on the membrane performance as the adsorption of polyelectrolyte was allowed to reach equilibrium. Zhang et al. [158] also determined that the deposition time of 1 h was sufficient to form uniform polyelectrolyte layers on the polyamide substrate for preparing pervaporation membranes. They further showed that the polyelectrolyte macromolecules (i.e., PEI) at a medium concentration of 0.02 monomol/L have more chance to interact with the oppositely charged polyelectrolyte. Typically, the concentration of polyelectrolytes for LbL membranes is below 0.2 wt% to form ladder-like structures [11]. According to Wang et al.[159], GO formed voids and agglomeration at high concentrations of GO (more than 100 mg/L), while GO could not fully cover the PEI layer at low concentrations (lower than 100 mg/L). Therefore, in the present study, the GO solution was diluted to 100 mg/L for the fabrication of the GO layer, and the concentration of PEI solution was 0.02 monomol/L. As the conditions of polyelectrolyte

deposition (e.g., the concentrations, deposition time, temperature and pH) were not optimized, the separation performance obtained with the PEI/GO LbL membranes does not represent the best membrane performance that could be reached. The chlorine-treated substrate was initially soaked in DI water overnight to remove sodium hypochlorite residue, and then it was mounted in a stainless steel membrane cell. To build up one PEI/GO bilayer, the chlorine-treated substrate was brought into contact with: (a) a positively charged PEI solution (0.02 monomol/L, 1 h, 25°C), (b) DI water (30 min, 25°C), (c) a negatively charged GO solution (100 ppm, 1h, 25°C), and (d) DI water (30 min, 25°C), consecutively. For convenience of discussion, the term 'PEI/GO LbL' was used throughout this study to refer to the resultant membrane. All the depositions were accomplished in a single-sided surface deposition approach. The average total thickness of the dry membranes (the bilayer plus TFC polyamide substrate) used in this study was 127 μm, as measured at different points using a digital micrometer.

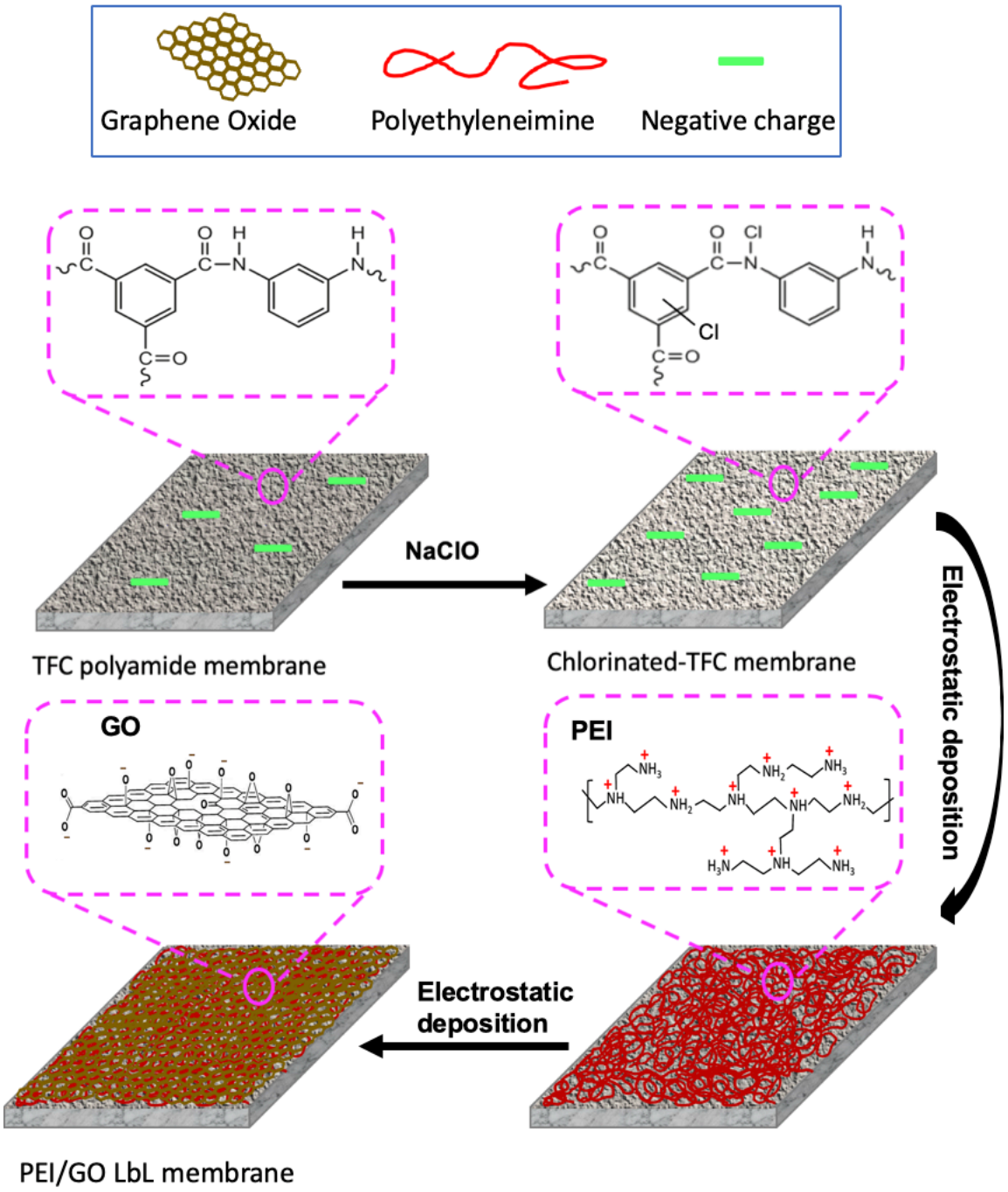

Figure 3. 1 Schematic diagram for the LbL assembly of PEI/GO membranes (one bilayer).

3.2.5 Evaluation of the pervaporation performance

The desalination experiments were conducted using a laboratory-scale pervaporation set-up, shown schematically in Fig 3.2. The as-prepared membrane with an effective surface area of 17.4 cm^2 was placed in the pervaporation apparatus. The pre-heated feed solution was pumped from the feed tank to the membrane surface, and the retentate was circulated back to the feed tank. The downstream pressure was maintained below 1.7 kPa absolute using a vacuum pump. The permeate was condensed and collected at specific time intervals in a cold glass trap immersed in liquid nitrogen. The pervaporation desalination performance of the GO/PEI LbL membrane was characterized by water flux (J) and salt rejection (R) under steady-state conditions, which were generally reached in about 1 h. The water flux was determined by evaluating the weight (Q) of permeate collected over a specific period of time (t) through a membrane with an effective area (A):

$$J = \frac{Q}{At} \tag{3.1}$$

The salt rejection was determined as follows:

$$R = \frac{(C_f - C_p)}{Cf} \times 100\% \tag{3.2}$$

where C_f and C_p are the salt concentrations in the feed and permeate, respectively [160].

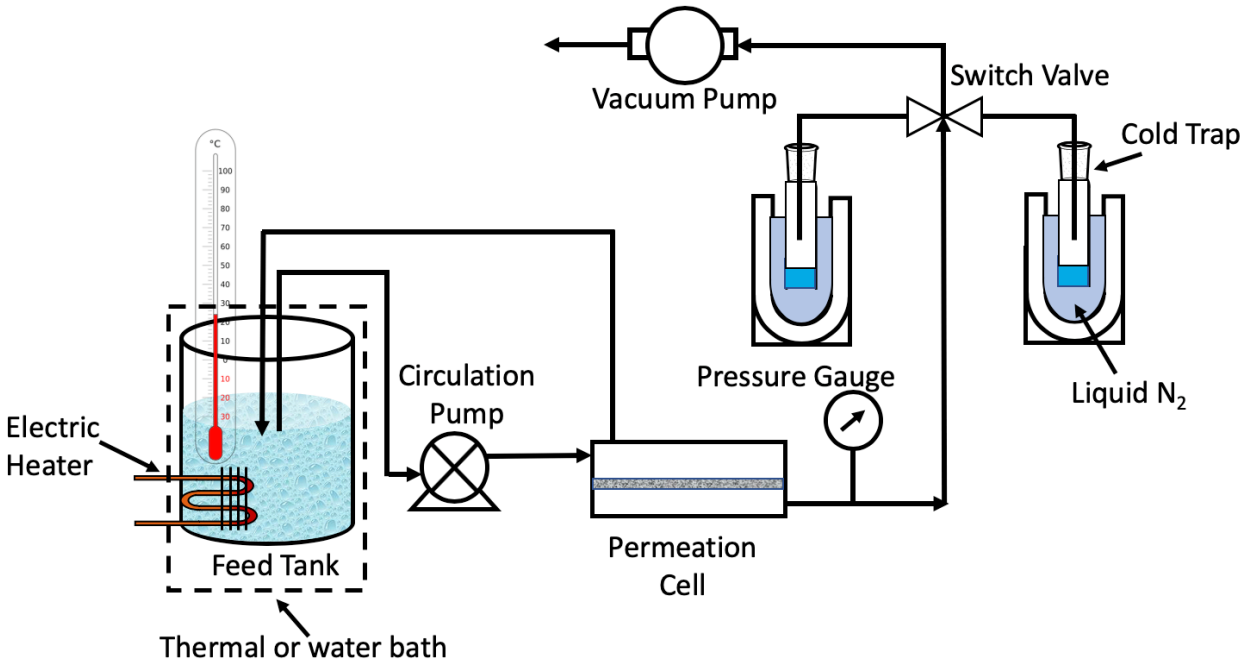

Figure 3. 2 Schematic diagram of the pervaporation set-up.

A feed temperature in the range of 22-65°C was maintained using a thermal bath. The salt concentrations were in a range of 2-20 wt%, to represent saline water. A conductivity meter (WTW inoLab Cond Level 2) was used to determine the salt concentrations of feed and permeate solutions. Water removed by the membrane was compensated for by adding the same amount of water into the feed to maintain a constant composition during each experimental test. Note that no salt precipitation or crystallization on the permeate side of the LbL membrane was detected throughout the entire experiment. After completion of a pervaporation run for each salt, the membrane was rinsed by flushing DI water on the feed side for 1 h to wash away any salt from its surface, followed by pervaporation with pure water for 1 h.

3.3 Results and discussion

3.3.1 Characteristics of GO

Fig 3.3 presents the results for the characterization of GO with XRD and FTIR. Fig 3.3(a) shows the spectrum of GO with a typical diffraction peak at 2θ=10.7° with the *d* spacing value of 0.8 nm. This result is in agreement with those reported elsewhere [153,161]. Fig 3.3(b) presents the FTIR spectrum of the GO nanosheets associated with different functional groups. The results confirm that the characteristics peaks of GO with the presence of –OH stretching in hydroxyl groups at 3253 cm^{-1}, C=O stretching vibration in carboxyl groups at 1738 cm^{-1}, unoxidized sp^2 aromatic C=C bonds at cm^{-1} 1620, the bending vibration of C-OH at 1418 cm^{-1}, and the stretching vibration of C–O in epoxy and alkoxy groups at 1220 and 1085 cm^{-1}, respectively. The presence of polar functional groups, especially the —OH functional groups, results in the hydrophilic nature of GO [50,161].

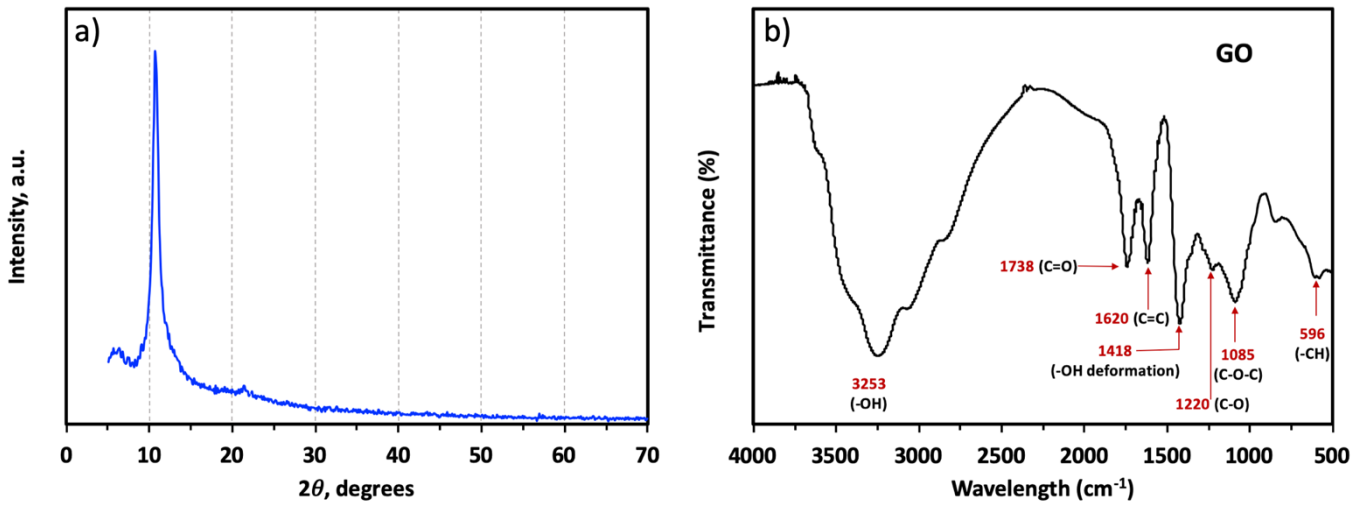

Figure 3. 3 a) XRD and b) FTIR spectra of GO nanosheets.

3.3.2 Polyamide membrane surface modification

3.3.2.1 Chlorination of polyamide membranes

Fig 3.4 shows the performance of the pristine polyamide membrane for pervaporative desalination of 20 wt.% NaCl feed solution before and after treatment with NaClO at different concentrations for 2 h.

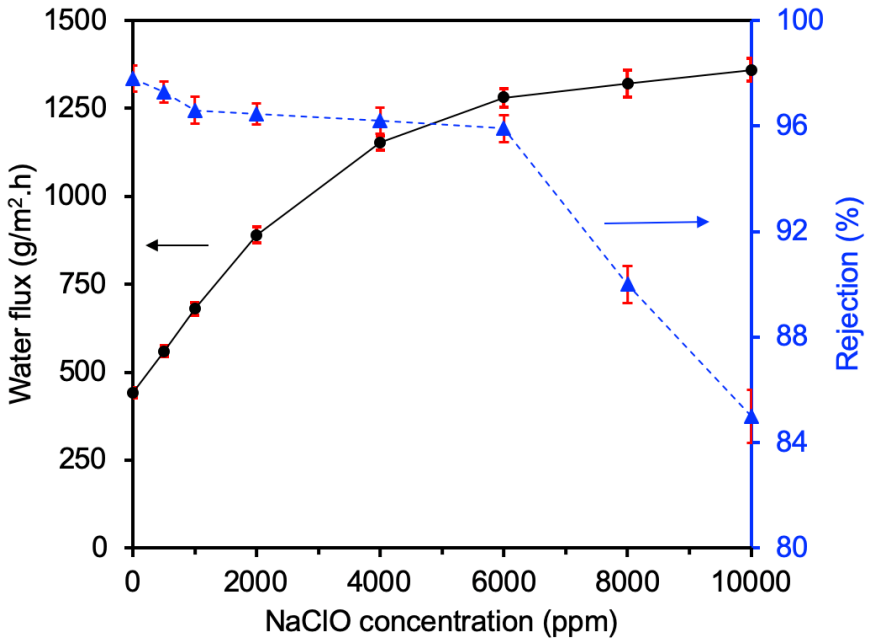

Figure 3. 4 Effects of NaClO concentration on the permeation flux and salt rejection of TFC polyamide membranes; Experimental conditions: Chlorine treatment 2h and room temperature (22°C). Pervaporation operating condition: feed NaCl concentration 20 wt% and room temperature. Data points show mean ± standard deviation (SD) for n = 5 replicate runs.

The original TFC polyamide membrane without chlorine treatment showed a permeation flux of 441 g/(m^2 h) and a salt rejection of 97.8%. After treatment with NaClO at 6000 ppm for 2 h, the permeation flux was almost tripled, while the salt rejection decreased by about 2 %. Such a chlorine-treated polyamide membrane with relatively low permeation resistance is considered to be a favorable substrate for the deposition of polyelectrolytes. Chlorine attack at a higher dosage

of NaClO would penetrate the membrane interior and degrade the polyamide layer by opening up the pores, causing a remarkable reduction in salt rejection. The chlorination of polyamide membranes lowered their resistance to mass transport, resulting in higher permeation fluxes and lower salt rejections. The pervaporation data reported in Fig 3.4 (at each NaClO concentration) represent the average of five measurements (n=5) under identical conditions and the experimental errors in the flux were less than 11% at a NaClO concentration up to 6000 ppm. At higher NaClO concentrations, the experimental error increased up to 17%, presumably due to degradation of membrane surface after additional chlorination. The experimental errors in salt rejection were less than 1%. Before the deposition of polyelectrolytes, the reproducibility of the chlorinated TFC polyamide membrane was checked. TFC polyamide membranes were treated with NaClO at 6000 ppm for 2 h for several times and tested under identical conditions.

3.3.2.2 LbL self-assembly

Attempts were made to improve the pervaporation performance using an LbL self-assembly approach. Fig 3.5(a) shows the pure water flux of chlorine-treated TFC polyamide membrane at various operating temperatures after deposition of PEI and GO layers. The pure water fluxes of the original and chlorine-treated TFC polyamide membranes are also presented for comparison. The salt rejection of the PEI/GO LbL membrane was increased to over 99.99% at all salt concentrations in the feed studied. The water flux did not significantly decrease after deposition of PEI/GO bilayer, suggesting the PEI and GO formed a very thin layer through the LbL self-assembly. Moreover, both PEI and GO are hydrophilic, and the tortuous nanochannels between the well-stacked GO nanosheets can be considered as a pathway for water molecules, and the GO inter-sheet spacing determines the selectivity of the membrane [34,50,162,163]. To confirm the hydrophilicity of the membranes, the contact angles of water on the surfaces of the original

polyamide and GO/PEI LbL membranes were measured (Fig 3.5(b)). The contact angle of the polyamide substrate tended to decrease from 33.2° to around 27° after chlorine treatment and deposition with the PEI/GO bilayer. Baskoro et al. deposited GO onto the top surface of a porous polyvinylidene fluoride-poly acrylic acid (PVDF-PAA) layer to form a dense ultrathin separation layer, and they also showed that a thin GO layer could improve the membrane performance compared with a GO-free membrane [135]. Fig 3.5(c) shows the XRD patterns of original TFC polyamide, chlorine-treated TFC polyamide, and GO/PEI LbL membranes. It can be observed that all these membranes displayed three diffraction peaks at $2\theta \sim 17.9$, 22.9 and 26.1°, related to *d* spacing values of 0.48, 0.39 and 0.34 nm, respectively. Similar observations have been reported by Ali et al. [164]. The peaks of the chlorine-treated TFC membrane were the same as the original TFC polyamide membrane, showing that the polyamide membrane maintained its structure after chlorine treatment. The 2θ value observed at 12.6° in PEI/GO LbL membrane showed that PEI was successfully attached to the GO layers. Moreover, it showed a decrease in the spacing between GO layers with the addition of PEI (decreasing from 0.8 to 0.7 nm). This decrease in *d* scaping value may be attributed to the ionic crosslinking between GO and PEI, forming closer stacking structure [165].

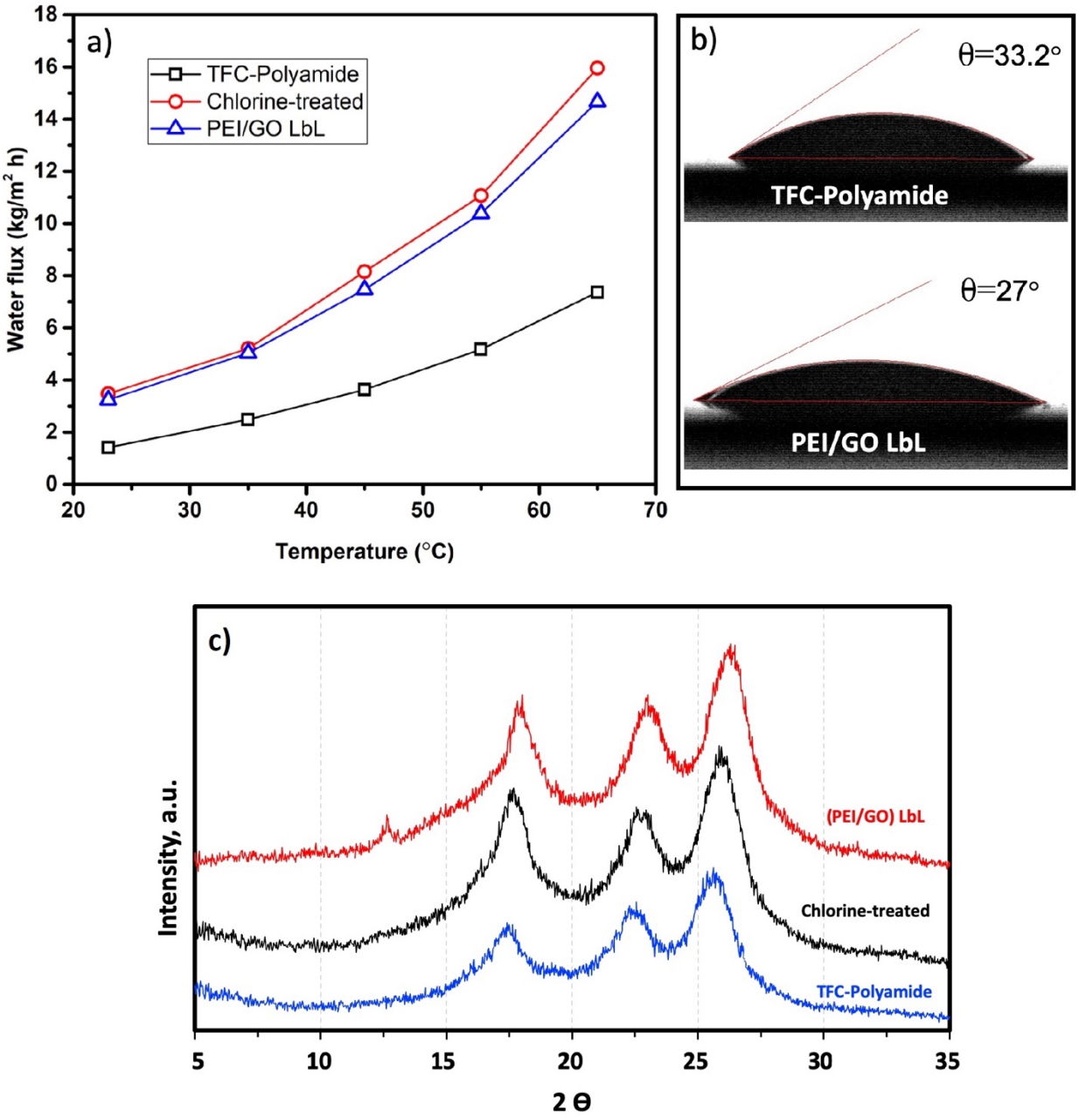

Figure 3. 5 (a) The pure water flux of the original and chlorine-treated TFC polyamide membrane and GO/PEI LbL membranes at various temperature, (b) the contact angles of water on the surfaces of TFC polyamide and PEI/GO LbL membranes, and (c) XRD patterns of TFC polyamide, chlorine-treated TFC polyamide and GO/PEI LbL membranes.

Fig 3.6 shows the ATR-FTIR spectra of pristine TFC polyamide, chlorine-treated polyamide and PEI/GO LbL membranes. The characteristic peaks at 1544, 1598, 1660 and 3363 cm^{-1} were attributed to N-H in-plane bending (amide II), C=C ring stretching, C=O stretching (amide I) and N-H stretching (amide II), respectively [166,167]. After chlorination, the intensities of the peaks at 1544, 1598 and 3363 cm^{-1} decreased, which shows that hydrogens in amide and aromatic ring were replaced by chlorine [168]. The broad peak at ~3363 cm^{-1} was intensified in the PEI/GO LbL membrane compared to that for chlorinated polyamide substrate. It can be assigned to the stretching vibrations of O-H in GO and N-H stretching (amide II) in PEI [119], showing assembly of GO nanosheets on the PEI layer. It has been reported that the intensity of this peak increases when increasing the amount of GO on the surface layer or increasing the number of GO/PEI bilayers [169]. The intensity of N-H bend also increased at ~ 1544 cm^{-1} due to assembling of PEI in the bilayer [142,159].

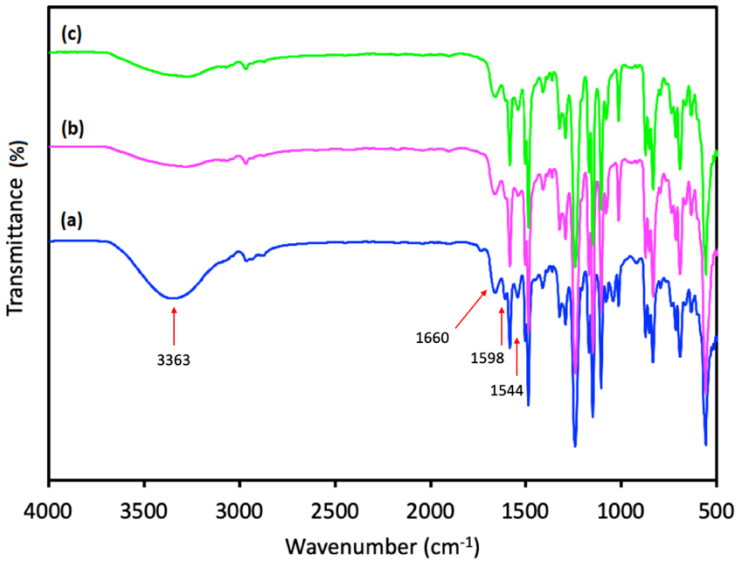

Figure 3. 6 ATR-FTIR spectra of (a) pristine TFC polyamide , (b) chlorine-treated polyamide and (c) PEI/GO LbL membranes.

Fig 3.7 shows the 3-D and 2-D AFM images of the surface morphology of the original polyamide and PEI/GO LbL membranes. The bright and dark regions are peaks and valleys, respectively [170]. The values of mean roughness (Ra) tend to decline after the deposition of PEI and GO on the membrane surface. The Ra values of the original polyamide membrane and PEI/GO LbL membranes are 61.1nm to 50.6nm, respectively. The smaller Ra value of the LbL membrane might be attributed to the coverage of modified TFC polyamide membrane surface with PEI and GO, resulting in the denser structure of the membrane. Moreover, it shows the formation of the bilayer on the substrate.

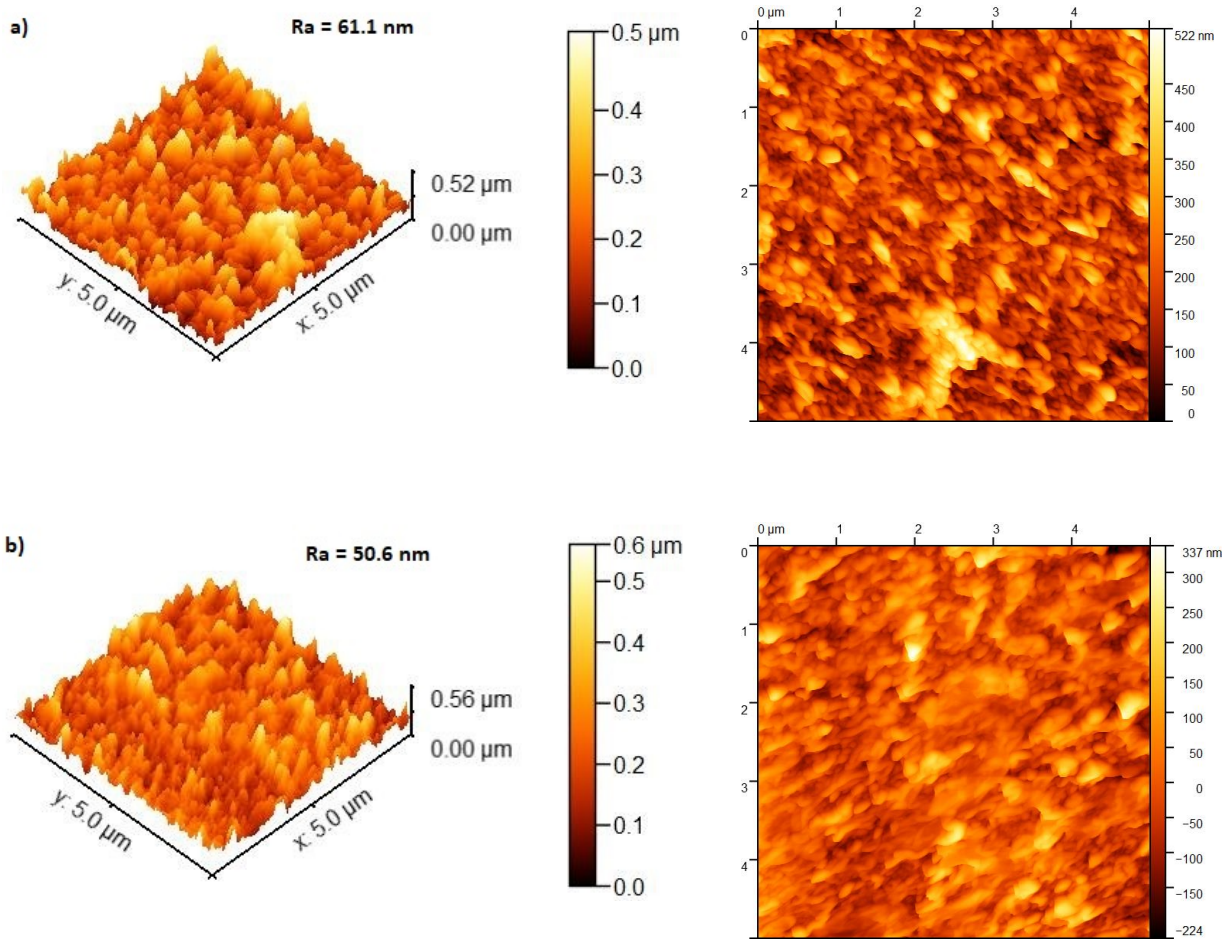

Figure 3. 7 3-D and 2-D AFM images of the (a) original TFC polyamide membrane and (b) PEI/GO LbL membrane, (scanned area: 5 µm × 5 µm).

3.3.3 Pervaporative desalination with the LbL membrane

The pervaporation desalination performance of the LbL membrane was tested at different feed solution salt concentrations and temperatures. In this work, the rejection of salts (NaCl, Na_2SO_4, $MgSO_4$, $MgCl_2$) remained high (~99.9%) regardless of the difference in the operating conditions. One reason for a high salt rejection in the pervaporation process is the non-volatility of the salts which prevents them from entering the vapor phase on the permeate side. However, the operating conditions have substantial effects on the permeability of water. Water molecules, the major component of the feed solution, are favorably sorbed in and diffused through the membrane, because of the affinity of PEI and GO to water that helps form hydrogen bonds [34,50]. The effects of operating conditions on water flux will be discussed in more details in the following.

3.3.3.1 The effects of feed temperature

The effects of feed temperature on the pervaporation desalination performance of the PEI/GO LbL membrane was presented in Fig 3.8. The operating temperature is a major factor in the pervaporation process as it affects both the solubility and diffusivity of the permeating species through the membrane as well as the driving force for permeation [171]. The water flux increased with an increase in temperature at all feed concentrations. Water fluxes of 13.7 kg/(m^2 h) and 8.4 kg/(m^2 h) were achieved for feed NaCl concentration of 2 wt% and 20 wt%, respectively, at 65°C. The partial vapor pressure difference between the feed and permeate is considered to be the driving force. At higher operating temperatures, the water vapor pressure on the feed side increases almost exponentially as predicted based on the Clausius Clapeyron equation. Therefore, at a given vacuum applied to the permeate side of the membrane, a higher driving force and water flux were obtained. Based on the Eyring theory, diffusion occurs when a molecule has enough energy to prevail over a potential barrier and reach a new equilibrium state. Increasing the feed temperature provokes the

motion of the polymer chains and speeds up the diffusion and transport of water molecules in the membrane [34]. Therefore, water molecules are able to diffuse into the free volume of the polymer matrix more easily, creating a higher water flux [172]. As shown in Fig 3.8, water flux through the membrane is also affected by the salts present in the feed. Though no salts were detected in the permeate, the salt molecules may enter the membrane. The diffusion coefficients in polymers are sensitive to penetrant size and shape [173]. Therefore, as a rule of thumb, when the size of salt molecules decreases, its rate of diffusion increases. Because they are not volatile, they can hardly enter the vapor phase.

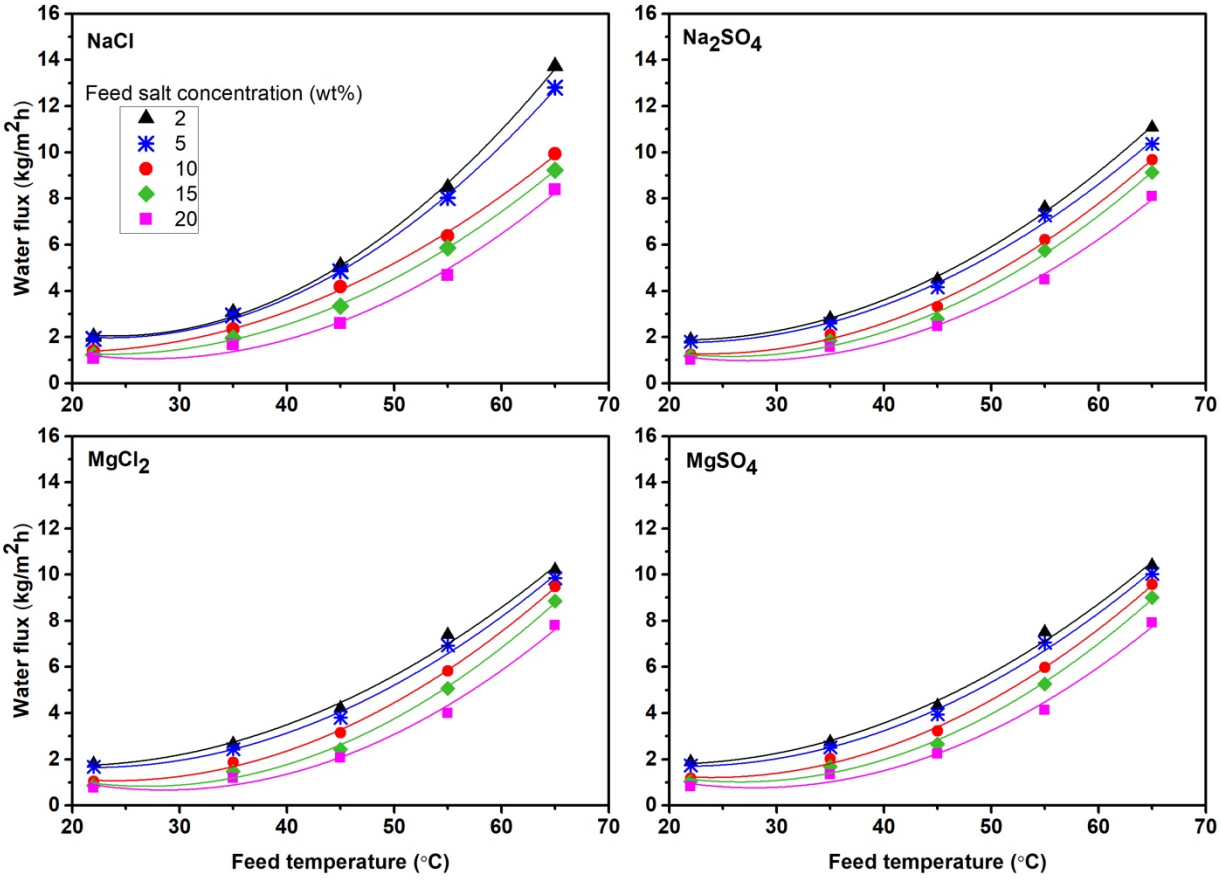

Figure 3. 8 The effects of feed temperature on water permeation fluxes.

The overall temperature dependence of the water permeation flux for pervaporation follows an Arrhenius type of relationship [34,171].

$$J = J_0 \, exp\left(-\frac{E_J}{RT}\right) \tag{3.3}$$

where J_0 is the pre-exponential factor, R is the gas constant, T is the absolute temperature, and E_J is the apparent activation energy for permeation. The Arrhenius plots for the permeation of water through the PEI/GO LbL membrane for the salt-water systems at various feed salt concentrations are presented in Fig 3.9, where the water fluxes showed a linear relationship with the reciprocal the absolute temperature.

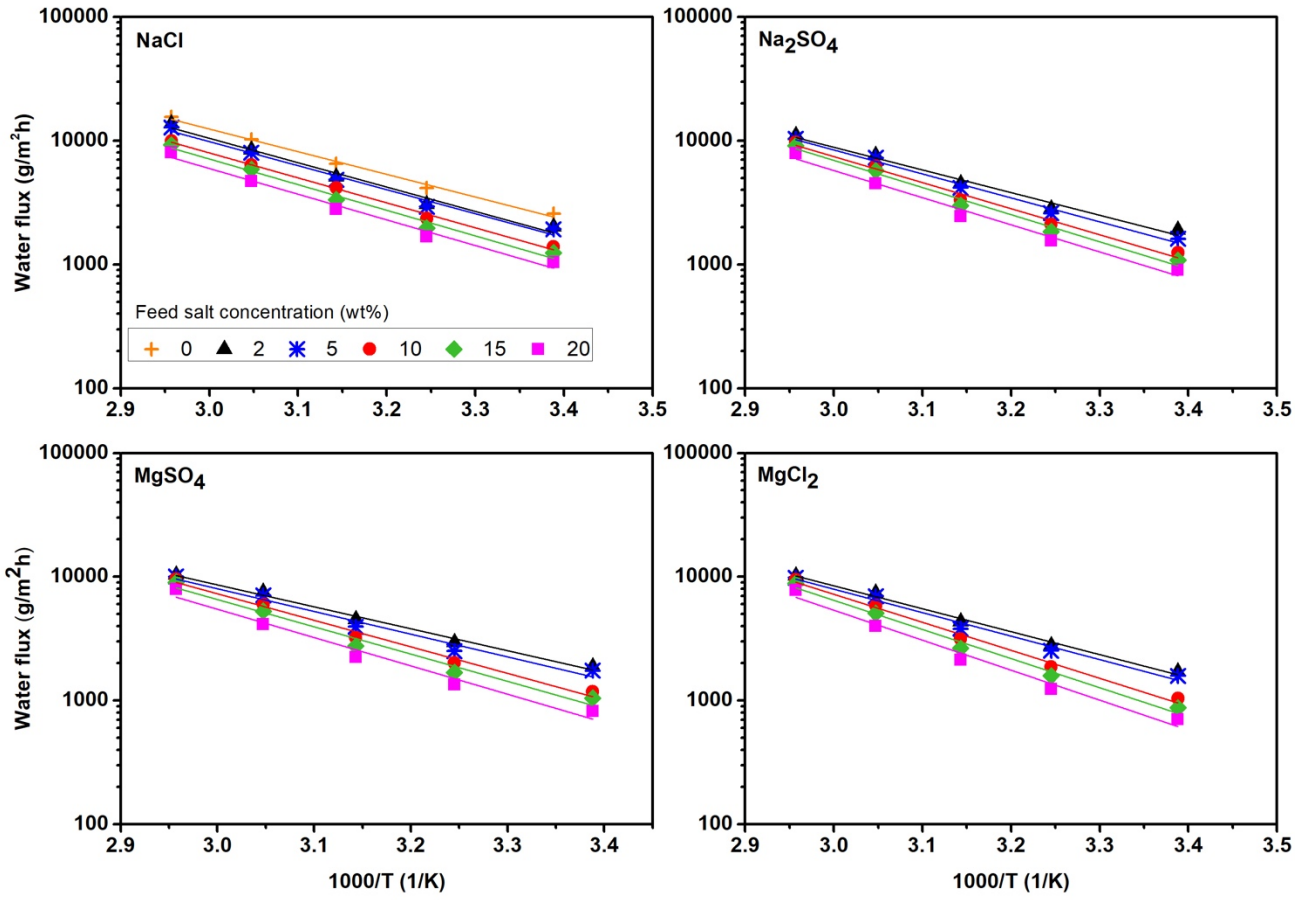

Figure 3. 9 Arrhenius plot of the water permeation fluxes for various salt concentrations.

The activation energies for water permeation, E_J, through the membrane is presented in Table 3.1. The positive value of E_J indicates that water flux has a positive correlation with temperature. The E_J values increased as the feed salt concentration increased from 2.0 to 20.0 wt%, and there was no significant difference in E_J for water permeation of the four different salt solutions. At a higher feed water concentration, the activation energy was tended to be lower due to the swelling effect of the membrane, which can considerably increase the free volume and water molecule diffusion [34]. In general, the relatively low apparent activation energy can be ascribed to the unique structure of GO that allows water molecules to diffuse through the spaces between nanosheets, and the hydrophilic nature of PEI. On the other hand, Jiraratananon et al. reported that water clustering lessens at higher temperatures, resulting in higher water permeation [174].

Table 3. 1 Activation energies for water permeation from salt solutions at different concentrations.

	E_J (kJ/mol)	E_p (kJ/mol)	E_J - E_p (kJ/mol)	ΔH_V [a] (kJ/mol)
Water	37.00	-3.29	40.29	40.71
NaCl				
2%	37.67	-2.65	40.32	40.68
5%	37.15	-3.14	40.29	40.66
10%	38.60	-1.69	40.29	40.64
15%	39.61	-0.68	40.28	40.61
20%	39.67	-0.62	40.29	40.58

	E_J (kJ/mol)	E_p (kJ/mol)	E_J - E_p (kJ/mol)	ΔH_V [a] (kJ/mol)
Na_2SO_4	35.03	-5.25	40.28	40.71
2%	35.04	-5.24	40.28	40.70
5%	40.3	0.017	40.28	40.69
10%	40.4	0.12	40.28	40.68
15%	40.4	0.12	40.28	40.67
20%				
$MgCl_2$				
2%	34.71	-5.57	40.28	40.70
5%	35.46	-4.82	40.28	40.69
10%	43.30	3.01	40.29	40.68
15%	45.40	5.10	40.30	40.66
20%	44.94	4.64	40.30	40.64
$MgSO_4$				
2%	34.33	-5.96	40.29	40.70
5%	35.11	-5.18	40.29	40.70
10%	41.01	0.73	40.28	40.69
15%	42.12	1.83	40.29	40.67
20%	43.77	3.50	40.27	40.66

[a] Heat of vaporization of water determined with ASPEN.

To investigate the effects of temperature on the membrane permeability, the permeance of the membrane (P/l) to water permeation was calculated using a permeation flux normalized by the driving force for permeation, which also normally follows an Arrhenius type of temperature dependence [171]:

$$\left(\frac{P_i}{l}\right) = \frac{J_i}{p_i^s x_i \gamma_i - p_i^p y_i} = \left(\frac{P_{i0}}{l}\right) \exp\left(-\frac{E_{pi}}{RT}\right) \quad (3.4)$$

where $\left(\frac{P_i}{l}\right)$, p^s, γ, p^p and E_p are, respectively, the permeance of the membrane to permeant i, the saturated vapor pressure of pure component i, the activity coefficient in the liquid phase (calculated by the Pitzer equation of state), the permeate vapor pressure (which is generally negligible in pervaporation), and the activation energy for permeation, based on membrane permeability. x and y are the mole fractions of water in the feed and permeate, respectively.

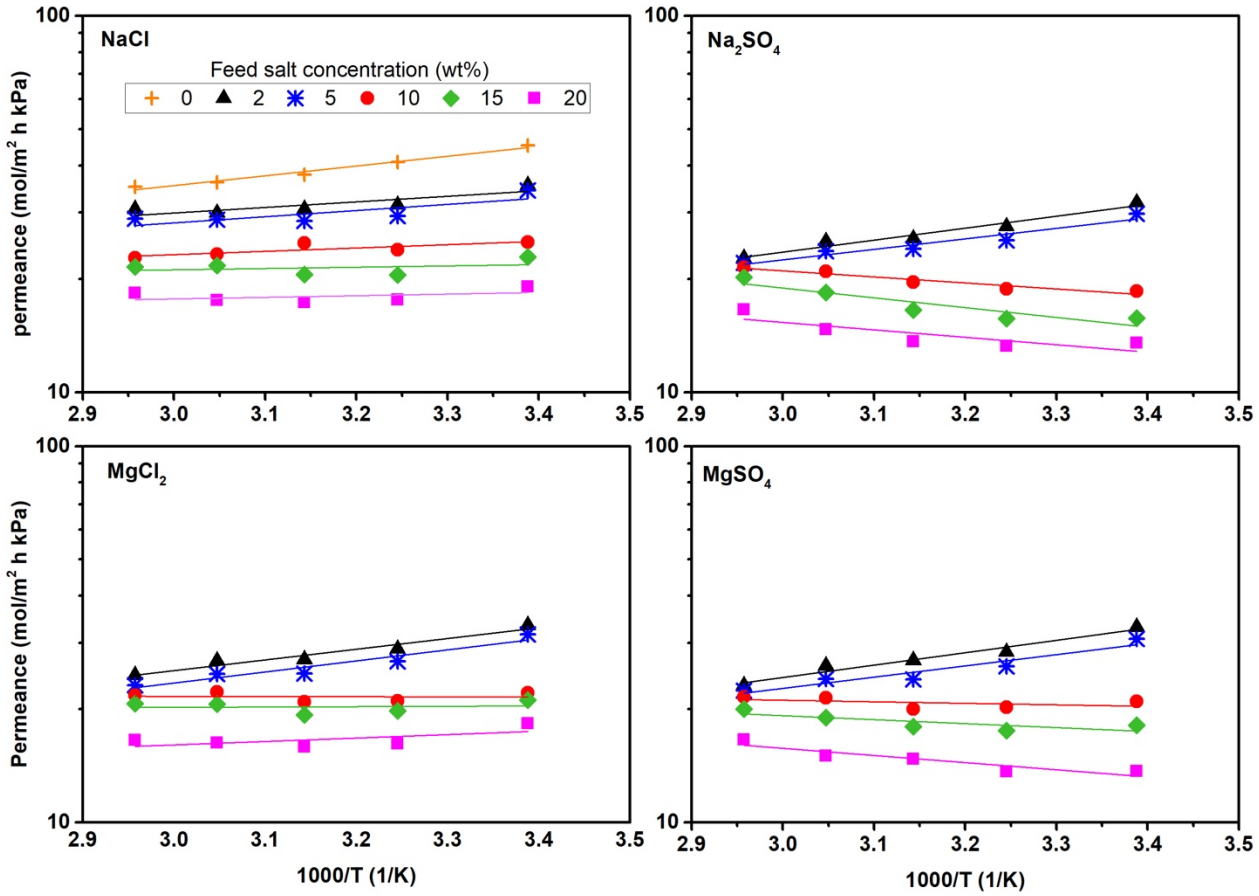

Figure 3. 10 Effects of temperature on permeance of water through GO-PEI LbL membrane at different feed salt concentrations.

Fig 3.10 shows the membrane permeance as a function of reciprocal temperature on a semi-log scale. As can be seen, the permeance of water in the membrane may increase or decrease with an increase in the operating temperature. The activation energy of permeation for various feed, E_p, which can be obtained from the slope of the Arrhenius plot, is listed in Table 3.1. Based on the solution-diffusion model, the permeability coefficient is equal to the product of the diffusion and solubility coefficients. Thus, E_p is equal to the activation energy for diffusion (E_D) plus the heat of sorption (ΔH_s) (i.e., $E_p = E_D + \Delta H_s$). Whereas E_D has a positive value, the heat of sorption (ΔH_s) can be either negative or positive depending upon whether the sorption process is

exothermic or endothermic. Negative values of E_p for the water permeation imply that the sorption process is exothermic (i.e., $\Delta H_s < 0$) and temperature affects exothermic sorption more than it affects diffusion, causing a decline in membrane permeability. E_p can be also estimated from $E_p = E_J - \Delta H_V$, where ΔH_V is the heat of vaporization [31]. Accordingly, the ΔH_V values of water for the different feed solutions at temperatures ranging from 25-65 °C were determined and presented in Table 3.1. The ΔH_V values obtained using ASPEN are comparable with the calculated ΔH_V values.

3.3.3.2 The effects of feed concentration

Fig 3.11 shows how salt concentration in the feed solution affected the pervaporation performance of a PEI/GO LbL membrane when the salt concentration increased from 2.0 to 20.0 wt% at different feed temperatures. In general, the water flux decreases at higher salt concentrations, which is consistent with results reported elsewhere [34,50]. This trend became more remarkable at higher temperatures. In pervaporation, the feed concentration directly affects the sorption of permeating species at the membrane/liquid interface, and the diffusion rate of the component in the membrane depends on the concentration gradient [174]. When the salt concentration in the feed solution increases, the mass transfer coefficient of water and consequently the rate of water diffusion into the membrane are expected to decrease. When the salt concentration was increased from 2.0 wt% to 20.0 wt% on the feed side, the concentration of water decreased from 98.0 wt% to 80.0 wt%, leading to the lowered partial vapour pressure of water. Additionally, at higher temperatures, feed salt concentration had more significant effects on water flux because the saturated water vapor pressure is affected by temperature as mentioned earlier. For example, the water vapour pressure at 65°C is much different to that at room temperature. On the other hand, increased salt concentration will reduce the available diffusion

space for water molecules, and consequently reduce the water flux.

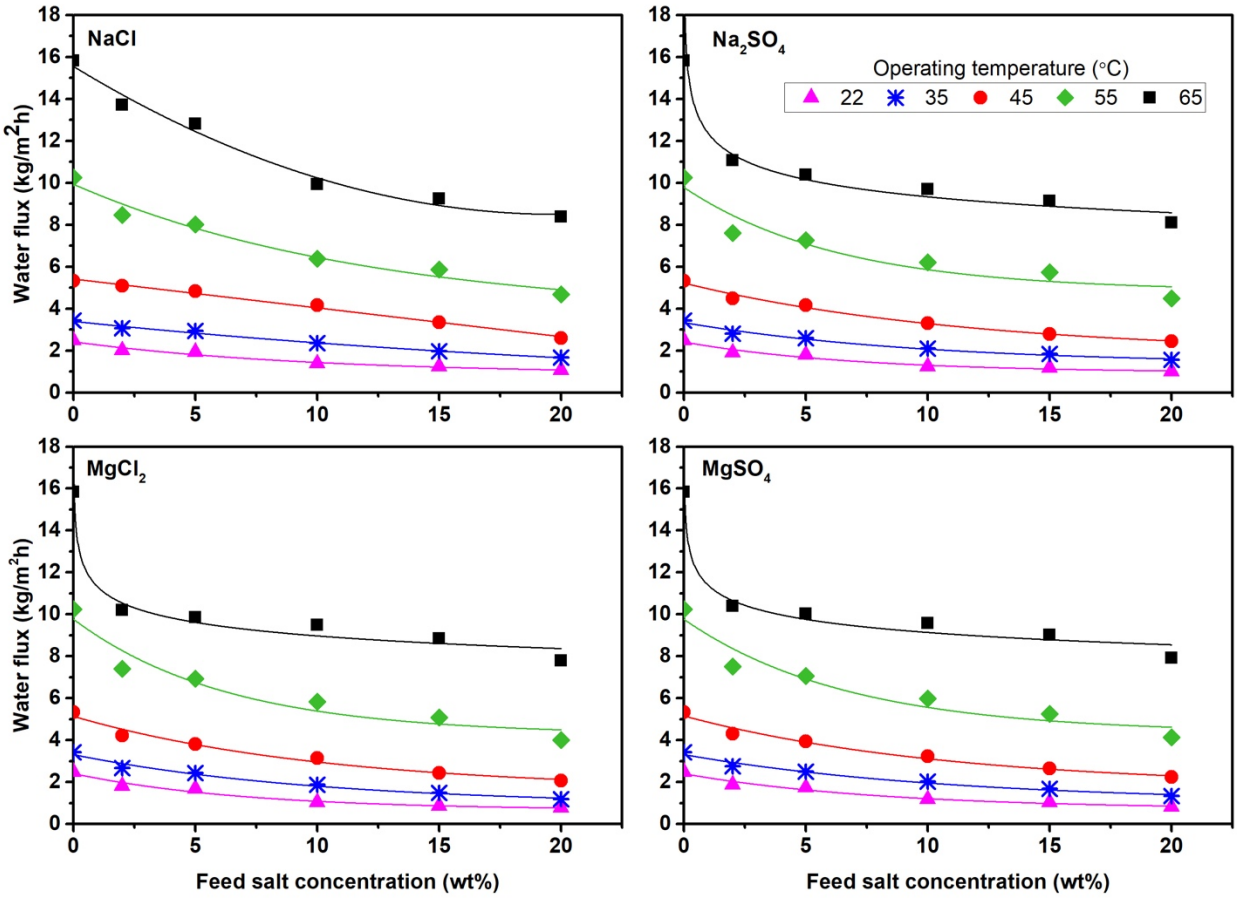

Figure 3. 11 Effects of feed salt concentration on water flux at different temperatures.

Table 3.2 compares the pervaporative desalination performance of the PEI/GO LbL membrane with other membranes reported in the literature [34,50,123,131,175–177]. For a feed salt concentration of 200g/L, the PEI/GO LbL membrane showed a water flux of 8.4 kg/m^2 h, which is more than 10 times higher than the water flux of the PEBA membrane used under the same operating conditions [178]. Qian et al. [177] found that there was fouling on the surface of chitosan/GO mixed matrix membranes after 35 h of operation with a 5wt% feed NaCl concentration. Huang et al. [176] reported that the polyimide/GO hollow fiber membrane had a

water flux of 15.6 kg/m^{2}h for seawater desalination at 90 ºC. Feng et al. [175] reported water flux of 10.7 kg/m^{2}h for a polyimide/GO mixed matrix membrane at 75 ºC for seawater desalination; however, there was no information available on the long term stability of the membrane. The other membranes listed in Table 3.2 were not applied for the desalination of high-salinity water.

Table 3. 2 Pervaporative desalination performance of different membranes.

Membrane	Feed NaCl (g/L)	Temperature (ºC)	Flux (kg/(m^2 h))	Rejection (%)	Ref.
GO/Polyacrylonitrile	35	30	14.3	>99.8	[50]
Poly(vinyl alcohol)/maleic acid/silica	2	65	11.7	>99.9	[34]
Poly(vinyl alcohol)/maleic acid/silica	2	22	6.93	>99.5	[123]
Crosslinked Poly(vinyl alcohol)/Laponite	30	60	51.2	>99.9	[131]
Polyimide/GO	100	75	10.7	>99.8	[175]
Polyimide/GO	35	90	15.6	>99.9	[176]
Chitosan/GO	100	60	16.2	>99.9	[177]
PEI/GO LbL	20	65	13.7	>99.9	This study
PEI/GO LbL	50	65	12.8	>99.9	This study
PEI/GO LbL	100	65	10	>99.9	This study
PEI/GO LbL	200	65	8.4	>99.9	This study

Moreover, the pressure required for membrane-based desalination using RO at a high salinity of 55,000 mg/L with a high recovery of above 35% would require a feed pressure that is beyond the acceptable pressure of membrane modules. For instance, to overcome the osmotic pressure, the feed pressure required for brackish water desalination is expected to range from 6 to 30 bar, whereas those for seawater desalination is 60 to 80 bar [179]. The osmotic pressure for the feed water with a salinity of 200 g/L NaCl (this study) is estimated to be more than 180 bar at 25ºC [180], which is extremely challenging for the current generation of RO.

Membrane distillation (MD) is an alternative process that is similar to pervaporation for desalination of water. Different types of MD configurations have been used to separate aqueous feed solutions using hydrophobic membranes, namely direct contact MD, air gap MD, vacuum MD, and sweeping gas MD. Table 3.3 summarizes several types of MD performances for a rough comparison with the performance of the LbL membranes prepared in this study. Banat and Simandl [181] used a polyvinylidene fluoride (PVDF) flat membrane for desalination of seawater via air gap MD, and a permeation flux of 1 kg/m^{2}h was obtained at a temperature of 40 ºC. Yun et al. [182] reported a permeation flux of 6.1 kg/m^{2}h at a feed NaCl concentration of 24.6 wt% at 43 ºC via direct contact MD using PVDF membranes. Hsu et al. [183] investigated two types of MD configurations using a Millipore polytetrafluoroethylene (PTFE) membrane, and they found a permeate flux of 1 and 0.5 kg/m^{2}h at 5 ºC for feed NaCl concentrations of 5 and 3 wt%, respectively, when direct contact MD and air gap MD were used. Gryta et al. [184] reported that capillary polypropylene membranes soaked in salt solutions were wetted faster than those soaked in distilled water. Most of the MD studies reported issues of fouling and wetting of the membranes. Therefore, the feed flowrate has an important effect on the MD membrane performance [126]. In general, the PEI/GO LbL membranes prepared in this study have a high permeation flux for

pervaporative desalination when compared to the afore-mentioned MD membranes.

Table 3. 3 MD performance of different membranes.

Membrane	MD module	Feed NaCl (g/L)	Temperature (ºC)	Flux (kg/(m^2 h))	Rejection (%)	Ref.
PVDF	Air gap	Seawater	40	1	<5ppm salt permeate	[181]
PVDF	Direct contact	250	43	6.1	99.9	[182]
PTFE	Direct contact	5	5	1	Conductivity 7-12 s/cm	[183]
PTFE	Air gap	3	5	0.5	Conductivity 7-12 s/cm	[183]
PVDF	Direct contact	3.5	60	16	-	[185]
PP	Vacuum	Na: 0.0344 mol/l Cl: 0.0166 mol/l	85	4.1	-	[186]
PTFE	Vacuum	150	48	7.9	-	[187]
PVDF-HFT	Direct contact	3	50	2.88	99.3	[188]

PVDF: polyvinylidene fluoride, PTFE: polytetrafluoroethylene, PP: polypropylene, PVDF-HFT: polyvinylidene fluoride-hexafluoropropylene

3.3.3.3 Long-term stability for pervaporation desalination

Fig 3.12 shows the separation performance of the PEI/GO LbL membrane with one bilayer for pervaporation desalination of high salinity water (NaCl concentration 20 wt%) at 35 °C for ~ 220 h. There was no significant change in permeation flux while maintaining a high salt rejection (~ 99.9%) over the entire test duration, which shows the long-term stability of the membrane for desalinating high-salinity water.

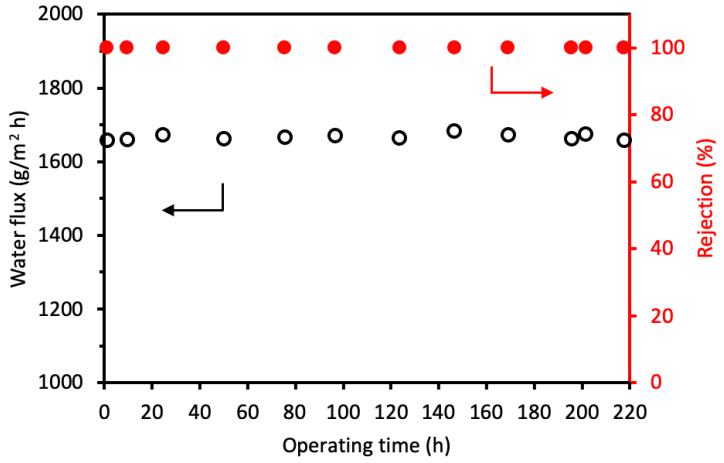

Figure 3. 12 The long term performance of the PEI/GO membrane for desalination of high salinity water at 35 °C. NaCl concentration in feed water 20 wt%.

3.4 Conclusions

A thin-film-composite polyamide membrane was surface modified by chlorine treatment followed by electrostatic deposition of polyethyleneimine and graphene oxide, leading to a new type of layer-by-layer self-assembly membrane. The PEI/GO LbL membrane was successfully fabricated and tested for desalination of high salinity water at salt concentrations up to 20 wt%. The effects of operating temperature and feed concentration on water permeation were studied. The chlorination treatment of the thin polyamide active layer resulted in the more hydrophilic and negatively charged surface, which was favorable for subsequent electrostatic adsorption of PEI and GO. The resultant membrane performed better than the original polyamide membrane in terms of water permeability, and it was applicable for desalination of high salinity water with a high rejection of salts (~ 99.9%). The study also revealed the positive correlation between temperature and water flux due to the augmented driving force for water permeation. The temperature dependence of water flux followed an Arrhenius type of relationship, and the activation energy for water permeation varied from 34 to 45 kJ/mol. Water flux declined when increasing feed salt

concentration from 2.0 to 20 wt% because of the reduced driving force for permeation. Water flux as high as 8.4 kg/(m^2h) was obtained for a feed solution of 20 wt% NaCl at 65°C. This study showed that the surface modification of the membrane via the LbL self-assembly requires a small amount of PEI and GO nanosheets to help overcome the trade-off effect encountered by typical TFC membranes to improve both water flux and salt rejection.

Chapter 4

Layer-by-layer assembly of graphene oxide/polyethyleneimine on TFC polyamide membranes for dehydration of ethylene glycol via pervaporation

4.1 Introduction

Pervaporation, effective membrane-based technology for liquid separation, is a well-established method for dehydrating organic solvents, particularly those with high-boiling points such as ethylene glycol [145,189]. In the past years, pervaporation has drawn considerable attention in industries dealing with energy and quality challenges related to ethylene glycol (EG) dehydration. EG is a non-volatile organic compound with two hydroxyl groups, and it has a wide range of applications due to its physical properties, some of which are listed in Table 4.1 [190–192].

EG is widely employed as an antifreeze and coolant in automobiles, as a precursor to manufacturing polyester and polyethylene terephthalate, and as a hydrate inhibitor of natural gas in the oil and gas industries [191]. However, a drawback of using EG is its toxicity, which is an environmental concern. Thus, it is imperative to recover EG from water. From both an environmental and economic points of view, conventional separation processes as distillation and multi-stage evaporation require a large amount such of thermal energy to separate water and EG,

since high-pressure steam is required in the reboiler due to the high boiling point of EG [189,190,193]. Therefore, from an energy consumption viewpoint, pervaporation is an alternative process which can be used at low heat levels, especially if coupled with waste heat, solar, or geothermal heat sources [5].

Table 4. 1 The physical properties of EG and water.

	EG	Water
Molecular weight (g/mol)	62	18
Molecular diameter (Å)	4.3	2.7
Molecular volume ($Å^3$)[a]	92.4	29.9
Boiling point (°C)	197.3	100
Melting point (°C)	-13	0.0
Refractive index, nD, at 25°C	1.43	1.33
Solubility in Water/EG at 20°C (wt%)	100	100
Vapor pressure at 25°C (kPa)	0.88×10^{-2}	3.17
Heat of vaporization at 1 atm (kJ/mol)	58.9	40.7

[a] The molecular volume is calculated by the molecular weight divided by the density and the Avogadro number [192].

For effective pervaporation dehydration of aqueous organics, hydrophilic non-porous membranes are generally exploited [14]. For such membranes, layer-by-layer (LbL) assembly offers a low-cost, versatile and structurally controllable technique to build up nanoscale anionic-cationic multilayers. The LbL assembly is performed through the alternative cyclic deposition of oppositely charged polyelectrolyte solutions (or nanoparticle suspensions) onto a charged substrate [77,194]. Since polyelectrolytes are hydrophilic and each deposited bilayer is nanometer, this bottom-up approach helps reduce the mass transfer resistance of the membrane and results in a higher permeation flux. Electrostatic interaction is the main driving force for the bilayer buildup,

and hydrogen bonding also helps assembly once the building blocks encompass functional groups as hydrogen bond acceptors or donors [195–197]. LbL assembly membranes have been studied for pervaporation [16,145], reverse osmosis (RO) [119], nanofiltration (NF) [16,198], and forward osmosis (FO) [17]. Zhang et al. [145] prepared an LbL membrane using seven bilayers of polyethyleneimine/poly(acrylic acid) (PEI/PAA) for EG dehydration, with a separation factor of over 410 at 22°C when the feed water concentration was less than 20 wt%.

Two factors are essential in preparing membranes via LbL assembly: appropriate substrates and polyelectrolytes. Thin film composite (TFC) polyamide membranes are a preferred substrate for LbL assembly membranes due to 1) its negatively charged surface, which makes it ready for polycation deposition, and 2) its thin dense skin layer, which reduces the number of polyelectrolyte depositions needed to obtain a durable membrane with sufficient selectivity [119,145].

Recently, graphene oxide (GO) has been shown to offer a solid "brick-and-mortar" LbL structure assembly [17,108,194]. Each individual GO nanosheet possesses a unique carbon nanostructure with abundant hydrophilic functional groups, allowing faster passage of water, almost without friction. GO is thus an ideal candidate nanomaterial for membranes [108,121]. Once GO nanosheets are dispersed in water, they act as polyanions due to the ionization of the hydroxyl and carboxyl groups. Subsequently, they can interconnect with polycations such as polyethyleneimine (PEI) through electrostatic and hydrogen bonding [17,138,194]. As a result, the multilayered membranes applied in water-related separations have enhanced stabilities compared to GO layers alone.

Numerous studies have reported the promising performance by incorporation of GO to modify the surface properties of a substrate through LbL assembly. For instance, Zhao et al. [199] developed gelatin (GE)/GO membranes via LbL self-assembly on hydrolyzed polyacrylonitrile

(H-PAN) ultrafiltration membranes as substrates for the pervaporative dehydration of ethanol. They obtained a permeation flux of 2,275 g/m^{2}h and a permeate water concentration of 98.7 wt% at 350 K for a feed water concentration of 20 wt% with 10.5 bilayers. They also confirmed the desirable long-term stability of the GE/GO multilayer membranes. Mi et al. [17] prepared a membrane via LbL assembling GO nanosheets on porous poly(acrylonitrile) (PAN) support which was attached to poly(allylamine hydrochloride) (PAH) mainly by electrostatic interactions for an FO process. The membrane exhibited a tight structure with a high rejection of about 99% to sucrose, and the thickness of each GO-PAH bilayer was reported to be about 16.5 nm. Grunlan et al. [118] demonstrated that membranes with tightly packed nanostructures prepared using ten bilayers of branched polyethyleneimine (bPEI) and GO on PET had impressive gas selectivity. Another study [194] by the same group showed that a membrane prepared with five bilayers of chitosan (CS), polyacrylic acid (PAA) and GO had excellent barrier properties for gas separation, and the thickness of the bilayers was reported to be ~44 nm. The membrane had a highly oriented structure of GO layers.

Thus, the objective of this study was to explore the potential use of PEI and GO in fabricating membranes via LbL self-assembly for pervaporative dehydration of ethylene glycol (EG). PEI was used as a positively charged polyelectrolyte due to its amine functional groups in its backbone. Furthermore, its hydrophilic nature is favorable for forming the structure of water-permeating membranes. By pairing PEI and GO, strong intermolecular hydrogen bonding is expected to occur in addition to electrostatic attractions.

To the best knowledge of the authors, no prior study has considered the self-assembly of PEI/GO on chlorinated TFC polyamide membranes for the dehydration of EG via pervaporation. PEI/GO bilayers are expected to offer a preferential passageway for the transport of water

molecules. This work examined the effects of temperature and feed water concentration on the membrane performance to investigate the permeability and selectivity of the membranes. Furthermore, the pervaporation dehydration of EG in the presence of salt (i.e., NaCl) was studied, since aqueous EG solutions in gas and chemical processing usually include salts (e.g., 110-800 mg/L sodium [200]). The effects of the number of bilayers on the membrane performance were also considered to gain an insight into the relation among membrane thickness, mass transfer resistance, permeation flux, and selectivity. The morphology and hydrophilicity of the PEI/GO LbL membranes with a different number of bilayers were explored by using atomic force microscopy (AFM) and contact angle measurement, respectively.

4.2 Experimental

4.2.1 Materials

A commercially available thin-film composite polyamide membrane with non-woven fabric support produced by interfacial polymerization (supplied by GE Water) was used as a dense substrate. Graphite flakes were obtained from Alfa Aesar. To oxidize graphite into GO, potassium permanganate ($KMnO_4$, >99%, Merck), phosphoric acid (H_3PO_4, 85% solution in water, Acros), hydrogen peroxide 30% (H_2O_2, 30%) and sulfuric acid (H_2SO_4, 95-98%, Sigma-Aldrich) were used. Moreover, hydrochloric acid (HCl, 37%, Merck), ethanol (Sigma-Aldrich) and de-ionized water were used for rinsing the synthesized GO. Branched polyethylenimine, (PEI, average $M_w \sim$ 25,000, Sigma-Aldrich) was used as a polycation and the polycation solution has a pH of ~ 10. Sodium hypochlorite (NaClO, 14.5% available chlorine, BDH Chemicals) was used for the chlorine treatment of TFC polyamide surface. De-ionized water was used to prepare aqueous solutions of EG with desired feed concentrations. The prepared GO solution was well-sonicated

for 15 min before usage, and the GO suspension was used as an anionic component at its natural pH (~ 6).

4.2.2 The preparation of GO aqueous solution

Applying an improved GO synthesis method proposed by Marcano et al. [153], GO nanosheets were produced from graphite powders. This method provides a larger amount of hydrophilic oxidized graphene materials with fewer defects in the basal plane than the GO prepared by the conventional Hummers' method [154]. Briefly, 3 g of natural graphite flakes and 18 g of $KMnO_4$ were gradually added to an acid mixture composed of 360 mL of H_2SO_4 and 40 mL of H_3PO_4 under stirring conditions. The reaction was allowed to occur at 50°C for 16 h. Afterward, the mixture was cooled to room temperature and poured onto 400 mL of ice-water, followed by addition of H_2O_2 (~3 mL), causing a color change from dark purple to golden. The mixture was centrifuged at 3500 rpm to decant away large aggregates and supernatant, and the remaining solid materials were washed with 10% HCl (2×) and ethanol (4×) solutions, respectively. After each washing step, the mixtures were centrifuged to remove the supernatant. The resulting uniform and brown GO suspension was used as an anionic solution in self-assembly technique.

4.2.3 The preparation and characterization of GO/PEI LbL membranes

Fig. 4.1 shows a schematic of the LbL deposition. First, the TFC polyamide support membrane was treated with an aqueous chlorine solution, i.e., sodium hypochlorite, of 6000 PPM for 2 h to impart strong negative surface charges (denoted as Cl-TFC for convenience of discussion). The active polyamide skin layer became thinner and less compact due to the controlled chlorination [143,152]. The Cl-TFC substrate was initially soaked in DI water overnight to remove sodium hypochlorite residue. Then to build up a bilayer, the PEI aqueous solution (positively charged,

0.02 monomol/L) and GO aqueous solution (negatively charged, 100 mg/L) was deposited onto the Cl-TFC surface for 30 min, respectively. It should be mentioned that each deposition step was followed by rinsing with DI water for 10 min to remove the physically adsorbed excess polyelectrolytes. This cycle was repeated for building up additional bilayers. The resulting membranes were dried in a vacuum oven at 45°C for 2 h. The resulting LbL assembled membrane was designated as $(PEI/GO)_x$, where x refers to the number of bilayers. The surface hydrophilicity of the membranes with a different number of bilayers was evaluated by conducting static contact angle measurement with a contact angle goniometer (VCA 2500 XE, AST Products) at room temperature. The average contact angle value of three arbitrary locations was reported for each membrane sample (for an average water droplet size of 2 μL). The surface morphology and roughness of the membranes were characterized using a tapping mode atomic force microscopy (AFM) (Bruker Innova, USA). To confirm the chemical structures of GO nanosheets and LbL membranes, Fourier Transform Infrared spectroscopy (FTIR, Bruker Tensor 27 IR) was used over the wavelength range of 500 to 4000 cm^{-1}.

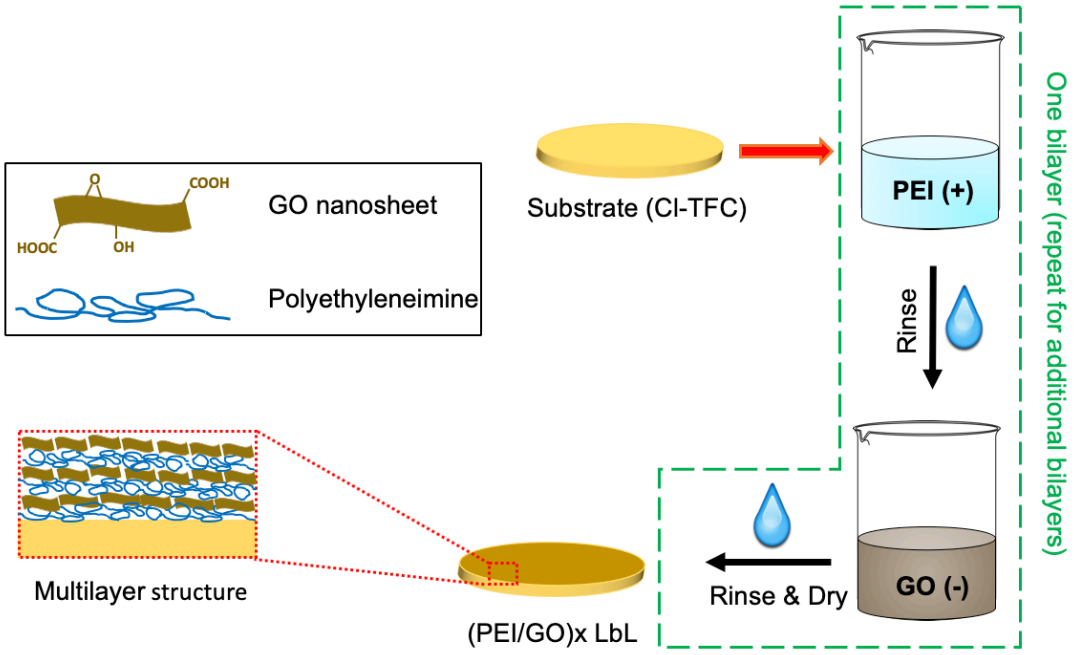

Figure 4. 1 Schematic of the LbL deposition process.

4.2.4 Pervaporation study

The performance of the prepared membranes was evaluated in a laboratory-scale pervaporation apparatus. The membrane with a permeation area of 17.4 cm^2 was placed with the active side facing the feed-solution. The downstream side was evacuated using a vacuum pump and maintained under 0.1 kPa absolute. The permeate vapor was collected over a specific period of time using cold glass traps immersed in liquid nitrogen, then analyzed for composition by a refractometer (Atago 3810, PAL-1). The permeation flux (J, g/m^2h) and separation factor (α) were determined as follows:

$$J = \frac{Q}{At} \tag{4.1}$$

$$\alpha = \frac{Y/(1-Y)}{X/(1-X)} \quad (4.2)$$

where Q is the total weight of the permeate collected at a specific experimental time (t) over the effective membrane area (A); and X and Y are the mass fractions of water in the feed and permeate solutions, respectively. The partial fluxes of EG and water were determined from the permeate composition and total flux. The experimental data were recorded once no further difference in the permeate flux and composition could be detected, and an average of at least three measurements was conducted to ensure reproducibility.

An operating temperature in the range of 22-65°C was maintained using a thermal bath. The feed water concentrations were in a range of 0.1-18 wt%. Water removed by the membrane was compensated for by adding the same amount of water to the feed to maintain a consistent composition during pervaporation experiments. Moreover, the pervaporative dehydration of EG was studied in the presence of inorganic salt. Note that no salt precipitation or crystallization on the permeate side of the LbL membrane was detected throughout the entire experiment. After completion of a pervaporation run in the presence of salt, the feed side of the membrane was rinsed with DI water for 2 h to wash away any salt, followed by pervaporation with pure water for 2 h. The experimental data reported representing the average values from at least three measurements.

4.3 Results and discussion

4.3.1 Effects of feed concentration on the dehydration of ethylene glycol

To study the effects of feed water concentration on the pervaporative dehydration of EG using the $(PEI/GO)_3$ membrane, the experiments were undertaken for feed water concentrations ranging from 0.1 to 18 wt% at 35 °C. This range is relevant to industrial applications, e.g., the dehydration

of natural gas using EG [171]. Fig. 4.2 shows the water concentration in the permeate, separation factor, total and partial permeation fluxes as a function of feed water concentration. The permeate water concentration increased from 66.5 to 95 wt% when increasing the feed water from 0.1 to 18 wt%. The vapor-liquid equilibrium (VLE) data of binary mixtures of EG and water are also plotted to compare pervaporation separation and traditional distillation [201]. The dehydration of EG by pervaporation is a more selective and efficient than distillation, particularly at low feed water concentrations. The total permeation flux increased almost linearly from 56 to 402 (g/m^2h) with an increase in the feed water concentration from 0.1 to 18 wt%, while the partial flux of water was comparable with the total permeation flux and drastically increased with an increase in feed water concentration. Meanwhile, the partial flux of EG increased very slightly (Fig. 4.2 d).

An increase in feed water concentration enhances the driving force for permeation of water through the membrane and swelling of the membrane, giving water molecules the ability to diffuse through the membrane more effortlessly; whereas the opposite happens for EG permeation. The permeation flux of water was much higher than that of EG, and the total permeation flux is predominantly manipulated by the water flux, implying that water is preferentially permeable through the membrane. The high water permeability may result from the relatively small kinetic size of water molecules and the stronger affinity between water and the outmost GO layer in the membrane.

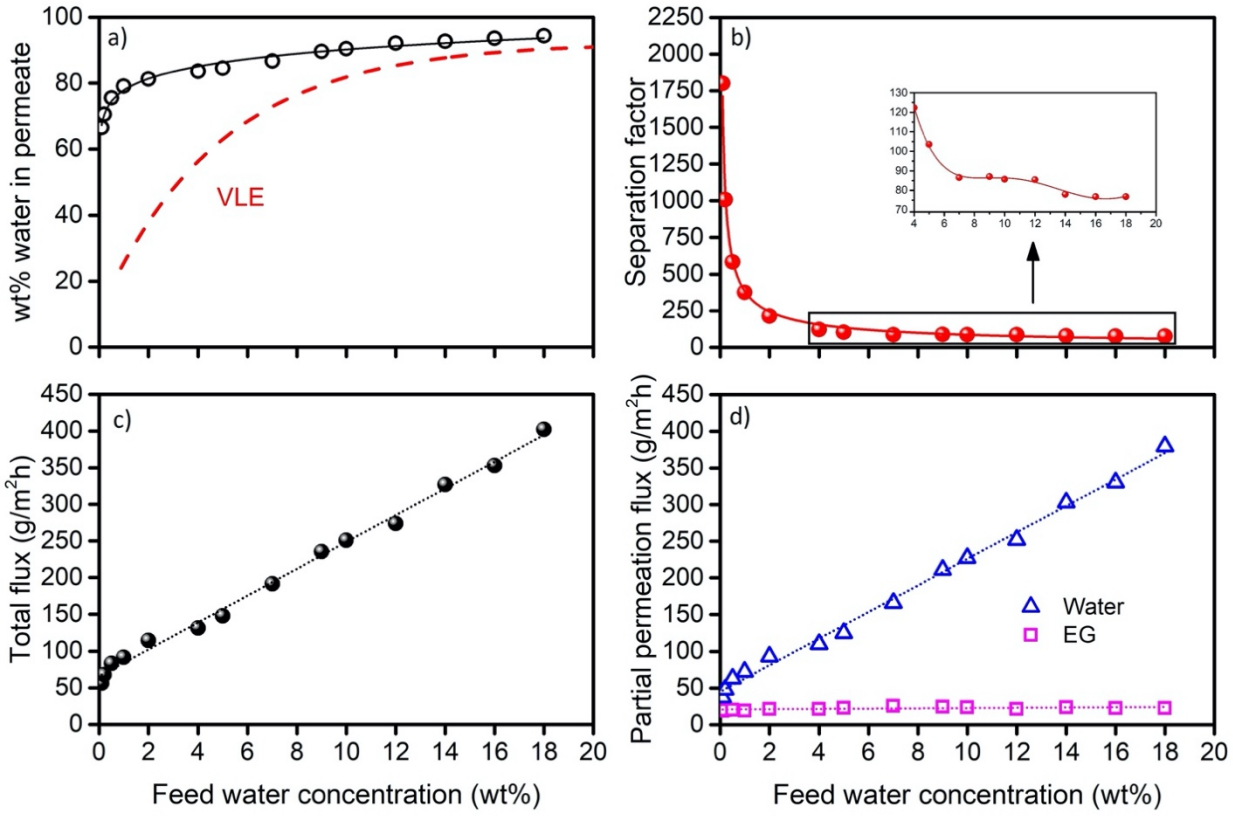

Figure 4. 2 Effects of feed water concentration on (a) water content in permeate, (b) separation factor, (c) total permeation flux, and (d) partial permeation flux through $(PEI/GO)_3$ membrane. Temperature: 35 °C.

There is a trade-off relationship between the permeation flux and separation factor. The separation factor of the $(PEI/GO)_3$ membrane tended to decrease when the feed water content increased (Fig. 4.2 c**)**. The separation factor reduction is more significant at lower feed water concentrations (i.e., 0.1-2.0 wt%), and a further increase in the feed water concentration had a slight impact on the separation factor. The PEI/GO LbL membrane with 3 bilayers exhibited a very high separation factor for the dehydration of EG at low feed water concentrations, which confirms the permselectivity of the membrane. For instance, at feed water concentrations of 0.1,

0.2, and 0.5 wt%, separation factors of 1800, 1008, and 583 were observed, respectively. Similar trends were reported for dehydration of EG using different hydrophilic membranes [171,189].

4.3.2 The effects of operating temperature

Temperature is an important operating parameter in pervaporation as it affects both the solubility and diffusivity of the permeating species through the membrane, as well as the driving force for permeation [171,189]. Fig. 4.3(a) shows the partial fluxes of water and EG through the $(PEI/GO)_3$ membrane as a function of temperature, where the temperature dependence of the fluxes followed an Arrhenius type of relationship. The partial vapor pressure difference between the feed and permeate may be considered to be the driving force. The permeation fluxes of both water and EG increased exponentially with temperature for all feed concentrations.

The increased permeation fluxes at higher temperatures may be attributed to 1) the partial vapor pressures of both water and EG increased as the operating temperature increased, which enhanced the driving forces for their transport through the membrane; 2) faster diffusion occurred at higher temperatures as the permeant molecules became more active and energetic; and 3) the thermal energy would provoke the motion of polymer chains, enlarging the free volume of the membrane [34,172]. Increasing temperature, at a given feed water concentration, appeared to affect the permeation of EG more considerably than that of water; consequently, the separation factor experienced a drop with a rise in temperature, as shown in Fig. 4.3(b). The EG flux, for example, was increased from 14.1 to 44 g/(m^2h), while water flux increased from 54.4 to 96.2 g/(m^2h) with an increase in temperature from 25 to 60 °C at a feed water concentration of 0.5 wt%.

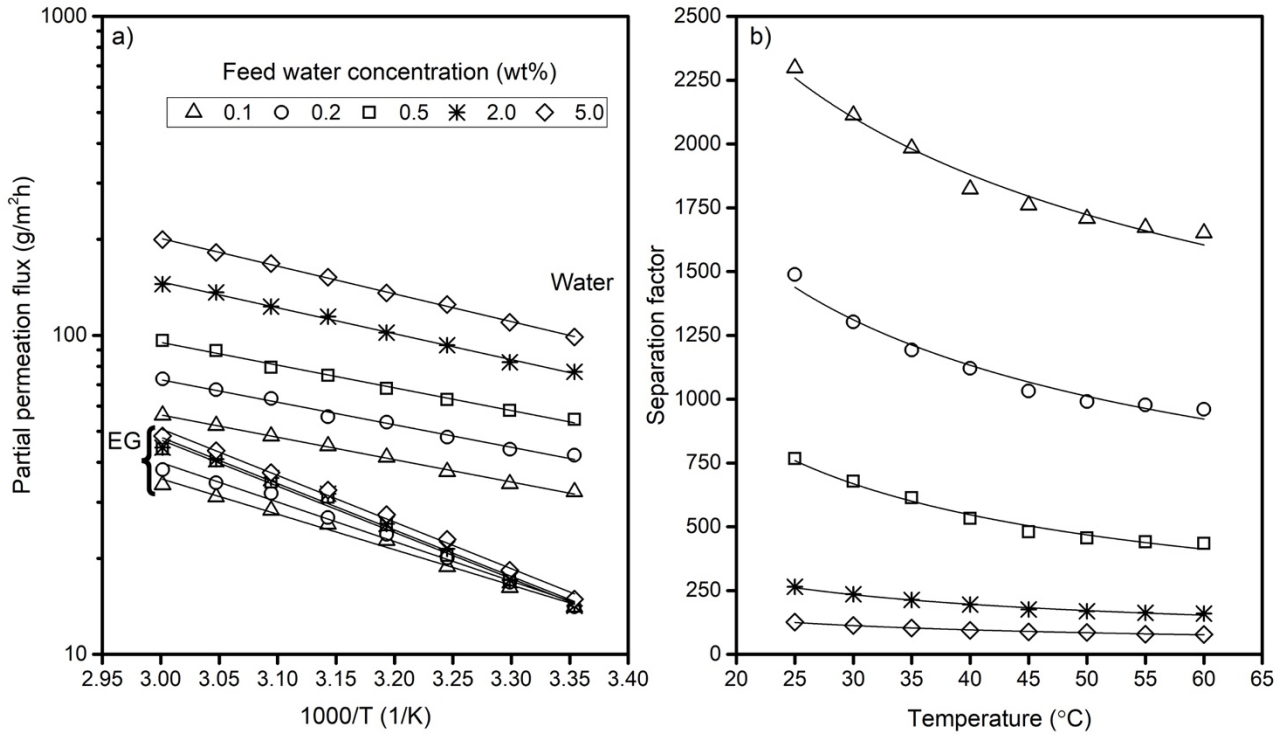

Figure 4. 3 Effects of temperature on (a) the partial permeation fluxes of water and EG; and (b) separation factor using membrane $(PEI/GO)_3$ at different feed water concentrations.

The temperature dependence of the permeation flux fits an Arrhenius type of relationship:

$$J = J_0 exp\ (-\frac{E_J}{RT}) \quad (4.3)$$

where J_0 is the pre-exponential factor, R is the gas constant, T is the absolute temperature, and E_J is the apparent activation energy for permeation that depends on the activation energy for diffusion and the heat of sorption [171]. E_J shows the overall effects of temperature on the permeation flux, which has accounted for the driving force for mass transport.

Fig. 4.4 shows the apparent activation energies, E_J, for the permeation of EG and water at different feed water concentrations ranging from 0.1-5.0 wt%. The apparent activation energy for

both water and EG permeation increased with an increase in the feed water concentration. The activation energy for water permeation appeared to be lower than that for EG permeation (i.e., $E_{J,water} < E_{J,EG}$). This finding may be ascribed to 1) water having a lower heat of vaporization (i.e., 40.7 kJ/mol) than EG (i.e., 53.2 kJ/mol); therefore, the vapor pressure of EG increases more significantly than the vapor pressure of water with increasing the feed temperature; and 2) water having a smaller kinetic molecular size than EG, and needing to overcome a lower energy barrier to diffuse through the membrane. Increasing temperature, in other words, can augment the diffusivity of the larger component more than that of the smaller component [173].

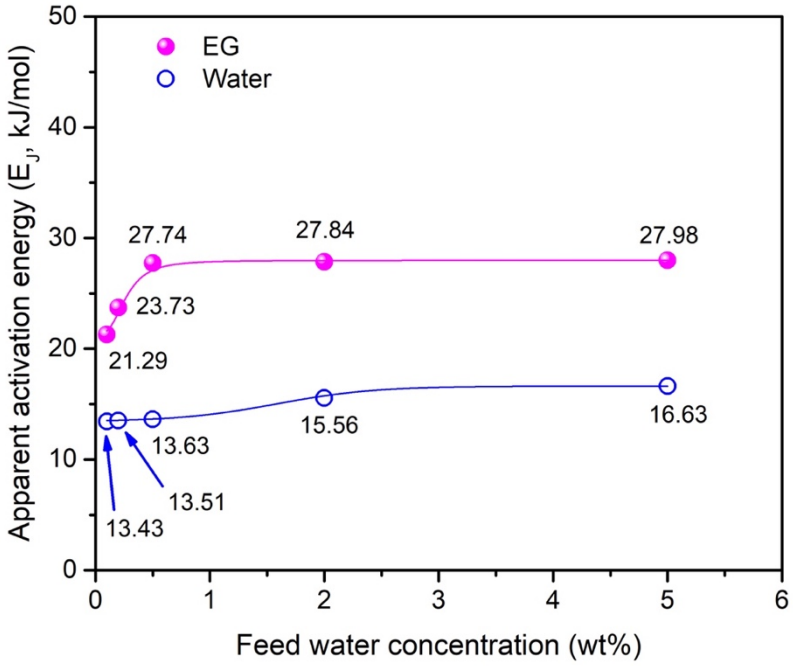

Figure 4. 4 Apparent activation energies for permeation of water and EG based on permeation flux at different feed water concentrations.

To explore the effects of temperature on the membrane permeance (or permeability), the permeance of the membrane was calculated by normalizing the permeation flux by the driving force and an Arrhenius type of temperature dependence also applies:

$$\left(\frac{P_i}{l}\right) = \frac{J_i}{P_i^s x_i \gamma_i - p^p y_i} = \left(\frac{P_{i0}}{l}\right) \exp\left(\frac{E_{Pi}}{RT}\right) \quad (4.4)$$

where $\left(\frac{P_i}{l}\right)$, p^s, γ, p^p, E_p, x and y are, respectively, the permeance of the membrane to permeant *i*; the saturated vapor pressure of pure component *i,* which can be calculated from the Antoine equation [202]; the activity coefficient in the liquid phase, calculated from the Wilson equation with the help of Aspen Plus [189]; the permeate vapor pressure, which is generally negligible in pervaporation; the activation energy, based on membrane permeability; and the mole fraction of water in the feed and permeate.

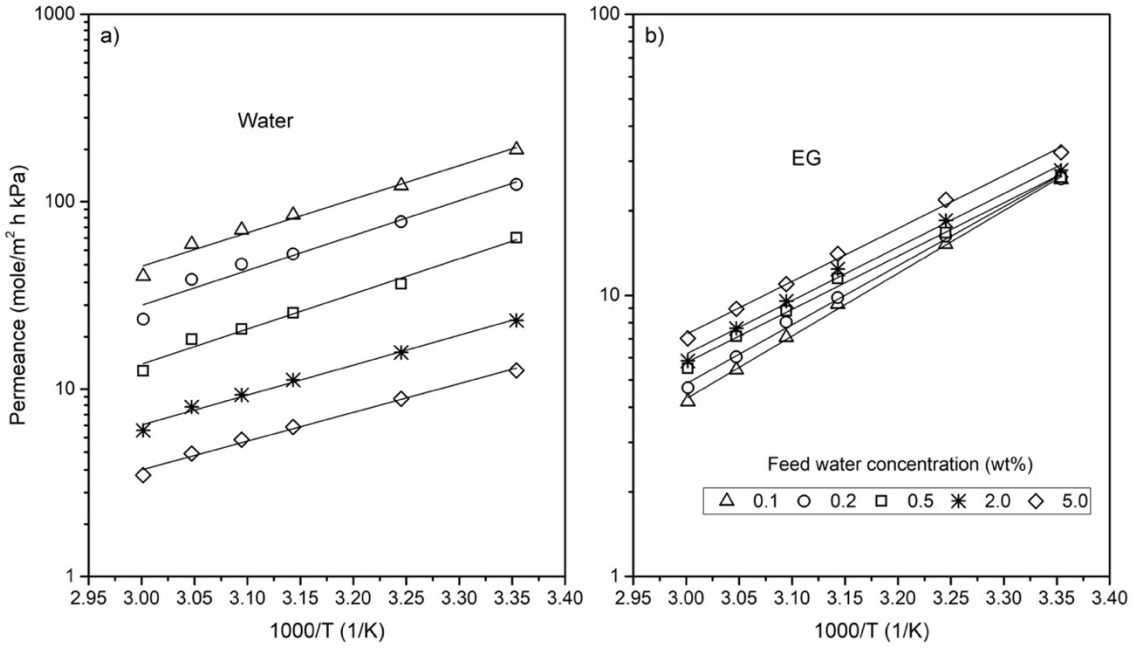

Figure 4. 5 Effects of temperature on the permeance of (a) water, and (b) EG through $(PEI/GO)_3$ membrane at different feed water concentrations.

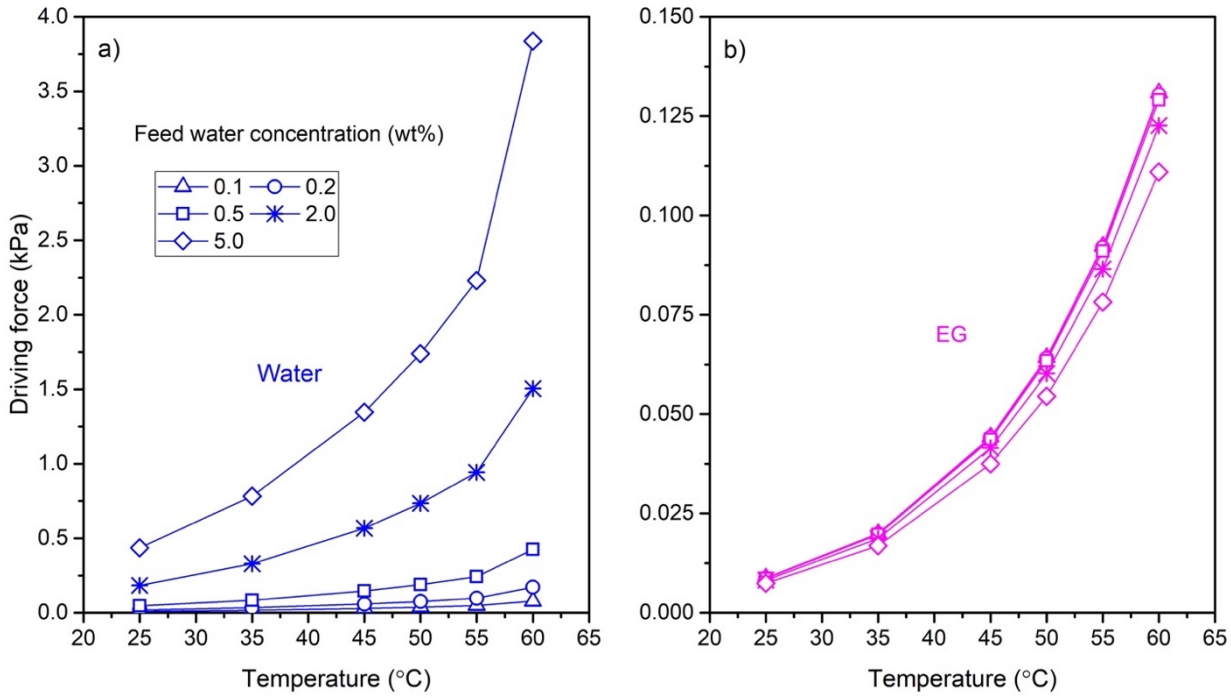

Figure 4. 6 Effects of temperature on the driving force of (a) water, and (b) EG molecules through $(PEI/GO)_3$ membrane at different feed water concentrations.

Table 4. 2 Activation energies of permeation of water and EG based on membrane permeance (E_p) through $(PEI/GO)_3$ membrane at different feed water concentrations.

Feed water concentration (wt%)	$E_{p,water}$ (kJ/mol)	$E_{p,EG}$ (kJ/mol)
0.1	-34.3	-42.7
0.2	-35.6	-40.2
0.5	-35.8	-36.2
2.0	-30.6	-36.4
5.0	-29.3	-36.0

Fig. 4.5 shows the membrane permeance as a function of reciprocal temperature and Table 4.2 summarizes the E_p data for EG and water. In particular, at a given temperature, the permeance of water through the membrane was higher than that of EG at low feed water concentrations. However, the opposite trend is true for the permeance of water when a feed water concentration was 5 wt%. Similar results were observed with other hydrophilic membranes for dehydration of EG [171,189]. The water clustering increased at higher feed water concentrations, resulting in lower water diffusion in the membrane [203]. Furthermore, separation in pervaporation is the sum of evaporation of the feed liquid and membrane selectivity [204]. At 5 wt% feed water concentration in the range of temperatures studied, the water/EG permeance ratio (selectivity) of the membrane (which is 0.4-0.5) was low; however, the membrane showed separation factors of 126 to 78. It implies that the separation achieved was more due to the selective evaporation, and the membrane had low impact on the separation [205]. Therefore, a membrane with more number of bilayers may potentially be required for the dehydration of EG with more than 5 wt% feed water concentration.

Fig. 4.5. also shows that the membrane permeance tended to decrease with a rise in temperature for both EG and water (to a greater extent), implying that temperature had a negative impact on the membrane permeance. As pervaporation occurs as per the solution-diffusion model, the permeability coefficient equals the product of the diffusion and solubility coefficients. Thus, E_p is equal to the activation energy for diffusion (E_D) plus the heat of sorption (ΔH_s) (i.e., $E_p = E_D + \Delta H_s$) [31]. Whereas E_D has a positive value, the enthalpy of sorption (ΔH_s) can be negative or positive depending upon whether the sorption process is exothermic or endothermic. Negative values of E_p for both water and EG permeation imply that the sorption process is exothermic (i.e., $\Delta H_s < 0$) and temperature affects the exothermic sorption more than it affects diffusion, causing

a decline in the membrane permeance. Moreover, the increase in permeation flux for each component strongly related to the increase in their saturated vapor pressures and thus driving force. Similar phenomena for dehydration of EG via pervaporation were reported in the literature [171,189,206]. In addition, Fig. 4.6 shows the calculated driving forces for each individual component at different feed water concentrations as a function of temperature, which is in line with the results in Fig. 4.5. Water had a higher driving force than EG, and the percentage decrease in water permeance is lower compared to EG permeance at all feed water concentrations.

4.3.3 The effects of salt on the dehydration of EG

NaCl and EG are commonly present in gas and chemical processing. The former occurs as the water phase produced is brine. Only a few studies have evaluated the pervaporation performance of ternary organics-water-salt mixtures [171,207–209]. The present study attempted to explore the performance of the $(PEI/GO)_3$ membrane for the dehydration of EG in the presence of NaCl, at different feed salt concentrations and operating temperatures. It was found that the $(PEI/GO)_3$ membrane was stable at the considered operating conditions. For instance, the membrane showed a total permeation flux of 91.6 g/m^2h and a separation factor of 375 for a feed water concentration of 1 wt% at 35°C. This membrane showed approximately the consistent pervaporation performance after conducting pervaporation experiments with different feed solutions (e.g., binary and ternary mixtures) at various temperatures ranging from 25 to 60 °C for about 4 months, with a total permeation flux of 94.5 g/m^2h and a separation factor of 363 for a feed water concentration of 1 wt% at 35°C, i.e., ~ 3.06 and 3.20 % changes in total permeation flux and separation factor, respectively.

Effects of feed salt concentration on the membrane performance in the ternary system

Fig. 4.7 presents the variations in separation factor, the water content in the permeate, total permeation flux, and partial permeation fluxes of water and EG for an EG-water-NaCl system as a function of feed NaCl concentration at a fixed temperature of 35 °C. The feed water concentration was on a salt-free basis. The water content in the permeate increased with an increase in NaCl content in the feed, particularly at lower feed water concentrations. For instance, when the feed NaCl content was increased from 0 to 0.5 wt%, the percentage increase in the permeate water concentration at a feed water concentration of 0.5 wt% was approximately 15.4 %; whereas, these values for the feed water concentrations of 2.0 wt% and 5.0 wt% are about 12.1% and 9.9%, respectively.

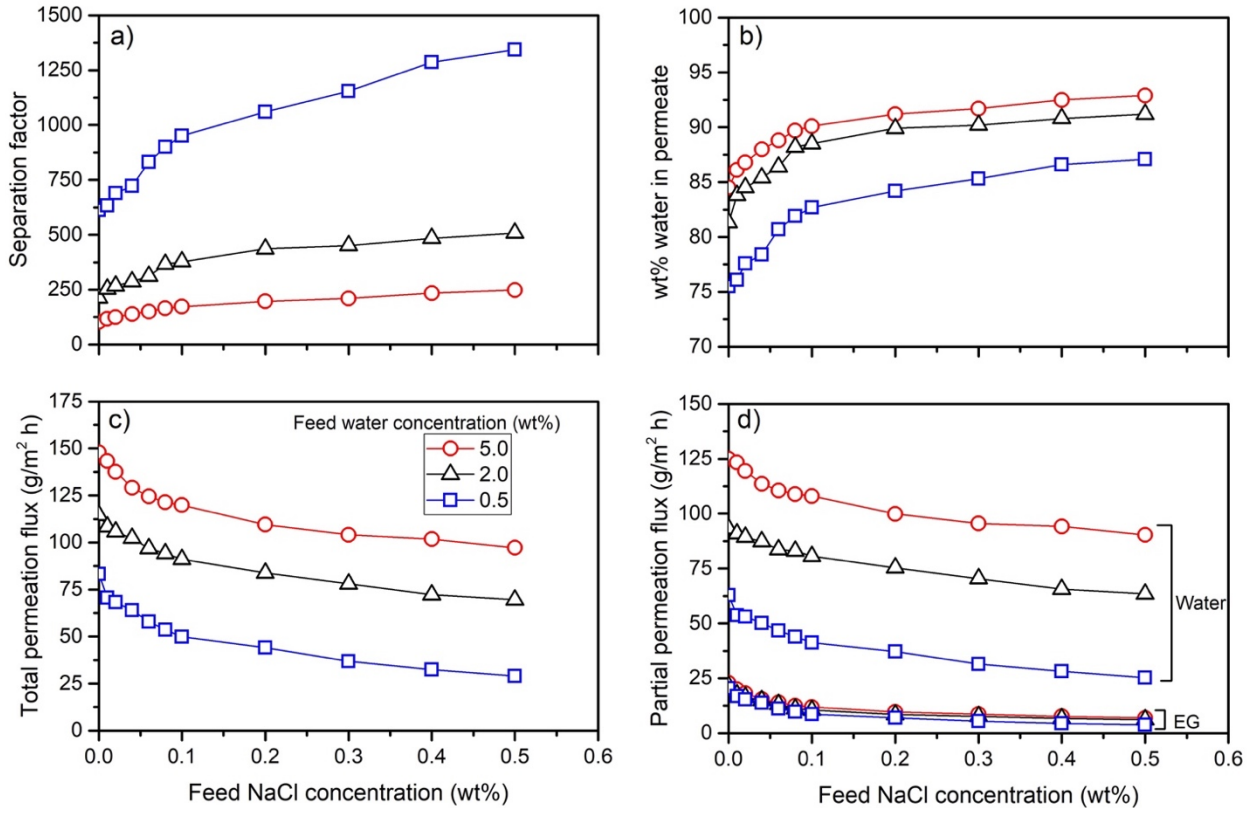

Figure 4. 7 Effects of feed NaCl concentration on (a) separation factor, (b) water content in permeate, (c) total permeation flux, and (d) partial permeation fluxes of water and EG through $(PEI/GO)_3$ membrane at 35 °C.

Based on Raoult's law, adding non-volatile NaCl to water decreased water vapor pressure, resulting in a lower driving force. In addition, the activity of water decreased due to the interactions with NaCl molecules, resulting in less membrane swelling [207,209,210]. Note that no salt precipitation or crystallization on the permeate side of the membrane was detected throughout the entire experiment. Moreover, no flux reduction was observed over time during the dehydration experiments for all feed NaCl concentrations, since probably salt did not physically block the membrane surface.

Effects of feed temperature on the pervaporation performance in a ternary system

Fig. 4.8 presents the effects of temperature on the partial fluxes of water and EG through $(PEI/GO)_3$ membrane, in the presence of salt, where the logarithmic fluxes and reciprocal temperature followed a linear relation. Experiments were performed by changing the feed NaCl concentration (i.e., 0-0.4 wt%) while keeping the feed water concentration constant at 0.5 wt% (salt-free basis). The permeation fluxes of both water and EG increased exponentially with the temperature at all feed NaCl concentrations when the temperature increased from 25 to 60 °C. It can be determined from the slope of the lines that the temperature dependency of water permeation flux was more remarkable at higher concentrations of feed NaCl, while the opposite happened for EG permeation. The apparent activation energies (E_J) for water and EG in the presence of NaCl are shown in Fig. 4.9. Note that the sodium chloride is more soluble in water than in EG [211], and the vapor pressure of EG and water decrease by salt concentration.

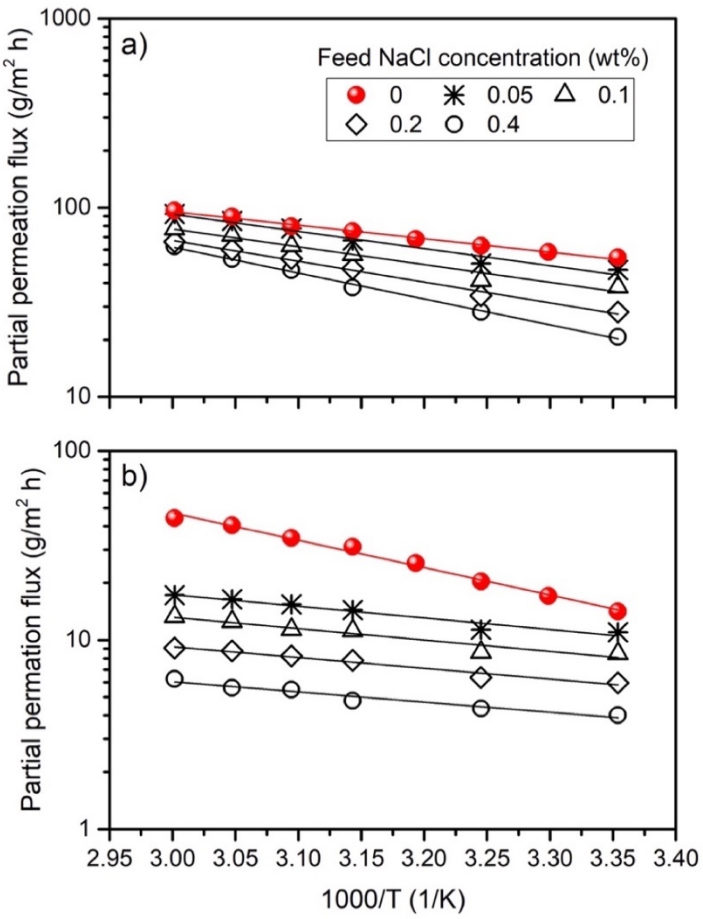

Figure 4. 8 Effects of temperature on permeation fluxes of (a) water and (b) EG at different feed NaCl contents, feed water concentration: 0.5 wt% (salt-free basis), and $(PEI/GO)_3$ membrane.

The apparent activation energy for permeation of water noticeably increased with an increase in NaCl content in the feed. The opposite was observed for EG, though the decrease in activation energy for EG was much more gradual. With an increase in temperature, the vapor pressure of water increased more noticeably than the vapor pressure of EG in the presence of salt, resulting in a higher water concentration in the permeate and the separation factor as shown in Fig. 4.10.

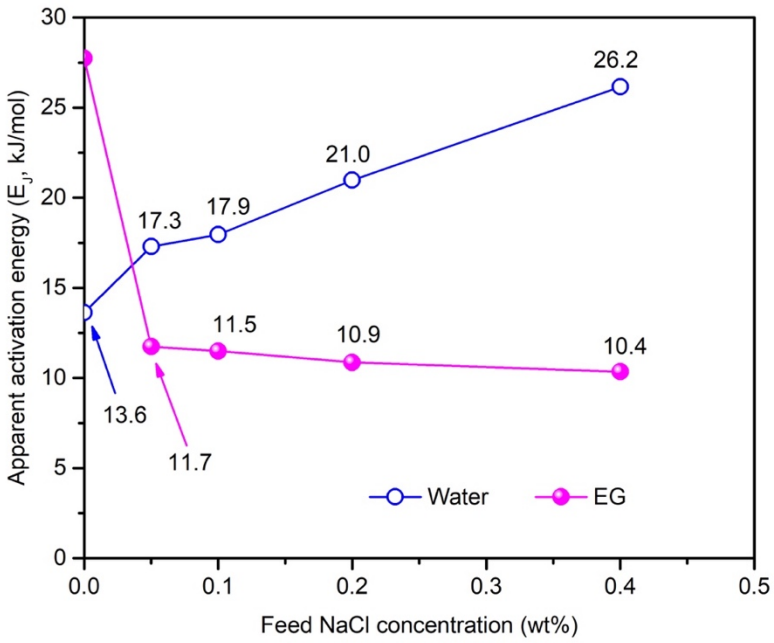

Figure 4. 9 Apparent activation energies (E_J) for permeation of water and EG based on permeation flux at different feed NaCl concentrations. Feed water concentration 0.5 wt% (salt-free basis), $(PEI/GO)_3$ membrane.

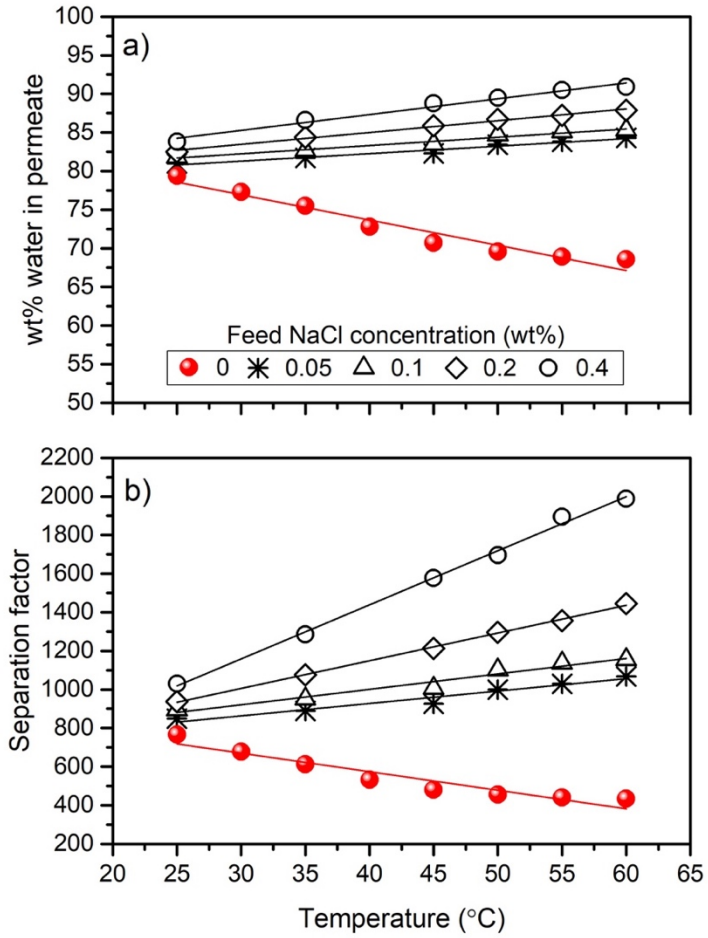

Figure 4. 10 Effects of temperature on: (a) water concentration in permeate, and (b) separation factor at different feed NaCl concentrations. Feed water concentration 0.5wt% (salt-free basis), $(PEI/GO)_3$ membrane.

4.3.4 Importance of number of bilayers to pervaporation performance

Fig. 4.11 shows the effects of the number of bilayers on total flux, separation factor, and partial permeation fluxes of water and EG, a feed with 5 wt% water was used at a fixed temperature of 35 °C. With an increase in the number of bilayers, the total permeation flux decreased while the separation factor increased. For instance, the total flux decreased from 163.7 to 101.8 (g/m^2 h) (i.e., a 38% decline) when the number of bilayers changed from 1 to 15; whereas the separation

factor increased from 82.6 to 204.5 (i.e., increased by 148%). Increasing the number of bilayers from 1 to 15 caused the EG flux to drop by almost 72%, while the water flux dropped by about 30%. Therefore, the membrane became more selective with an increase in the number of bilayers and the greater decrease in EG flux may be attributed to a larger molecule size of EG than water. The increase in selectivity was also at the expense of reduced permeance. Note that there might be non-selective interfacial defects when the number of bilayers was low. Defect-free membranes with stable active layers can be formed by increasing the depositions of PEI and GO layers.

The membrane resistance is expected to increase proportionally when the membrane thickness increases [10]. Based on the resistance-in-series approach, the overall mass transfer resistance of a component in composite membranes is the sum of the resistance in the bilayers and a substrate. A straight line should be attained by plotting inverse flux as a function of the number of bilayers (Fig. 4.12). The slope of the line gives the mass transfer resistance related to per bilayer, and the intercept gives the mass transfer resistance related to the substrate [212]. Table 4.3 presents data of membrane resistance for permeation of water and EG. As expected, the mass transfer resistance of the bilayers and substrate showed a positive correlation with the number of bilayers (Appendix D). The mass transfer resistance per bilayer for permeation of EG is higher than that of water, which indicates that the selectivity can be controlled by the number of bilayers. The substrate resistance for permeation of water and EG in an original TFC membrane without chlorine treatment (at the same feed concentration and operating temperature) were 11.2×10^{-2} and 3.2×10^{-2} ($\frac{m^2.h.kPa}{mol}$), respectively. It confirms that the TFC membrane resistance for permeation of components decreased after chlorine treatment (see Table 4.3). However, it should be noted that at 5wt% feed water concentration, the intrinsic membrane selectivity was low and separation obtained with such a substrate was mostly due to the different relative volatility of EG and water

(see Figure 4.5). Therefore, the selectivity of the LbL membrane can be improved by depositing an additional number of PEI/GO bilayers on the substrate. Moreover, the straight lines suggest that the bilayer build-up was uniform. Liu et al. [213] reported that the thickness of an active layer is directly correlated with the number of bilayers. The diffusion pathway length and the mass transfer resistance for both water and EG molecules increased with the addition of bilayers, thereby decreasing the permeation flux. Table 4.4 shows a comparison of the pervaporation performance of the $(GO/PEI)_x$ LbL membranes prepared in this study with other membranes reported in the literature.

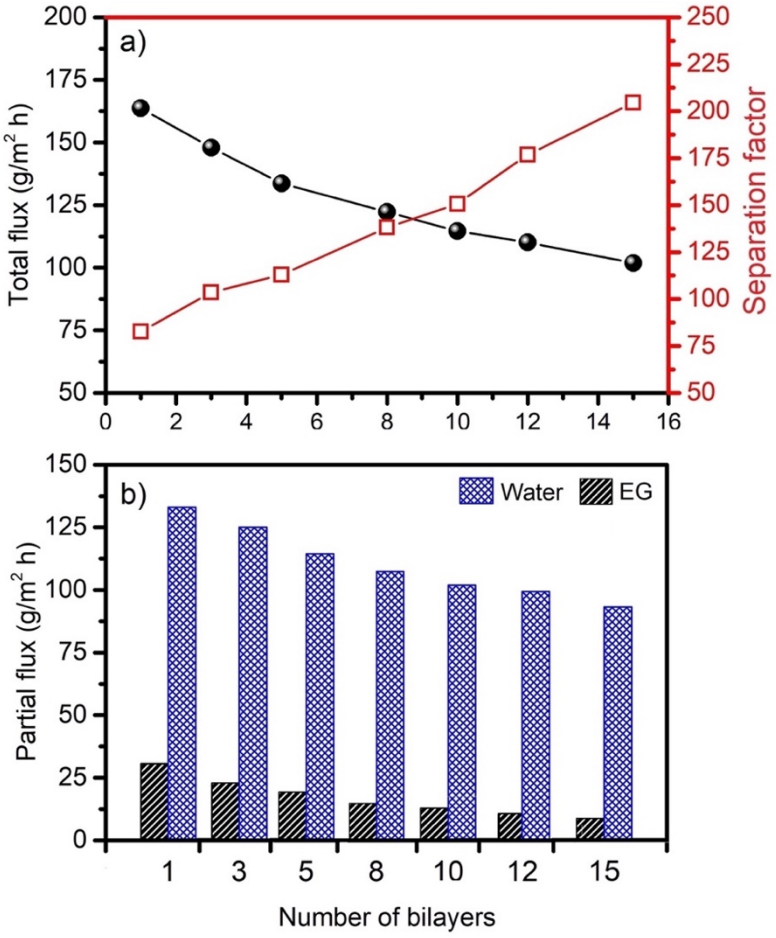

Figure 4. 11 Effects of the number of bilayers on (a) total flux and separation factor, and (b) partial permeation fluxes of water and EG. Feed water concentration: 5 wt%, operating temperature: 35 °C.

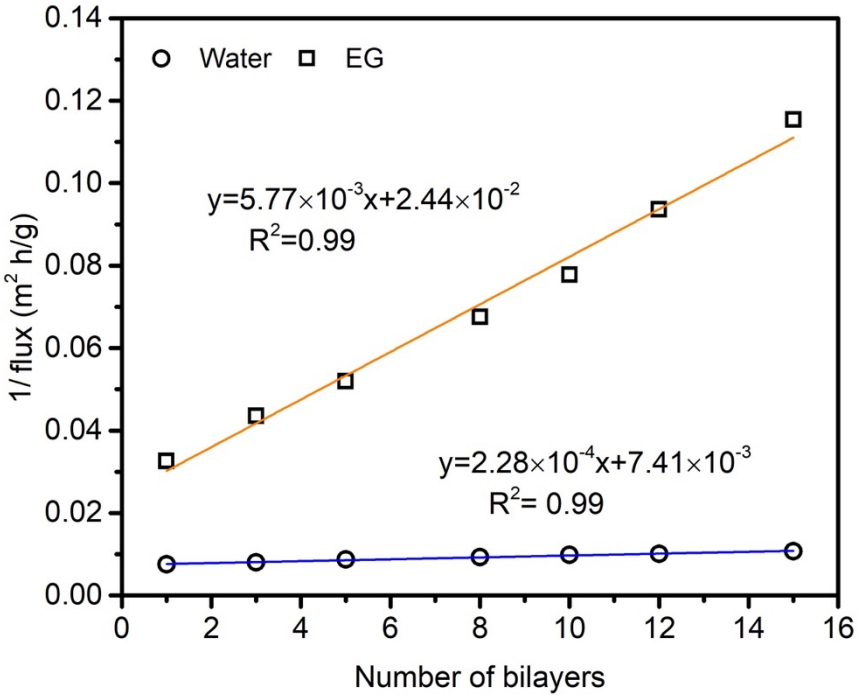

Figure 4. 12 Inverse of the partial flux of water and EG as a function of the number of bilayers. Feed composition: 5wt% water, operating temperature: 35 ºC.

Table 4. 3 Membrane resistance for permeation of water and EG. Feed composition: 5wt% water, operating temperature: 35 ºC.

Component	Resistance per bilayer ($\frac{m^2.h.kPa}{mol}$)	Substrate ($\frac{m^2.h.kPa}{mol}$)
EG	6.05×10^{-3}	2.55×10^{-2}
Water	3.21×10^{-3}	10.43×10^{-2}

Table 4. 4 A comparison of pervaporation performance of membranes for dehydration of ethylene glycol.

Membrane	Feed water concentration (wt%)	Temperature (°C)	Flux (g/m^2h)	Separation factor	Ref.
CS/PAA PECM	20	70	165	258	[214]
CS/PAA PECM	20	70	216	105	[215]
PEI/PAA-polyamide	3	40	400	340	[143]
PEI/PAA-polyamide	10	22	12	410	[145]
PES-PD/Polyamide/PD	2.4	38	81	388	[171]
PES-PD/Polyamide/PD	19.2	38	429	196	[171]
$(PEI/GO)_3$ LbL	2	35	114	213	This work
$(PEI/GO)_3$ LbL	5	35	148	103	This work
$(PEI/GO)_{15}$ LbL	5	35	102	205	This work

CS: Chitosan, PAA: poly(acrylic acid), PECM: polyelectrolyte complex membrane, PEI: polyethyleneimine, PES: polyethersulfone, PD: polydopamine, PVA: polyvinyl alcohol

4.3.5 Characterization of the membrane surface with different bilayers

ATR-FTIR was used to confirm the functional groups of PEI/GO LbL membrane with a different number of bilayers. Fig 4.13 shows the ATR-FTIR spectra of GO, Cl-TFC polyamide (a), $(PEI/GO)_3$ LbL (b), $(PEI/GO)_8$ LbL (c), and $(PEI/GO)_{12}$ LbL (d) membranes. The characteristics peaks of GO were observed at 3253 cm^{-1} (–OH stretching in hydroxyl groups), 1738 cm^{-1} (C=O stretching vibration in carboxyl groups), 1620 cm^{-1}(unoxidized sp^2 aromatic C=C bonds), 1418 cm^{-1} (the bending vibration of C-OH) , and 1220 and 1085 cm^{-1} (the stretching vibration of C–O in epoxy and alkoxy groups, respectively) [161,216]. The characteristic peaks of the membranes were observed at 1544 cm^{-1} (N—H in-plane bending, amide II), 1598 cm^{-1} (C=C

ring stretching), 1660 cm^{-1} (C=O stretching, amide I) and 3363 cm^{-1} (N—H stretching, amide II) which are related to the Cl-TFC substrate [168]. The broad peak at ~3363 cm^{-1} was intensified in PEI/GO membrane with different bilayers compared to that of the chlorinated substrate. It can be assigned to the stretching vibrations of the O—H groups in GO nanosheets and N—H stretching (amide II) in PEI structure, showing successful assembly of GO on the PEI layer. The intensity of this peak increased by increasing the amount of GO on the surface layer or number of bilayers [119,169].

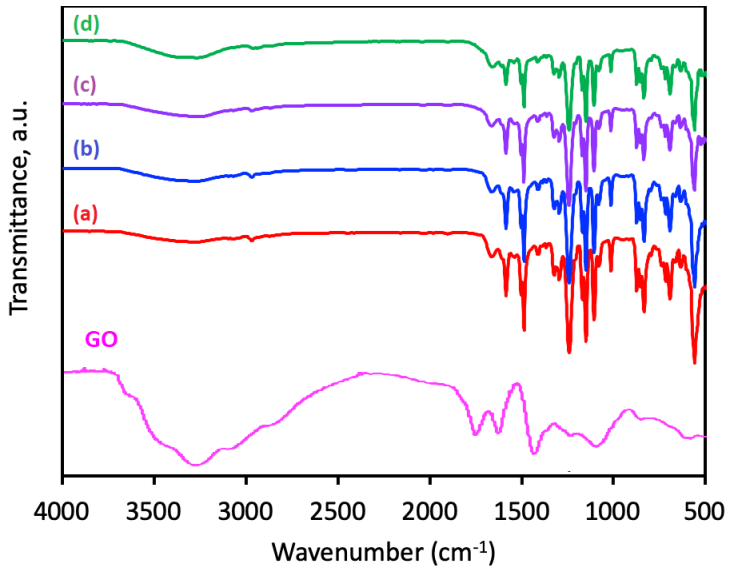

Figure 4. 13 ATR-FTIR spectra of GO, Cl-TFC polyamide (a), $(PEI/GO)_3$ LbL (b), $(PEI/GO)_8$ LbL (c), and $(PEI/GO)_{12}$ LbL (d) membranes

The mean surface roughness (Ra) values of the (PEI/GO) membranes decreased with an increase in the number of bilayers, which was confirmed by the AFM. Fig. 4.14 shows the 3-D and 2-D images of the surface morphology of the membranes with different bilayers. The bright and dark regions are peaks and valleys, respectively [170]. The Ra value of the (PEI/GO) membrane decreased from 41.02 nm to 20.91 nm when the number of bilayers increased from 3

to 12, respectively. This finding may relate to the depositing PEI and GO preferentially covered the valley regions of the membranes.

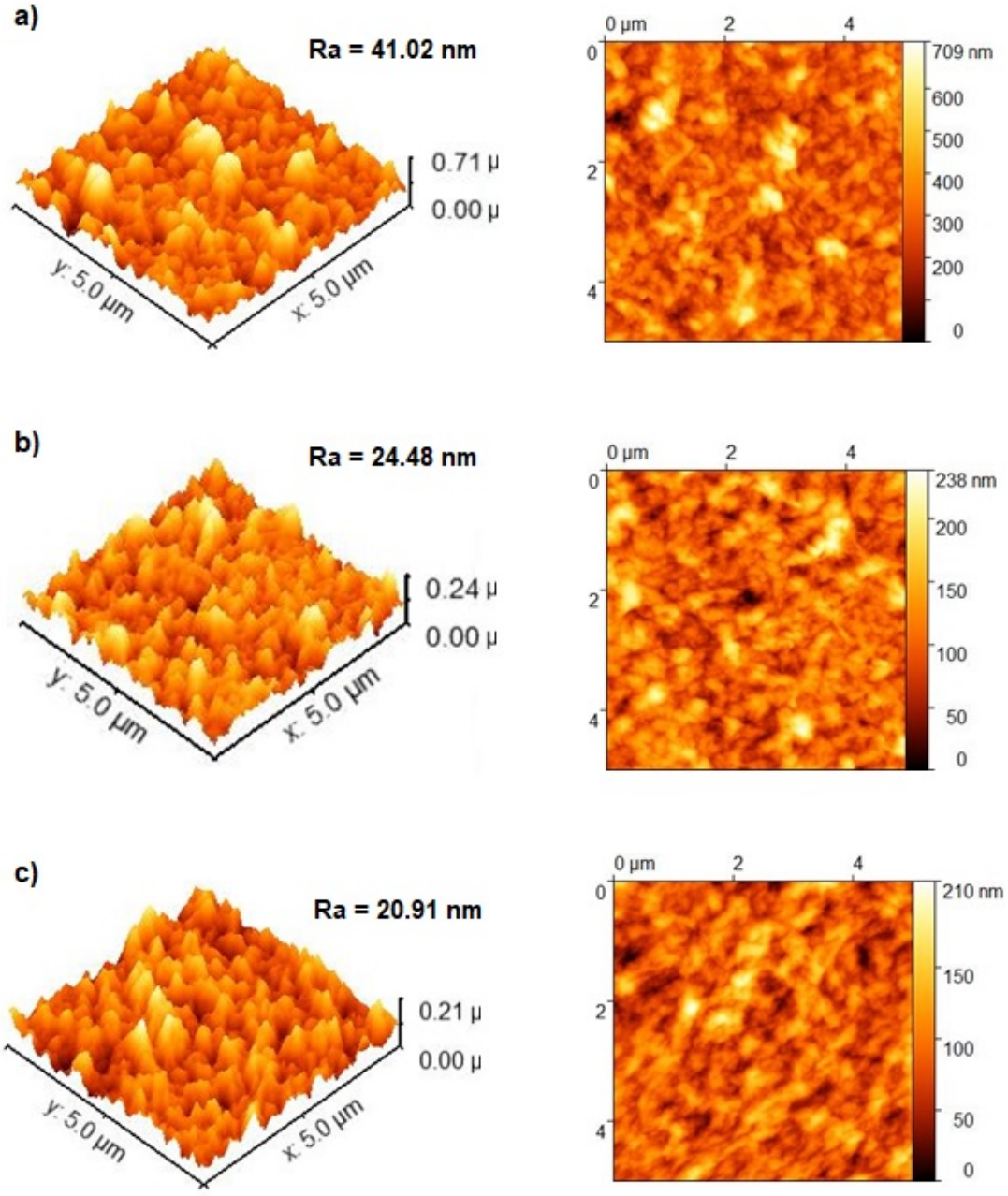

Figure 4. 14 3D and 2D AFM images of the (a) $(PEI/GO)_3$, (b) $(PEI/GO)_8$, and (c) $(PEI/GO)_{12}$ LbL membranes, (scanned area: 5 µm × 5 µm).

Furthermore, the water contact angles of the (PEI/GO) membranes with different bilayers were measured. As shown in Fig. 4.15, all membranes are hydrophilic, and their water contact angles increased from 41.5° to 54.2° when the number of bilayers increased from 3 to 15, respectively. This finding may attribute to the increasing content of GO nanosheets on the membrane surface as the GO nanosheets contain hydrophobic aromatic regions and abundant hydrophilic groups on the defect regions or around the boundaries [198]. Moreover, the increase of water contact angles was probably owing to the decrease of surface roughness at a higher number of bilayers.

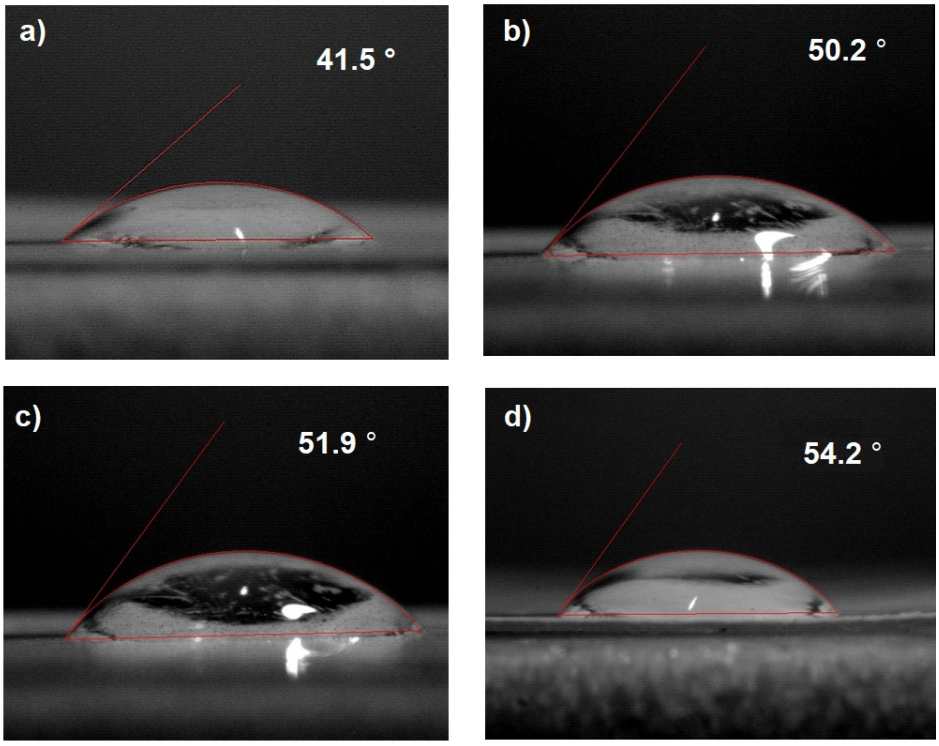

Figure 4. 15 Water contact angle measurements of (a) $(PEI/GO)_3$, (b) $(PEI/GO)_8$, (c) $(PEI/GO)_{12}$, and (d) $(PEI/GO)_{15}$.

4.4 Conclusions

In this study, PEI/GO LbL membranes with a different number of bilayers have been fabricated and studied for the dehydration of EG via pervaporation. The impacts of temperature, feed concentration, and the number of bilayers for pervaporation of binary water/EG, and ternary water/EG/salt mixtures were examined. The following conclusions may be made:

(1) The alternate deposition of oppositely charged GO and PEI on the chlorinated TFC polyamide was shown to be successful for assembly of the membrane under electrostatic interactions and hydrogen bonds between ionized carboxyl groups on GO and protonated groups on PEI. The PEI/GO membrane with three bilayers had considerably good permeation flux and selectivity for the dehydration of EG, presumably due to the dense ultrathin surface layer.

(2) An increase in feed temperature resulted in a higher permeation flux but a lower separation factor for the dehydration of EG. The separation factor decreased by temperature for the separation of binary water/EG solution. However, the reverse was true when salt was present in the feed because the vapor pressure of water increased more noticeably than the vapor pressure of EG.

(3) The presence of NaCl in the feed mixture decreased the permeation flux and increased the water concentration in the permeate. Therefore, pervaporation seemed to be an attractive technique for simultaneous separating out salt and EG from the feed stream.

(4) Membrane performance could be tailored by adjusting the number of bilayers. Membrane resistance per bilayer for permeation of water was lower than that for EG (for feed water concentration of 5 wt%); however, the opposite was true for substrate resistance. As a result,

with an increase in the number of bilayers, the selectivity of the LbL membrane could be improved.

Chapter 5

Thin film composite membranes via layer-by-layer assembly of graphene oxide and polyethyleneimine for ethanol and isopropanol dehydration

5.1 Introduction

Pervaporation, a promising membrane-based technology, is applied in three main areas: 1) dehydration of organic solvents, 2) recovery of organic compounds from water, and 3) separation of organic-organic liquids [4,10,21]. The dehydration of alcohols is the most developed area of applications, especially when the feed has only a low quantity of water (<20 wt%) [6,11]. Among the alcohols, ethanol (EtOH) is the most common renewable biofuel resource [217], and isopropanol (IPA) is widely used in electronic and pharmaceutical industries where high purity IPA is needed [218]. Both EtOH and IPA form azeotropes with water at an alcohol concentration of around 96 and 88 wt%, respectively [3,218]. Some of the physical properties of EtOH, IPA and water are listed in Table 5.1. Compared with the traditional separation processes such as adsorption and distillation, pervaporation is generally a cost/energy-effective approach to breaking azeotropes and removing a trace amount of water [218], mainly because pervaporation is particularly suitable for removing minor components from the bulk feed [11]. Moreover, the separation mechanism of pervaporation is based on solution-diffusion, and only the latent heat of evaporation of the

permeate is needed for the separation. Therefore, pervaporation is not limited by thermodynamic vapor-liquid equilibrium (VLE) and can be used in the separation of azeotropic or close-boiling mixtures [4]. Integrating pervaporation with other conventional separation processes appears to be effective to further improve the separation performance [3].

Table 5. 1 Physical property of EtOH, IPA, and water.

	Ethanol	Isopropanol	Water
Molecular weight (g/mol)	46	60	18
Kinetic diameter (Å)	4.3	4.6	2.7
Molar volume (10^{-6} m^3/mol)	58	76	18
Molecular diameter (nm)[a] (25°C)	0.57	0.62	0.39
Hydrogen bonding parameter[b] $(MPa)^{0.5}$ (25°C)	19.4	16.4	42.3
Boiling point (°C)	78	82	100
Solubility parameter[a] ($MPa^{-0.5}$)	26.5	23.5	47.8
Refractive index, nD (25°C)	1.36	1.37	1.33
Vapor pressure (25°C) (kPa)	7.8	5.8	3.1
Heat of vaporization at 1 atm (kJ/mol)	38.6	44.0	40.7

[a] From reference [75]
[b] From reference [219].

A key component for dehydration of organic solvents is hydrophilic (or water permselective) membranes [51], and layer-by-layer (LbL) assembly is one of the well-known methods to fabricate nanoscale anionic-cationic multilayers on a substrate through sequential deposition of oppositely charged polyelectrolyte solutions or nanoparticle suspensions [77,194]. LbL membranes have a significant affinity to water molecules, and the deposited nanolayers offer improved water transport through the membrane [11,220]. The main driving force for the assembly buildup is

coulombic (electrostatic) interactions between oppositely charged ions, and hydrogen bonding is another means of assembly [51]. This bottom-up approach was first introduced by Iler [221], and it received great attention for nanoassembly after work of Decher et al. [77,82]. In 1998, Tieke et al. used LbL membranes for pervaporative separation of EtOH/water [222]. Since then, a variety of LbL membranes have been successfully prepared for gas separation [222,223], pervaporation [222,223], reverse osmosis (RO) [119], forward osmosis [17], and nanofiltration (NF) [16,198].

The LbL membranes are prone to swelling when exposed to alcohol/water mixtures due to their hydrophilic nature. Both water and alcohol are polar and can swell the polyelectrolyte layers. Therefore, nanolayers formed by cation-anion interactions are not stable when extreme swelling and interchain stretching occur, resulting in a low selectivity [51,75]. Kim et al. [224] described that polyelectrolyte multilayer performed differently for the organic/water mixtures, and the polymer coils can be softened or contracted in different organic solvents. Zhang et al. [75] confirmed that EtOH and IPA can wash away some polyelectrolyte macromolecules deposited onto polyamide membranes, and Poptoshev et al. [225] showed that polyelectrolytes multilayers may disassemble in certain organic solvents, resulting in the film collapse. In such cases, chemical crosslinking may be used to alleviate membrane swelling and to augment membrane stability and performance [75,226]. Membrane crosslinking restricts polymer-chain mobility and leads to stiffer more-compact membrane structures. Crosslinked membranes usually show a lower permeation flux and higher separation factor because of increased diffusion resistance after crosslinking [57,220,227]. Aldehydes are often used as crosslinking agents as they are highly reactive with many functional groups in polymers commonly used for pervaporation membranes [57,75,216,228–230].

To prepare membranes via LbL assembly, selecting appropriate substrates and polyelectrolytes are of primary importance. In this study, thin film composite (TFC) polyamide membrane was chosen as a substrate because of its negative surface charge, which favors the deposition of polycation. Moreover, the number of polyelectrolyte depositions needed to prepare a defect-free permselective membrane was reduced due to its thin dense skin layer [75,119]. Graphene oxide (GO) and polyethyleneimine (PEI) were used as the anionic and cationic depositing components, respectively. GO nanosheets hold a unique carbon nanostructure with abundant hydrophilic functional groups, allowing faster passage of water. In addition, GO nanosheets functioned as polyanions when dispersed in water due to the ionization of hydroxyl and carboxyl groups. Consequently, the nanosheets can interconnect with polycations (e.g., PEI) through electrostatic attraction and hydrogen bonding [17,108,138,194]. Therefore, GO may be used as an appropriate candidate anionic nanomaterial to offer a solid "brick-and-mortar" LbL structure. On the other hand, PEI is a polycation due to its amine functional groups in the backbone, and its hydrophilic nature makes it a popular choice for constructing water-permeating membranes. To improve the performance of the prepared LbL membranes, glutaraldehyde (GA) was used as a crosslinking agent. GA can react with the amine groups in PEI and hydroxy groups in GO, as schematically illustrated in Fig. 5.1 [75,216,231].

To our best knowledge, no reports are currently available in the literature on the preparation of PEI/GO LbL membranes assembled on a TFC substrate and chemically crosslinked with GA for alcohol dehydration via pervaporation. The objective of this research was to fabricate PEI/GO LbL membranes by crosslinking each bilayer for EtOH and IPA dehydration. The effects of crosslinking conditions (e.g., temperature, time, and crosslinker concentration) on the permeation flux and separation factor were investigated, and the effects of the interactions of these factors

were evaluated through a two-level factorial design. The results were used to find the optimal ranges of the crosslinking parameters by considering the trade-off between permeation flux and separation factor. Then, a membrane prepared within the proposed optimal ranges was further studied for pervaporation separation. The as-prepared membrane was initially tested to compare its performance for the alcohol dehydration at different feed concentrations and operating temperatures. The effects of the number of bilayers on the membrane performance were then investigated to correlate membrane thickness, mass transfer resistance, permeation flux, and selectivity. Water sorption uptake was measured to study the degree of swelling of the bilayers. The long-term stability of the crosslinked membrane was also investigated. The morphology and hydrophilicity of the (PEI/GO) LbL membranes with different bilayers were examined using atomic force microscopy (AFM) and contact angle measurements, respectively.

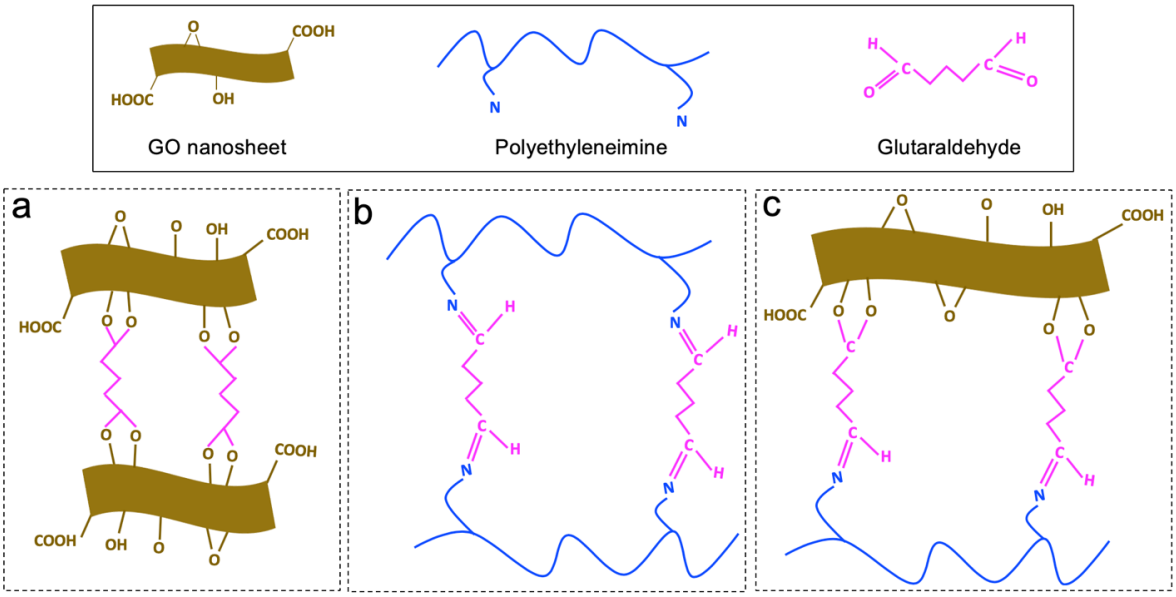

Figure 5. 1 Schematic crosslinking mechanism of (a) graphene oxide, (b) polyethyleneimine, and (c) polyethyleneimine and graphene oxide with GA.

5.2 Experimental

5.2.1 Materials

A commercial thin-film composite polyamide membrane produced by interfacial polymerization (supplied by GE water) was used as a substrate. Graphite flakes were obtained from Alfa Aesar Chemical Manufacturing Company. Graphite was oxidized into GO using potassium permanganate ($KMnO_4$, >99%, Merck), phosphoric acid (H_3PO_4, 85% solution in water, Acros), hydrogen peroxide 30% (H_2O_2, 30%, Sigma-Aldrich) and sulfuric acid (H_2SO_4, 95-98%, Sigma-Aldrich) [153]. The synthesized GO nanosheets were rinsed with hydrochloric acid (HCl, 37%, Merck), ethanol (Sigma-Aldrich) and De-ionized (DI) water. Branched polyethyleneimine (PEI, average $M_w \sim$ 25,000, Sigma-Aldrich) was used as a polycation. The TFC polyamide surface was then treated with sodium hypochlorite solution (NaClO, 14.5% available chlorine, BDH Chemicals) before being used as a substrate for LbL assembly. GO suspension was used as an anionic component at its natural pH (~ 6), and the prepared GO solution was well-sonicated for 15 min before use. Glutaraldehyde (GA, 25% in water, Sigma-Aldrich) was employed as a crosslinking agent. Isopropanol was purchased from Fisher Scientific. Aqueous solutions of alcohols with desired feed concentrations were prepared with DI water.

5.2.2 The preparation of GO/PEI LbL membrane preparation

GO nanosheets were produced from graphite powder following an improved method [153], resulting in a large amount of hydrophilic oxidized graphene materials with fewer defects in the basal plane as compared to GO prepared by the original Hummers' method [153,154]. The uniform GO solution was diluted to the desired concentration before use. Fig. 5.2 is a schematic of the LbL process for membrane preparation. The TFC polyamide support membrane was initially treated with an aqueous chlorine solution, (sodium hypochlorite concentration 6000 ppm), for 30 min to

impart a strong negatively charged surface (denoted as Cl-TFC). The active polyamide skin layer became thinner and less compact through controlled chlorination [143,152]. The Cl-TFC substrate was then soaked in DI water overnight to remove sodium hypochlorite residue. To build up an individual bilayer, the Cl-TFC polyamide substrate membrane was brought into contact with: (a) a solution of cationic PEI (0.02 monomol/L, 45 min), (b) pure water (15 min), (c) a solution of anionic GO (100 ppm, 45 min), and (d) pure water (15 min), respectively. To fabricate a crosslinked LbL membrane, GA solutions at given concentrations were brought into contact with the membrane after steps (b) or (d). It should be mentioned that each crosslinking step was also followed by rinsing with DI water. Deposition of the solutions onto the membranes was carried out in a stainless steel membrane cell. The thin separating structure of the membrane was built up by the repetition of the sequential deposition steps. In each deposition step, a polyelectrolyte or GO layer was adsorbed to induce surface charge reversal [232]. The resulting membranes were dried in a vacuum oven at 45°C overnight. For convenience of discussion, the crosslinked LbL membrane was designated as XL$(PEI/GO)_z$, where z refers to the number of PEI/GO bilayers, and the LbL membrane without crosslinking was denoted as $(PEI/GO)_z$.

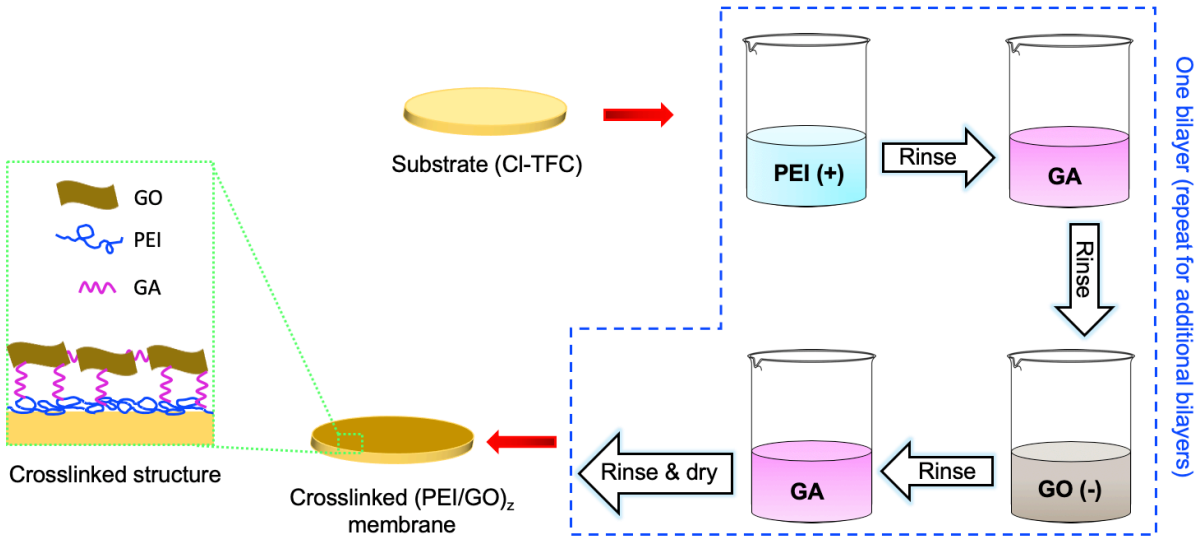

Figure 5. 2 Schematic diagram for membrane fabrication.

5.2.3 Membrane characterization

The surface hydrophilicity of membranes with different numbers of bilayers was evaluated by conducting static contact angle measurement with a contact angle goniometer (VCA 2500 XE, AST Products) at room temperature. The average value of contact angles at three arbitrary locations was reported for each membrane sample using an average water droplet size of 2 μL. The surface morphology and roughness of the membranes were characterized using atomic force microscopy (AFM) (Bruker Innova, USA). To confirm the chemical structures of GO nanosheets and LbL membranes, Fourier Transform Infrared spectroscopy (FTIR, Bruker Tensor 27 IR) was used over a wavelength range of 500 to 4000 cm^{-1}.

The sorption uptake of water in the PEI/GO bilayers was measured as follows: (1) samples of the same area of the Cl-TFC substrate (W_1) and XL(PEI/GO)$_7$ (W_2) were dried in a vacuum oven overnight to remove the moisture, (2) the pre-weighed dry membranes was immersed in DI water

at room temperature for 48h to allow the membranes to reach sorption equilibrium, (3) After gentle wiping dry of water drops off the membrane surface with tissue papers, the weights of the Cl-TFC substrate (W_3) and XL(PEI/GO)$_7$ (W_4) were determined. The degree of swelling (S) of the PEI/GO bilayers in water was determined with regard to water sorption uptake in the bilayers per g of the surface of the bilayer:

$$S = \frac{(W_4 - W_3) - (W_2 - W_1)}{(W_2 - W_1)} \quad (5.1)$$

5.2.4 Pervaporation study

Pervaporation experiments were performed for the separation of EtOH/water and IPA/water mixtures. The dehydration performance of the LbL membranes measured in terms of permeation flux (J) and separation factor (α). The membrane area for permeation was 17.4 cm^2, and it was mounted in the permeation cell with the PEI/GO bilayers facing the feed solution. The downstream side was evacuated using a vacuum pump and maintained below 0.1 kPa absolute. The permeate vapor was collected periodically at specific time intervals using cold glass traps immersed in liquid nitrogen, and the permeate sample was analysed using an Atago 3810 refractometer. The total permeation flux was determined from the weight of collected permeate (V) over a period of time (t):

$$J = {}^{V}/_{At} \quad (5.2)$$

where A is membrane area for permeation.

The separation factor, which measures the extent of the pervaporation separation, is determined as:

$$\alpha = \frac{Y/(1-Y)}{X/(1-X)} \quad (5.3)$$

where *X* and *Y* are the mass fraction of water in the feed and permeate solutions, respectively. The partial fluxes of alcohol and water can be found from the permeate composition and total flux. The experimental data, recorded when no further difference in the permeate flux and composition could be detected, represent an average of five measurements under identical conditions. Note that water-enriched permeate removed by the membrane was compensated for by adding the same amount into the feed to maintain a constant composition during each experimental test.

5.2.5 Factorial design study

In order to assess the impacts of individual factors involved in membrane crosslinking (i.e., concentration, time and temperature) on the permeation flux and separation factor, a two-level factorial design was considered to provide additional information on the potential interactions that can hardly be identified using the classical "one-variable-at-a-time" method [233]. A total of eight experiments were performed to capture all combinations of the levels of the factors. The variable factors and their values are presented in Table 5.2, where the codes "+" and "-" indicate the "high" and "low" levels of a factor, respectively. Table 5.3 presents the experimental design where three replicates were conducted for each run.

Table 5. 2 Variables, their coded levels used in the factorial design.

Variables		-	+
A	Crosslinker concentration (wt%)	0.3	2
B	Crosslinking time (h)	0.16	2
C	Crosslinking temperature (ºC)	22	55

Multiple linear regression (MLR) analysis was used to determine the relationship between the response (i.e., flux and separation factor) and the variables. Based on fitting a linear function with respect to main and interaction coefficients for each response, MLR is commonly used to estimate the coefficient of model parameters. The significance of each model term is then assessed through the analysis of variance (ANOVA) table (**Appendix E**).

Table 5. 3 Experimental runs and results for two-level factorial study for EtOH dehydration at 22° C and feed concentration of 98 wt% EtOH.

Membrane No.	Factors			Responses	
	A	B	C	J (g/m^2 h)	α
N1	-	-	-	1231	37.6
N2	-	+	-	639	69.4
N3	+	-	-	802.3	57.5
N4	+	+	-	339	113.2
N5	-	-	+	1055	48.4
N6	-	+	+	536	99.5
N7	+	-	+	754	82.4
N8	+	+	+	279	128.5

Since the interaction terms are considered in the MLR analysis, the data are normalized with respect to the mean and standard deviation of each parameter to provide a comparable coefficient for each term as the scales of the factors are different. In the present study, Data Analysis Toolpak and Minitab (Minitab® 17.2.1) were used to determine main effects (i.e., A, B and C), two-way interactions (i.e., AB, AC, and BC) and three-way interaction effect (ABC).

5.3 Results and discussion

5.3.1 Experimental design for ethanol dehydration

Table 5.3 shows the pervaporation results for EtOH dehydration with the eight membranes prepared based on a 2^3 factorial design. For ease of comparison, the separation factor is also plotted against corresponding permeation flux in Fig. 5.3.

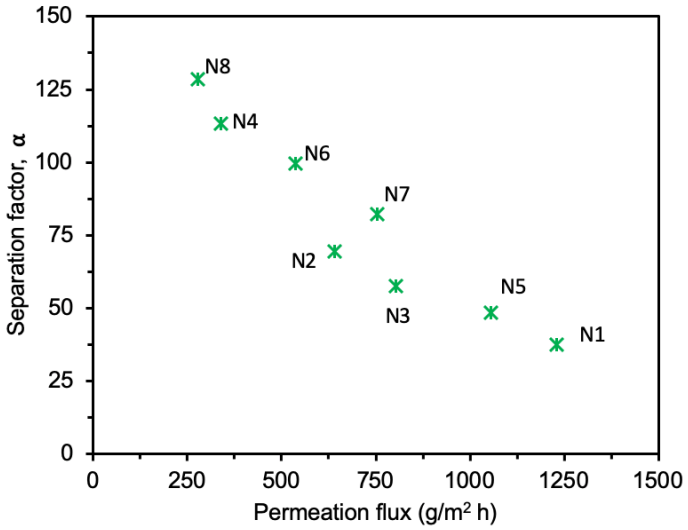

Figure 5. 3 The membrane separation factor vs. permeation flux. The membrane numbers are given in Table 5.3.

Table 5.4 shows the MLR analysis for individual response. In statistics, a probability value (p-value) can be viewed as the probability that the relationships in data are caused by chance. A p-value for each term tests the null hypothesis that the coefficient is equal to zero (no effect). A small p-value (< 0.01, for a 99% confidence interval) means that a result is most probably not caused by chance, indicating that there is an underlying relationship in the data [234]. A small p-value indicates that the null hypothesis can be rejected. In other words, a factor that has a smaller p-value is likely to have a more significant impact as the changes in the factor's value are related to the

changes in the response variable. Conversely, a larger (insignificant) p-value suggests that changes in the factor are not associated with changes in the response. The impacts of all three individual factors are statistically significant on the flux and separation factor since the p-values are smaller than 0.01. Among the interaction terms, BC is not significant for the flux, and AC is insignificant for the separation factor (p-value > 0.01). Using the coefficient values calculated by ANOVA, the linear model for 2^3 factorial designs can be expressed as (Appendix E):

$$J = 703.26 - 165.93\mathrm{A} - 260.43\mathrm{B} - 47.89\mathrm{C} + 23.26\mathrm{AB} + 24.46\mathrm{AC} + 7.32\mathrm{BC} - 12.80\mathrm{ABC} \quad (R^2 > 0.99) \tag{5.4}$$

$$\alpha = 79.52 + 16.14A + 23.58B + 10.34C + 2.39AB - 0.04AC + 1.21BC - 3.83ABC \quad (R^2 > 0.99) \tag{5.5}$$

Table 5. 4 ANOVA table for the MLR analysis on the permeation flux and separation factor for EtOH dehydration.

	Flux, J		Separation factor, α	
Terms	Coefficients	P-value	Coefficients	P-value
A	-165.93	<0.0001	16.14	<0.0001
B	-260.43	<0.0001	23.58	<0.0001
C	-47.89	<0.0001	10.34	<0.0001
AB	23.26	<0.0001	2.39	<0.0001
AC	24.46	<0.0001	-0.04	0.3510
BC	7.32	0.0307	1.21	<0.0001
ABC	-12.80	0.0009	-3.83	<0.0001

As mentioned earlier, a smaller value of p means a more significant impact on membrane performance. The significance of model parameters that indicate which terms have a higher impact on the responses was determined and then visualized through re-scaling of p-values (i.e., $-\log_{10}$(p-value) (Fig. 5.4).

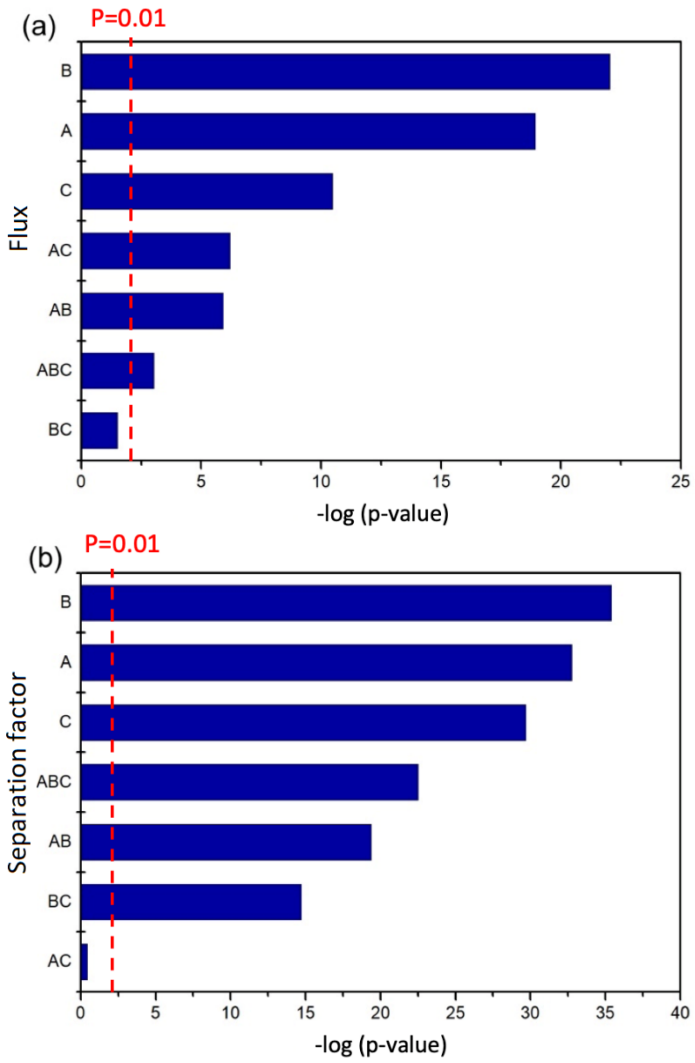

Figure 5. 4 Contribution plot of individual and interaction terms for: (a) flux, and (b) separation factor.

Based on the factorial design results, the following observations can be made for the separation of EtOH/water mixtures:

(1) The main effects are more significant than the interaction effects for both permeation flux and separation factor, and the impact of the interaction effects cannot always be neglected though.

(2) The main effect B (i.e., crosslinking time) is the most significant parameter affecting both flux and separation factor. Crosslinker concentration is the second-largest contributor, and crosslinking temperature is the least important. The main reasons for these changes are discussed in details at the end of this section.

(3) Most effects have opposite signs for the MLR coefficients with respect to the permeation flux and separation factor, which agrees with the common trade-off relation observed.

It may be pointed out that a factorial design experiment can effectively reveal the significance of factors influencing the membrane performance, which ultimately helps to optimize the membrane, but the results cannot be extrapolated beyond the range of study due to the linearity assumption used in the data analysis [233,235].

The negative/positive impacts of an individual parameter on the membrane performance are also represented in Fig. 5.5 **(**main effects) and Fig. 5.6 (interaction effects). All these factors have a negative correlation with the flux, meaning an increase in such a factor results in a lower flux (Fig. 5.5a**)**. Conversely, these factors correlate positively with the separation factors (Fig. 5.5b). Table 5.5 shows the swelling degrees of the PEI/GO bilayers in water at different crosslinking conditions. The degree of swelling in water for $(PEI/GO)_7$ membrane without crosslinking was 7.85 ± 0.1 (g water/g bilayers). Increasing the crosslinking time and temperature or/and crosslinker concentration augments the degree of crosslinking and decreases the degree of

swelling. The space between polymer chains decreased in the crosslinked membranes, which enhanced membrane rigidity and compactness. Accordingly, the penetrant molecules (i.e., EtOH and water) were less permeable due to the increased diffusion resistance and reduced free volume. Moreover, the larger molecules (i.e., EtOH) became increasingly difficult to pass through the crosslinked membrane, resulting in a higher separation factor [3].

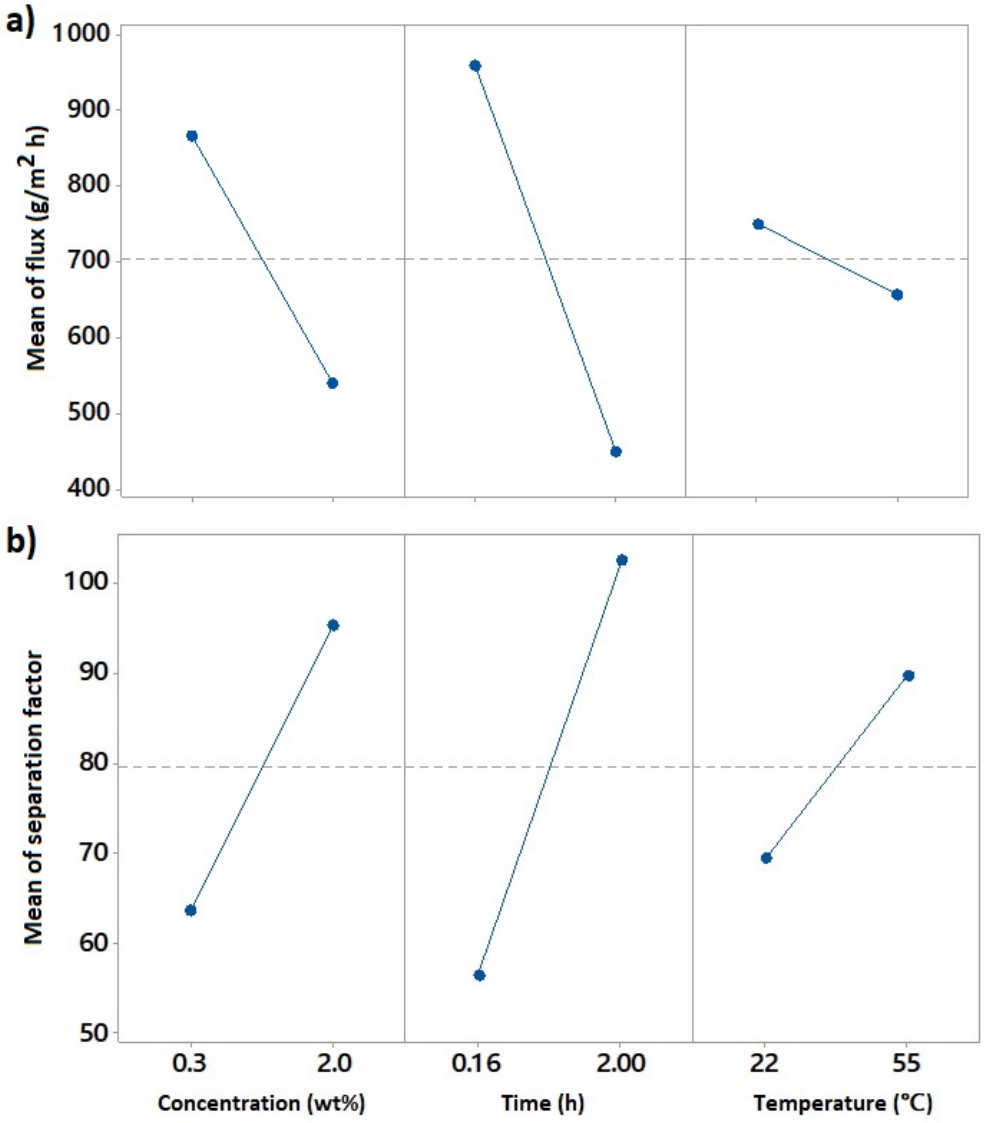

Figure 5. 5 Main effect plots for (a) flux and (b) separation factor.

Table 5. 5 Sorption uptake of water in PEI/GO bilayers (seven bilayers) at different crosslinking conditions.

Crosslinking condition			Degree of swelling in water (g water/g bilayers)
Reaction time (h)	Concentration (wt%)	Temperature (°C)	
0.16	2	22	5.66 ± 0.01
0.5	1	22	6.28 ± 0.05
0.5	2	22	4.58 ± 0.07
1	2	22	4.45 ± 0.04
2	2	22	3.50 ± 0.06
1	0.3	55	4.00 ± 0.08
1	1	55	3.40 ± 0.01

The interaction effects indicate how the relationship between an individual parameter and the response depends on the value(s) of one or more factors. Fig. 5.6 displays the mean values of the responses (i.e., permeation flux and separation factor) on the y-axis for the levels of one factor on the x-axis and a separate line for each level of other factors. Parallel lines in these plots indicate no interaction among these factors, while non-parallel lines show the possibility of interactions. The greater the departure from parallel indicates a stronger interaction effect. Based on the data in Fig. 5.6, most of the lines in the interaction plots appear to be parallel, and there is no clear evidence of an interaction between the main factors of the study between the considered levels. That is, the effects of crosslinker concentration and temperature and time of crosslinking reaction on the flux and separation factor are not influenced by other factors. Based on interaction plots, there seems to be no interaction among the individual factors for the selected ranges.; however, there may be a chance for the interaction of concentration and temperature (AC term) at concentrations higher than 2% (Fig. 5.6a).

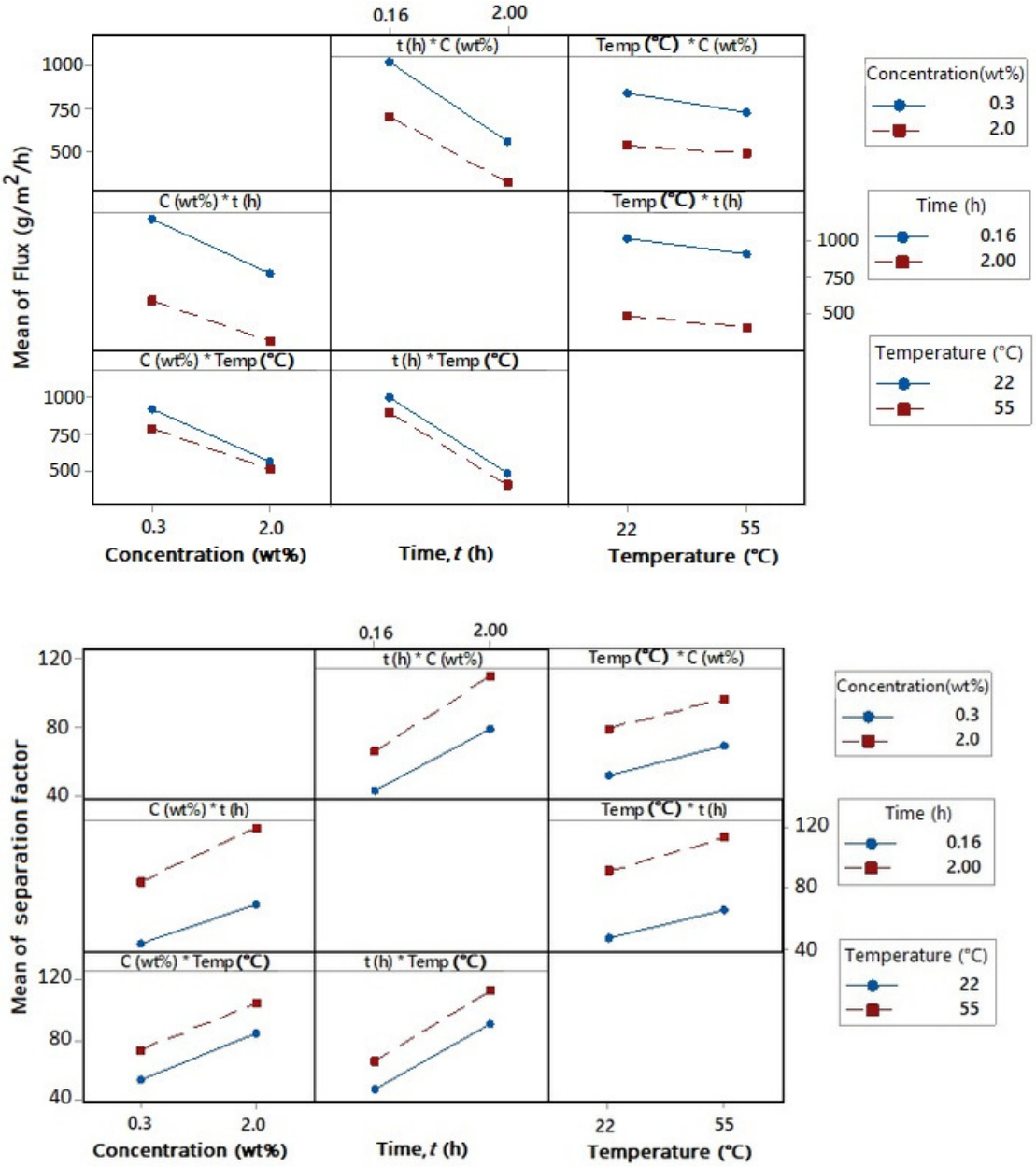

Figure 5. 6 Interaction plots for (a) flux and (b) separation factor.

As mentioned earlier, the impact of concentration and time on both flux and separation factor is more significant than that of temperature (Fig 5.5 and 5.6). To further assess the overall effect of concentration and time on the responses over the selected ranges, additional experimental

studies were also carried out by considering the crosslinker concentration and time over a broader range, while keeping crosslinking temperature fixed at room temperature (22 ºC).

5.3.2 Effects of crosslinker concentration and reaction time on ethanol dehydration performance

The effects of GA concentration (in the range 0.3-2wt%) on the pervaporation performance were studied using the $(PEI/GO)_7$ LbL membrane crosslinked at a constant time of 0.5 h, and the effects of crosslinking time were studied (over a period of 0.16-2.0 h) using the $(PEI/GO)_7$ LbL membrane crosslinked at 2wt% of GA. The flux and separation factor of these membranes were tested at feed water concentrations of 2, 6, 12, and 20 wt%.

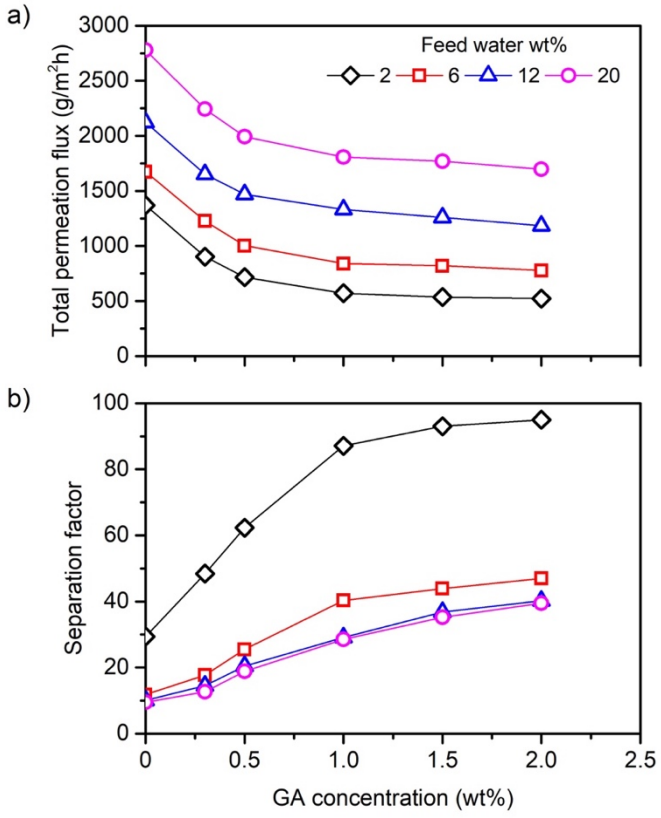

Figure 5. 7 Effects of GA concentration on (a) flux and (b) separation factor. Crosslinking temperature: 22 ºC, crosslinking time: 0.5h.

Fig. 5.7 shows the total permeation flux and separation factor at various feed concentrations as a function of GA concentration. With an increase in GA concentration, the total flux tends to decrease while the separation factor increases. These changes are less significant above a GA concentration of 1 wt%. The increase in the separation factor is more noticeable at lower feed water concentrations than higher feed water concentrations.

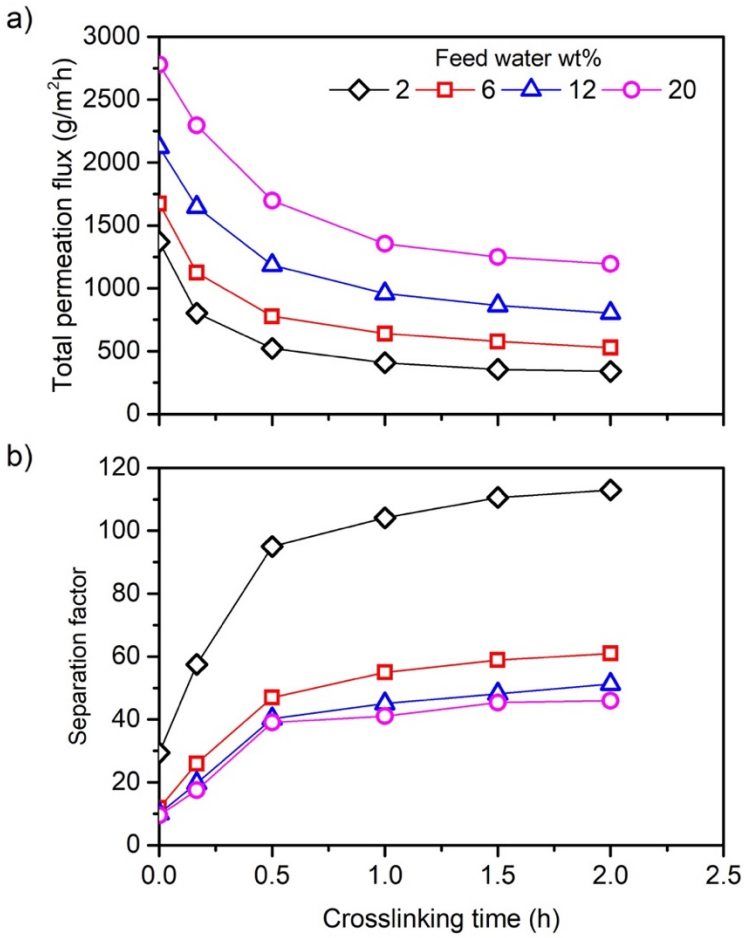

Figure 5. 8 Effect of crosslinking time on the (a) flux and (b) separation factor. Crosslinking temperature: 22ºC, crosslinker concentration: 2wt%.

Fig. 5.8 shows the total fluxes and separation factors of the membranes at different feed concentrations as a function of GA reaction time. Comparing Fig. 5.7 with 5.8, similar trends are observable for both fluxes and separation factors with increasing reaction time. These findings can be attributed to an increased crosslinking degree. The degree of crosslinking increases over time and GA concentration since the GA molecules are able to penetrate deeper into the membrane. In principle, as the crosslinking density increases, the PEI chains and GO nanosheets are restricted, resulting in more packed structure of the membrane that is increasingly resistant to the penetrant molecules. Therefore, the permeation fluxes decrease and the separation factors increase. Due to the trade-off relation, the membrane fabrication conditions can be optimized based on the permeation flux or separation factor, but rarely both. Membranes with a 0.5 h crosslinking time and 1.0 wt% of GA concentration were selected for further study. The membranes crosslinked at room temperature (22ºC) were used in subsequent studies. Further investigations were performed to determine the suitability of the membrane for EtOH and IPA dehydration.

5.3.3 Effects of feed concentration on the dehydration of ethanol and isopropanol

Figs. 5.9-5.12 show the total permeation flux, water concentration in permeate, water partial flux and separation factor of XL(PEI/GO)$_7$ LbL membranes for the dehydration of EtOH and IPA, respectively, as a function of feed water concentrations at 22 ºC. For comparison, the results of un-crosslinked (PEI/GO)$_7$ LbL membrane are also provided. The flux and separation factor showed similar trends for both EtOH/water and IPA/water mixtures when the feed water concentration is increased. The crosslinked membrane had a lower permeation flux than the un-crosslinked membrane over feed water concentration tested (2.0 to 20.0 wt%); however, the separation factor

increased significantly. For instance, at a feed water concentration of 2wt% in EtOH/water mixture, the un-crosslinked membrane showed a total permeation flux of 1369 g/m^{2}h and the separation factor of 30; whereas the crosslinked membrane showed a total permeation flux of 571 g/m^{2}h and the separation factor of 87. At a feed water concentration of 2wt% in IPA/water mixture, the un-crosslinked membrane showed a total permeation flux of 1266 g/m^{2}h and the separation factor of 58; whereas the crosslinked membrane showed a total permeation flux of 495 g/m^{2}h and the separation factor of 209. The total permeation flux is manipulated mainly by the water flux. The driving force (fugacity) of water increases at the feed side, while that of alcohol decreases as the feed water content increases (Appendix C). In addition, the higher water permeation is partially due to the relatively small kinetic size of water molecules and the stronger affinity between water and the membrane surface. The separation factors of both un-crosslinked and crosslinked membranes decreased with an increase in feed water concentration. These membranes are hydrophilic and will swell with an increase in water concentration. Therefore, both water and alcohol permeant molecules can diffuse through the membrane with less effort, leading to a decline in the separation factor. However, the outmost skin layer became more selective after crosslinking, causing a more than threefold increase in the separation factor for the dehydration of EtOH and IPA.

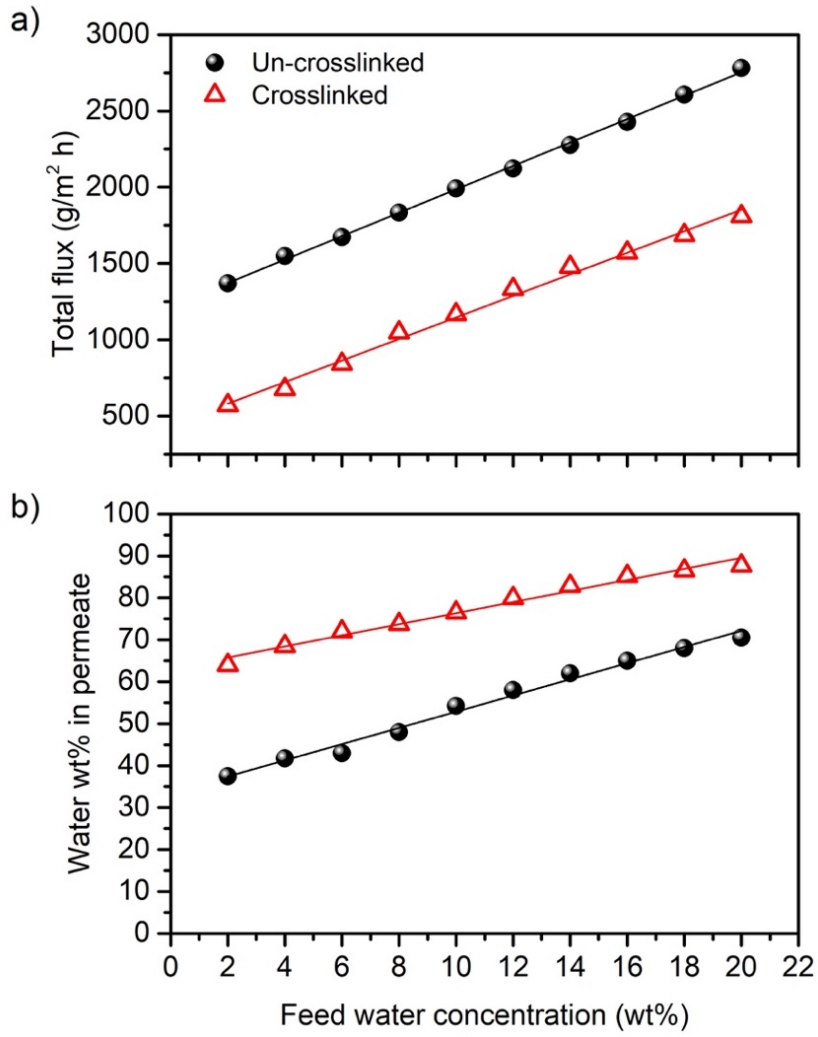

Figure 5. 9 Effects of feed water concentration on (a) total permeation flux and (b) water concentration in permeate for the un-crosslinked and crosslinked $(PEI/GO)_7$ membranes. Feed: EtOH/water. Crosslinking conditions: temperature 22 ºC, concentration 1 wt%, and time 30min.

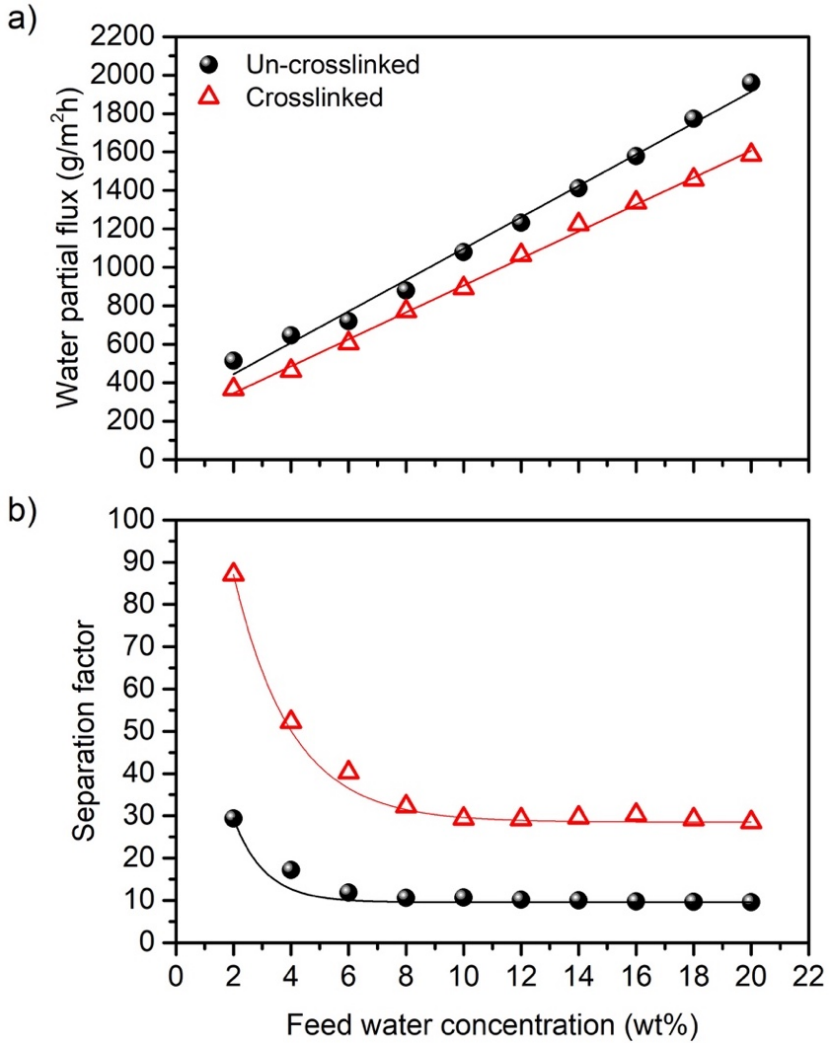

Figure 5. 10 Effects of feed water concentration on (a) water partial flux and (b) separation factor for the un-crosslinked and crosslinked $(PEI/GO)_7$ membranes. Feed: EtOH/water. Crosslinking conditions: temperature 22 ºC, concentration 1 wt%, and time 30min.

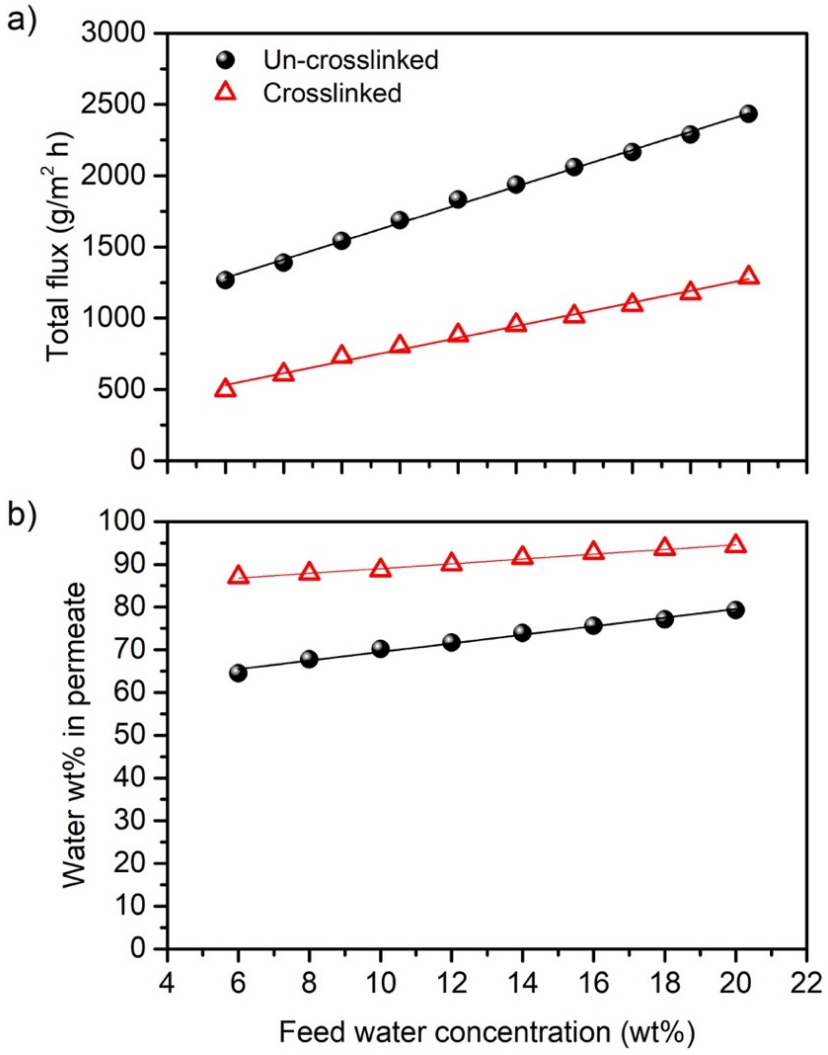

Figure 5. 11 Effects of feed water concentration on (a) total permeation flux and (b) water concentration in permeate for the un-crosslinked and crosslinked $(PEI/GO)_7$ membranes. Feed: IPA/water. Crosslinking conditions: temperature 22 ºC, concentration 1 wt%, and time 30min.

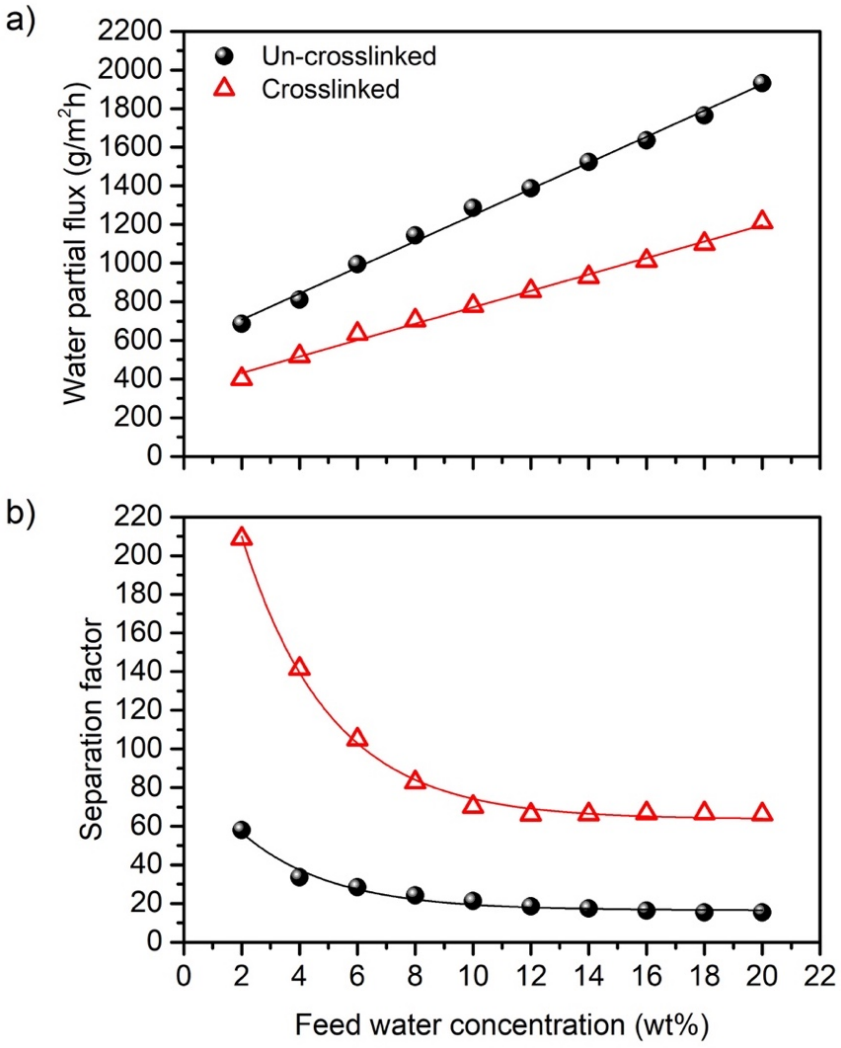

Figure 5. 12 Effects of feed water concentration on (a) water partial flux and (b) separation factor for the un-crosslinked and crosslinked $(PEI/GO)_7$ membranes. Feed: IPA/water. Crosslinking conditions: temperature 22 ºC, concentration 1 wt%, and time 30min.

At a given feed water concentration, the total permeation flux for EtOH dehydration is higher than that for IPA dehydration, and this can be attributed to the alcohols molecular sizes (Table 5.1). EtOH can diffuse through the membrane faster than IPA. Additionally, based on the hydrogen bonding parameters of the permeants, water has the highest hydrogen bonding capacity, followed

by EtOH and then IPA. This implies that water has a strong affinity to the hydrophilic LbL membrane. Also, EtOH has a higher solubility in the membrane than IPA, resulting in a greater membrane swelling effect from the EtOH/water mixture. In terms of separation factor, it is easier to separate out the alcohol with larger molecules [236]. Thus, EtOH can form clusters with water, which then pass through the membranes [21]. As a consequence, the EtOH/water mixture has a lower separation factor and higher flux than the IPA/water mixture. In terms of water partial flux, at a given feed water concentration (wt%), the driving force of water in the IPA/water mixture is higher than that of water in the EtOH/water mixture (Appendix C).

5.3.4 Effects of feed temperature on dehydration performance of ethanol and isopropanol

Figs. 5.13-5.16 show the EtOH and IPA dehydration performance of the XL(PEI/GO)$_7$ membrane, respectively, as a function of temperature at various feed water concentrations. Similar trends can be observed with an increase in temperature. The permeation fluxes of both the water and alcohols increased as the temperature increased from 22 to 60°C. The partial vapor pressure difference between the feed and permeate is considered to be the driving force. The partial vapor pressures of both water and alcohols increased as the temperature augmented, which enhanced the driving force for mass transport through the membrane. Moreover, the permeant molecules have more kinetic energy at higher temperatures, leading to faster molecular diffusion. At a given feed water concentration, temperature affected the flux of alcohol relatively more than that of water; therefore, the separation factor slightly decreased. The total permeation flux in EtOH/water mixture is higher than the total permeation flux in IPA/water mixture, and the opposite is true for the separation factor.

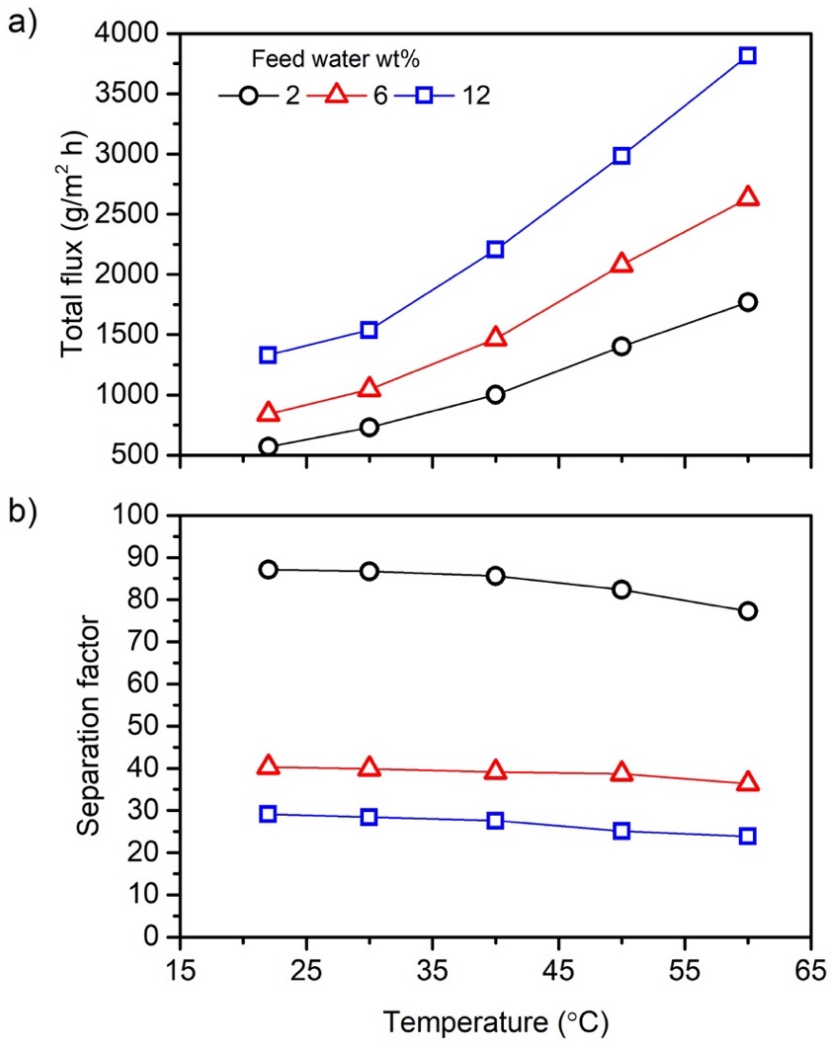

Figure 5. 13 Effects of temperature on (a) total permeation flux and (b) separation factor for separation of water from EtOH using XL(PEI/GO)$_7$ membrane at different feed water concentrations.

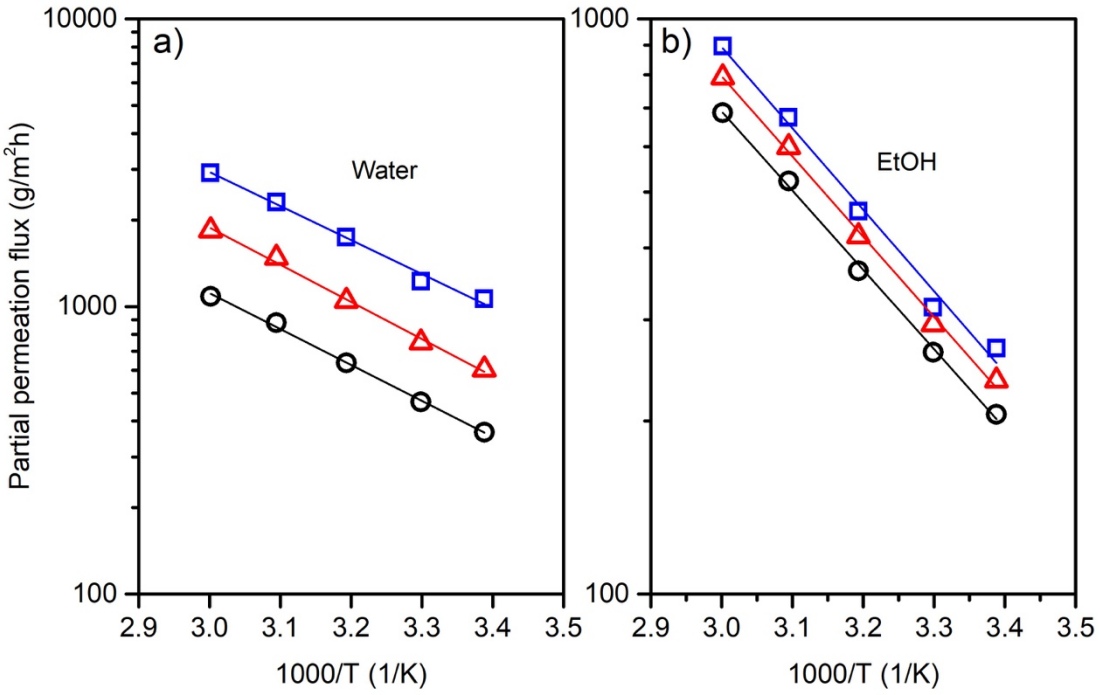

Figure 5. 14 Effects of temperature on permeation fluxes of (a) water and (b) EtOH using XL(PEI/GO)$_7$ membrane at different feed water concentrations.

The temperature dependence of the permeation flux follows an Arrhenius type of relationship:

$$J = J_0 \, e^{(-\frac{E_J}{RT})} \tag{5.6}$$

where J_0 is the pre-exponential factor, R is the gas constant, T is the absolute temperature, and E_J is the apparent activation energy for permeation that depends on the activation energy for diffusion and the heat of sorption [171]. E_J represents the overall effects of temperature on the permeation flux. Tables 5.6 and 5.7 summarize the apparent activation energies, E_J, for the permeation of alcohol and water in the EtOH/water and IPA/water mixtures, respectively. There is a small variation in the apparent activation energies for both the water and alcohols permeation flux with an increase in the feed water concentration. The activation energy for water permeation is lower

than that for alcohols permeation (i.e., $E_{J,water} < E_{J,alcohol}$). Water has a smaller kinetic molecule size than both alcohols and needs to overcome a lower energy barrier to diffuse through the membrane. Comparably, the $E_{J,EtOH}$ is lower than $E_{J,IPA}$ at different feed water concentrations.

Table 5. 6 Activation energies of permeation of water and EtOH based on permeation flux and permeance through XL(PEI/GO)$_7$ at different feed water concentrations.

Feed water concentration (wt%)	$E_{J,water}$ (kJ/mol)	$E_{p,water}$ (kJ/mol)	$E_{J,EtOH}$ (kJ/mol)	$E_{p,EtOH}$ (kJ/mol)
2	23.7	-20.2	25.7	-19.7
6	22.3	-22.0	25.8	-19.8
12	24.6	-21.2	25.8	-19.6

Table 5. 7 Activation energies of permeation of water and IPA based on permeation flux and permeance through XL(PEI/GO)$_7$ at different feed water concentrations.

Feed water concentration (wt%)	$E_{J,water}$ (kJ/mol)	$E_{p,water}$ (kJ/mol)	$E_{J,IPA}$ (kJ/mol)	$E_{p,IPA}$ (kJ/mol)
2	23.9	-19.7	26.3	-15.8
6	24.7	-21.1	26.7	-15.5
12	22.6	-19.0	27.1	-15.0

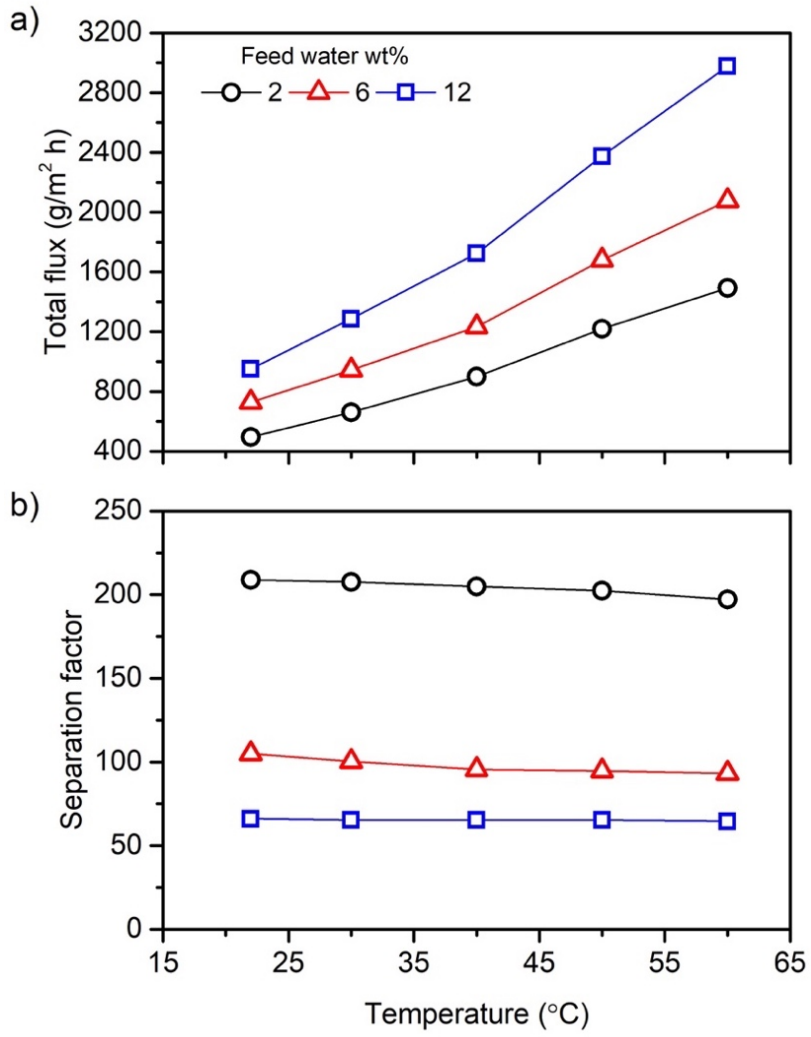

Figure 5. 15 Effects of temperature on (a) total permeation flux and (b) separation factor for separation of water from IPA using XL(PEI/GO)$_7$ membrane at different feed water concentrations.

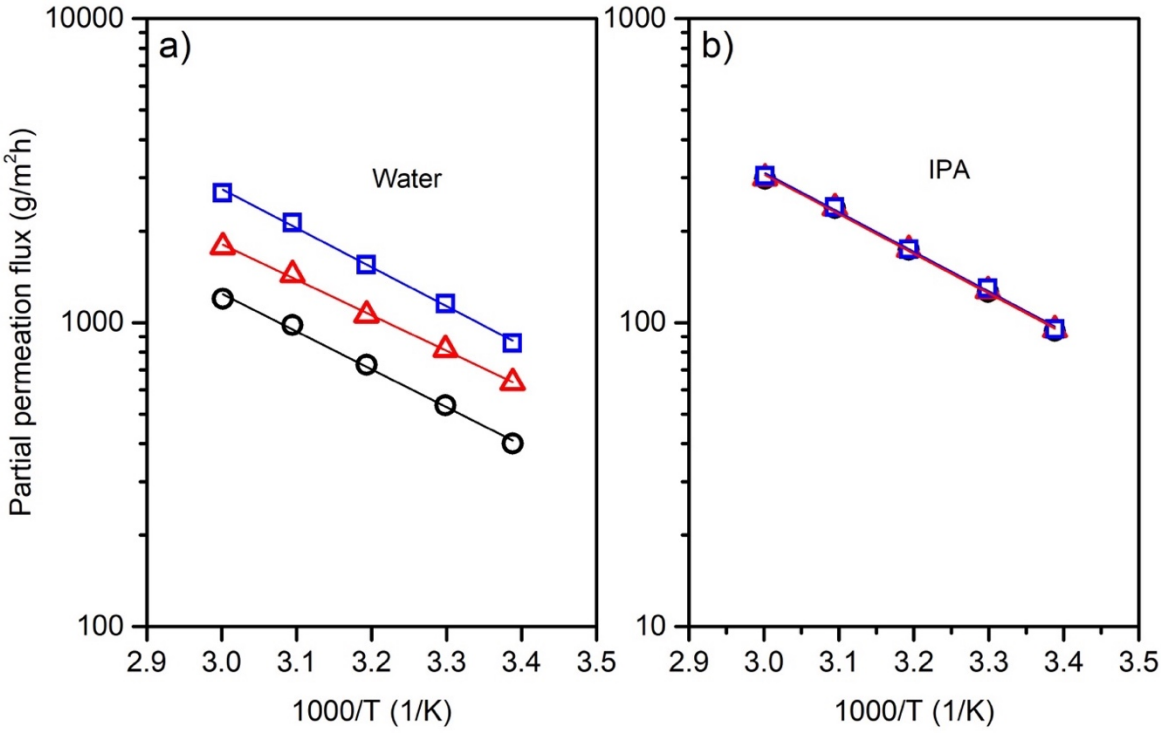

Figure 5. 16 Effects of temperature on permeation fluxes of (a) water and (b) IPA using XL(PEI/GO)$_7$ membrane at different feed water concentrations.

The permeance of the membrane, from calculated permeation flux normalized by the driving force, and the temperature dependence of membrane permeance was found to follow Arrhenius type relationship [171]:

$$\left(\frac{P_i}{l}\right) = \frac{J_i}{P_i^s x_i \gamma_i - p^p y_i} = \left(\frac{P_{i0}}{l}\right) e^{\left(-\frac{E_{Pi}}{RT}\right)} \quad (5.7)$$

where $\left(\frac{P_i}{l}\right)$, p^s, γ, p^p, E_p, x and y are, respectively, the permeance of the membrane to permeant i; the saturated vapor pressure of pure component i (calculated from the Antoine equation); the activity coefficient in the liquid phase (calculated by using the Wilson equation of state with the help of Aspen Plus; the permeate vapor pressure (which is generally negligible in pervaporation);

the activation energy (based on membrane permeability); and the mole fraction of water in the feed and permeate.

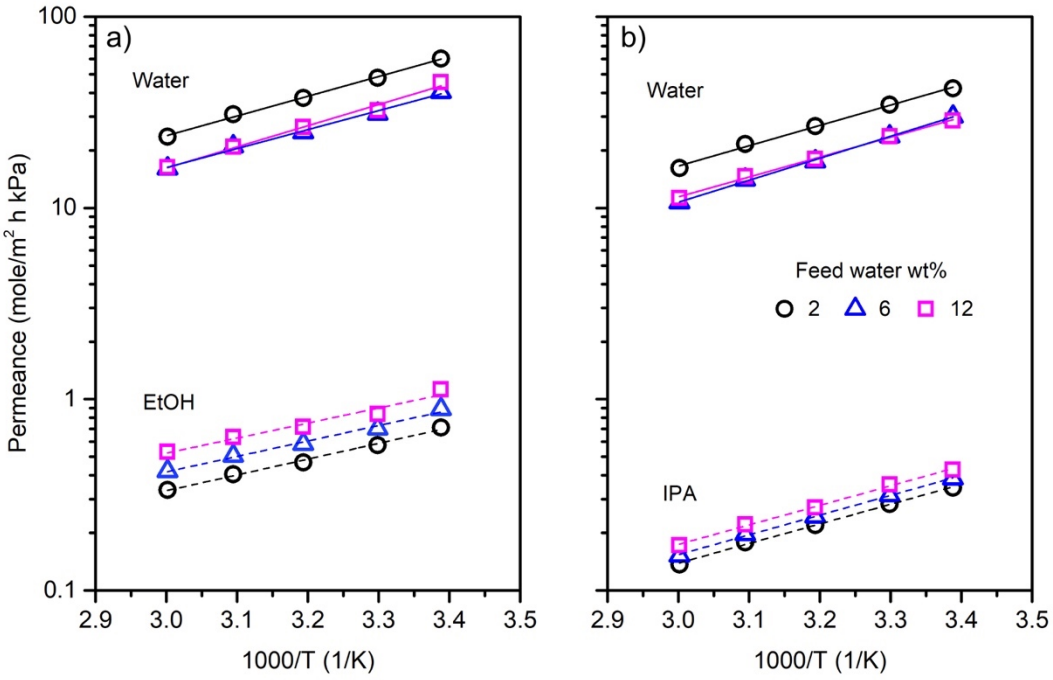

Figure 5. 17 Effects of temperature on permeance of water and alcohols through the XL(PEI/GO)$_7$ membrane at different feed water concentrations: a) EtOH/water mixture, and b) IPA/water mixture.

Fig. 5.17 shows the calculated membrane permeance for different feed mixtures of EtOH/water and IPA/water, as a function of reciprocal temperature. The E_p data for the permeants in EtOH and IPA dehydration are also shown in Tables 5.6 and 5.7. The permeance of water in the membrane is well over the permeance of the alcohols. The membrane permeance tended to decrease with an increase in temperature for both alcohols and water (to a greater extent), implying that temperature has a negative impact on the membrane permeance. Based on the solution-diffusion model, the permeability coefficient is equal to a product of the diffusion and solubility

coefficients. Thus, E_p is equal to the activation energy for diffusion (E_D) plus the heat of sorption (ΔH_s) (i.e., $E_p = E_D + \Delta H_s$) [31]. Whereas E_D has a positive value, the enthalpy of sorption (ΔH_s) can be negative or positive depending upon whether the sorption process is exothermic or endothermic. Negative values of E_p for both water and alcohol permeation imply that the sorption process is exothermic (i.e., $\Delta H_s < 0$) and temperature affects exothermic sorption more than it affects diffusion, causing a decline in the membrane permeance. Moreover, the increase in permeation flux of each component with temperature is predominantly related to the increased saturated vapor pressure and thus the increased driving force for permeation. Similar phenomena for dehydration of EtOH and IPA via pervaporation were reported previously [236]. In addition, Tables S1 and S2 (Appendix C) show the calculated driving forces (fugacity) for individual component transport at different feed water concentrations and temperatures, which is aligned with the results in Fig 5.17.

5.3.5 Importance of number of bilayers on pervaporation performance

The pervaporation performance of XL(PEI/GO)$_z$ membranes with different numbers of bilayers was assessed for dehydrating an alcohol solution containing 6 wt% water at 50°C. Figs. 5.18 and 5.19 show the partial fluxes, total flux, and separation factor as a function of the number of bilayer for dehydrating EtOH and IPA, respectively. Based on the results, the total permeation flux tends to decrease, while the separation factor steadily improves as the number of bilayers increases. For instance, the total flux of the EtOH/water and IPA/water mixtures decreased by 42% (from 2670 to 1539 (g/m^{2}h)) and 35% (from 1964 to 1452 (g/m^{2}h)), respectively, when the number of bilayers was increased from 3 to 14. The separation factor increased by about 65% (in the EtOH/water mixture from 26 to 75, and in the IPA/water mixture from 62 to 180).

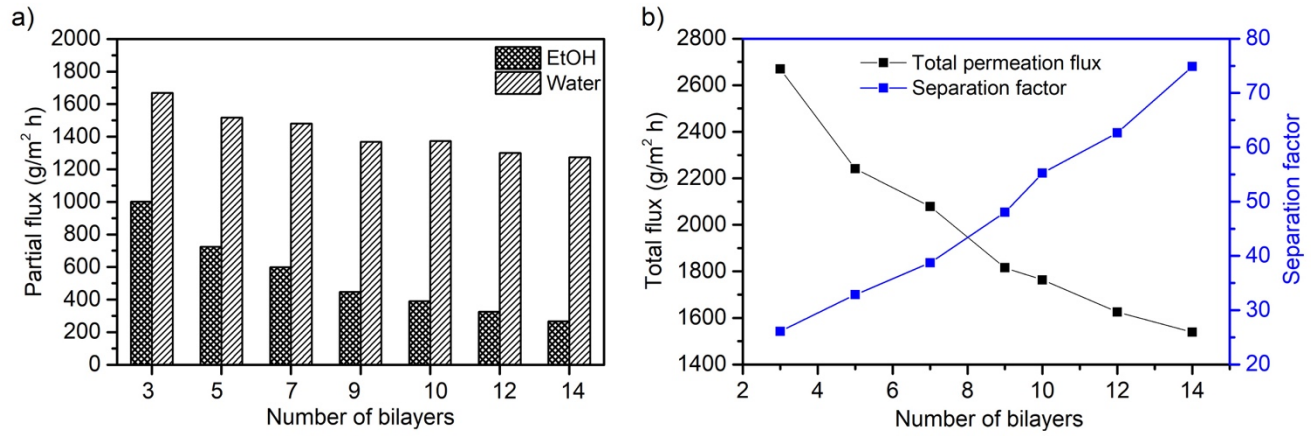

Figure 5. 18 Effect of the number of bilayer on the (a) partial fluxes of water and EtOH and (b) total flux and separation factor, feed water concentration: 6 wt%, feed temperature: 50 °C.

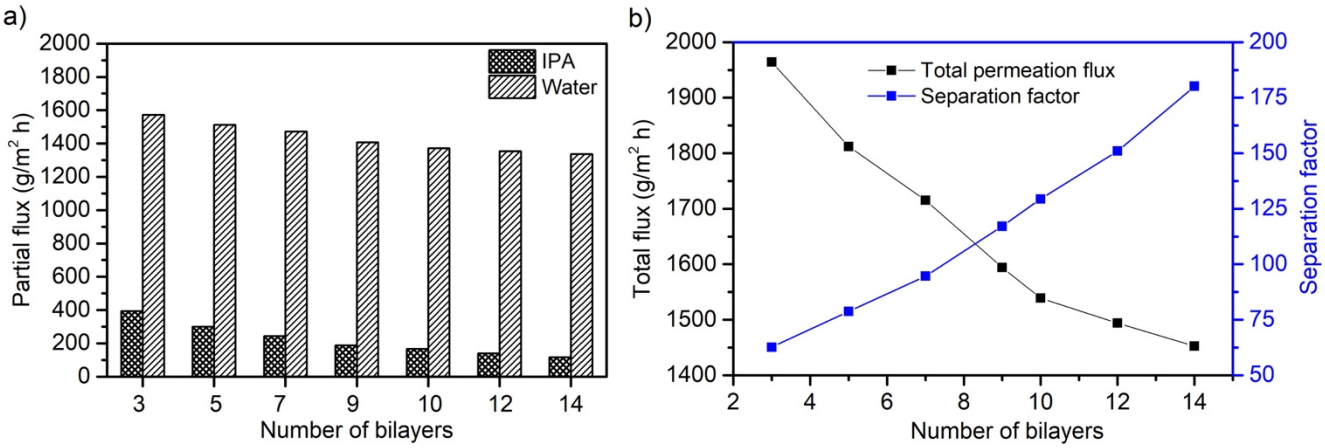

Figure 5. 19 Effect of the number of bilayer on the (a) partial fluxes of water and IPA and (b) total flux and separation factor, feed water concentration: 6 wt%, feed temperature: 50 °C.

The thickness of the active layer of the membrane increases with the number of the bilayer, and the inverse of permeation flux is proportional to the membrane thickness [213]. Based on the resistance-in-series model [10], the overall mass transfer resistance of a component in a composite membrane is the sum of the mass transfer resistance of the bilayer and the substrate. A straight line

is obtained by plotting the inverse flux as a function of the number of bilayers (Fig. 5.20). From the slope of the line, the mass transfer resistance related to per bilayer can be determined, and from the intercept of the line, the mass transfer resistance of the substrate can be calculated [212]. Based on the results (Table 5.8 and Appendix D), the mass transfer resistance of the alcohols per bilayer, and the substrate were much higher than that of water. As expected, the mass transfer resistance also increased for water and alcohols when the number of bilayers increased. The straight lines suggest that the bilayer build-up was uniform. Moreover, when the number of bilayers increases, the diffusion pathway length also increases, as does the diffusion resistance for water, EtOH and IPA molecules, leading to a decrease in the permeation flux [213]. The more significant decline in the alcohol flux can be attributed to the alcohols having larger sizes than water (Table 5.1). Since the overall mass transfer resistance is affected by the mass transfer resistance in the bilayers, the separation factor depends on the membrane thickness as well. The membrane performance can be fine-tuned by controlling the number of bilayers. Table 5.9 compares the pervaporation performance of the XL(GO/PEI)$_z$ LbL membrane prepared in this research with those of other membranes reported in the literature.

Table 5. 8 Membrane resistance for permeation of different alcohol/water mixtures. Feed composition: 6 wt% water, operating temperature: 50 °C.

Mixture	Component	Resistance per bilayer ($\frac{m^2.h.kPa}{mol}$)	Substrate ($\frac{m^2.h.kPa}{mol}$)
1	EtOH	2.96×10^{-1}	1.15×10^{-1}
	Water	1.18×10^{-3}	3.98×10^{-2}
2	IPA	6.88×10^{-1}	7.00×10^{-1}
	Water	1.10×10^{-3}	6.22×10^{-2}

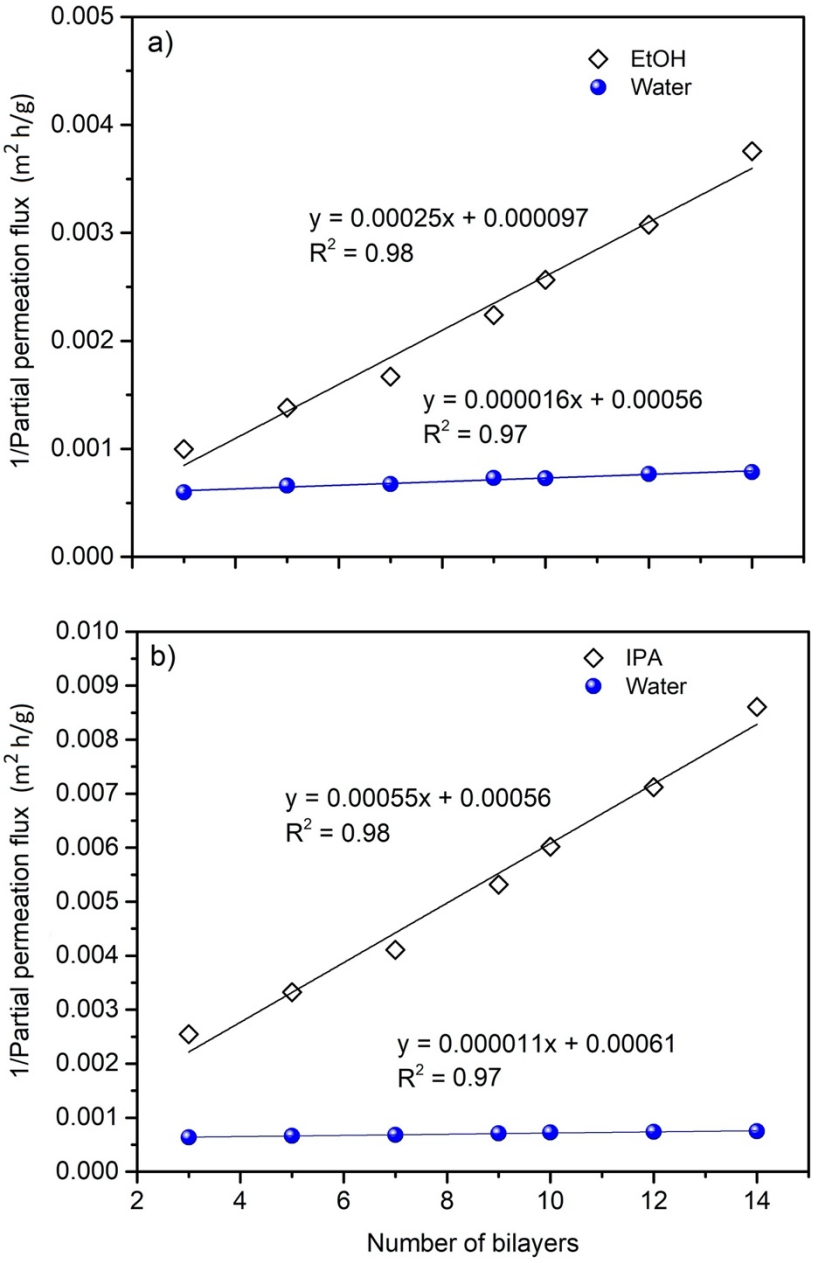

Figure 5. 20 Inverse of the partial flux of (a) water and EtOH, and (b) water and IPA as a function of the number of bilayers. Feed water concentration: 6 wt%, operating temperature: 50 °C.

Table 5. 9 Performance benchmarking of the XL(PEI/GO)$_z$ membranes with pervaporation membranes in the literature for different alcohol/water mixtures.

Membrane	Substrate	Feed solvent content (wt%)	J (g/m^{2}h)	α	T (ºC)	Ref.
EtOH/water						
Sodium alginate/chitosan	-	95	70	1110	60	[235]
(PEI/PSS)$_{60}$	PAN/PET	93.8	540	21	58.5	[223]
(PAM/PAA)$_3$	CA	90	100	80	25	[237]
(PEI/PAA)$_4$	PES	95	374	18	40	[64]
(PEI/PAA)$_{2.5}$ [a]	PAN	95	314	604	70	[63]
(PEI/GO)$_7$	Cl-TFC	98	1770	77	60	This study
(PEI/GO)$_{14}$	Cl-TFC	94	1540	75	50	This study
IPA/water						
Sodium alginate/chitosan	-	90	554	2010	60	[235]
(PEI/PSS)$_6$	PA-6[b]	70	1430	6.6	50	[238]
(PEI/PAA)$_6$	PA-6[b]	70	670	3330	50	[238]
(PEI/PAA)$_6$	PAN	92.1	500	2900	50	[12]
(PDDA/PSS)$_6$	PA-6[b]	70	1850	2.7	50	[238]
(PEI/GO)$_7$	Cl-TFC	98	1494	197	60	This study
(PEI/GO)$_{14}$	Cl-TFC	94	1336	180	50	This study

PSS: poly(styrene sulfonate sodium salt); PAN: polyacrylonitrile; PET: polyethyleneterephthalate ; PAM: polyallylamine; PAA: polyacrylic acid ; CA: cellulose acetate; PDDA: poly(diallyldimethylammonium chloride).
[a] The membrane prepared by dynamic LbL adsorption; [b] Carboxyl functionalized polyamide-6.

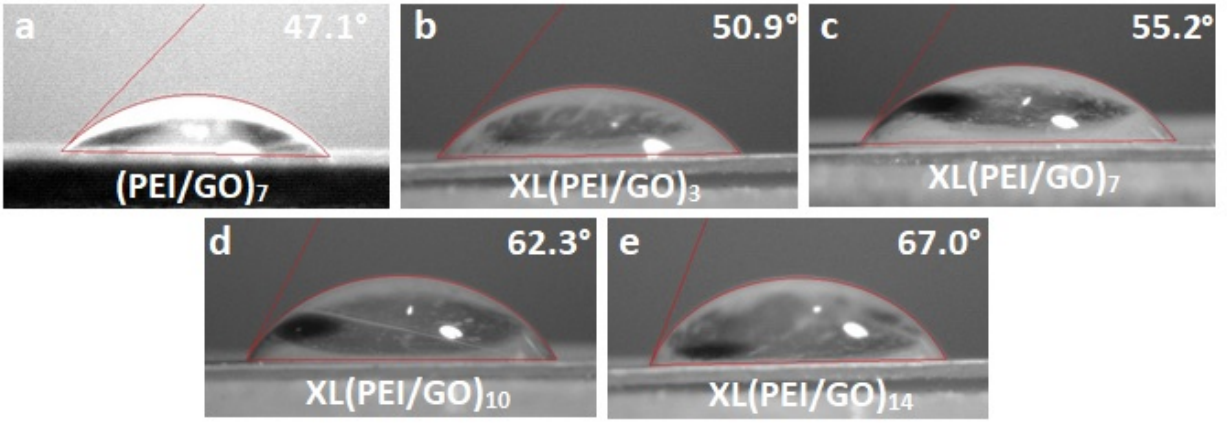

Figure 5. 21 Water contact angle on (a) $(PEI/GO)_7$, (b) $XL(PEI/GO)_3$, (c) $XL(PEI/GO)_7$, (d) $XL(PEI/GO)_{10}$, and (e) $XL(PEI/GO)_{14}$ membranes.

The water contact angle on the crosslinked membranes with different bilayers was measured. For comparison, the contact angle on the un-crosslinked LbL membrane was also provided. As shown in Fig. 5.21, all membranes were hydrophilic with water contact angles less than 90°. The water contact angle of the (PEI/GO) membrane with seven bilayers increased from 47.1° to 55.2° after crosslinking with GA. The contact angle in the crosslinked membranes increased to 67° after deposition of 14 bilayers. These results may be attributed to the hydrophobic carbon chain of GA [216]. Moreover, crosslinking the GO layer decreased the amount of hydroxyl groups on the GO nanosheets that can form strong bonds with water.

Fig 5.22 shows the FTIR spectra of the $XL(PEI/GO)_7$ LbL (a), $(PEI/GO)_7$ LbL (b) and chlorine-treated TFC polyamide membranes (c). For comparison, the FTIR spectrum of GO nanosheets was added (inset) in the figure. The characteristic peaks of GO were observed at 3253 cm^{-1} (–OH stretching in hydroxyl groups), 1738 cm^{-1} (C=O stretching vibration in carboxyl groups), 1620 cm^{-1}(unoxidized sp^2 aromatic C=C bonds), 1418 cm^{-1} (the bending vibration of C-OH) , and 1220 and 1085 cm^{-1} (the stretching vibration of C–O in epoxy and alkoxy groups, respectively)

[161,216,239]. The characteristic peaks of the membranes were observed at 1544 cm^{-1} (N-H in-plane bending, amide II), 1598 cm^{-1} (C=C ring stretching), 1660 cm^{-1} (C=O stretching, amide I) and 3363 cm^{-1} (N-H stretching, amide II). The broad peak at ~3363 cm^{-1} was intensified in $(PEI/GO)_7$ LbL membrane compared to that of chlorinated substrate. It can be assigned to the stretching vibrations of the O-H groups in GO nanosheets and N-H stretching (amide II) in PEI structure. In addition, the enhanced intensities of -CH stretching at 2950 and 2845 cm^{-1} in the crosslinked membrane imply the introduction of glutaraldehyde [16,119,169,216].

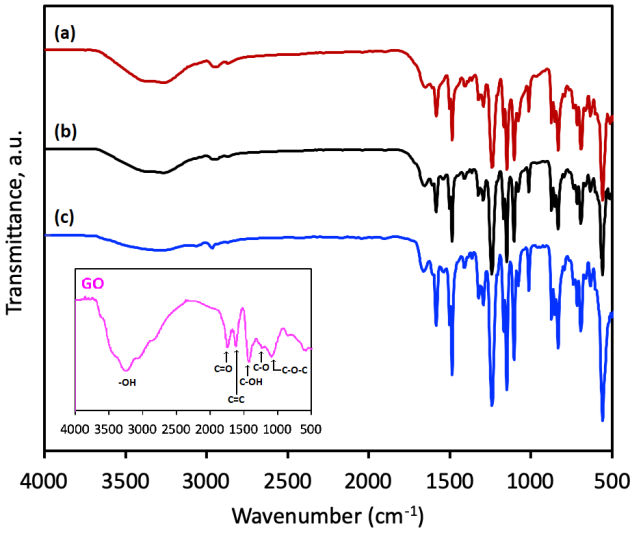

Figure 5. 22 FTIR spectra of the (a) XL(PEI/GO)7 LbL, (b) (PEI/GO)7 LbL, and (c) chlorine-treated TFC polyamide membranes. Inset: GO nanosheets. Crosslinking condition: time 0.5h, GA concentration 1.0 wt% at 22 ºC.

The mean surface roughness (Ra) values of the $(PEI/GO)_7$ membrane increased with an increase in the number of bilayers and degree of crosslinking, which was confirmed by the AFM. Fig. 5.23 shows the 3-D and 2-D images of the surface morphology of the un-crosslinked and crosslinked membranes. The Ra value of the (PEI/GO) membrane with seven bilayers increased

from 50.8nm to 78.8nm after crosslinking with GA. The Ra values in the crosslinked membranes increased to 97.9 and 128.2 after deposition of 10 and 14 bilayers, respectively. The actual contact area between the feed and the skin layer increased as the surface roughness increased.

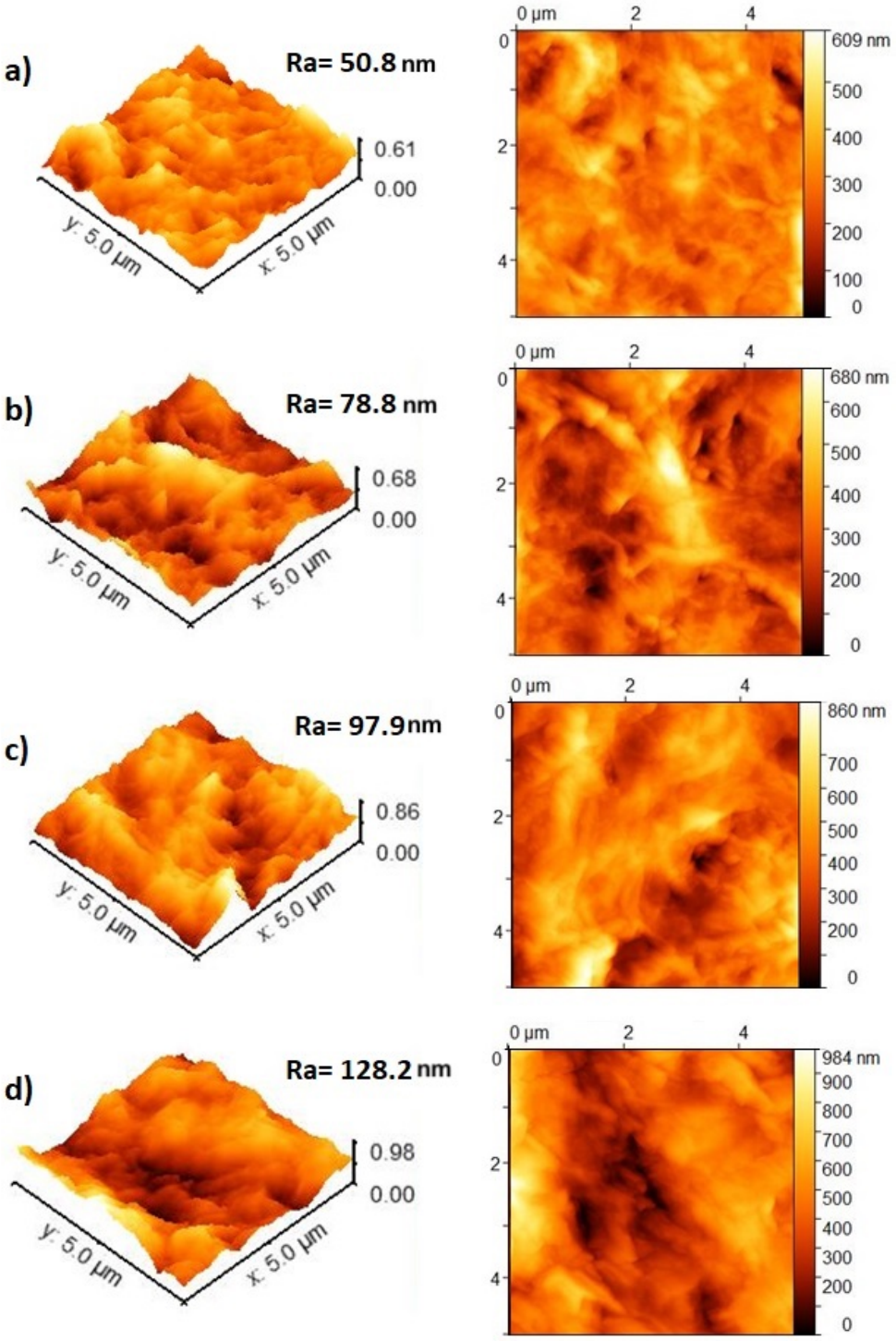

Figure 5. 23 3D and 2D AFM images of the (a) $(PEI/GO)_7$, (b) $XL(PEI/GO)_7$, (c) $XL(PEI/GO)_{10}$, and $XL(PEI/GO)_{14}$ LbL membranes, (scanned area: 5 µm × 5 µm).

5.3.6 Long-term stability for alcohol dehydration

Fig. 5.24 shows the separation performance of the crosslinked PEI/GO membrane with seven bilayers for pervaporation dehydration of EtOH and IPA for ~ 210 h at 50 °C and feed water concentration of 6 wt%. There were no significant changes in total permeation flux and water concentration in permeate during the operating time, signifying the long-term stability of the membrane and its potential for industrial EtOH and IPA dehydration applications.

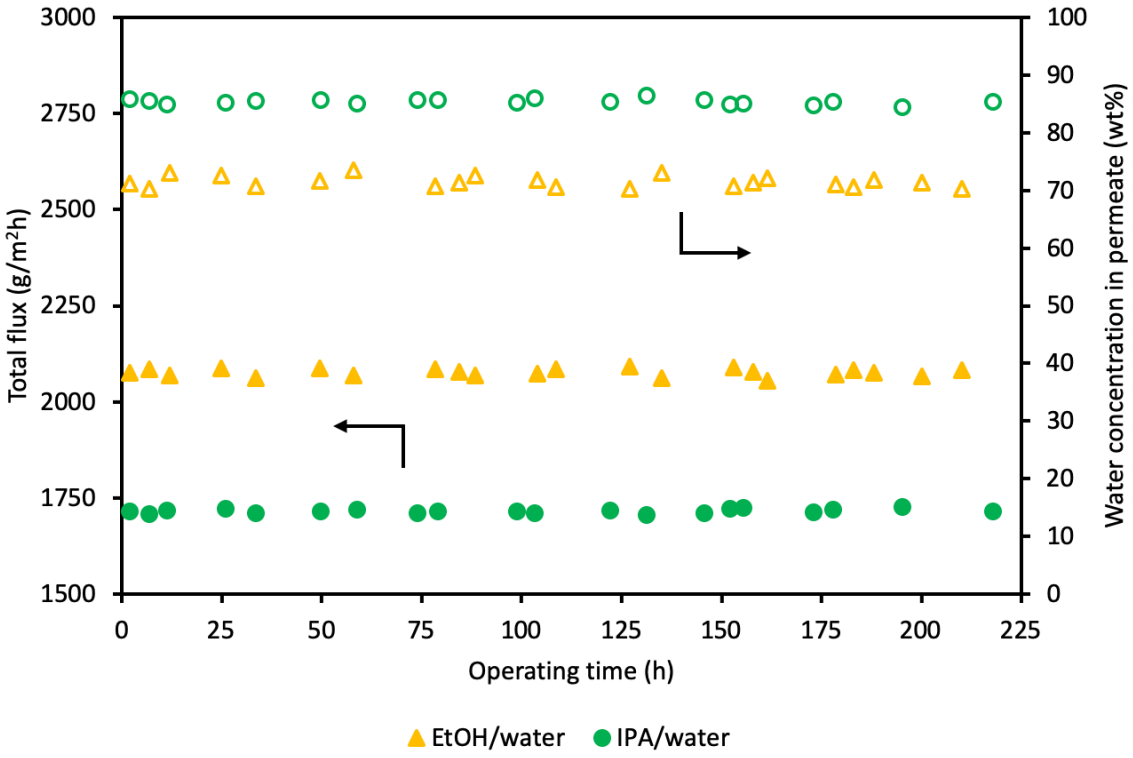

Figure 5. 24 The long term pervaporation performance of the XL(PEI/GO)$_7$ membrane for dehydration of EtOH and IPA at 50 °C and feed water concentration of 6 wt%.

5.4 Conclusions

This study has explored the preparation of LbL self-assembled membranes using PEI and GO, followed by crosslinking with glutaraldehyde (GA). The membranes were tested for the dehydration of ethanol (EtOH) and isopropanol (IPA) via pervaporation. The following conclusions can be drawn:

1) An MLR analysis showed that, of the three main effects, the GA concentration and crosslinking time had a greater influence on membrane performance than crosslinking temperature did. However, the impact of the interaction effects cannot be neglected.
2) The impacts of the two significant main factors, i.e., the GA concentration and crosslinking time, on the performance of the crosslinked membranes were explored individually at a fixed crosslinking temperature of 22 ºC. The crosslinking time of 0.5 h and GA concentration of 1.0 wt% appeared to be within the optimum crosslinking range. Experimental results for the dehydration of EtOH and IPA showed that the crosslinked (PEI/GO) LbL membrane with seven bilayers has considerably good permeation flux and separation factor.
3) An increase in the operating temperature resulted in a higher permeation flux and lower separation factor. It is more challenging to separate out EtOH than IPA, due to the smaller molecular size of EtOH and its greater hydrogen bonding parameter.
4) $E_{J,water}$ is the lowest, whereas $E_{J,IPA}$ is the greatest. Therefore, water needs to overcome a lower energy barrier to pass through the membrane than the alcohols.
5) By adjusting the number of bilayers, the membrane performance could be tailored. Membrane resistance for permeation of water was lower than that for alcohols. Increasing the number of bilayers could increase the separation factor, while the permeation flux decreased.

6) The long-term stability of the XL(PEI/GO)$_7$ membrane showed that there were no significant variations in total permeation flux and water concentration in permeate during ~ 210 h at 50 °C, implying the membrane potential for industrial alcohol dehydration applications.

Chapter 6

General comparison of membrane performance for the different pervaporation separations

In this study, different types of PEI/GO LbL membranes were prepared. PEI/GO LbL membrane with one bilayer was used for pervaporative desalination, but it was not permselective enough for dehydration of organic solvents. Thus, PEI/GO LbL membranes with the different numbers of bilayers were applied for dehydration of EG, and LbL membranes crosslinked with GA were used for dehydration of EtOH and IPA. In all pervaporation systems, the activation energies of permeation of the penetrants based on permeation flux (E_J) and permeance (E_P) at different feed water concentrations were calculated and discussed in detail. The activation energy data for desalination of high salinity-water, dehydration of EG, and dehydration of EtOH and IPA were tabulated in Tables 6.1, 6.2 and 6.3, respectively. As mentioned in Chapter 2, the value of E_J is always positive while the value of E_P can be either positive or negative depending on the value of activation energy for diffusion (E_D) and the heat of sorption (ΔH_s).

In pervaporative desalination, the feed solutions contained non-volatile salts with different concentrations. The pure water flux of the PEI/GO LbL membrane with one bilayer was 5 kg/m^{2}h at 35°C. The water permeation flux decreased to 1.7 kg/m^{2}h at 35°C when NaCl concentration in

the feed reached 20 wt%. The salt rejection remained high under all operating conditions. As shown in Table 6.1, E_J is positive, and increases with an increase in the feed salt concentration; the E_J values are comparable with those reported in the literature [34,50,123]. E_P values for water permeation are small positive and negative values. Negative values of E_P mean that the temperature affected exothermic sorption more than it affected diffusion during the permeation process. With an increase in feed salt concentration, the activation energy for water tended to increase, which may be attributed to the lower swelling of the membrane [34].

For dehydration of EG, the LbL membrane with one PEI/GO bilayer showed a total flux of 164 g/m^{2}h with a separation factor of 82 for a feed water concentration of 5 wt% at 35 °C. The total flux is much lower than the water flux in desalination for the same membrane. The main reason is the difference in the feed composition. EG is an organic compound with a high boiling point, while inorganic salt is a non-volatile component. Activation energies were calculated for the PEI/GO membrane with three bilayers (see Table 6.2). With an increase in feed water concentration, the E_J values for both water and EG slightly increased. This is similar to the results observed with other hydrophilic membranes for dehydration of EG [171]. All E_P values are negative for this system, implying that the permeability coefficient in the membrane decreased with increasing temperature. Generally, the diffusivity selectivity and permselectivity of a membrane decrease when temperature increases [240]. The values of E_J for water are smaller than that for EG due to the lower heat of vaporization of water. Furthermore, more permeable permeants often have lower activation energies than less permeable permeants because the most permeable components have smaller molecules sizes and the diffusion activation energy usually increases with penetrant size [27].

Table 6. 1 Activation energies of permeation of water based on permeation flux (E_J) and permeance (E_P) at different feed water concentrations through the PEI/GO LbL membrane.

Feed water concentration (wt%)	$E_{J,water}$ (kJ/mol)	$E_{p,water}$ (kJ/mol)	Water flux (kg/m^2h) at 35°C
100 (pure water)	37.0	-3.3	5.0
NaCl/water mixture			
98	37.7	-2.6	3.1
95	37.1	-3.1	2.9
90	38.6	-1.7	2.4
85	39.6	-0.7	2.0
80	39.7	-0.6	1.7
Na_2SO_4/water mixture			
98	35.0	-5.2	2.8
95	35.0	-5.2	2.6
90	40.3	0.02	2.1
85	40.4	0.1	1.8
80	40.4	0.1	1.6
$MgCl_2$/water mixture			
98	34.7	-5.6	2.7
95	35.5	-4.8	2.4
90	43.3	3.0	1.9
85	45.4	5.1	1.5
80	44.9	4.6	1.2
$MgSO_4$/water mixture			
98	34.3	-6.0	2.8
95	35.1	-5.2	2.5
90	41.0	0.7	2.1
85	42.1	1.8	1.7
80	43.8	3.5	1.3

Table 6. 2 Activation energies of permeation of water and EG based on permeation flux (E_J) and permeance (E_P) at different feed water concentrations through the $(PEI/GO)_3$ LbL membrane.

Feed water concentration (wt%)	$E_{J,water}$ (kJ/mol)	$E_{p,water}$ (kJ/mol)	$E_{J,EG}$ (kJ/mol)	$E_{P,EG}$ (kJ/mol)	Total flux (g/m^2h) at 35°C	Separation factor
0.1	13.4	-34.3	21.3	-42.7	56	1800
0.2	13.5	-35.6	23.7	-40.2	68	1008
0.5	13.6	-35.8	27.7	-36.2	83	583
2.0	15.6	-30.6	27.8	-36.4	114	213
5.0	16.6	-29.3	28.0	-36.0	148	103

For dehydration of EtOH and IPA, the PEI and GO layers were crosslinked with GA to enhance membrane selectivity. The crosslinked PEI/GO LbL membrane with seven bilayers showed a flux of 1 kg/m^2h and a separation factor of 86 for EtOH dehydration and a flux of 0.9 kg/m^2h and a separation factor of 204 for IPA dehydration, at a feed water concentration of 2 wt% at 40 °C. Crosslinking restricted the polymer chain motions, decreased the free volume of the polymer and reduced swelling of the membrane [57,227]. Consequently, the permeation flux decreased and selectivity increased. Generally, the permeation flux in dehydration of alcohols is lower than the permeation flux in desalination of water. The total fluxes in dehydration of EtOH and IPA were higher than the total flux in dehydration of EG due to the different feed compositions and interactions between penetrants-penetrants and penetrants-membranes.

As can be seen in Table 6.3, the apparent activation energy of water in the EtOH/water and IPA/water systems is comparable to that of water in the EG/water system. In addition, E_J for water permeation is lower than that for EtOH and IPA permeation. Water is a smaller molecule than the alcohols, and therefore it has a lower energy barrier to overcome to pass through the membrane. It should be also mentioned that the E_J for EtOH is slightly lower than E_J for IPA at different feed water concentrations, and this may be related to the smaller molecule size of EtOH than IPA. Temperature showed more significant effects on permeation of EtOH and IPA than water

permeation. The activation energies for both water and alcohols did not change much with temperature.

Table 6. 3 Activation energies of permeation of water and alcohol based on permeation flux (E_J) and permeance (E_P) at different feed water concentrations through the crosslinked $(PEI/GO)_7$.

Feed water concentration (wt%)	$E_{J,water}$ (kJ/mol)	$E_{p,water}$ (kJ/mol)	$E_{J,alcohol}$ (kJ/mol)	$E_{p,alcohol}$ (kJ/mol)	Total flux (g/m^2h) at 40°C	Separation factor
EtOH/water						
2	23.7	-20.2	25.7	-19.7	1003	86
6	22.3	-22.0	25.8	-19.8	1466	39
12	24.6	-21.2	25.8	-19.6	2206	27
IPA/water						
2	23.9	-19.7	26.3	-15.8	899	204
6	24.7	-21.1	26.7	-15.5	1235	95
12	22.6	-19.0	27.1	-15.0	1726	65

Briefly, the values of E_J for water permeation in desalination of water is greater than that for water permeation in dehydration of organic solvents. It implies that the effect of temperature on water permeation flux is more significant in water desalination than solvent dehydration. Water needs to overcome a higher energy barrier to diffuse through the PEI/GO membrane in water desalination than in solvent dehydration. It should be noted that the PEI/GO LbL membranes used in these applications were not the same, and they had different bilayers and were further crosslinked in case of dehydration of EtOH and IPA.

Comparing dehydration of EG and dehydration of EtOH and IPA, it was shown that the PEI/GO LbL membrane had a higher total flux for EtOH and IPA dehydration than dehydration of EG. The opposite trend is true for the separation factor. The LbL membrane with three bilayers was more selective to water permeation in the dehydration of EG than the crosslinked PEI/GO LbL membrane with seven bilayers in the dehydration of EtOH and IPA. The values of E_J for

water permeation in dehydration of EtOH and IPA are higher than that for water permeation in dehydration of EG. It shows that temperature affected alcohol/water separation more significantly than EG/water separation. Crosslinking of the bilayers was shown to be an effective method to develop next generation pervaporation membranes for dehydration applications.

All the PEI/GO LbL membranes prepared in this study were hydrophilic, and the PEI/GO membrane with one bilayer was the most hydrophilic (with a water contact angle of 27°) among all the membranes tested. After deposition of additional bilayers (i.e., 3 bilayers), the contact angle increased to 41°, which may be attributed to the higher compactness of membrane and increased the content of GO on the membrane surface as GO contains hydrophobic aromatic regions. The crosslinked membrane with three bilayers showed a water contact angle of 51°. This may be ascribed to the hydrophobic carbon chain of the crosslinker GA [216] and its penetration to the interior during the crosslinking of each bilayer. In addition, crosslinking the GO layer decreased the amount of hydroxyl groups on the GO nanosheets that can form strong bonds with water. Nonetheless, such a change in surface hydrophilicity was not significant enough to change the mass transfer resistance per bilayer.

Chapter 7

General conclusions, contributions, and recommendations

7.1 General conclusions

The objectives of this study were to investigate the preparation of novel layer-by-layer (LbL) self-assembled membranes using polyethyleneimine (PEI) and graphene oxide (GO) for desalination of high-salinity water and dehydration of organic solvents via pervaporation. This work was divided into three parts; first, the PEI/GO LbL membrane was prepared, characterized and investigated for pervaporative desalination using different common salts (Chapter 3). After it was found that the LbL membrane with only one PEI/GO bilayer was efficient for pervaporative desalination of non-volatile salts, further investigations were carried out to assess the LbL membrane performance for dehydration of high boiling-point ethylene glycol (EG) with and without the presence of salt in the feed (Chapter 4). Finally, the performance of the PEI/GO LbL membranes was improved with the help of crosslinking for the dehydration of alcohols (Chapter 5).

In the first objective of the thesis, a preliminary study on the chlorination of thin film composite (TFC) polyamide membrane showed that the chlorine-treated polyamide membrane was a promising substrate for preparing LbL membrane. After chlorination, pure water flux increased

twofold and the membrane showed more hydrophilicity. The FTIR spectra of the membrane surfaces confirmed the formation of the LbL PEI/GO membrane. The X-Ray Diffraction (XRD) patterns of membranes showed a slight decrease in the *d* spacing between GO layers with the addition of PEI, which may be attributed to ionic crosslinking between GO and PEI to a certain extent to form a more closely stacked structure. It was shown that the LbL membrane with only one bilayer was suitable for pervaporative desalination of high-salinity water. A water flux of 8.4 kg/(m^2 h) was achieved at a feed NaCl concentration of 200 g/L at 65°C. The rejection of all the model salts (i.e., NaCl, Na_2SO_4, $MgSO_4$, and $MgCl_2$) was high (~99.9%) under all operating conditions. Water permeation flux increased with an increase in temperature mainly due to an increase in the driving force for permeation. The water flux decreased with an increase in salt concentration since the sorption of water at the membrane/liquid interface and the diffusion rate of water in the membrane was affected by the salt concentration.

The second objective, which focused on the preparation and characterization of PEI/GO LbL membranes for pervaporative dehydration of EG, resulted in a number of interesting findings. The PEI/GO LbL membrane with three bilayers was shown to be more selective and efficient than distillation, especially at lower feed water concentration. The $(PEI/GO)_3$ LbL membrane was preferentially permeable to water. A permeation flux of 114 g/(m^2h) and a separation factor of 213 were achieved at 35 ºC for a feed with 2wt% water. At feed water concentrations of 0.1, 0.2, and 0.5 wt%, separation factors of 1800, 1008, and 583 were observed, respectively. The effect of operating temperature was more significant on EG flux than water permeation flux; subsequently, the separation factor experienced a drop. For a feed water concentration of 2 wt%, the total flux increased to 190 g/m^2h with a separation factor of 160 when the temperature was increased to 60 °C. Since salt and EG are commonly present in gas and chemical processing, the effects of NaCl

present in the feed on the dehydration of EG were also investigated. Both the total flux and separation factor increased with temperature in the presence of salt, and the effect of temperature was more significant on water flux. With an increase in the salt concentration, the separation factor increased at all feed water concentrations, while the total flux decreased.

The effects of number of bilayers on the dehydration of EG showed that when the number of bilayers increased from 1 to 15, the total flux decreased by 38% (164 to 102 g/m^2h) and the separation factor increased by 148% (from 83 to 205). An analysis with the resistance-in-series model showed that the mass transfer resistance per bilayer for EG permeation was higher than that of water. By building up more PEI/GO bilayers, the LbL membrane became more selective to water. The PEI/GO LbL membranes had water contact angles less than 54°, confirming their hydrophilicity. Moreover, the mean surface roughness (Ra) of the LbL membrane decreased to 21 nm after depositing 15 number of bilayers, which could be ascribed to the coverage of the membrane surface by PEI and GO.

Finally, the PEI/GO LbL membranes were crosslinked using glutaraldehyde (GA) for pervaporative dehydration of ethanol (EtOH) and isopropanol (IPA). With a two-level factorial design, the optimal ranges of the crosslinking parameters were found as: a GA concentration of 1wt%, and a crosslinking time of 30 min at room temperature. After crosslinking, the sorption uptake of water in the PEI/GO bilayers (seven bilayers) decreased from 7.9 to 3.4 (g water/g bilayer), confirming more-compact membrane structures after crosslinking. The crosslinked $(PEI/GO)_7$ LbL membrane showed an improved permselectivity for dehydration of EtOH and IPA, whereas the separation factor decreased slightly with temperature due to the restriction of polymer chain mobility. The total flux for EtOH dehydration was higher than that for IPA dehydration, attributing to the penetrant size, polarity and hydrogen bonding parameters. Based on the

resistance-in-series approach, the mass transfer resistances per PEI/GO bilayer to EtOH and IPA are much higher than to water, and so was resistance of the substrate. However, the permselectivity of the substrate was not high enough as shown by the low water/alcohol permeance ratio (i.e., 3 for water/EtOH and 12 for water/IPA). PEI/GO bilayer showed a permeance ratio of 250 and 620 for water/EtOH and water/IPA, respectively, implying that the membrane was much more permselective after deposition of bilayers on the substrate.

To summarize, the results of this study showed that the PEI/GO LbL membranes with different number of bilayers are promising for pervaporative desalination of high salinity water and dehydration of organic solvents. The effects of operating conditions on membrane performance were observed. LbL membranes with different number of bilayers were prepared and analyzed based on resistance-in-series model. Overall, the membranes compared favorably with other membranes reported in the literature. The membrane characterizations have not been addressed in details, and additional work is needed to have a better understanding of the membranes.

7.2 Recommendations for future work

Based on the research findings, the following are suggested for further studies to provide helpful insights:

Characterization of the PEI/GO LbL membrane

The first recommendation is to characterize PEI/GO LbL membranes using field emission scanning electron microscopy (FESEM) and transmission electron microscopy (TEM) to assist in confirming the nanoscale wall structure that is generated by the LbL deposition and thickness of the membrane. Also, a quartz crystal microbalance (QCM) can provide more insights about the

mass increment and behaviors of the GO nanosheets and PEI chains. For instance, the mass ratio of deposited GO and PEI can be found and compared.

Further improvement of PEI/GO LbL membrane for dehydration applications

The $(PEI/GO)_3$ LbL membrane showed a high separation factor especially at low feed water concentrations. However, the total flux was still not very high (compared to alcohol dehydration). The opposite is true for dehydration of alcohols using crosslinked $(PEI/GO)_7$ membrane; high permeation flux and low separation factor. Further studies can be carried out to improve the selectivity of alcohol dehydration, and the total flux of EG dehydration. For these improvements the other types of crosslinker such as glyoxal, trimesoyl chloride, and glyoxylic acid can be applied. In addition, either PEI or GO layers, or both, can be crosslinked, and the results compared. The condition of chlorination can be also optimized for the dehydration of EG. The other LbL preparation methods and polyelectrolyte solution conditions may make an improvement in LbL membrane performance, as discussed below in detail.

LbL Preparation methods

In this research, the membranes were prepared by a static LbL process (single-sided deposition). Two other preparation methods can be considered: a dynamic LbL process in which the deposition solution moves continuously in a deposition process (a rotator, shaker or stirrer can be used), and an electric field (EF) process in which electrode plates are placed at the two sides of the substrate and solution, and a DC power supply is used to connect the electrodes and generate a uniform electric field, without the electrodes touching the solution or substrate material. Both methods might offer a better choice of the deposition as the distribution of the polyelectrolytes on the substrate would improve. Moreover, the two methods may also offer such advantages over the static LbL process as shorter preparation time, fewer deposition layers, reduced use of

polyelectrolyte solutions, and even distribution of polyelectrolyte [64,241]. In the presence of an electric field, the PEI and GO showed ordered stretched chains and nanosheets [242].

Polyelectrolyte solution

To explore the effects of PEI and GO solution pH, concentrations, deposition time and temperature, and the presence of salt in deposition solutions on the pervaporative performance of the membranes. A longer deposition time might allow more polyelectrolyte to diffuse to the oppositely charged surface, which may help repair any defects on the membrane surface. With an increase in the deposition temperature, the polyelectrolytes will become more energetic, and their diffusion will be faster. Consequently, they will be adsorbed by the substrate faster. pH is an important parameter that directly influences the degree of ionization of polyelectrolytes in solutions and subsequently the growth and adsorption amount of polyelectrolytes. The presence of salt in polyelectrolyte solution changes polymer conformation (polymer coils become denser).

Dehydration of other organics

In this study, LbL formed on chlorine-treated TFC polyamide membranes were used for pervaporative desalination of water and dehydration of ethylene glycol, ethanol, and isopropanol. To further investigate the pervaporation performance of PEI/GO LbL membranes, the application of such membranes can be extended to pervaporative dehydration of other organic solvents (e.g., butanol, triethylene glycol and acetic acid). The effects of feed concentration, operating temperature, and the presence of inorganic components in feed on membrane performance can be studied.

6.3 Summary of research contributions

In this study, the chlorinated TFC polyamide membranes were used for the first time as substrates for the LbL deposition of PEI and GO. The membranes were applied to pervaporative desalination of high-salinity water, dehydration of high-boiling organic compound (e.g., ethylene glycol), and dehydration of azeotropic mixtures (e.g., ethanol/water and isopropanol/water mixtures). A portion of the pervaporative desalination study in Chapter 3 has been published in *Separation and Purification Technology* 234 (2020) 116077. A manuscript based on dehydration of EtOH and IPA study is under review in *Chemical Engineering Science.* A manuscript on dehydration of EG has been submitted to *Journal of membrane science*.

It was for the first time that the PEI/GO LbL membranes has been applied for pervaporative desalination and dehydration of ethylene glycol, to the best of the author's knowledge. Moreover, no reports are currently available in the literature on the preparation of PEI/GO LbL membranes crosslinked with glutaraldehyde for alcohol dehydration. Effects of temperature and feed concentration as the most influential parameters on the membranes performance was investigated at different pervaporation applications and discussed in details. The effects of three main factors in the crosslinking of PEI and GO layers were investigated for the first time in the literature to better understand the effect of crosslinking on the membrane performance. It was shown that crosslinking time and crosslinker concentration were the most significant parameters.

The effects of bilayers on the performance of a LbL membrane has not been investigated in details in the literature. It was usually explained based on the thickness of the bilayers estimated from SEM images. This is the first study reporting the effects of bilayers on pervaporative performance based on the resistance-in-series model. This approach allows researchers to better understand how the bilayers and substrate influence the membrane performance. These findings

enhance our understanding of the concepts of the resistance of per bilayer and substrate resistance of the LbL membranes.

The PEI/GO LbL membranes with different bilayers showed potential for application in the pervaporative treatment of high-salinity water, the dehydration of ethylene glycol, and the dehydration of ethanol and isopropanol. In all studied applications, the LbL membranes showed great stability, which makes them a promising candidate to use.

Reference

[1] M. Elimelech, W.A. Phillip, The future of seawater desalination: energy, technology, and the environment, Science. 333 (2011) 712 – 717.

[2] Global membrane water and wastewater treatment market report, (2019, January) Retrieved from https://www.grandviewresearch.com/industry-analysis/

[3] P.D. Chapman, T. Oliveira, A.G. Livingston, K. Li, Membranes for the dehydration of solvents by pervaporation, J. Membr. Sci. 318 (2008) 5–37.

[4] Y.K. Ong, G.M. Shi, N.L. Le, Y.P. Tang, J. Zuo, S.P. Nunes, T.S. Chung, Recent membrane development for pervaporation processes, Prog. Polym. Sci. 57 (2016) 1–31.

[5] Q. Wang, N. Li, B. Bolto, M. Hoang, Z. Xie, Desalination by pervaporation: A review, Desalination. 387 (2016) 46–60.

[6] S.P. Nunes, K.-V. Peinemann, Membrane Technology in the Chemical Industry, Wiley, 2001.

[7] S.-L. Wee, C.-T. Tye, S. Bhatia, Membrane separation process—Pervaporation through zeolite membrane, Sep. Purif. Technol. 63 (2008) 500–516.

[8] U. Sander, P. Soukup, Design and operation of a pervaporation plant for ethanol dehydration, J. Membr. Sci. 36 (1988) 463–475.

[9] R. Ruutenhuch, Membrane separation systems: recent developments and future directions., Chemie Ing. Tech. 64 (1992) 584.

[10] X. Feng, R.Y.M. Huang, Liquid separation by membrane pervaporation: A review, Ind. Eng. Chem. Res. 36 (1997) 1048–1066.

[11] Q. Zhao, Q.F. An, Y. Ji, J. Qian, C. Gao, Polyelectrolyte complex membranes for pervaporation, nanofiltration and fuel cell applications, J. Membr. Sci. 379 (2011) 19–45.

[12] Z. Zhu, X. Feng, A. Penlidis, Self-assembled nano-structured polyelectrolyte composite membranes for pervaporation, Mater. Sci. Eng. C. 26 (2006) 1–8.

[13] J. Xu, X. Feng, C. Gao, Surface modification of thin-film-composite polyamide membranes for improved reverse osmosis performance, J. Membr. Sci. 370 (2011) 116–123.

[14] R.W. Baker, Membrane Technology and Applications, 3rd ed., Wiley, 2012.

[15] Y. Zhou, S. Yu, C. Gao, X. Feng, Surface modification of thin film composite polyamide membranes by electrostatic self deposition of polycations for improved fouling resistance, Sep. Purif. Technol. 66 (2009) 287–294.

[16] N. Wang, S. Ji, G. Zhang, J. Li, L. Wang, Self-assembly of graphene oxide and polyelectrolyte complex nanohybrid membranes for nanofiltration and pervaporation, Chem. Eng. J. 213 (2012) 318–329.

[17] M. Hu, B. Mi, Layer-by-layer assembly of graphene oxide membranes via electrostatic interaction, J. Membr. Sci. 469 (2014) 80–87.

[18] H.M. Hegab, Y. Wimalasiri, M. Ginic-Markovic, L. Zou, Improving the fouling resistance of brackish water membranes via surface modification with graphene oxide functionalized chitosan, Desalination. 365 (2015) 99–107.

[19] P.A. Kober, Pervaporation, perstillation and percrystallization, J. Membr. Sci. 100 (1995) 61–64.

[20] I. Blume, J.G. Wijmans, R.W. Baker, The separation of dissolved organics from water by pervaporation, J. Membr. Sci. 49 (1990) 253–286.

[21] P. Shao, R.Y.M. Huang, Polymeric membrane pervaporation, J. Membr. Sci. 287 (2007) 162–179.

[22] H.K. Lonsdale, The growth of membrane technology, J. Membr. Sci. 10 (1982) 81–181.

[23] J.G. Wijmans, R.W. Baker, The solution-diffusion model: a review, J. Membr. Sci. 107 (1995) 1–21.

[24] M. Mudler, Basic Principles of Membrane Technology, Springer, 2012.

[25] T. Okada, T. Matsuura, Predictability of transport equations for pervaporation on the basis of pore-flow mechanism, J. Membr. Sci. 70 (1992) 163–175.

[26] E. Nagy, Chapter 18 - Membrane Gas Separation, 2nd Ed., Elsevier, 2019, 457–481.

[27] K. Ghosal, B.D. Freeman, Gas separation using polymer membranes: an overview, Polym. Adv. Technol. 5 (1994) 673–697.

[28] B. Freeman, Y. Yampolskii, I. Pinnau, Materials science of membranes for gas and vapor separation, John Wiley & Sons, 2006.

[29] D.R. Paul, Polymeric Gas Separation Membranes, CRC press, 2018.

[30] W.M. Lee, Selection of barrier materials from molecular structure, Polym. Eng. Sci. 20 (1980) 65–69.

[31] X. Feng, R.Y.M. Huang, Estimation of activation energy for permeation in pervaporation processes, J. Membr. Sci. 118 (1996) 127–131.

[32] Y.P. Kuznetsov, E. V Kruchinina, Y.G. Baklagina, A.K. Khripunov, O.A. Tulupova, Deep desalination of water by evaporation through polymeric membranes, Russ. J. Appl. Chem. 80 (2007) 790–798.

[33] E. Huth, S. Muthu, L. Ruff, J.A. Brant, Feasibility assessment of pervaporation for desalinating high-salinity brines, J. Water Reuse Desal. 4 (2014) 109–124.

[34] Z. Xie, D. Ng, M. Hoang, T. Duong, S. Gray, Separation of aqueous salt solution by pervaporation through hybrid organic–inorganic membrane: Effect of operating conditions, Desalination. 273 (2011) 220–225.

[35] Y. Zhu, R.G. Minet, T.T. Tsotsis, A continuous pervaporation membrane reactor for the study of esterification reactions using a composite polymeric/ceramic membrane, Chem. Eng. Sci. 51 (1996) 4103–4113.

[36] H. Bruschke, Industrial application of membrane separation processes, Pure Appl. Chem. 67 (1995) 993.

[37] R.Y.M. Huang, Pervaporation Membrane Separation Processes, Elsevier, 1991.

[38] C. Guizard, A. Bac, M. Barboiu, N. Hovnanian, Hybrid organic-inorganic membranes with specific transport properties: Applications in separation and sensors technologies, Sep. Purif. Technol. 25 (2001) 167–180.

[39] F. Peng, L. Lu, H. Sun, Z. Jiang, Analysis of annealing effect on pervaporation properties of PVA-GPTMS hybrid membranes through PALS, J. Membr. Sci. 281 (2006) 600–608.

[40] M. Drobek, C. Yacou, J. Motuzas, A. Julbe, L. Ding, J.C. Diniz da Costa, Long term pervaporation desalination of tubular MFI zeolite membranes, J. Membr. Sci. 415–416 (2012) 816–823.

[41] E. Korin, I. Ladizhensky, E. Korngold, Hydrophilic hollow fiber membranes for water desalination by the pervaporation method, Chem. Eng. Process. Process Intensif. 35 (1996) 451–457.

[42] E. Korngold, E. Korin, I. Ladizhensky, Water desalination by pervaporation with hollow fiber membranes, Desalination. 107 (1996) 121–129.

[43] C.H. Cho, K.Y. Oh, S.K. Kim, J.G. Yeo, P. Sharma, Pervaporative seawater desalination using NaA zeolite membrane: Mechanisms of high water flux and high salt rejection, J. Membr. Sci. 371 (2011) 226–238.

[44] S.G. Chaudhri, B.H. Rajai, P.S. Singh, Preparation of ultra-thin poly(vinyl alcohol) membranes supported on polysulfone hollow fiber and their application for production of pure water from seawater, Desalination. 367 (2015) 272–284.

[45] M.C. Duke, J. O'Brien-Abraham, N. Milne, B. Zhu, J.Y.S. Lin, J.C. Diniz da Costa, Seawater desalination performance of MFI type membranes made by secondary growth, Sep. Purif. Technol. 68 (2009) 343–350.

[46] H.J. Zwijnenberg, G.H. Koops, M. Wessling, Solar driven membrane pervaporation for desalination processes, J. Membr. Sci. 250 (2005) 235–246.

[47] S. Wijaya, M.C. Duke, J.C. Diniz da Costa, Carbonised template silica membranes for desalination, Desalination. 236 (2009) 291–298.

[48] B. Liang, K. Pan, L. Li, E.P. Giannelis, B. Cao, High performance hydrophilic pervaporation composite membranes for water desalination, Desalination. 347 (2014) 199–206.

[49] W. An, X. Zhou, X. Liu, P.W. Chai, T. Kuznicki, S.M. Kuznicki, Natural zeolite clinoptilolite-phosphate composite membranes for water desalination by pervaporation, J. Membr. Sci. 470 (2014) 431–438.

[50] B. Liang, W. Zhan, G. Qi, S. Lin, Q. Nan, Y. Liu, B. Cao, K. Pan, High performance graphene oxide/polyacrylonitrile composite pervaporation membranes for desalination applications, J. Mater. Chem. A. 3 (2015) 5140–5147.

[51] S.I. Semenova, H. Ohya, K. Soontarapa, Hydrophilic membranes for pervaporation: An analytical review, Desalination. 110 (1997) 251–286.

[52] X. Qiao, T.S. Chung, Diamine modification of P84 polyimide membranes for pervaporation dehydration of isopropanol, AIChE J. 52 (2006) 3462–3472.

[53] M.L. Gimenes, L. Liu, X. Feng, Sericin/poly(vinyl alcohol) blend membranes for pervaporation separation of ethanol/water mixtures, J. Membr. Sci. 295 (2007) 71–79.

[54] L. Liang, E. Ruckenstein, Polyvinyl alcohol-polyacrylamide interpenetrating polymer network membranes and their pervaporation characteristics for ethanol-water mixtures, J. Membr. Sci. 106 (1995) 167–182.

[55] K.S.V.K. Rao, M.C.S. Subha, M. Sairam, N.N. Mallikarjuna, T.M. Aminabhavi, Blend membranes of chitosan and poly(vinyl alcohol) in pervaporation dehydration of isopropanol and tetrahydrofuran, J. Appl. Polym. Sci. 103 (2007) 1918–1926.

[56] W. Zhang, G. Li, Y. Fang, X. Wang, Maleic anhydride surface-modification of crosslinked chitosan membrane and its pervaporation performance, J. Membr. Sci. 295 (2007) 130–138.

[57] R.Y.M. Huang, R. Pal, G.Y. Moon, Crosslinked chitosan composite membrane for the pervaporation dehydration of alcohol mixtures and enhancement of structural stability of chitosan/polysulfone composite membranes, J. Membr. Sci. 160 (1999) 17–30.

[58] R.Y.M. Huang, R. Pal, G.Y. Moon, Characteristics of sodium alginate membranes for the pervaporation dehydration of ethanol–water and isopropanol–water mixtures, J. Membr. Sci. 160 (1999) 101–113.

[59] M.D. Kurkuri, U.S. Toti, T.M. Aminabhavi, Syntheses and characterization of blend membranes of sodium alginate and poly(vinyl alcohol) for the pervaporation separation of water + isopropanol mixtures, J. Appl. Polym. Sci. 86 (2002) 3642–3651.

[60] Y.Q. Dong, L. Zhang, J.N. Shen, M.Y. Song, H.L. Chen, Preparation of poly(vinyl alcohol)-sodium alginate hollow-fiber composite membranes and pervaporation dehydration characterization of aqueous alcohol mixtures, Desalination. 193 (2006) 202–210.

[61] H.A. Tsai, M.J. Hong, G.S. Huang, Y.C. Wang, C.L. Li, K.R. Lee, J.Y. Lai, Effect of DGDE additive on the morphology and pervaporation performances of asymmetric PSf hollow fiber membranes, J. Membr. Sci. 208 (2002) 233–245.

[62] Y.C. Wang, Y.S. Tsai, K.R. Lee, J.Y. Lai, Preparation and pervaporation performance of 3,3-bis[4-(4-aminophenoxy)phenyl] phthalide based polyimide membranes, J. Appl. Polym. Sci. 96 (2005) 2046–2052.

[63] G. Zhang, H. Yan, S. Ji, Z. Liu, Self-assembly of polyelectrolyte multilayer pervaporation membranes by a dynamic layer-by-layer technique on a hydrolyzed polyacrylonitrile ultrafiltration membrane, J. Membr. Sci. 292 (2007) 1–8.

[64] G. Zhang, W. Gu, S. Ji, Z. Liu, Y. Peng, Z. Wang, Preparation of polyelectrolyte multilayer membranes by dynamic layer-by-layer process for pervaporation separation of alcohol/water mixtures, J. Membr. Sci. 280 (2006) 727–733.

[65] K.R. Lee, R.Y. Chen, J.Y. Lai, Plasma deposition of vinyl acetate onto Nylon-4 membrane for pervaporation and evapomeation separation of aqueous alcohol mixtures, J. Membr. Sci. 75 (1992) 171–180.

[66] W.S. Hung, M. De Guzman, S.H. Huang, K.R. Lee, Y.C. Jean, J.Y. Lai, Characterizing free volumes and layer structures in asymmetric thin-film polymeric membranes in the wet condition using the variable monoenergy slow positron beam, Macromolecules. 43 (2010) 6127–6134.

[67] B. Khorshidi, T. Thundat, B.A. Fleck, M. Sadrzadeh, A novel approach toward fabrication of high performance thin film composite polyamide membranes, Sci. Rep. 6 (2016) 22069.

[68] S.H. Huang, C.J. Hsu, D.J. Liaw, C.C. Hu, K.R. Lee, J.Y. Lai, Effect of chemical structures of amines on physicochemical properties of active layers and dehydration of isopropanol through interfacially polymerized thin-film composite membranes, J. Membr. Sci. 307 (2008) 73–81.

[69] W.C. Chao, S.H. Huang, Q. An, D.J. Liaw, Y.C. Huang, K.R. Lee, J.Y. Lai, Novel interfacially-polymerized polyamide thin-film composite membranes: Studies on characterization, pervaporation, and positron annihilation spectroscopy, Polymer. 52 (2011) 2414–2421.

[70] J. Zuo, J.Y. Lai, T.S. Chung, In-situ synthesis and cross-linking of polyamide thin film composite (TFC) membranes for bioethanol applications, J. Membr. Sci. 458 (2014) 47–57.

[71] P. Sukitpaneenit, T.S. Chung, Fabrication and use of hollow fiber thin film composite membranes for ethanol dehydration, J. Membr. Sci. 450 (2014) 124–137.

[72] S.H. Huang, G.J. Jiang, D.J. Liaw, C.L. Li, C.C. Hu, K.R. Lee, J.Y. Lai, Effects of the polymerization and pervaporation operating conditions on the dehydration performance of interfacially polymerized thin-film composite membranes, J. Appl. Polym. Sci. 114 (2009) 1511–1522.

[73] S.H. Huang, W.S. Hung, D.J. Liaw, C.H. Lo, W.C. Chao, C.C. Hu, C.L. Li, K.R. Lee, J.Y. Lai, Interfacially polymerized thin-film composite polyamide membranes: Effects of annealing processes on pervaporative dehydration of aqueous alcohol solutions, Sep. Purif. Technol. 72 (2010) 40–47.

[74] Y. Liu, M. Zhu, Q. Zhao, Q. An, J. Qian, K. Lee, J. Lai, The chemical crosslinking of polyelectrolyte complex colloidal particles and the pervaporation performance of their membranes, J. Membr. Sci. 385–386 (2011) 132–140.

[75] Y. Zhang, J.W. Rhim, X. Feng, Improving the stability of layer-by-layer self-assembled membranes for dehydration of alcohol and diol, J. Membr. Sci. 444 (2013) 22–31.

[76] A. Toutianoush, L. Krasemann, B. Tieke, Polyelectrolyte multilayer membranes for pervaporation separation of alcohol/water mixtures, Colloids Surfaces A Physicochem. Eng. Asp. 198–200 (2002) 881–889.

[77] G. Decher, Fuzzy nanoassemblies: toward layered polymeric multicomposites, Science. 277 (1997) 1232–1237.

[78] B.F. Abu-Sharkh, Structure and mechanism of formation of polyelectrolyte multilayers, Polymer. 47 (2006) 3674–3680.

[79] R. Steitz, W. Jaeger, R. v. Klitzing, Influence of charge density and ionic strength on the multilayer formation of strong polyelectrolytes, Langmuir. 17 (2001) 4471–4474.

[80] R. Netz, J.F. Joanny, Complexation between a semiflexible polyelectrolyte and an oppositely charged sphere, Macromolecules. 32 (1999) 9026–9040.

[81] S.Y. Park, M.F. Rubner, A.M. Mayes, Free energy model for layer-by-layer processing of polyelectrolyte multilayer films, Langmuir. 18 (2002) 9600–9604.

[82] G. Decher, J.D. Hong, Buildup of ultrathin multilayer films by a self-assembly process: II. consecutive adsorption of anionic and cationic bipolar amphiphiles and polyelectrolytes on charged surfaces, Ber. Bunsenges. Phys. Chem. 95 (1991) 1430–1434.

[83] G.B. Sukhorukov, E. Donath, H. Lichtenfeld, E. Knippel, M. Knippel, A. Budde, H. Möhwald, Layer-by-layer self assembly of polyelectrolytes on colloidal particles, Colloids Surfaces A Physicochem. Eng. Asp. 137 (1998) 253–266.

[84] P. Lavalle, C. Gergely, F.J.G. Cuisinier, G. Decher, P. Schaaf, J.C. Voegel, C. Picart, Comparison of the structure of polyelectrolyte multilayer films exhibiting a linear and an exponential growth regime: An in situ atomic force microscopy study, Macromolecules. 35 (2002) 4458–4465.

[85] Y. Lvov, F. Essler, G. Decher, Combination of polycation/polyanion self-assembly and Langmuir-Blodgett transfer for the construction of superlattice films, J. Phys. Chem. 97 (1993) 13773–13777.

[86] X. Arys, A. Laschewsky, A.M. Jonas, Ordered polyelectrolyte "multilayers". 1. Mechanisms of growth and structure formation: A comparison with classical fuzzy "multilayers," Macromolecules. 34 (2001) 3318–3330.

[87] F. Caruso, E. Rodda, D.N. Furlong, K. Niikura, Y. Okahata, Quartz crystal microbalance study of DNA immobilization and hybridization for nucleic acid sensor development, Anal. Chem. 69 (1997) 2043–2049.

[88] M. Yin, J. Qian, Q. An, Q. Zhao, Z. Gui, J. Li, Polyelectrolyte layer-by-layer self-assembly at vibration condition and the pervaporation performance of assembly multilayer films in dehydration of isopropanol, J. Membr. Sci. 358 (2010) 43–50.

[89] B.Y. Kim, M.L. Bruening, pH-dependent growth and morphology of multilayer dendrimer/poly(acrylic acid) films, Langmuir. 19 (2003) 94–99.

[90] W. Lenk, J. Meier-Haack, Polyelectrolyte multilayer membranes for pervaporation separation of aqueous-organic mixtures, Desalination. 148 (2002) 11–16.

\

[91] G. Zhang, X. Gao, S. Ji, Z. Liu, Electric field-enhanced assembly of polyelectrolyte composite membranes, J. Membr. Sci. 307 (2008) 151–155.

[92] P. Zhang, J. Qian, Q. An, X. Liu, Q. Zhao, H. Jin, Surface morphology and pervaporation performance of electric field enhanced multilayer membranes, J. Membr. Sci. 328 (2009) 141–147.

[93] P. Zhang, J. Qian, Y. Yang, Q. An, X. Liu, Z. Gui, Polyelectrolyte layer-by-layer self-assembly enhanced by electric field and their multilayer membranes for separating isopropanol–water mixtures, J. Membr. Sci. 320 (2008) 73–77.

[94] D. Carrière, R. Krastev, M. Schönhoff, Oscillations in solvent fraction of polyelectrolyte multilayers driven by the charge of the terminating layer, Langmuir. 20 (2004) 11465–11472.

[95] M.D. Miller, M.L. Bruening, Correlation of the swelling and permeability of polyelectrolyte multilayer films, Chem. Mater. 17 (2005) 5375–5381.

[96] S.E. Burke, C.J. Barrett, Swelling behavior of hyaluronic acid/polyallylamine hydrochloride multilayer films, Biomacromolecules. 6 (2005) 1419–1428.

[97] J.W. Rhim, Y.K. Kim, Pervaporation separation of MTBE–methanol mixtures using cross-linked PVA membranes, J. Appl. Polym. Sci. 75 (2000) 1699–1707.

[98] S. Xiao, X. Feng, R.Y.M. Huang, Trimesoyl chloride crosslinked chitosan membranes for CO2/N2 separation and pervaporation dehydration of isopropanol, J. Membr. Sci. 306 (2007) 36–46.

[99] T. Uragami, T. Matsuda, H. Okuno, T. Miyata, Structure of chemically modified chitosan membranes and their characteristics of permeation and separation of aqueous ethanol solutions, J. Membr. Sci. 88 (1994) 243–251.

[100] J. Ren, C. Jiang, Transport phenomena of chitosan membrane in pervaporation of water-ethanol mixture, Sep. Sci. Technol. 33 (1998) 517–535.

[101] Y.N. Kwon, J.O. Leckie, Hypochlorite degradation of crosslinked polyamide membranes: I. Changes in chemical/morphological properties, J. Membr. Sci. 283 (2006) 21–26.

[102] Y.N. Kwon, J.O. Leckie, Hypochlorite degradation of crosslinked polyamide membranes: II. Changes in hydrogen bonding behavior and performance, J. Membr. Sci. 282 (2006) 456–464.

[103] J. Glater, S. Hong, M. Elimelech, The search for a chlorine-resistant reverse osmosis membrane, Desalination. 95 (1994) 325–345.

[104] D. Wu, J. Martin, J.R. Du, Y. Zhang, D. Lawless, X. Feng, Effects of chlorine exposure on nanofiltration performance of polyamide membranes, J. Membr. Sci. 487 (2015) 256–270.

[105] D.R. Dreyer, S. Park, C.W. Bielawski, R.S. Ruoff, The chemistry of graphene oxide, Chem. Soc. Rev. 39 (2010) 228–240.

[106] S.T. Nguyen, O.C. Compton, Graphene oxide, highly reduced graphene oxide, and graphene: Versatile building blocks for carbon-based materials, Small. 6 (2010) 711–723.

[107] J.T. Chen, Y.J. Fu, Q.F. An, S.C. Lo, S.H. Huange, W.S. Hunga, C.C. Hu, K.R. Lee, J.Y. Lai, Tuning nanostructure of graphene oxide/polyelectrolyte LbL assemblies by controlling

pH of GO suspension to fabricate transparent and super gas barrier films, Nanoscale. 5 (2013) 9081–9088.

[108] M. Hu, B. Mi, Enabling graphene oxide nanosheets as water separation membranes, Environ. Sci. Technol. 47 (2013) 3715–3723.

[109] X. Zhao, Q. Zhang, Y. Hao, Y. Li, Y. Fang, D. Chen, Alternate multilayer films of poly(vinyl alcohol) and exfoliated graphene oxide fabricated via a facial layer-by-layer assembly, Macromolecules. 43 (2010) 9411–9416.

[110] L.J. Cote, J. Kim, V.C. Tung, J. Luo, F. Kim, J. Huang, Graphene oxide as surfactant sheets, Pure Appl. Chem. 83 (2010) 95–110.

[111] A.J. Paulista Neto, E.E. Fileti, Elucidating the amphiphilic character of graphene oxide, Phys. Chem. Chem. Phys. 20 (2018) 9507–9515.

[112] A.J. Paulista Neto, E.E. Fileti, Impact of edge groups on the hydration and aggregation properties of graphene oxide, J. Phys. Chem. B. 122 (2018) 2578–2586.

[113] A.J.P. Neto, V. V Chaban, E.E. Fileti, Hydration peculiarities of graphene oxides with multiple oxidation degrees, Phys. Chem. Chem. Phys. 19 (2017) 32333–32340.

[114] F. Kim, L.J. Cote, J. Huang, Graphene oxide: surface activity and two-dimensional assembly, Adv. Mater. 22 (2010) 1954–1958.

[115] L. Xu, J. Teng, L. Li, H.-D. Huang, J.-Z. Xu, Y. Li, P.-G. Ren, G.-J. Zhong, Z.-M. Li, Hydrophobic graphene oxide as a promising barrier of water vapor for regenerated cellulose nanocomposite films, ACS Omega. 4 (2019) 509–517.

[116] X. Chen, G. Liu, H. Zhang, Y. Fan, Fabrication of graphene oxide composite membranes and their application for pervaporation dehydration of butanol, Chinese J. Chem. Eng. 23 (2015) 1102–1109.

[117] L. Zhao, H. Zhang, N.H. Kim, D. Hui, J.H. Lee, Q. Li, H. Sun, P. Li, Preparation of graphene oxide/polyethyleneimine layer-by-layer assembled film for enhanced hydrogen barrier property, Compos. Part B Eng. 92 (2016) 252–258.

[118] Y.H. Yang, L. Bolling, M.A. Priolo, J.C. Grunlan, Super gas barrier and selectivity of graphene oxide-polymer multilayer thin films, Adv. Mater. 25 (2013) 503–508.

[119] W. Choi, J. Choi, J. Bang, J.H. Lee, Layer-by-layer assembly of graphene gxide nanosheets on polyamide membranes for durable reverse-osmosis applications, ACS Appl. Mater. Interfaces. 5 (2013) 12510–12519.

[120] M.A. Shannon, P.W. Bohn, M. Elimelech, J.G. Georgiadis, B.J. Mariñas, A.M. Mayes, Science and technology for water purification in the coming decades, Nature. 452 (2008)

301.

[121] D. Cohen-Tanugi, J.C. Grossman, Water desalination across nanoporous graphene, Nano Lett. 12 (2012) 3602–3608.

[122] H. Wang, S. Ding, H. Zhu, F. Wang, Y. Guo, H. Zhang, J. Chen, Effect of stretching ratio and heating temperature on structure and performance of PTFE hollow fiber membrane in VMD for RO brine, Sep. Purif. Technol. 126 (2014) 82–94.

[123] Z. Xie, M. Hoang, T. Duong, D. Ng, B. Dao, S. Gray, Sol–gel derived poly(vinyl alcohol)/maleic acid/silica hybrid membrane for desalination by pervaporation, J. Membr. Sci. 383 (2011) 96–103.

[124] M. Baghbanzadeh, D. Rana, C.Q. Lan, T. Matsuura, Zero thermal input membrane distillation, a zero-waste and sustainable solution for freshwater shortage, Appl. Energy. 187 (2017) 910–928.

[125] D.M. Warsinger, J. Swaminathan, E. Guillen-Burrieza, H.A. Arafat, J.H. Lienhard V, Scaling and fouling in membrane distillation for desalination applications: A review, Desalination. 356 (2015) 294–313.

[126] L.D. Tijing, Y.C. Woo, J.-S. Choi, S. Lee, S.-H. Kim, H.K. Shon, Fouling and its control in membrane distillation—A review, J. Membr. Sci. 475 (2015) 215–244.

[127] M. Gryta, Fouling in direct contact membrane distillation process, J. Membr. Sci. 325 (2008) 383–394.

[128] M. Gryta, Influence of polypropylene membrane surface porosity on the performance of membrane distillation process, J. Membr. Sci. 287 (2007) 67–78.

[129] M. Gryta, Long-term performance of membrane distillation process, J. Membr. Sci. 265 (2005) 153–159.

[130] M.D.C. García-Payo, M.A. Izquierdo-Gil, C. Fernández-Pineda, Wetting study of hydrophobic membranes via liquid entry pressure measurements with aqueous alcohol solutions, J. Colloid Interface Sci. 230 (2000) 420–431.

[131] A. Selim, A.J. Toth, E. Haaz, D. Fozer, A. Szanyi, N. Hegyesi, P. Mizsey, Preparation and characterization of PVA/GA/Laponite membranes to enhance pervaporation desalination performance, Sep. Purif. Technol. 221 (2019) 201–210.

[132] E. Drioli, S. Zhang, A. Basile, On the coupling effect in pervaporation, J. Membr. Sci. 81 (1993) 43–55.

[133] Y. Ying, W. Ying, Q. Li, D. Meng, G. Ren, R. Yan, X. Peng, Recent advances of nanomaterial-based membrane for water purification, Appl. Mater. Today. 7 (2017) 144–

158.

[134] B. Liang, W. Zhan, G. Qi, S. Lin, Q. Nan, Y. Liu, B. Cao, K. Pan, polyacrylonitrile composite pervaporation membranes for desalination applications, J. Mater. Chem. A Mater. Energy Sustain. 3 (2015) 5140–5147.

[135] F. Baskoro, C.B. Wong, S.R. Kumar, C.W. Chang, C.H. Chen, D.W. Chen, S.J. Lue, Graphene oxide-cation interaction: Inter-layer spacing and zeta potential changes in response to various salt solutions, J. Membr. Sci. 554 (2018) 253–263.

[136] G.R. Xu, S.H. Wang, H.L. Zhao, S.B. Wu, J.M. Xu, L. Li, X.Y. Liu, Layer-by-layer (LBL) assembly technology as promising strategy for tailoring pressure-driven desalination membranes, J. Membr. Sci. 493 (2015) 428–443.

[137] B.G. Choi, Y.S. Huh, Y.C. Park, D.H. Jung, W.H. Hong, H. Park, Enhanced transport properties in polymer electrolyte composite membranes with graphene oxide sheets, Carbon N. Y. 50 (2012) 5395–5402.

[138] D. Li, M.B. Müller, S. Gilje, R.B. Kaner, G.G. Wallace, Processable aqueous dispersions of graphene nanosheets, Nat. Nanotechnol. 3 (2008) 101.

[139] J. Lee, H.R. Chae, Y.J. Won, K. Lee, C.H. Lee, H.H. Lee, I.C. Kim, J. min Lee, Graphene oxide nanoplatelets composite membrane with hydrophilic and antifouling properties for wastewater treatment, J. Membr. Sci. 448 (2013) 223–230.

[140] R.R. Nair, H.A. Wu, P.N. Jayaram, I. V Grigorieva, A.K. Geim, Unimpeded permeation of water through helium-leak-tight graphene-based membranes, Science. 335 (2012) 442–444.

[141] N. Wei, X. Peng, Z. Xu, Understanding water permeation in graphene oxide membranes, ACS Appl. Mater. Interfaces. 6 (2014) 5877–5883.

[142] Q. Nan, P. Li, B. Cao, Fabrication of positively charged nanofiltration membrane via the layer-by-layer assembly of graphene oxide and polyethylenimine for desalination, Appl. Surf. Sci. 387 (2016) 521–528.

[143] J. Xu, X. Feng, C. Gao, Surface modification of thin-film-composite polyamide membranes for improved reverse osmosis performance, J. Membr. Sci. 370 (2011) 116–123.

[144] Z. Zhu, X. Feng, A. Penlidis, Layer-by-layer self-assembled polyelectrolyte membranes for solvent dehydration by pervaporation, Mater. Sci. Eng. C. 27 (2007) 612–619.

[145] Y. Zhang, J.W. Rhim, X. Feng, Improving the stability of layer-by-layer self-assembled membranes for dehydration of alcohol and diol, J. Membr. Sci. 444 (2013) 22–31.

[146] P.T. Hammond, Recent explorations in electrostatic multilayer thin film assembly, Curr.

Opin. Colloid Interface Sci. 4 (1999) 430–442.

[147] B. Mi, Graphene oxide membranes for ionic and molecular sieving, Science. 343 (2014) 740 – 742.

[148] Y. Zhou, S. Yu, C. Gao, X. Feng, Surface modification of thin film composite polyamide membranes by electrostatic self deposition of polycations for improved fouling resistance, Sep. Purif. Technol. 66 (2009) 287–294.

[149] W.J. Lau, A.F. Ismail, N. Misdan, M.A. Kassim, A recent progress in thin film composite membrane: A review, Desalination. 287 (2012) 190–199.

[150] J. Glater, S. Hong, M. Elimelech, The search for a chlorine-resistant reverse osmosis membrane, Desalination. 95 (1994) 325–345.

[151] H.D. Raval, J.J. Trivedi, S.V. Joshi, C.V. Devmurari, Flux enhancement of thin film composite RO membrane by controlled chlorine treatment, Desalination. 250 (2010) 945–949.

[152] N.P. Soice, A.R. Greenberg, W.B. Krantz, A.D. Norman, Studies of oxidative degradation in polyamide RO membrane barrier layers using pendant drop mechanical analysis, J. Membr. Sci. 243 (2004) 345–355.

[153] D.C. Marcano, D. V Kosynkin, J.M. Berlin, A. Sinitskii, Z. Sun, A. Slesarev, L.B. Alemany, W. Lu, J.M. Tour, Improved synthesis of graphene oxide, ACS Nano. 4 (2010) 4806–4814.

[154] W.S. Hummers, R.E. Offeman, Preparation of graphitic oxide, J. Am. Chem. Soc. 80 (1958) 1339.

[155] Y.-H. Yang, F.A. Malek, J.C. Grunlan, Influence of deposition time on layer-by-layer growth of clay-based thin films, Ind. Eng. Chem. Res. 49 (2010) 8501–8509.

[156] G. Decher, J.B. Schlenoff, Multilayer thin films: sequential assembly of nanocomposite materials, John Wiley & Sons, 2006.

[157] Y. Huang, J. Sun, D. Wu, X. Feng, Layer-by-layer self-assembled chitosan/PAA nanofiltration membranes, Sep. Purif. Technol. 207 (2018) 142–150.

[158] Y. Zhang, Layer-by-layer Self-assembly Membranes for Solvent Dehydration by Pervaporation, (2013).

[159] T. Wang, J. Lu, L. Mao, Z. Wang, Electric field assisted layer-by-layer assembly of graphene oxide containing nanofiltration membrane, J. Membr. Sci. 515 (2016) 125–133.

[160] J.P.G. Villaluenga, P. Godino, M. Khayet, B. Seoane, J.I. Mengual, Pervaporation of alcohols and methyl tert-butyl ether through a dense poly(2,6-dimethyl-1,4-phenylene

oxide) membrane, Ind. Eng. Chem. Res. 43 (2004) 2548–2555.

[161] G.S. Lai, W.J. Lau, P.S. Goh, A.F. Ismail, N. Yusof, Y.H. Tan, Graphene oxide incorporated thin film nanocomposite nanofiltration membrane for enhanced salt removal performance, Desalination. 387 (2016) 14–24.

[162] W.S. Hung, Q.F. An, M. De Guzman, H.Y. Lin, S.H. Huang, W.R. Liu, C.C. Hu, K.R. Lee, J.Y. Lai, Pressure-assisted self-assembly technique for fabricating composite membranes consisting of highly ordered selective laminate layers of amphiphilic graphene oxide, Carbon N. Y. 68 (2014) 670–677.

[163] S.C. George, S. Thomas, Transport phenomena through polymeric systems, Prog. Polym. Sci. 26 (2001) 985–1017.

[164] M.E.A. Ali, F.M. Hassan, X. Feng, Improving the performance of TFC membranes via chelation and surface reaction: applications in water desalination, J. Mater. Chem. A. 4 (2016) 6620–6629.

[165] Y. Tian, Y. Cao, Y. Wang, W. Yang, J. Feng, Realizing ultrahigh modulus and high strength of macroscopic graphene oxide papers through crosslinking of mussel-inspired polymers, Adv. Mater. 25 (2013) 2980–2983.

[166] Y. Li, Y. Su, Y. Dong, X. Zhao, Z. Jiang, R. Zhang, J. Zhao, Separation performance of thin-film composite nanofiltration membrane through interfacial polymerization using different amine monomers, Desalination. 333 (2014) 59–65.

[167] S. Liu, F. Fang, J. Wu, K. Zhang, The anti-biofouling properties of thin-film composite nanofiltration membranes grafted with biogenic silver nanoparticles, Desalination. 375 (2015) 121–128.

[168] G. Zeng, G. Lian, Y. Zhang, L. Gan, Y. Zhou, J. Qiu, B. van der Bruggen, J. Shen, Potential applications of abandoned aromatic polyamide reverse osmosis membrane by hypochlorite degradation, RSC Adv. 6 (2016) 12263–12271.

[169] J. Yin, G. Zhu, B. Deng, Graphene oxide (GO) enhanced polyamide (PA) thin-film nanocomposite (TFN) membrane for water purification, Desalination. 379 (2016) 93–101.

[170] M. Khayet, J.P.G. Villaluenga, M.P. Godino, J.I. Mengual, B. Seoane, K.C. Khulbe, T. Matsuura, Preparation and application of dense poly(phenylene oxide) membranes in pervaporation, J. Colloid Interface Sci. 278 (2004) 410–422.

[171] D. Wu, J. Martin, J. Du, Y. Zhang, D. Lawless, X. Feng, Thin film composite membranes comprising of polyamide and polydopamine for dehydration of ethylene glycol by pervaporation, J. Membr. Sci. 493 (2015) 622–635.

[172] M.C. Burshe, S.B. Sawant, J.B. Joshi, V.G. Pangarkar, Sorption and permeation of binary

water-alcohol systems through PVA membranes crosslinked with multifunctional crosslinking agents, Sep. Purif. Technol. 12 (1997) 145–156.

[173] K. Ghosal, B.D. Freeman, Gas separation using polymer membranes : an overview, Polym. Adv. Technol. 5 (1994) 673–697.

[174] R. Jiraratananon, A. Chanachai, R.Y.. Huang, D. Uttapap, Pervaporation dehydration of ethanol–water mixtures with chitosan/hydroxyethylcellulose (CS/HEC) composite membranes: I. Effect of operating conditions, J. Membr. Sci. 195 (2002) 143–151.

[175] B. Feng, K. Xu, A. Huang, Synthesis of graphene oxide/polyimide mixed matrix membranes for desalination, RSC Adv. 7 (2017) 2211–2217.

[176] A. Huang, B. Feng, Synthesis of novel graphene oxide-polyimide hollow fiber membranes for seawater desalination, J. Membr. Sci. 548 (2018) 59–65.

[177] X. Qian, N. Li, Q. Wang, S. Ji, Chitosan/graphene oxide mixed matrix membrane with enhanced water permeability for high-salinity water desalination by pervaporation, Desalination. 438 (2018) 83–96.

[178] D. Wu, A. Gao, H. Zhao, X. Feng, Pervaporative desalination of high-salinity water, Chem. Eng. Res. Des. 136 (2018) 154–164.

[179] L.F. Greenlee, D.F. Lawler, B.D. Freeman, B. Marrot, P. Moulin, Reverse osmosis desalination: Water sources, technology, and today's challenges, Water Res. 43 (2009) 2317–2348.

[180] Y. Luo, B. Roux, Simulation of osmotic pressure in concentrated aqueous salt solutions, J. Phys. Chem. Lett. 1 (2010) 183–189.

[181] F.A. Banat, J. Simandl, Desalination by membrane distillation: A parametric study, Sep. Sci. Technol. 33 (1998) 201–226.

[182] Y. Yun, R. Ma, W. Zhang, A.G. Fane, J. Li, Direct contact membrane distillation mechanism for high concentration NaCl solutions, Desalination. 188 (2006) 251–262.

[183] S.T. Hsu, K.T. Cheng, J.-S. Chiou, Seawater desalination by direct contact membrane distillation, Desalination. 143 (2002) 279–287.

[184] M. Gryta, J. Grzechulska-Damszel, A. Markowska, K. Karakulski, The influence of polypropylene degradation on the membrane wettability during membrane distillation, J. Membr. Sci. 326 (2009) 493–502.

[185] G. Chen, X. Yang, R. Wang, A.G. Fane, Performance enhancement and scaling control with gas bubbling in direct contact membrane distillation, Desalination. 308 (2013) 47–55.

[186] C.M. Tun, A.G. Fane, J.T. Matheickal, R. Sheikholeslami, Membrane distillation crystallization of concentrated salts—flux and crystal formation, J. Membr. Sci. 257 (2005) 144–155.

[187] J.-P. Mericq, S. Laborie, C. Cabassud, Vacuum membrane distillation of seawater reverse osmosis brines, Water Res. 44 (2010) 5260–5273.

[188] L. García-Fernández, M.C. García-Payo, M. Khayet, Effects of mixed solvents on the structural morphology and membrane distillation performance of PVDF-HFP hollow fiber membranes, J. Membr. Sci. 468 (2014) 324–338.

[189] S.Y. Hu, Y. Zhang, D. Lawless, X. Feng, Composite membranes comprising of polyvinylamine-poly(vinyl alcohol) incorporated with carbon nanotubes for dehydration of ethylene glycol by pervaporation, J. Membr. Sci. 417–418 (2012) 34–44.

[190] Y. Wang, M. Gruender, T.S. Chung, Pervaporation dehydration of ethylene glycol through polybenzimidazole (PBI)-based membranes. 1. Membrane fabrication, J. Membr. Sci. 363 (2010) 149–159.

[191] H. Yue, Y. Zhao, X. Ma, J. Gong, Ethylene glycol: properties, synthesis, and applications, Chem. Soc. Rev. 41 (2012) 4218–4244.

[192] R.Y.M. Huang, N.R. Jarvis, Separation of liquid mixtures by using polymer membranes. II. Permeation of aqueous alcohol solutions through cellophane and poly(vinyl alcohol), J. Appl. Polym. Sci. 14 (1970) 2341–2356.

[193] X. Feng, R.Y.M. Huang, Pervaporation with chitosan membranes. I. Separation of water from ethylene glycol by a chitosan/polysulfone composite membrane, J. Membr. Sci. 116 (1996) 67–76.

[194] P. Tzeng, B. Stevens, I. Devlaming, J.C. Grunlan, Polymer–graphene oxide quadlayer thin-film assemblies with improved gas barrier, Langmuir. 31 (2015) 5919–5927.

[195] G. Liu, Z. Jiang, C. Chen, L. Hou, B. Gao, H. Yang, H. Wu, F. Pan, P. Zhang, X. Cao, Preparation of ultrathin, robust membranes through reactive layer-by-layer (LbL) assembly for pervaporation dehydration, J. Membr. Sci. 537 (2017) 229–238.

[196] F.-X. Xiao, M. Pagliaro, Y.-J. Xu, B. Liu, Layer-by-layer assembly of versatile nanoarchitectures with diverse dimensionality: a new perspective for rational construction of multilayer assemblies, Chem. Soc. Rev. 45 (2016) 3088–3121.

[197] C. Cho, F. Xiang, K.L. Wallace, J.C. Grunlan, Combined ionic and hydrogen bonding in polymer multilayer thin film for high gas barrier and stretchiness, Macromolecules. 48 (2015) 5723–5729.

[198] L. Wang, N. Wang, J. Li, J. Li, W. Bian, S. Ji, Layer-by-layer self-assembly of

polycation/GO nanofiltration membrane with enhanced stability and fouling resistance, Sep. Purif. Technol. 160 (2016) 123–131.

[199] J. Zhao, Y. Zhu, F. Pan, G. He, C. Fang, K. Cao, R. Xing, Z. Jiang, Fabricating graphene oxide-based ultrathin hybrid membrane for pervaporation dehydration via layer-by-layer self-assembly driven by multiple interactions, J. Membr. Sci. 487 (2015) 162–172.

[200] J.A. Veil, M.G. Puder, D. Elcock, R.J. Redweik Jr., A white paper describing produced water from production of crude oil, natural gas, and coal bed methane., United States, 2004.

[201] R.H. Perry, D.W. Green, Perry's Chemical Engineers' Handbook, 7th ed., McGrow-Hill, 1999.

[202] C.L. Yaws, K. Narasimhan, Prasad, C. Gabbula, Yaws' Handbook of Antoine Coefficients for Vapor Pressure, 2nd Electr, Knovel, 2009.

[203] Y. Hirai, T. Nakajima, Sorption behavior of water vapor into polyelectrolyte complex of poly(acrylic acid)/poly(4-vinylpyridine), J. Appl. Polym. Sci. 37 (1989) 2275–2281.

[204] J.G. Wijmans, R.W. Baker, A simple predictive treatment of the permeation process in pervaporation, J. Membr. Sci. 79 (1993) 101–113.

[205] R.W. Baker, J.G. Wijmans, Y. Huang, Permeability, permeance and selectivity: A preferred way of reporting pervaporation performance data, J. Membr. Sci. 348 (2010) 346–352.

[206] Y. Wang, T.S. Chung, B.W. Neo, M. Gruender, Processing and engineering of pervaporation dehydration of ethylene glycol via dual-layer polybenzimidazole (PBI)/polyetherimide (PEI) membranes, J. Membr. Sci. 378 (2011) 339–350.

[207] D. Shah, D. Bhattacharyya, A. Ghorpade, W. Mangum, Pervaporation of pharmaceutical waste streams and synthetic mixtures using water selective membranes, Environ. Prog. 18 (1999) 21–29.

[208] E.G. Heisler, A.N.N.S. Hunter, J. Siciliano, R.H. Treadway, Solute and temperature effects in the pervaporation of aqueous alcoholic solutions, Science. 124 (1956) 77–79.

[209] A. Misra, F.W. Kroesser, R.A. Shelden, The effect of solutes on the pervaporation of water-methanol mixtures through cellophane, J. Polym. Sci. Polym. Symp. 41 (1973) 145–153.

[210] J. Yang, H. Li, J. Xu, J. Wang, X. Meng, K. Bai, J. Lu, Y. Zhang, D. Yin, Influences of inorganic salts on the pervaporation properties of zeolite NaA membranes on macroporous supports, Microporous Mesoporous Mater. 192 (2014) 60–68.

[211] H.M. Trimble, Solubilities of salts in ethylene glycol and in its mixtures with water, Ind. Eng. Chem. 23 (1931) 165–167.

[212] J.P.G. Villaluenga, M. Khayet, P. Godino, B. Seoane, J.I. Mengual, Analysis of the membrane thickness effect on the pervaporation separation of methanol/methyl tertiary butyl ether mixtures, Sep. Purif. Technol. 47 (2005) 80–87.

[213] G. Liu, Z. Jiang, C. Li, L. Hou, C. Chen, H. Yang, F. Pan, H. Wu, P. Zhang, X. Cao, Layer-by-layer self-assembled nanocomposite membranes via bio-inspired mineralization for pervaporation dehydration, J. Membr. Sci. 570–571 (2019) 44–52.

[214] C. Hu, R. Guo, B. Li, X. Ma, H. Wu, Z. Jiang, Development of novel mordenite-filled chitosan–poly(acrylic acid) polyelectrolyte complex membranes for pervaporation dehydration of ethylene glycol aqueous solution, J. Membr. Sci. 293 (2007) 142–150.

[215] C. Hu, B. Li, R. Guo, H. Wu, Z. Jiang, Pervaporation performance of chitosan–poly(acrylic acid) polyelectrolyte complex membranes for dehydration of ethylene glycol aqueous solution, Sep. Purif. Technol. 55 (2007) 327–334.

[216] D. Hua, R.K. Rai, Y. Zhang, T.S. Chung, Aldehyde functionalized graphene oxide frameworks as robust membrane materials for pervaporative alcohol dehydration, Chem. Eng. Sci. 161 (2017) 341–349.

[217] N. Vorayos, T. Kiatsiriroat, N. Vorayos, Performance analysis of solar ethanol distillation, Renew. Energy. 31 (2006) 2543–2554.

[218] X. Qiao, T.S. Chung, W.F. Guo, T. Matsuura, M.M. Teoh, Dehydration of isopropanol and its comparison with dehydration of butanol isomers from thermodynamic and molecular aspects, J. Membr. Sci. 252 (2005) 37–49.

[219] A. F. M. Barton, Handbook of Solubility Parameters and Other Cohesion Parameters, CRC Press, Boca Raton, Florida, 1983.

[220] B. Bolto, M. Hoang, Z. Xie, A review of membrane selection for the dehydration of aqueous ethanol by pervaporation, Chem. Eng. Process. Process Intensif. 50 (2011) 227–235.

[221] R.K. Iler, Multilayers of colloidal particles, J. Colloid Interface Sci. 21 (1966) 569–594.

[222] L. Krasemann, B. Tieke, Ultrathin self-assembled polyelectrolyte membranes for pervaporation, J. Membr. Sci. 150 (1998) 23–30.

[223] F. van Ackern, L. Krasemann, B. Tieke, Ultrathin membranes for gas separation and pervaporation prepared upon electrostatic self-assembly of polyelectrolytes, Thin Solid Films. 327–329 (1998) 762–766.

[224] B.-S. Kim, O. V Lebedeva, K. Koynov, H. Gong, G. Glasser, I. Lieberwith, O.I. Vinogradova, Effect of Organic Solvent on the Permeability and Stiffness of Polyelectrolyte Multilayer Microcapsules, Macromolecules. 38 (2005) 5214–5222.

[225] E. Poptoshev, B. Schoeler, F. Caruso, Influence of Solvent Quality on the Growth of Polyelectrolyte Multilayers, Langmuir. 20 (2004) 829–834.

[226] D.W. Mangindaan, G. Min Shi, T.S. Chung, Pervaporation dehydration of acetone using P84 co-polyimide flat sheet membranes modified by vapor phase crosslinking, J. Membr. Sci. 458 (2014) 76–85.

[227] M.N. Hyder, R.Y.M. Huang, P. Chen, Composite poly(vinyl alcohol)–poly(sulfone) membranes crosslinked by trimesoyl chloride: Characterization and dehydration of ethylene glycol–water mixtures, J. Membr. Sci. 326 (2009) 363–371.

[228] C. Qiu, S. Qi, C.Y. Tang, Synthesis of high flux forward osmosis membranes by chemically crosslinked layer-by-layer polyelectrolytes, J. Membr. Sci. 381 (2011) 74–80.

[229] S. Qi, C.Q. Qiu, Y. Zhao, C.Y. Tang, Double-skinned forward osmosis membranes based on layer-by-layer assembly—FO performance and fouling behavior, J. Membr. Sci. 405–406 (2012) 20–29.

[230] Q. Chen, P. Yu, W. Huang, S. Yu, M. Liu, C. Gao, High-flux composite hollow fiber nanofiltration membranes fabricated through layer-by-layer deposition of oppositely charged crosslinked polyelectrolytes for dye removal, J. Membr. Sci. 492 (2015) 312–321.

[231] B. Xia, C. Dong, Y. Lu, M. Rong, Y. Lv, J. Shi, Preparation and characterization of chemically-crosslinked polyethyleneimine films on hydroxylated surfaces for stable bactericidal coatings, Thin Solid Films. 520 (2011) 1120–1124.

[232] L. Krasemann, A. Toutianoush, B. Tieke, Self-assembled polyelectrolyte multilayer membranes with highly improved pervaporation separation of ethanol/water mixtures, J. Membr. Sci. 181 (2001) 221–228.

[233] X. Feng, R.Y.M. Huang, Preparation and performance of asymmetric polyetherimide membranes for isopropanol dehydration by pervaporation, J. Membr. Sci. 109 (1996) 165–172.

[234] General Electric, Design of Experiments in Protein Production and Purification, n.d. Retrieved from http://www.gelifesciences.co.kr/

[235] G. Young Moon, R. Pal, R.Y.M. Huang, Novel two-ply composite membranes of chitosan and sodium alginate for the pervaporation dehydration of isopropanol and ethanol, J. Membr. Sci. 156 (1999) 17–27.

[236] Y.M. Xu, T.S. Chung, High-performance UiO-66/polyimide mixed matrix membranes for ethanol, isopropanol and n-butanol dehydration via pervaporation, J. Membr. Sci. 531 (2017) 16–26.

[237] S.P. Kusumocahyo, T. Kanamori, T. Iwatsubo, K. Sumaru, T. Shinbo, Development of

polyion complex membranes based on cellulose acetate modified by oxygen plasma treatment for pervaporation, J. Membr. Sci. 208 (2002) 223–231.

[238] J. Meier-Haack, W. Lenk, D. Lehmann, K. Lunkwitz, Pervaporation separation of water/alcohol mixtures using composite membranes based on polyelectrolyte multilayer assemblies, J. Membr. Sci. 184 (2001) 233–243.

[239] E. Halakoo, X. Feng, Layer-by-layer assembly of polyethyleneimine/graphene oxide membranes for desalination of high-salinity water via pervaporation, Sep. Purif. Technol. 234 (2020) 116077.

[240] W.J. Koros, G.K. Fleming, Membrane-based gas separation, J. Membr. Sci. 83 (1993) 1–80.

[241] L.Y. Ng, A.W. Mohammad, C.Y. Ng, A review on nanofiltration membrane fabrication and modification using polyelectrolytes: Effective ways to develop membrane selective barriers and rejection capability, Adv. Colloid Interface Sci. 197–198 (2013) 85–107.

[242] L. Zhao, B. Yuan, Y. Geng, C. Yu, N.H. Kim, J.H. Lee, P. Li, Fabrication of ultrahigh hydrogen barrier polyethyleneimine/graphene oxide films by LBL assembly fine-tuned with electric field application, Compos. Part A Appl. Sci. Manuf. 78 (2015) 60–69.

Appendix A

Sample calculations

Pervaporation performance

Water permeate flux (desalination):

Feed: NaCl/water

Quantity of permeate collected (Q): 2 g

Effective area of the membrane (A): 17.35 cm^2

Time interval (Δt): 5min

Operating temperature (ºC): 25

Feed NaCl concentration (C_f): 200 g/L

Permeate NaCl concentration (C_p): ~ 0.2 g/L

$$J = \frac{Q}{A.\Delta t} = \frac{2}{17.35\times10^{-4}\times0.084} = 13723 \text{ (g/m}^2\text{ h)}$$

Salt rejection

$$R = \frac{C_f - C_p}{C_f} \times 100 = \frac{200 - 0.2}{200} \times 100 = 99.9\ \%$$

Water permeate flux (dehydration):

Feed: EG/water

Feed water concentration (X_w): 0.1 wt%

Effective membrane area (A): 17.35 cm^2

Time interval (Δt): 2h

Quantity of permeate collected (Q): 0.195 g

Water content in permeate (X_w): 66.5 wt%

$$J = \frac{Q}{A.\Delta t} = \frac{0.195}{17.35\times10^{-4}\times2} = 56.2 \text{ (g/m}^2\text{ h)}$$

Partial permeation flux

$J_{water} = J \times X_w = 56.2 \times 0.665 = 37.37$ (g/m^2 h)

$J_{EG} = J(1-X_w) = 56.2 \times (1- 0.665) = 18.826$ (g/m^2 h)

Separation factor

$$\alpha_{ij} = \frac{Y_i/Y_j}{X_i/X_j} = \frac{66.5/33.5}{0.1/99.9} = 1983$$

Membrane permeance and Driving force

Feed: EtOH/water

Feed water concentration (C_f): 2 wt%

Operating temperature: 295.15 K

Permeation flux of water (J_w): 365.2

Permeation flux of EtOH (J_w): 205

Saturated vapor pressure of water at 295.15 K (p_w^{sat}): 2.64 kPa

Saturated vapor pressure of EtOH at 295.15 K (p_w^s): 6.56 kPa

Mole fraction of water in feed (X_w): 0.0496

Mole fraction of EtOH in feed (X_w): 0.9503

Activity coefficient of water (γ_w): 2.5771

Activity coefficient of EtOH (γ_{EtOH}): 1.0019

Permeate vapor pressure of water (p^p): ~ 0 kPa

Mole fraction of water in permeate (Y_w): 0.9504

The permeance of water:

$$\frac{P_w}{l} = \frac{J_w}{X_w \gamma_w p_w^{sat} - Y_w p^p} = \frac{\frac{365.2}{18}}{0.0496 \times 2.57 \times 2.64} = 60.34 \ \frac{mol}{m^2.h\,.kPa}$$

$P_i^{sat} x_i \gamma_i =$ Driving force for component i

Driving force of water = $X_w \gamma_w p_w^{sat} = 0.33626$ kPa

Driving force of EtOH = $X_{EtOH} \gamma_{EtOH} p_{EtOH}^{sat} = 6.25$ kPa

Activation energy

Feed: EtOH/water

Feed water concentration (C_f): 2 wt%

$$\ln J = \ln J_0 - \frac{E_J}{R}\frac{1}{T}$$

$\text{Slope}_1 = -{}^{E_J}/_{R} = -2.876$

$E_J = -(-2.876 \times 8.314) = 23.91$

$$\ln({}^{P_w}/_{l}) = \ln(\frac{P_{w0}}{l}) - \frac{E_P}{R}\frac{1}{T}$$

$\text{Slope}_2 = -{}^{E_P}/_{R} = 2.37$

$E_P = -(2.37 \times 8.314) = -19.70$

Appendix B

Calibration curves by refractometer

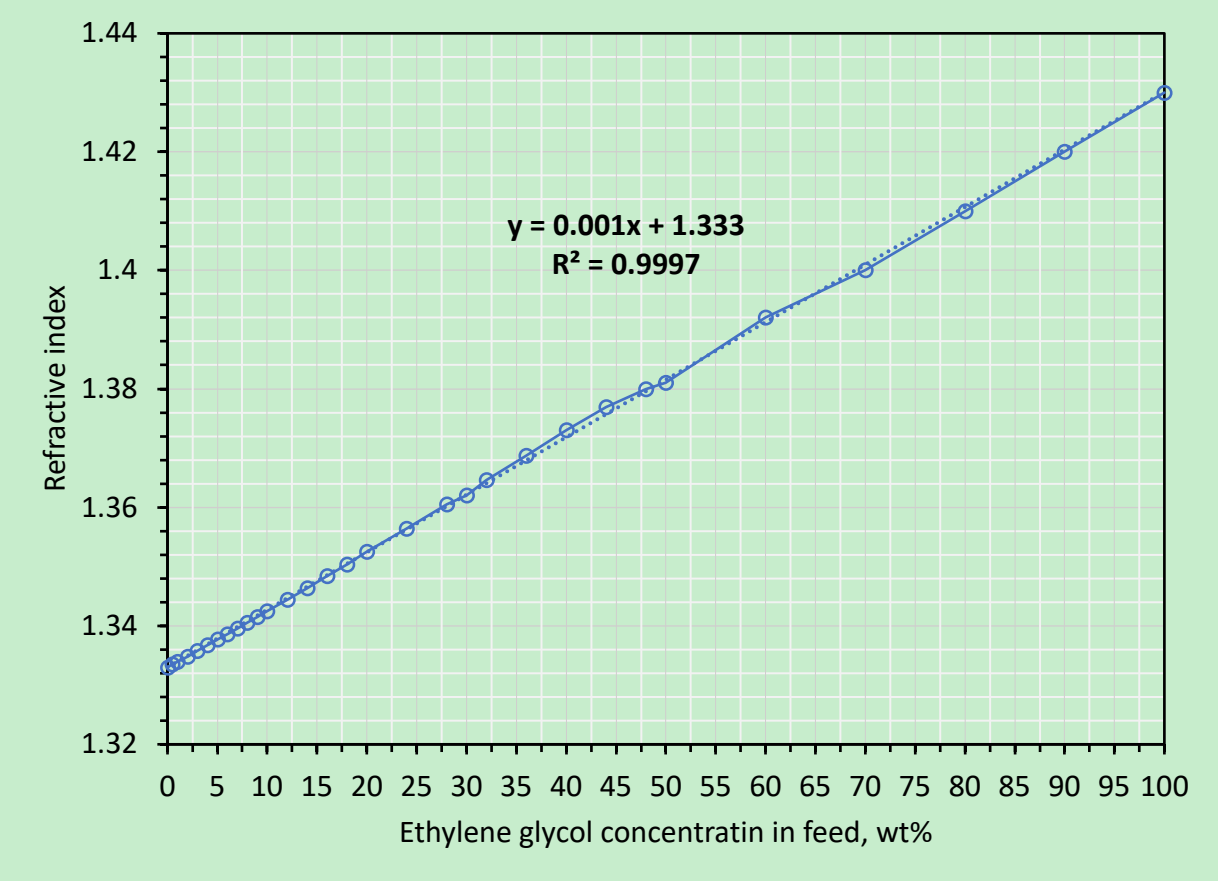

Figure S. 1 Calibration curve for ethylene glycol/water mixtures by refractometer. At room temperature: 22-23 ºC

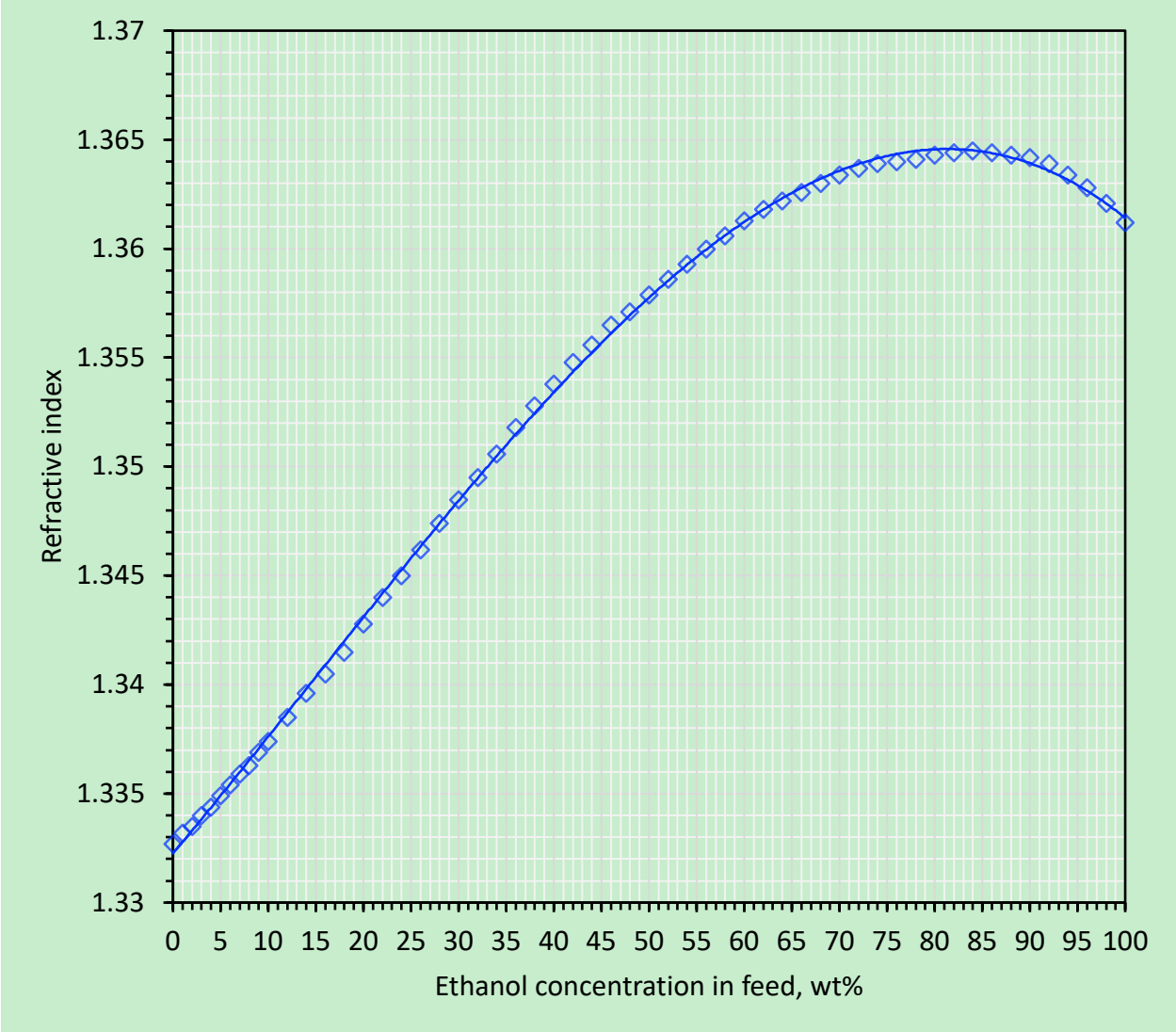

Figure S. 2 Calibration curve for ethanol/water mixtures by refractometer. At room temperature: 22-23 ºC

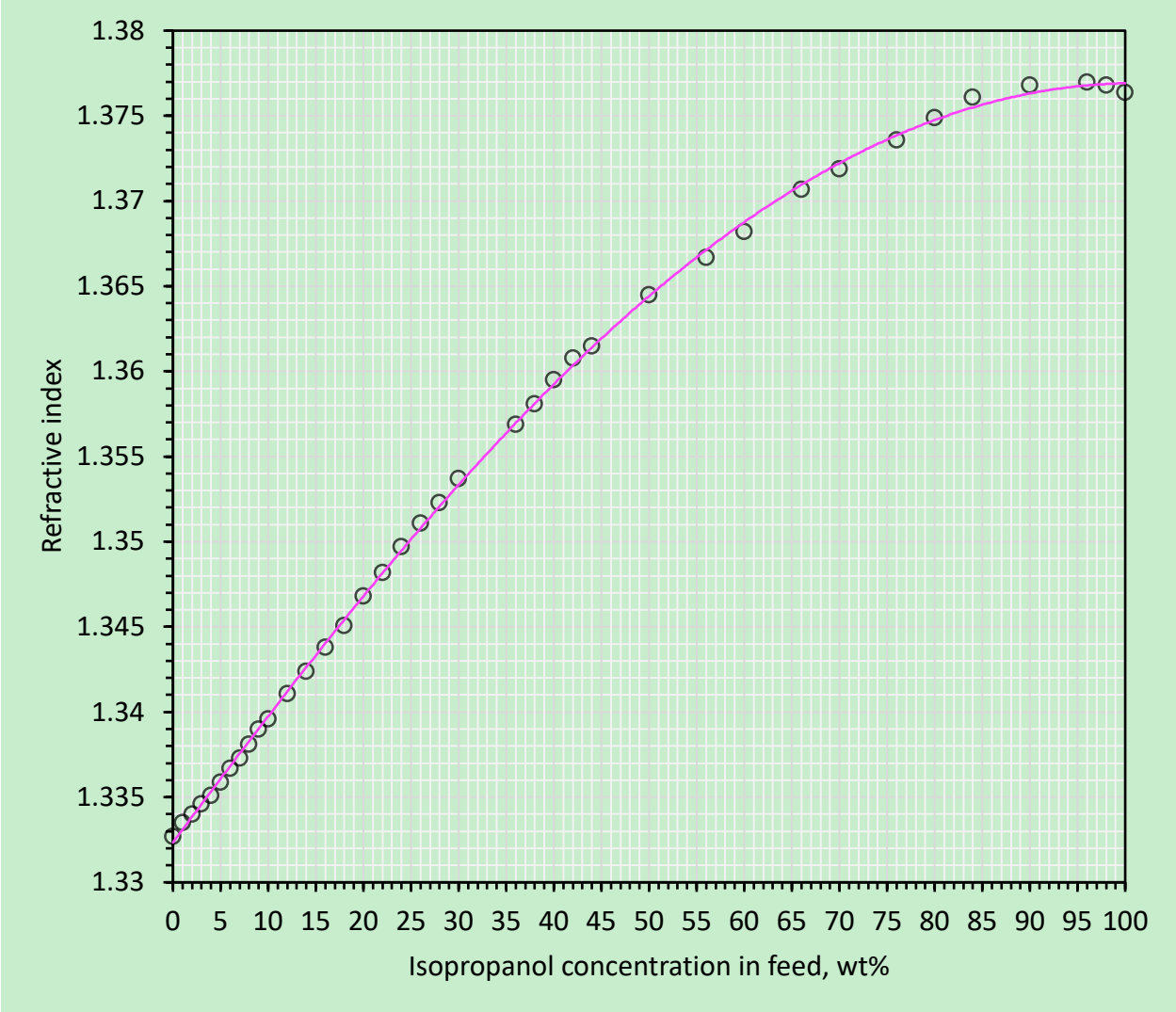

Figure S. 3 Calibration curve for isopropanol/water mixtures by refractometer. At room temperature: 22-23 ºC

Appendix C

Table S. 1 Thermodynamic properties of IPA/water mixtures and driving force for pervaporation at various temperatures and concentrations.

Feed water concentration (wt%)	Temperature (ºC)	γ_{IPA}	γ_{water}	p^s_{IPA} (kPa)	p^s_{water} (kPa)	Driving force of IPA (kPa)	Driving force of water (kPa)
2	22	1.004	3.138	4.820	2.634	4.532	0.527
	30	1.004	3.173	7.880	4.231	7.409	0.856
	40	1.004	3.205	13.938	7.358	13.104	1.505
	50	1.004	3.227	23.601	12.305	22.187	2.534
	60	1.004	3.242	38.444	19.870	36.139	4.110
6	22	1.033	2.539	4.820	2.634	4.108	1.175
	30	1.033	2.572	7.880	4.231	6.712	1.912
	40	1.033	2.605	13.938	7.358	11.868	3.368
	50	1.032	2.630	23.601	12.305	20.089	5.686
	60	1.032	2.648	38.444	19.870	32.709	9.247
12	22	1.113	2.017	4.820	2.634	3.689	1.663
	30	1.112	2.046	7.880	4.231	6.026	2.710
	40	1.111	2.075	13.938	7.358	10.650	4.779
	50	1.110	2.099	23.601	12.305	18.015	8.083
	60	1.109	2.118	38.444	19.870	29.314	13.171

Simulation method: WILSON at 25 ºC, 1 atm.

Table S. 2 Thermodynamic properties of EtOH/water mixtures and driving force for pervaporation at various temperatures and concentrations.

Feed water concentration (wt%)	Temperature (ºC)	γ_{EtOH}	γ_{water}	p^s_{EtOH} (kPa)	p^s_{water} (kPa)	Driving force of EtOH (kPa)	Driving force of water (kPa)
2	22	1.002	2.571	6.568	2.634	6.254	0.336
	30	1.002	2.577	10.412	4.231	9.915	0.541
	40	1.002	2.583	17.825	7.358	16.974	0.944
	50	1.002	2.589	29.369	12.305	27.965	1.581
	60	1.002	2.593	46.751	19.870	44.515	2.558
6	22	1.016	2.245	6.568	2.634	5.738	0.831
	30	1.016	2.252	10.412	4.231	9.095	1.338
	40	1.016	2.260	17.825	7.358	15.570	2.336
	50	1.016	2.267	29.369	12.305	25.649	3.918
	60	1.015	2.273	46.751	19.870	40.825	6.343
12	22	1.059	1.906	6.568	2.634	5.155	1.300
	30	1.058	1.913	10.412	4.231	8.171	2.095
	40	1.058	1.921	17.825	7.358	13.984	3.658
	50	1.057	1.929	29.369	12.305	23.032	6.141
	60	1.057	1.935	46.751	19.870	36.653	9.950

Simulation method: WILSON at 25 ºC, 1 atm.

Table S. 3 Thermodynamic properties of EG/water mixtures for pervaporation at various temperatures and concentrations.

Feed water concentration (wt%)	Temperature (°C)	γ_{EG}	γ_{water}	p^{s}_{EG} (kPa)	p^{s}_{water} (kPa)
0.1	25	1	0.869985	0.0088	3.170
	35	1	0.880947	0.0200	5.626
	45	1	0.891344	0.0444	9.590
	50	1	0.896343	0.0645	12.305
	55	1	0.901216	0.0926	15.702
	60	1	0.905968	0.1313	19.870
0.2	25	1	0.870573	0.0088	3.170
	35	1	0.881496	0.0200	5.626
	45	1	0.891854	0.0444	9.590
	50	1	0.896834	0.0645	12.305
	55	1	0.901689	0.0926	15.702
	60	1	1	0.1313	19.870
0.5	25	1	0.872322	0.0088	3.170
	35	1	0.883127	0.0200	5.626
	45	1	0.893369	0.0444	9.590
	50	1	0.898293	0.0645	12.305
	55	1	0.903092	0.0926	15.702
	60	1	1	0.1313	19.870
2.0	25	1	0.880705	0.0088	3.170
	35	1	0.890935	0.0200	5.626
	45	1	0.900616	0.0444	9.590

Feed water concentration (wt%)	Temperature (ºC)	γ_{EG}	γ_{water}	p^{s}_{EG} (kPa)	p^{s}_{water} (kPa)
	50	1	0.905265	0.0645	12.305
	55	1	0.909792	0.0926	15.702
	60	1	0.914202	0.1313	19.870
5.0	25	0.997454	0.895812	0.0088	3.170
	35	0.997661	0.904965	0.0200	5.626
	45	0.997856	0.913601	0.0444	9.590
	50	0.99795	0.917738	0.0645	12.305
	55	0.998042	0.921761	0.0926	15.702
	60	0.998131	0.998131	0.1313	19.870

Appendix D

Water/EtOH mixture
Feed water concentration: 6wt%
Operating Temperature: 50 ºC

Table S. 4 Total resistance of water and EtOH in the membrane as a function of number of bilayers.

# bilayers	$(1/flux)_{water}$-(m^2 h/g)	$(1/flux)_{EtOH}$-(m^2 h/g)	$(Driving\ force)_{water}$-(kPa)	$(Driving\ force)_{EtOH}$-(kPa)	$(Total\ resistance)_{water}$-($m^2$ h kPa/mol)	$(Total\ resistance)_{EtOH}$-($m^2$ h kPa/mol)
3	0.00060	0.00099	3.92	25.65	0.0423	1.180
5	0.00066	0.00138	3.92	25.65	0.0465	1.632
7	0.00068	0.00167	3.92	25.65	0.0477	1.974
9	0.00073	0.00224	3.92	25.65	0.0515	2.646
10	0.00072	0.00256	3.92	25.65	0.0513	3.031
12	0.00077	0.00307	3.92	25.65	0.0542	3.635
14	0.00078	0.00375	3.92	25.65	0.0554	4.439

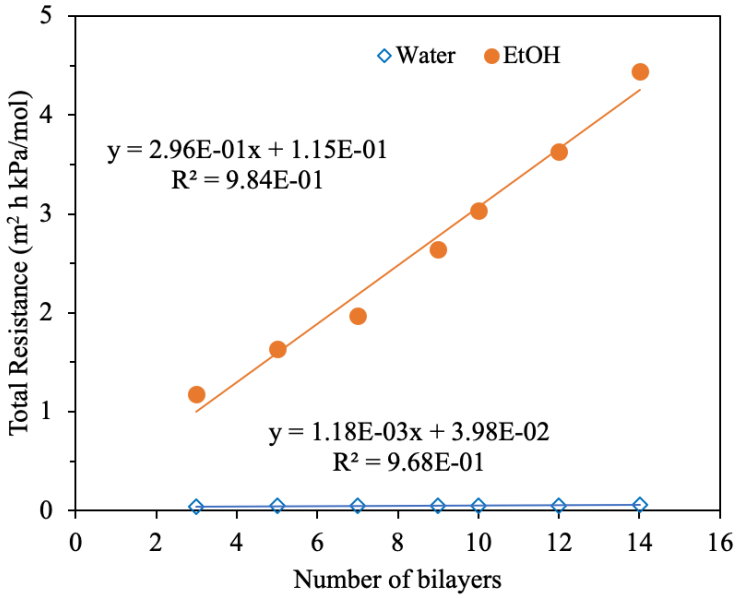

Figure S. 4 Total resistance as a function of number of bilayers for water and EtOH. Feed water concentration: 6wt%, Operating Temperature: 50 ℃

Water/IPA mixture
Feed water concentration: 6wt%
Operating Temperature: 50 ºC

Table S. 5 Total resistance of water and IPA in the membrane as a function of number of bilayers.

# bilayers	$(1/flux)_{water}$-(m^2 h/g)	$(1/flux)_{IPA}$-(m^2 h/g)	$(Driving\ force)_{water}$-(kPa)	$(Driving\ force)_{IPA}$-(kPa)	$(Total\ resistance)_{water}$-($m^2$ h kPa/mol)	$(Total\ resistance)_{IPA}$-($m^2$ h kPa/mol)
3	0.00063	0.00254	5.68	20.09	0.0650	3.073
5	0.00066	0.00332	5.68	20.09	0.0676	4.014
7	0.00068	0.00410	5.68	20.09	0.0695	4.957
9	0.00071	0.00531	5.68	20.09	0.0727	6.420
10	0.00073	0.00601	5.68	20.09	0.0745	7.264
12	0.00074	0.00712	5.68	20.09	0.0755	8.598
14	0.00075	0.00860	5.68	20.09	0.0765	10.391

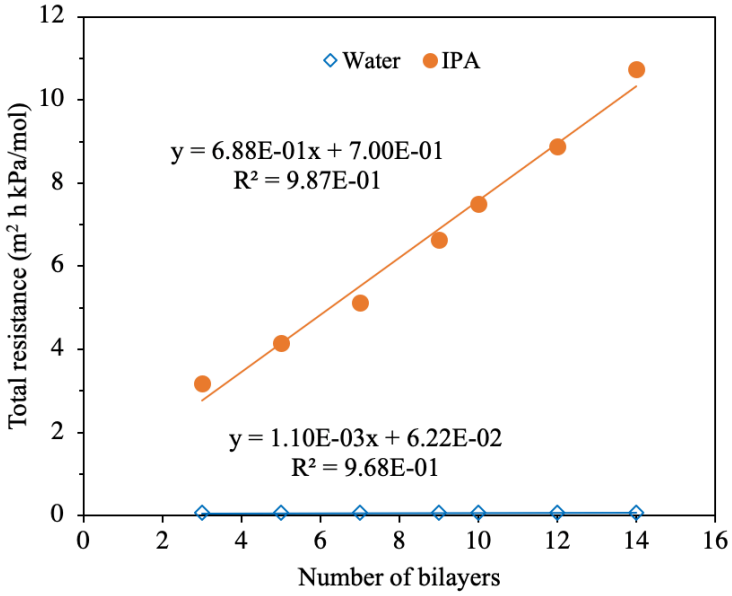

Figure S. 5 Total resistance as a function of number of bilayers for water and IPA. Feed water concentration: 6wt%, Operating Temperature: 50 ºC.

Water/EG mixture
Feed water concentration: 5wt%
Operating Temperature: 35 ºC

Table S. 6 Total resistance of water and EG in the membrane as a function of number of bilayers.

# bilayers	$(1/flux)_{water}$-(m^2 h/g)	$(1/flux)_{EG}$-(m^2 h/g)	$(Driving\ force)_{water}$-(kPa)	$(Driving\ force)_{EG}$-(kPa)	$(Total\ resistance)_{water}$-($m^2$ h kPa/mol)	$(Total\ resistance)_{EG}$-(m^2 h kPa/mol)
1	0.0075	0.0326	0.7822	0.0169	0.1058	0.0342
3	0.0080	0.0436	0.7822	0.0169	0.1126	0.0457
5	0.0087	0.0519	0.7822	0.0169	0.1230	0.0544
8	0.0093	0.0676	0.7822	0.0169	0.1310	0.0709
10	0.0098	0.0778	0.7822	0.0169	0.1382	0.0816
12	0.0100	0.0936	0.7822	0.0169	0.1416	0.0982
15	0.0107	0.1155	0.7822	0.0169	0.1510	0.1210

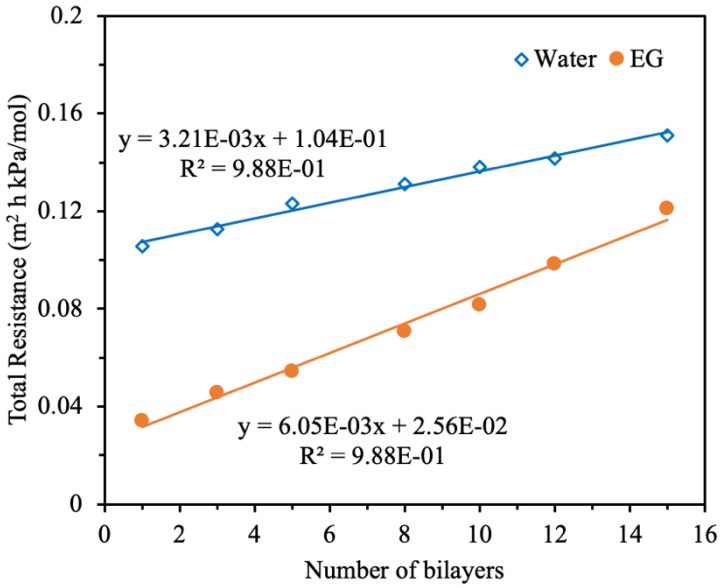

Figure S. 6 Total resistance as a function of number of bilayers for water and EG. Feed water concentration: 5wt%, Operating Temperature: 35 ºC

Appendix E

Summary of MLR analyses for flux

Regression Statistics	
Multiple R	0.99
R Square	0.99
Adjusted R Square	0.99
Standard Error	14.50
Observations	24

ANOVA

	df	*SS*	*MS*	*F*	*Significance F*
Regression	7	2275722.47	325103.21	1546.84	1.98×10^{-21}
Residual	16	3362.76	210.17		
Total	23	2279085.23			

Terms	Coefficients	Standard Error	t Stat	P-value	Lower 95%	Upper 95%	Lower 99.0%	Upper 99.0%
Intercept	703.27	2.96	237.65	8.10E-30	696.99	709.54	694.62	711.91
C (wt%)	-165.93	3.02	-54.89	1.20E-19	-172.34	-159.52	-174.76	-157.11
t (h)	-260.43	3.02	-86.15	9.01E-23	-266.83	-254.02	-269.26	-251.61
T (℃)	-47.88	3.02	-15.84	3.36E-11	-54.29	-41.47	-56.71	-39.05
C*t	23.25	3.08	7.53	1.20E-06	16.71	29.8	14.23	32.27
C*T	24.46	3.08	7.92	6.31E-07	17.91	31.01	15.43	33.47
t*T	7.32	3.08	2.37	0.0307	0.77	13.86	-1.7	16.33
C*t*T	-12.8	3.15	-4.05	0.000914	-19.5	-6.11	-22.01	-3.58

Summary of MLR analyses for separation factor

Regression Statistics	
Multiple R	0.99
R Square	0.99
Adjusted R Square	0.99
Standard Error	0.19
Observations	24

ANOVA

	df	*SS*	*MS*	*F*	*Significance F*
Regression	7	21698.47	3099.78	84539.50	2.53×10^{-35}
Residual	16	0.58	0.04		
Total	23	21699.06			

Terms	Coefficients	Standard Error	t Stat	P-value	Lower 95%	Upper 95%	Lower 99.0%	Upper 99.0%
Intercept	79.52	0.04	2034.46	9.79E-45	79.43	79.61	79.41	79.63
C (wt%)	16.14	0.04	404.12	1.67E-33	16.05	16.22	16.01	16.25
t (h)	23.58	0.04	590.46	3.86E-36	23.49	23.66	23.45	23.69
T (℃)	10.34	0.04	258.93	2.06E-30	10.25	10.42	10.22	10.45
C*t	2.39	0.04	58.52	4.30E-20	2.31	2.47	2.26	2.5
C*T	-0.04	0.04	-0.96	0.35	-0.12	0.04	-0.15	0.08
t*T	1.21	0.04	29.74	1.97E-15	1.12	1.29	1.09	1.33
C*t*T	-3.83	0.04	-91.99	3.16E-23	-3.92	-3.74	-3.95	-3.71